University of Southampton

Faculty of Environmental and Life Sciences

School of Ocean and Earth Sciences

The Correspondence of Morphological and Geochemical Trait Dynamics in Shifting Plankton Communities

by

Lorna Ellen Kearns

ORCID ID 0000-0001-9740-7410

Thesis for the degree of Doctor of Philosophy

September 2021

University of Southampton

Abstract

Faculty of Environmental and Life Sciences

School of Ocean and Earth Sciences

Doctor of Philosophy

The Correspondence of Morphological and Geochemical Trait Dynamics in Shifting Plankton Communities

by

Lorna Ellen Kearns

Humans are changing the Earth. What is unknown is how biotic communities and ecosystems will react to this change on both short and long timescales. The fossil record can provide us with a means of investigating ecosystem responses to long-term climatic fluctuations which can act as baselines for future anthropogenic induced change. How we utilize the fossil record is therefore of critical Importance. The high spatial and temporal resolution of the planktonic foraminifera fossil record provides an ideal system to investigate ecosystem responses to climatic fluctuations at multiple scales and levels. The primary objective of this thesis is to measure and understand the relationship between planktonic foraminifera and their environment, to enable a more biologically informative assessment of the fossil record. I created a diversity record of planktonic foraminifera through the Middle Eocene Climatic Optimum comprising of 22,800 individuals classified to three taxonomic levels and investigated the responses of these assemblages using effective diversity: a novel approach for Palaeogene and deep-time systems (Chapter 2). The results from this study show that analytical size fraction choice is a key determinant of diversity signals in deep-time and furthermore it is small species that maintain ecological function during transient climatic events. I then investigated a key component of these assemblages, *Subbotina*, using individual morphological and geochemical measurements to link their traits to the environment and assess their persistence through the climatic fluctuations of the Middle Eocene (Chapter 3). I found that longevity of *Subbotina* is a result of morphological and geochemical trait plasticity resulting in a wide ecological niche which in turn allowed for continued persistence and dominance through the Middle Eocene whilst other groups faltered. Next, I explored the relationship between geochemistry and morphology within a relatively recent system to understand the relationship between geochemistry, size, and genetically identified species (Chapter 4). The results showed that fine resolution geochemical analyses can be used to unpick the drivers of intraindividual variability. However, more work is needed to understand the drivers of geochemistry at the individual level which is possible using the methods I advocate and explore in this thesis. Together, these discoveries expand our understanding of how planktonic foraminifera communities are linked to their environment and demonstrate that by using the appropriate analytical approaches we can investigate this relationship in a more biologically meaningful way. Future studies on planktonic foraminifera will require the application of trait-based approaches through the integration of geochemistry, morphology, and diversity measurements to further our understanding of how past communities responded to climatic perturbations with an aim to inform our understanding of biotic responses to current and future anthropogenic change.

Table of Contents

Table of Tables

Table of Figures

Table of Figures

List of Accompanying Materials

Due to the size of the datasets generated in this thesis, all data where not provided in the Appendices is electronically available upon request and will be available as supplements to the manuscripts this thesis is composed of when they are published .

Chapter 2 is intended for submission to *Paleobiology*, and the corresponding datasets will be made publicly available following the acceptance and publication of this manuscript.

Chapter 3 is published in *Frontiers in Ecology and Evolution* which can be found here: https://doi.org/10.3389/fevo.2021.679722 including all supplementary material and data.

Chapter 4 is an invited resubmission to *Paleoceanography and Paleoclimatology*. All material will be made publicly available following the final acceptance of this manuscript.

Research Thesis: Declaration of Authorship

Print name: Lorna Kearns

Title of thesis: The Correspondence of Morphological and Geochemical Trait Dynamics in Shifting Plankton Communities

I declare that this thesis and the work presented in it are my own and has been generated by me as the result of my own original research.

I confirm that:

1. This work was done wholly or mainly while in candidature for a research degree at this University;
2. Where any part of this thesis has previously been submitted for a degree or any other qualification at this University or any other institution, this has been clearly stated;
3. Where I have consulted the published work of others, this is always clearly attributed;
4. Where I have quoted from the work of others, the source is always given. With the exception of such quotations, this thesis is entirely my own work;
5. I have acknowledged all main sources of help;
6. Where the thesis is based on work done by myself jointly with others, I have made clear exactly what was done by others and what I have contributed myself;
7. Parts of this work have been published as:-

Kearns, Lorna E., Steven M. Bohaty, K. M. Edgar, Sandra Nogué, and Thomas H. G. Ezard. 'Searching for Function: Reconstructing Adaptive Niche Changes Using Geochemical and Morphological Data in Planktonic Foraminifera'. *Frontiers in Ecology and Evolution* 9 (2021). https://doi.org/10.3389/fevo.2021.679722.

Signature: .....Date: .....

Acknowledgements

A thesis is both the sole achievement of one, who gets to bask in its glory, and the efforts of numerous individuals all of whom deserve to be recognized. I will do my best to acknowledge them here.

First and foremost, I would like to thank my supervisors Tom Ezard, Steve Bohaty, Kirsty Edgar and Sandra Nogué-Bosch, without whom this project would not have been possible. Tom has pushed me to achieve and experience more than I ever thought possible during my PhD. His constant encouragement has allowed me to fight an underlying anxiety of both mathematics and chemistry, so much so that my thesis is now overflowing with statistics and geochemistry. Furthermore, he has allowed me to travel the world to present my research expanding both my understanding and place in the world of academia. Steve has provided constant encouragement throughout my PhD and gave me the opportunity to participate in a research expedition which has gone on to shape how I think about and use palaeo data. Kirsty's vast knowledge of foraminifera and positive encouragement has helped me endlessly throughout my PhD. Sandra provided positivity and encouragement in abundance alongside dynamic conversations which have continuously shaped my research and will continue to do so into the future. In addition, I am extremely grateful for the patience given to me by Gavin Foster who, though not officially my supervisor, has patiently dealt with my constant questions since I first dove headfirst into the world of geochemistry all those years ago.

I have had the privilege to meet amazing people across the world who were kind enough to engage in my research for which I am very grateful. Closer to home the past 4 years would not have been possible without the NOCS Palaeo team, LALA lab group, NOCS PhD's and SPITFIRE PhD's. Special thanks should be given to Amy, Tereza and Max for being by side throughout the highs and lows of the past 4 years. Though not a PhD member of Southampton a special thank you goes to Hannah for being a constant support as we navigated the research experience in our host institutions.

I would like to thank my Dad who started me on this journey decades ago with his passion for Earth Sciences. Although there have been many twists and turns along the way I do believe that I am where I am meant to be because of him and his endless encouragement. My Mum has provided me with a space outside of academia to relax and unwind which I have come to appreciate more and more in the final years of my PhD and without which this thesis would not have been possible. Another big thank you should go to my grandparents who have provided endless support and encouragement.

And finally, thank you to James. This thesis would not have been possible without his constant laughter, love, and enthusiasm all of which have helped me to thrive during the final years of my PhD and even survive a global pandemic. I can't wait for my next adventure, whatever that may be, with him by my side.

Definitions and Abbreviations

Kyr ..... Thousands of years

Ma ..... Mega annum, Millions of years ago

Myr ..... Millions of years

EECO ..... Early Eocene Climatic Optimum

EOT ..... Eocene-Oligocene Transition

MECO ..... Middle Eocene Climatic Optimum

K-Pg ..... Cretaceous/Paleogene boundary

CCD ..... Carbonate compensation depth

CTD ..... Conductivity, Temperature and Depth

D ..... Effective Diversity

DIC ..... Dissolved inorganic carbon

Exp. ..... Expedition

Frag ..... Fragment

GLOW ..... GLObal Warming cruise

IODP ..... International Ocean Drilling Programme

ITCZ ..... Inter Tropical Convergence Zone

SL ..... Sensu lato subspecies of *G. ruber*

SLE ..... Sensu lato extreme of *G. ruber*

SS ..... Sensu stricto subspecies of *G. ruber*

SST ..... Sea surface temperature

H_S ..... Shannon's index

H_{GS} ..... Simpson's index

SR ..... Species Richness

$\delta^{18}O$ ..... Ratio of ^{16}O and ^{18}O

$\delta^{13}C$ ..... Ratio of ^{12}C and ^{13}C

Mg/Ca ..... Ratio of $^{24}Mg/^{43}Ca$

LA-ICP-MS ..... Laser ablation inductively coupled mass spectrometry

SEM ..... Scanning Electron Microscope

VPDB ..... Vienna Pee Dee Belemnite

AIC ..... Akaike Information Criterion

BIC ..... Bayesian Information Criterion

ANOVA ..... Analysis of variance

GAM ..... Generalized Additive Model

PCA ..... Principal Component Analysis

PC ..... Principal Component

β ..... Coefficient

s.e ..... Standard error

t ..... t statistic

p ..... *p*-value

GCV ..... Generalized Cross Validation

REML ..... Restricted maximum likelihood estimation

AIC_c ..... Akaike Information Criterion corrected for small sample size

edf ..... effective degrees of freedom

F ..... F-statistics

eta2[H] ..... Effect size

Chapter 1 Introduction

Humans are continuing to change Earth's climate (Eyring et al., 2021). The impacts of climate change are expected to persist and grow well into the future (Jackson and Overpeck, 2000; Pereira et al., 2010; Steffen et al., 2018). Climate change in turn is indirectly and directly affecting global biodiversity. Humans have negatively influenced biodiversity since the Quaternary when human populations expanded and contributed to the extinction of Quaternary megafauna (Barnosky, 2008). The current synergy of human induced climate change and anthropogenic activity, such as over exploitation and habitat loss (Diamond, 1984), mean biodiversity is now declining and is expected to increase in pace and magnitude into the coming centuries (Ceballos et al., 2015). Already 80 % of terrestrial land mass is influenced by human activity (Sanderson et al., 2002) and 44 % of plant and animal species have undergone local extinctions (Román-Palacios and Wiens, 2020) including terrestrial vertebrates (Dirzo et al., 2014; Ceballos, Ehrlich and Raven, 2020) and insects (Hallmann et al., 2017). Current rates of extinction are hypothesized to be 1000 times higher than expected background rates (Pimm et al., 2014) leading many researchers to believe we are entering the sixth mass extinction (Barnosky et al., 2011; Ceballos et al., 2015). Humanity is reliant on biodiversity and ecosystem services for sustainable living (Guo, Zhang and Li, 2010; Cardinale et al., 2012; Mace, Norris and Fitter, 2012), but how do we measure them most effectively?

Extinction is a tangible impact of anthropogenic change and can therefore dominate conservation efforts. Species richness has often, wrongfully, been used as the sole measure of diversity (e.g. Rockstrom et al., 2009). Diversity is complex and any measure should include measures of abundance, distribution, functional composition and interactions of species (Mace et al., 2014) all of which impact or can aid humanity. Abundance is the number of individuals within a taxonomical unit and is important as the balance between taxa can alter human access to resources. As an example, high abundances of locusts put millions of people at risk of famine (Dangles and Crespo Pérez, 2020). Understanding the spatial extent (distribution) of populations and its driving mechanisms is important for conservation efforts as well as ecological restoration with an aim to increase resource production. Functional composition is the distribution of traits that provide a function to an ecosystem. Understanding functional diversity is important as it can impact how communities respond to invasive species (Fried et al., 2019) and can inform our conservation efforts (Grenié et al., 2018). Finally, measuring and understanding how taxa interact with one another (species interactions) can aid our understanding of competition, which in turn can help conservation efforts such as informing our choices for reintroduction projects (Seddon, Armstrong and Maloney, 2007).

The focus of diversity should therefore not necessarily be on mitigating extinctions but rather understanding the drivers of diversity and the response of communities to these drivers in order to minimise future biodiversity loss (Montoya, Donohue and Pimm, 2017; Nadeau and Urban, 2019) and maintain a safe operating space for humanity (Rockstrom et al., 2009; Mace et al., 2014).

The resilient ability of ecosystems to persist is a key aspect of how feedbacks reinforce ecological stability of communities and thus the ecosystem services that those communities provide. To understand and predict the persistence of ecosystems on longer timescales we need to have baseline references and long-term perspectives both of which are benefits of using the fossil record. The fossil record can be used to understand on the long-term how communities respond to larger environmental perturbations which can act as a baseline reference to future anthropogenic change.

1.1 Controlling factors on diversity

Diversity is fundamentally a result of both macroevolution and microevolution. Macroevolution has many definitions (Hautmann, 2020), which in a broad sense can be defined as long-term evolution across and above the species level. The fossil record is therefore a record of macroevolutionary dynamics against a backdrop of a changing climate. In contrast microevolution is evolution within a population often occurring over a short period of time. Abiotic and biotic forcing influence both macroevolutionary and microevolutionary dynamics and therefore drive overall diversity.

Biotic factors are the foundation of the Red Queen hypothesis, which declares that evolution is primarily a result of biotic pressures such as competition (Stenseth and Smith, 1984; Van Valen, 1973). Conversely, the court jester model (Barnosky, 2001) hypothesises that diversity arises from unpredictable changes in the physical environment, or in other words, via abiotic forcing (Benton, 2009). Biotic drivers are commonly competition, predation, mutualisms, and symbiosis (Dunson and Travis, 1991; Lagomarsino et al., 2016) whilst abiotic factors are numerous including: temperature, salinity, water depth, and soil acidity (Dunson and Travis, 1991). Identifying whether biotic or abiotic drivers dominate diversity dynamic is fundamentally dependant on the scale of the observation (Benton, 2009; Ezard, Quental and Benton, 2016). On shorter timescales biotic factors tend to drive diversity whilst at time scales of more than 100,000 years abiotic factors have more visible impacts (Benton, 2009). The traditional belief is that abiotic factors drive

macroevolution (Barnosky, 2001; Benton, 2009), with biotic factors thought to be acting in the background rather than influentially.

Due to the scales needed to observe abiotic factors on longer timescales modern ecological experiments are limited, by their nature, to short time periods. Human longevity and funding mean most ecological experiments are limited to durations of less than one year with little replication (Estes et al., 2018). Whilst there are a few exceptions to this rule e.g., Park Grass (Silvertown et al., 2006) and Jena (Weisser et al., 2017), our empirical experimental evidence of modern ecological changes as a result of climate change are limited in time and scope. In addition to observational issues, our theoretical understanding of biodiversity is hindered due to the complexity of biodiversity and its responses to the climate change we are observing today.

1.2 Insights from the past.

Where modern ecological experiments falter, the natural experiments of the geological record can excel (Nogués-Bravo et al., 2018). The geological record has provided records of palaeoclimate that have refined climatic modelling and forecasts of future climate change (Eyring et al., 2021). Alongside a climatic record, the geology of the planet provides a discontinuous record of life against a backdrop of natural climate variation. Environmental disturbances occur on a variety of scales (Donohue et al., 2016), which are impossible to capture in short term modern ecological experiments but are preserved in the geological record (Jackson and Blois, 2015; Nogués-Bravo et al., 2018). Thus, the geological record allows us to investigate biotic responses to different magnitudes, paces, and durations of climatic fluctuations. Whilst the geological record cannot provide direct analogues to the future climate of Earth as we enter a climate space not experienced before (Jackson and Overpeck, 2000), it is heuristic (Fordham et al., 2020) and can provide a platform to investigate biotic responses to a wider variety of climate changes whilst accounting for evolution that a lot of biodiversity models, and therefore predictions, lack (Nadeau and Urban, 2019).

1.2.1 Abiotic and biotic drivers of macroevolution in the fossil record

Opposition to solely biotically driven macroevolution argues that competition alone cannot drive a species to complete extinction (Voje et al., 2015). Despite this there are examples of cases where extinctions have been caused in majority by competition. In spatially restricted environments such as lakes or islands this is predominantly caused by the artificial addition of a new species (Gill and Martinson, 1991; Kaufman, 1992). In less spatially restricted systems, the migration of new species can force ecologically similar taxa into a smaller space reducing the functionality of an ecosystem and increasing resource competition resulting in the long-term

reduction in speciation probability and increased extinction risk (Silvestro et al., 2015). Thus, the synergetic effect of biotic interactions has the potential to impact speciation and extinction on an observable and meaningful scale.

Macroevolution driven by abiotic drivers such as climate, volcanism and impact events have ample support due to paleontological evidence. This is a result of the strong signal that abiotic processes leave within the geological record (Ezard, Quental and Benton, 2016). Microfossil analysis has found that planktic foraminifera show a correlation between species richness and abiotic forcings (Fenton et al., 2016b) as well as a relationship between sea surface temperature and test size evolution (Schmidt, 2004). In marine megafauna, the extirpation of 36% of Pliocene genera has been attributed to the synergetic effects of neritic area reduction (27% mean area decrease), changes to ocean productivity and ocean circulation (Pimiento et al., 2017).

The above studies are just a few that focus on the drivers of macroevolution, yet these studies and others often treat abiotic and biotic forcings independently. This is somewhat simplistic and is a false dichotomy, with many studies now demonstrating that it is the interplay of biotic and abiotic drivers that control diversity dynamics (Ezard, Quental and Benton, 2016; Solórzano et al., 2019). An example of this interplay is the correlation of temperature and insect herbivory through all climatic perturbations through the late Paleocene and early Eocene in Bighorn Basin (Currano et al., 2017). This is hypothesized to be the result of temperature increases increasing insect metabolic rate and therefore increasing nutritional requirement (Currano et al., 2017). Additionally, temperature caused the northward migration of thermophilic insects, shown by specialized herbivory, increasing the number of insects in the area and thus strengthening biotic competition pressure.

1.2.2 The importance of measuring differences among individuals

When measuring macroevolutionary dynamics the focus tends to be on long-term population dynamics and how species and/or communities respond to stochastic environmental perturbations. Such research assumes that conspecific individual differences are either unimportant or not large enough to be ecologically important (Bolnick et al., 2003, 2011) and that responses to environmental perturbations will be independent of individual variability. This assumption has led to the omnipresent use of a mean-based approach in ecology (Violle et al., 2012) and a focus on measuring traits that are more variable between rather than within species (McGill et al., 2006).

Despite being considered inconsequential, individual variability invokes idiosyncratic responses of both species and individuals (Violle et al., 2012; Urban et al., 2016) to abiotic and biotic interactions as the basis of such interactions is at the level of the individual (Violle et al., 2012;

Kling et al., 2020). Quantitative research has shown that these individual differences are important for ecosystem processes (Crutsinger, 2006), coexistence and thus, species diversity (Imura, Toquenaga and Fujii, 2003; Lankau and Strauss, 2007; Agashe, 2009; Hart, Schreiber and Levine, 2016) and persistence in stochastic environments (Agashe, 2009; Godhe and Rynearson, 2017; Luxem, Ellwood and Strzepek, 2017; Henn et al., 2018).

Individuality can occur through trait plasticity such that the expression of a trait is dependent on the experience of that individual within a population or through genetics where genetic expression of a trait is different for each individual. The former permits an individual and thus community response and can aid persistence through climatic shifts such as those experienced by communities in sensitive environments such alpine plants (Henn et al., 2018) and albatrosses (Nevoux et al., 2010). Fixed or non-plastic trait variability between individuals allows large populations to increase their survival probability in fluctuating abiotic and biotic conditions by bet-hedging such as that shown in Antarctic phytoplankton clones (Luxem, Ellwood and Strzepek, 2017).

Therefore, a mean-based approach may overgeneralise community responses to climatic perturbations and thus oversimplify our responses and conservation efforts to anthropogenic climate change. However, a mean-based approach is still applied to both theoretical and empirical studies as measuring and modelling individual variability is difficult (Bolnick et al., 2003) and time consuming. An additional problem with measuring individual variability is that the sample size needed to measure individual variability is more difficult to predict (Araújo, Bolnick and Layman, 2011).

One way to circumnavigate the time-consuming nature of trait collection is to focus on measuring traits that are functionally important. Functional traits define the role of an organism in an ecosystem (Ezard and Purvis, 2016; Jax, 2005) at an individual level (Violle et al., 2007, 2012) and vary through time and space (Akçakaya et al., 2020). As functional traits capture how an organism interacts with the environment (Lacourse, 2009; Oksanen et al., 2019) they dictate an organism's fate during environmental perturbations (McGuire and Lauer, 2020). Functional traits in modern ecosystems can be identified through direct observations and identifying traits that are relevant to an organism's function (Boyé *et al.*, 2019; Brun, Payne and Kiørboe, 2017; Jax, 2005; Litchman and Klausmeier, 2008; Mace et al., 2014; Stuart-Smith *et al.*, 2013).

To solve the problem of unknown sample numbers and to promote research on individual variability, studies need to focus on systems that have large numbers of individuals that are easily measured on large temporal and spatial scales. These requirements mean the microfossil record is ideal to investigate individual based responses to abiotic and biotic drivers and macroevolutionary dynamics (Nogués-Bravo et al., 2018). However, the fossil record is often left

at the mercy of time and preservation (Jackson and Blois, 2015) which ultimately reduces individual numbers at narrow time slices which are needed for individual based analysis. The fossil record of planktonic foraminifera circumvents the common problems encountered by palaeoecologists as outlined by Jackson and Blois (2015) and therefore make an ideal study organism for diversity-based studies.

1.3 Planktonic foraminifera

In my thesis I use planktonic foraminifera to investigate both macro and microevolutionary dynamics against a backdrop of changing climate. Planktonic foraminifera are free-floating, single celled marine protists that are present in all modern ocean basins and are currently represented by ~ 50 species (Kucera, 2007). Foraminifera life span ranges from a few days to several weeks. Individuals grow by adding sequential chambers of calcite, which, upon death, sink to the ocean floor depositing their calcite tests (shell) (Hemleben, Spindler and Anderson, 1989). Evolving from benthic foraminifera (Darling et al., 2009), planktonic foraminifera have a high spatial and temporal record extending from the Jurassic period ~ 200 million years ago to the present day (Fraass, Kelly and Peters, 2015). In addition to excellent resolution across time and space, planktonic foraminifera exist in large populations producing ~ 2 Gt of calcite (Schiebel and Hemleben, 2008). Despite only ~ 1-2 % of this calcite reaching the sea floor (Schiebel and Hemleben, 2008), planktonic foraminifera have an enviable species level record with ~ 450 identified fossil species (Schiebel and Hemleben, 2008) which have at least an 81 % chance of detection in the Cenozoic Era (Ezard et al., 2011). Overall, this makes their fossil record equivalent or better than that of the best-preserved macroinvertebrate genus record (Ezard et al., 2011) with a fully revised morphological phylogeny for the Cenozoic Era (Aze et al., 2011).

1.3.1 Macroevolutionary patterns

As a ubiquitous part of marine life since the Jurassic period, the macroevolutionary record of planktonic foraminifera spans major events in Earth's history including extra-terrestrial impacts and tectonic reconfigurations as well as major and minor climatic fluctuations (Fraass, Kelly and Peters, 2015). As a result, the macroevolutionary patterns in the planktonic foraminifera record are understandably tied to such abiotic events (Schiebel and Hemleben, 2008). Though, such abiotic factors have been found to primarily drive extinction events with speciation driven predominantly by biotic forcings (Ezard et al., 2011).

Planktonic foraminifera emerged from benthic taxa in the Jurassic (Darling et al., 1997; Hart et al., 2003; Darling et al., 2009). A major evolutionary event of planktonic foraminifera occurred at the Cretaceous/Paleogene boundary (K-Pg) coincident with the Chicxulub asteroid impact event

(Schulte et al., 2010). At this event all but two macroperforate genera became extinct leaving an ocean devoid of the morphological and taxonomic complexity observed prior to the extinction (Lowery and Fraass, 2019). Following the K-Pg event, vacant ecological niches allowed for rapid initial diversification, but morphological diversity remained low (due to fewer available successful life strategies) only gradually increasing until the Middle Eocene when pre-K-Pg diversity was reached (Fraass, Kelly and Peters, 2015; Lowery and Fraass, 2019).

During the Eocene the modern relationship observed between planktonic foraminifera diversity and abiotic drivers broadened, leading to the development of the modern-day latitudinal diversity gradient (Fenton et al., 2016b). This macroevolutionary relationship with the environment is apparent in the large diversity decline from increased extinction rates and reduced origination rates on the approach to the Eocene-Oligocene transition (Ezard et al., 2011; Aze et al., 2011; Fraass, Kelly and Peters, 2015) coincident with Antarctic glaciation (Zachos et al., 2001; Westerhold et al., 2020). In the late Oligocene, origination rates increased, and extinction rates decreased driven by thermal differentiation in the oceans promoting diversification up until the middle Miocene (Wei and Kennett, 1986; Fraass, Kelly and Peters, 2015). Late Miocene diversity stagnation was followed by long term diversity decline in the Pliocene and Quaternary, which culminated in modern planktonic foraminifera communities. During this decline species richness and overall diversity declined due to both long term palaeoceanographic fluctuations alongside glacial-interglacial transitions (Berggren, 1969; Wei and Kennett, 1986).

1.3.2 Macroecological patterns

As well as temporal variability, planktonic foraminifera vary spatially with these patterns driven by environmental parameters. Temperature has regularly been thought of as the primary factor driving spatial variability explaining 90 % of geographical patterns of modern planktonic foraminifera in the Atlantic Ocean (Rutherford, D'Hondt and Prell, 1999). However, temporal models have shown that it is a combination of environmental parameters and not solely temperature that drives global planktonic foraminifera of spatial patterns (Fenton et al., 2016a).

Latitudinal thermal patterns lead to different thermal vertical gradients in the oceans with little to no thermocline in high latitudes and highly stratified waters in the tropics, which in turn changes the number of available niches (Rutherford, D'Hondt and Prell, 1999; Al-Sabouni, Kucera and Schmidt, 2007). In the tropics and subtropics, the water column is stratified with a strong thermocline creating multiple vertical niches for planktonic foraminifera to diversify into. In contrast, at high latitudes vertical niche partitioning is reduced due to a weakly stratified water column. This relationship between latitude and vertical niches results in the latitudinal diversity

gradient observed in modern oceans (Yasuhara et al., 2020), which formed in the Eocene as global temperature cooled and latitudinal thermal differences developed (Fenton et al., 2016b).

Latitudinal patterns also exist in the morphological distribution patterns of planktonic foraminifera with larger foraminifera found in the tropics (Schmidt, Thierstein and Bollmann, 2004). Fundamentally test size is controlled by biological processes such as metabolism, growth rate and resistance to starvation and predation (Schmidt, 2004; Rillo et al., 2020), which in turn are controlled by environmental factors primarily temperature (Schmidt, 2004; Burke et al., 2018). As in diversity, vertical temperature gradients correspond to size variability with stratified waters in tropical regions promoting specialization and larger foraminifera (Al-Sabouni, Kucera and Schmidt, 2007).

The relationship between size and temperature is not clear cut, however. The effect of temperature varies between species (Rillo et al., 2020). This interspecific relationship between abiotic forcing and size means inferences on overall size patterns are complex. During times of high diversity such as the Eocene test size is driven by temperature with an observable strong size - $\delta^{18}O$ value relationship, yet this relationship breaks down when diversity is reduced (Schmidt, Thierstein and Bollmann, 2004). Furthermore, analysis of nine species showed that only ~ 22 % species exhibited a statistically detectable positive correlation between temperature and size (Rillo et al., 2020).

1.3.3 Planktonic foraminifera ecology and its proxies

The microscopic nature of planktonic foraminifera mean they are nearly impossible to observe in-situ in natural populations. Consequently, our understanding of their ecology is based on plankton tows, culturing, accumulation rates and geochemical proxies. We know that foraminifera have various feeding strategies which vary between species ranging from a mixotrophic strategy through the harbouring of symbionts to omnivory feeding on marine snow and copepods (Hemleben, Spindler and Anderson, 1989). Additionally, we know that planktonic foraminifera live at different depths through the upper water column, which is reflected in the geochemistry of their tests (Emiliani, 1954a; Fairbanks, Wiebe and Bé, 1980; Fairbanks et al., 1982).

1.3.3.1 Feeding

Symbiotic foraminifera are restricted to the very upper water column and can either show obligate or facultative symbiont relationships (Hemleben, Spindler and Anderson, 1989). An obligate relationship allows some species of planktonic foraminifera to have a mixotrophic feeding strategy aiding its survival in oligotrophic waters. Contrastingly, facultative foraminifera

species are not reliant on the symbiotic relationship and as a result not all individuals within a species host symbiont.

Symbiosis in modern planktonic foraminifera can be identified through active chlorophyll fluorescence (Takagi et al., 2019). In the fossil record photosymbiotic foraminifera can be identified based on the relationship between stable carbon isotopes ($\delta^{13}C$) and test size (Spero, 1987; Spero and Deniro, 1987; Spero and Lea, 1993; Norris, 1996). Hosting symbionts alters the microenvironment of the foraminifer, thus changing the geochemistry of the test that precipitates from that environment. As symbionts preferentially uptake isotopically light carbon (^{12}C) the foraminifer's microenvironment is enriched in heavy carbon (^{13}C) which is then incorporated into the calcifying test. As planktonic foraminifera grow, they either host more symbionts or increase their symbiotic activity thus increasing the $\delta^{13}C$ values of their tests with increases in size (Spero and Deniro, 1987).

1.3.3.2 Depth habitat

In addition to feeding strategy, planktonic foraminifera ecology can be identified based on depth niche occupation using stable isotopes. Oxygen isotopes signals of foraminifera tests are determined by temperature dependant oxygen isotopic fractionation of seawater into foraminifera calcite resulting in $\delta^{18}O$ values increasing with depth as temperatures decrease (Fairbanks, Wiebe and Bé, 1980; Fairbanks et al., 1982). In contract, $\delta^{13}C$ values decrease as a function of depth due to the preferential uptake of isotopically light ^{12}C by symbionts and the remineralization of organic matter at depth releasing the light carbon back into the dissolved inorganic carbon (DIC) pool. Thus, surface dwelling planktonic foraminifera have low $\delta^{18}O$ values and high $\delta^{13}C$ values in comparison to those that live in the thermocline and subthermocline.

The relationship between depth habitat and $\delta^{18}O$ values are frequently used to make broad palaeoceanographic and palaeoclimatic observations (e.g., Edgar et al., 2013; Galazzo et al., 2014; Jehle et al., 2019; Metcalfe, Feldmeijer and Ganssen, 2019). Nonetheless, this relationship is complicated by the need to quantify $\delta^{18}O$ values of seawater and the impacts of seawater carbonate concentration (Spero et al., 1997; Bijma, Spero and Lea, 1999a; Pearson, 2012) as well as biological disequilibrium effects or "vital effects" (Epstein et al., 1951; Urey et al., 1951; Erez, 1978; Spero and Williams, 1989; Spero, Lerche and Williams, 1991; Weiner, 2005; Si and Aubry, 2018).

To mediate these effects, other geochemical proxies such as Mg/Ca values have been used to generate alternative temperature records based on planktonic foraminifera depth habitat. Mg/Ca thermometry is based on the observation that the incorporation of Mg^{2+} is controlled by temperature increasing as temperature increases (Barker et al., 2005), thus planktonic

foraminifera living in the upper water column have high Mg/Ca values compared to those living in the thermocline. This proxy has been applied to many areas such as studying glacial-interglacial cycles (Schmitt et al., 2019), seasonality (Steinke et al., 2010; Wit et al., 2010), sea-level changes (Lea et al., 2002) and even deep time surface ocean temperatures (Creech et al., 2010; Evans and Mller, 2012).

The Mg/Ca proxy is not free from issues, however. One of the main issues is that continued analysis and application of fine scale analytical methods such as Laser Ablation Inductively Coupled Plasma Mass Spectrometry (LA-ICP-MS) have revealed genetic (Blackmon and Todd, 1959; Bentov and Erez, 2006) and ecological controls on Mg incorporation (Eggins, Sadekov and De Deckker, 2004; Sadekov, Eggins and Deckker, 2005; Sadekov et al., 2008; Fehrenbacher et al., 2017; Holland et al., 2020). However, this proxy (Mg/Ca) has also revealed key aspects of planktonic foraminiferal ecology such as diurnal (Fehrenbacher et al., 2017) and ontogenetic migration (Anand and Elderfield, 2005; Bolton et al., 2011; Dueñas-Bohórquez et al., 2011). The key into using these proxies is detailed integration of geochemical and ecological knowledge.

In Chapter 4 I use LA-ICP-MS derived Mg/Ca values of surface dwelling extant planktonic foraminifera *Globigerinoides ruber* to investigate subspecies variability and its impact on palaeoceanographic reconstructions.

1.3.3.3 Morphology and morphological classification

Planktonic foraminifera show a wide degree of morphological variation driven by evolutionary history and ecology (Hsiang, Elder and Hull, 2016). Splitting planktonic foraminifera by morphological characteristics can be done at the coarsest level by looking at wall textures and primarily the size of perforations on the test walls. Macroperforate foraminifera have “large” perforations of > 4 µm; this clade dominates planktonic foraminifera research due to their resolved taxonomy and phylogeny (Aze et al., 2011). Microperforate foraminifera, in comparison to macroperforate, possess microperforations of < 1 µm and often have a seemingly smooth wall texture. Owing to their small size, microperforate taxa are not commonly studied and their phylogeny has yet been resolved despite research showing that microperforate taxa may provide insights into the origination of planktonic foraminifera (Darling et al., 2009) and could provide paleoenvironmental insights (Liu and Olsson, 1992; Hernitz Kucenjak, 2014; Luciani et al., 2020). Medioperforate forms have pore sizes between 1 – 4 µm (Li Qianyu and Radford, 1991) and include muricate forms such as *Acarinina spp.* and *Morozovelloides spp.* that are often grouped within macroperforate taxa (i.e., Aze et al., 2011).

Following classification based on perforation size, planktonic foraminifera are divided based on the presence/absence of spines and gross morphology which varies from simple, common, near

spherical forms such as in *Orbulinoides spp.* to highly complex, rare, shapes such as digitate forms (e.g., *Hantkinena spp.*). Further splitting to the species' level is then based on finer scale morphological traits such as supplementary apertures, pore size, sutural position, and chamber size differing inter- and intra-specifically. Whilst these fine scale morphological traits can be used for species identification, as I show in Chapter 4, caution should be taken when doing so as advances in genetic analysis have shown that cryptic variation is commonplace in planktonic foraminifera (de Vargas et al., 1999; Darling and Wade, 2008; Aurahs et al., 2011). Whilst the morphological based species concept sometimes doesn't correspond to genetics in planktonic foraminifera (Aurahs et al., 2011), gross morphology is consistent within genera indicating morphology does reflect a broader metric of evolutionary relatedness (Jablonski and Finarelli, 2009; Morard et al., 2019).

1.4 The importance of measuring the correct variables

Macroevolutionary and macroecological studies have progressed greatly in the past few decades (Beck et al., 2012). Increased emphasis on data collation has built large publicly available databases of contemporary (GBIF (gbif.org)) and palaeontological (e.g. PBDB (paleobiodb.org); Neotoma (Williams et al., 2018) and Triton (Fenton et al., 2021)) species occurrence data, as well as global trait databases (e.g. TRY (Kattge et al. 2020); LEDA (Kleyer et al. 2008) and BIEN (Enquist et al. 2016)). In addition, work is being done to collate previously collected trait data into useable frame works (e.g., Brun, Payne and Kiørboe, 2017; McLean *et al.*, 2019) and to generate new datasets (e.g., Stuart-Smith *et al.*, 2013). This wealth of data means that we can now do more analyses than ever before. But to be useful we need these analyses to be as a biologically meaningful as possible.

One way to analyse data in a more biologically meaningful way is to identify trait-environment relationships also known as ecometrics (Eronen et al., 2010). Ecometrics allow the same interactions between organisms and environment to be measured and compared across spatial and temporal scales in a taxon-free way that links the past and present (Eronen et al., 2010). For ecometrics to work a trait-environment relationship needs to be identified through direct observations or identifying correlations based on underlying mechanical function. Examples of widely applied ecometrics based on observations are the relationship of gross leaf (Bailey and Sinnott, 1915; Greenwood et al., 2004; Peppe et al., 2011) and tooth (Liu et al., 2012; Fortelius et al., 2016; Oksanen et al., 2019) morphology to climate and body size to temperature (Hunt and Roy, 2006; L. Trip *et al.*, 2014; Audzijonyte *et al.*, 2020).

In my thesis I generate records of traits and test whether they are linked to climatic variability. In Chapter 2, I generate a record of planktonic foraminifera classified by morphological and

ecological traits across the Middle Eocene in the North Atlantic. Applying a new methodology to deep time (Hill numbers), I investigate millennial scale community dynamics in response to the environmental fluctuations. In Chapter 3, I build on this work to investigate how individuals within a population respond to the Middle Eocene Climatic Optimum. In addition, using individually resolved geochemical and morphological methods I investigate whether commonly cited trait-environment relationships in extant planktonic foraminifera persist in deep time. In Chapter 4, I then investigate whether traits within individuals are consistent geochemically and morphologically within a commonly used planktonic foraminifera and discuss the implications for both palaeoceanographic and palaeoecological studies.

1.4.1 Taxonomic scale

Planktonic foraminifera have an enviable resolution for macroevolutionary, microevolutionary and ecological based studies, but a high resolution also provides opportunities regarding the best level to analyse these organisms at, and how consistent common approximations are when inferring whether species trends are consistent at higher (genus) and lower (subspecies) levels. Whilst species level is the most used taxonomic level, cryptic diversity can make the species level analysis unreliable, as I show in Chapter 4. In addition, species level taxonomy requires specialists and well-preserved samples which decreases in probability the older the specimens are. In Chapter 2 and 3, I show how genera-based studies can circumvent preservation and specialist issues which in turn allows broad ecological interpretation of data. In addition to taxonomic classification in Chapter 2, I also use trait-based classification grouping foraminifera into morphogroups and ecogroups based on morphological and geochemical traits (Aze et al., 2011) informing our understanding of morphological and ecological responses to transient warming events. Ultimately, all taxonomic classifications are subject to decisions around the chosen scale of analysis. My thesis contributes to the debate as to the utility of the species in showing that there are occasions when more resolved (subspecies) and less resolve (genera) analyses are analytically sufficient depending on the research question and environmental setting.

1.4.2 Diversity: Hill numbers

Biodiversity is commonly expressed at either a local, discrete scale (α-diversity), between different habitats or time samples (β-diversity) and at more encompassing scales (γ-diversity) (Colwell, 2009; Lamanna et al., 2014). Although β-diversity allows us to measure community responses to long-timescale abiotic forcings, deciding how to measure this element of diversity is contentious (Ellison, 2010). In Chapter 2, I will assess diversity responses to the MECO using Hill numbers. Hill numbers are a long-standing method recently revisited as being the best way to

measure β-diversity (Jost, 2007; Ellison, 2010), but which has not yet been tested in deep time environments and on the temporal averaging of samples.

Common diversity measures such as species richness (SR), Shannon's index (H_S) and Simpson's evenness (H_{GS}) are singular measures of diversity used in isolation of each other. This isolation is despite being based upon the same fundamental measure (species occurrence) and forming part of a diversity continuum. Hill numbers combines these dimensions of diversity by presenting a continuum of diversity from SR to H_{GS} in one image. In addition, using different data Hill numbers can also incorporate many aspects of diversity such as phylogenetic (Chao, Chiu and Jost, 2010), functional (Chiu and Chao, 2014) and taxonomic diversity.

1.4.3 Functional Traits

Ecometrics requires the identification of trait-environment relationships. In deep time systems, where direct observational studies are impossible, their use necessitates the identification of correlations between the organism and environment (Eronen et al., 2010). This can be done at the level of the individual in planktonic foraminifera through the identification of functional traits. Using ecogeochemical proxies, we can infer depth habitat (Pearson, 2012) and photosymbiotic activity (Spero and Deniro, 1987; Eggins, Sadekov and De Deckker, 2004; Edgar et al., 2013), which can be combined with morphological and climatic measurements to identify organismal ecology and function. From this approach we know, for example, that spine functionality is related to feeding (Hemleben et al., 1991) and pore size probably corresponds to gas exchange gas exchange (Bé, 1968; Baumfalk et al., 1987; Burke et al., 2018). However, gross morphological traits such as test size and shape are highly variable with unidentified function despite being easily and ubiquitously measured.

In Chapter 3, I investigate whether size exhibits any suggestions of functionality in thermocline dwelling genera against a backdrop of climatic perturbations during the Middle Eocene on millennial time scales in deep time. In Chapter 4, I then investigate the relationship between size and geochemical measures to the link between geochemistry and morphology within a species complex that is the workhorse of much of palaeoceanography and palaeoclimatology.

1.5 Research objectives and questions

1.5.1 Chapter 2

I. How did planktonic foraminifera diversity respond to transient warming during the Middle Eocene Climatic Optimum (MECO) in the mid-latitude North Atlantic?

II. How does analytical choice of size fraction impact inferences of diversity change across climatic perturbations?

1.5.2 Chapter 3

I. How consistent are hypothesized functional traits in planktonic foraminifera across the Middle Eocene Climatic Optimum?
II. How did the planktonic foraminifera genus *Subbotina* rise to dominance through the middle Eocene despite substantial thermal changes in its depth habitat?
III. How did the thermal and trophic structure of the upper water column respond to palaeoceanographic changes in Northwest Atlantic during the Middle Eocene?

1.5.3 Chapter 4

I. Does intraspecific variability in *Globigerinoides ruber* match the definition of genetically inferred subspecies?
II. What are the impacts of intraspecific and intra-chamber size variation on Mg/Ca values in *Globigerinoides ruber?*

Chapter 2 Small but mighty: how overlooked smallest species maintain community structure through Middle Eocene climate change

2.1 Abstract

Understanding current and future biodiversity responses to a changing climate is pivotal as anthropogenic climate change continues. To aid our understanding more data and robust analytical methods are required. Understanding biodiversity responses is complicated though by the multitude of available metrics to quantify dynamics, and through the sampling protocols we apply. Here, we use the data-rich fossil record to calculate effective diversity (=Hill numbers) for the first time on Paleogene planktonic foraminifer using 22,830 individual tests, in two different test size fractions, across seven million years featuring the transient warming interval of the Middle Eocene Climatic Optimum (MECO) ~40 million years ago (Ma) at study sites in the mid-latitude North Atlantic. Using generalized additive models (GAMs), we investigate the driving factors of planktonic foraminiferal responses to climatic fluctuations. Morphological and generic diversity decreased following the MECO, but palaeoceanographic changes did not alter planktonic foraminiferal depth habitat occupation through this period. After correcting for any effects of fossil fragmentation, we show divergent trajectories between the typical size-selected community and a more holistic selection including more smaller species. The larger assemblages show more rapid biodiversity declines than smaller ones, raising fundamental questions about how communities respond to climate excursions and which species are likely to dominate the environments of the future.

2.2 Introduction

Biodiversity is multifaceted; so how should it be summarised succinctly? The ubiquitous starting point is to generate records of taxa abundance resulting in records of richness. Species are regarded as the most intuitive unit of biology and the fundamental measure of diversity by many researchers (e.g., Colwell et al. 1994; Purvis and Hector 2000; Mace et al. 2012; Hohenegger 2014), making species the most common currency for diversity studies. Biologically, species are ideal as they have independent evolutionary trajectories and histories (Purvis and Hector, 2000). Furthermore, the idea of a species is understandable to both researchers and the general public

(Purvis and Hector, 2000; Baum, 2009; Chiarucci, Bacaro and Scheiner, 2011; Reydon, 2019) aiding conservation and public engagement efforts. From a palaeobiological perspective, species are fundamental for defining biostratigraphic ages of sediments and understanding evolution (Hohenegger, 2014). However, determining "true" species richness requires a "perfect" sample. In modern systems, approximately 300 species are discovered or described every day (Purvis and Hector, 2000), making a perfect sample impossible to achieve, particularly in palaeoecological samples that are at the mercy of time and preservation (Jackson and Blois, 2015). Thus, the goal is to find a sufficient way of representing an assemblage.

Measuring only common taxa in any sample or environment may be most informative as common taxa are more abundant and therefore the most detectable and influential components of ecosystems (Lennon et al., 2004; Gaston, 2008; Hannisdal et al., 2017). Thus, it is hypothesized that common taxa contribute more to assemblage richness than rare taxa (Lennon et al., 2004; Gaston, 2008). Furthermore, for a taxon to become common there is a complex interplay of traits and environmental influences, as well as historical and spatial dynamics (Gaston, 2008), meaning common taxa can potentially inform our understanding of diversity drivers. Yet, to be common is in itself rare. Very few species are common (Gaston and Fuller, 2007; Gaston, 2008; Hannisdal et al., 2017), so by only measuring common species a large proportion of information is discarded. Fluctuating abundances in rare species may be more ecologically informative, potentially acting as "canaries" providing early warning signals for ecosystem collapse (Doncaster et al., 2016), insights into palaeoceanographic change (Ishino and Suto, 2020) and a focus for conservation efforts (Gaston, 2008). However, taxa vary spatially, influencing diversity patterns at any single location in time and space (Patzkowsky and Holland, 2007). Consequently, what is rare in one sample or area may be common in another (Colwell, 2009). Perhaps it is not what is rare that is important but instead what is absent from a sample, or so called "Dark Diversity" (Pärtel, Szava-Kovats and Zobel, 2011). On a theoretical level, far less is known about the role of rare species in their ecosystem (Lyons et al., 2005), meaning they are easier to dismiss as unimportant components of an ecosystem and therefore are often ignored (Chao et al., 2014).

To be common, rare or absent, is a relative measure (Preston, 1948), and relative abundance requires the counting of everything to make such conclusions. Biodiversity is complex and exists on a continuum in multiple dimensions that consequently cannot be comprehensively summarised by a singular number (Purvis and Hector, 2000; Colwell, 2009a; Reich et al., 2012). Presenting diversity in integrated ways is an ideal solution (Ellison, 2010). Such methods exist: effective numbers, or Hill numbers (Hill, 1973), integrate richness, evenness and dominance in one encompassing image (Figure 2.1). A drawback of effective numbers is the need for large amounts of individuals, meaning their applications are limited to abundant taxa. To this end, effective numbers have been applied to a range of modern-day taxa including tropical ants (Chao

et al., 2014), spiders (Chao et al., 2014) and bacteria (Kang et al., 2016). Palaeoecological applications have been focused on the Quaternary investigating the link between climate and diversity in deep ocean ostracods (Yasuhara et al., 2008, 2016), nematodes (Yasuhara et al., 2016) as well as pelagic planktonic foraminifera (Yasuhara et al., 2020).

Conceptually, Hill numbers are the effective number of equally abundant taxa required to give the same diversity presented in the sample (Hill, 1973; Jost, 2010a; Chao et al., 2014). Whilst Hill numbers, like traditional indices such as Shannon's index (H_S) and Simpson's index (H_{GS}), can be presented as single numbers, they normally present diversity (D; Figure 2.1) as a function of q, which determines how rare taxa are weighted in relation to abundant taxa (Figure 2.1). Therefore, the best representation of Hill numbers is as a function of *q*. In uneven assemblages, this line is a non-linear curve (Figure 2.1) that links the three traditional indices in one image. In addition to being an integrative measure of diversity, Hill numbers also obey the replication principle (Hill, 1973). The replication principle is the requirement that when two equal assemblages with no shared taxa and equivalent relative abundances are combined the diversity of the pooled assemblage is doubled (Hill, 1973; Chiu and Chao, 2014). This fundamental principle is not obeyed in entropy measures such as Shannon's index. The replicable nature of Hill numbers makes them suitable for detecting diversity changes as a result of environmental perturbations whether they be anthropogenic such as oil spills (Heritier-Robbins et al., 2021; McClain, Nunnally and Benfield, 2019; Miller et al., 2020) or, as in the present study, geologically transient climatic events. The commonality of units at all levels of *q* means that inferences can be made regarding magnitudes of change (Jost, 2007, 2010a; Chao et al., 2014), sample and locality differences (Hill, 1973; Chao, Chiu and Jost, 2014), as well as enabling the transformation to commonly used general entropy metrics such as Shannon's index and Simpson's index. In addition, Hill numbers can be applied to other aspects of diversity such as phylogenetic (Chao, Chiu and Jost, 2010), functional (Chiu and Chao, 2014) and taxonomic (Chao, Chiu and Jost, 2014) diversity.

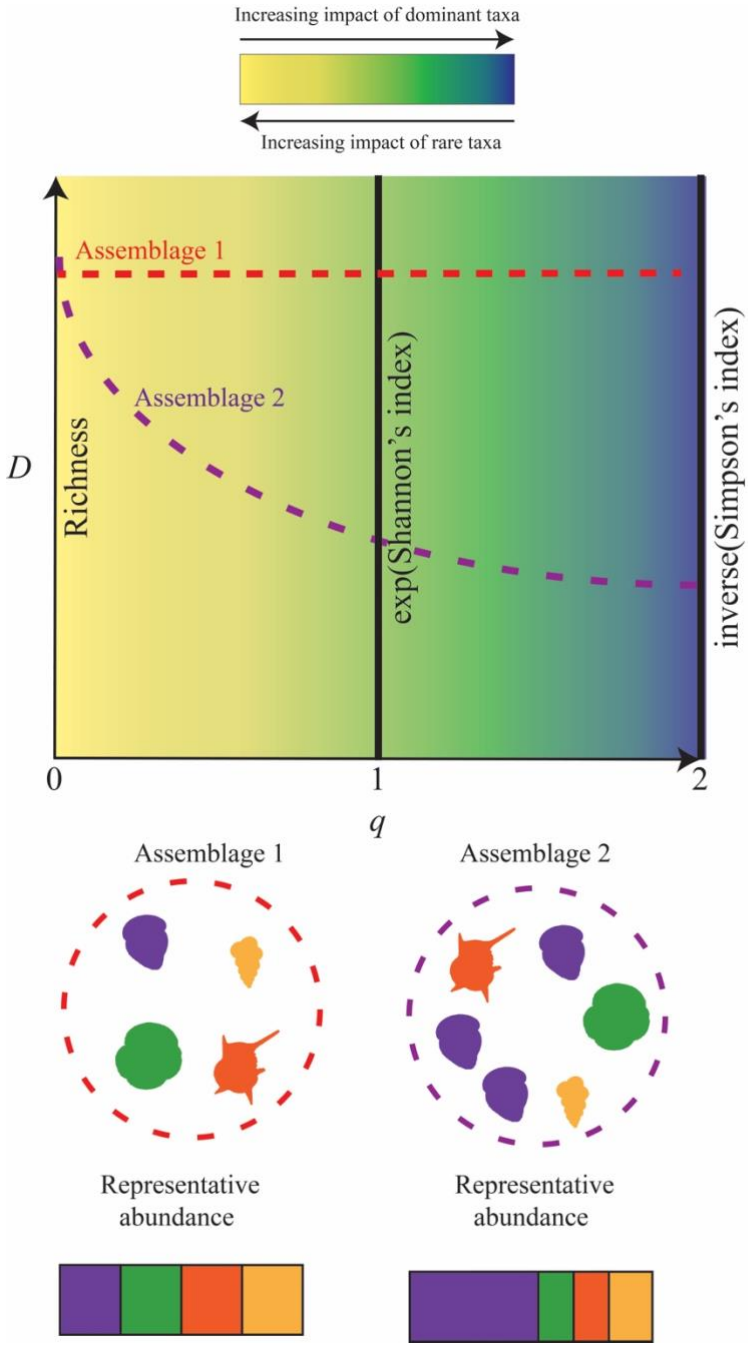

Figure 2.1 Schematic representation of Hill numbers and how q is related to D. The gradient of colour represents the weight given to abundance with more weight given as you move to the right. Simplified relationship between diversity line shape and the underlying assemblage. Each line is generated from an assemblage containing 4 taxa. Assemblage 1 is represented equally within the assemblage, so the resulting diversity line is horizontal. The y-intercept is the same for both assemblages as they have the same number of unique taxa (4), but assemblage 2 has a steep gradient as the purple taxon is more abundant than green, red, or orange. The silhouettes represent typical planktonic foraminifera of our study interval.

To be meaningful, however, Hill number calculations require sufficient and careful sampling protocols. Here, for the first time, we calculate Hill numbers for a deep time community outlining best practices for sample analysis by tracking planktonic foraminifera diversity changes across the Middle Eocene Climatic Optimum (MECO), ~ 40 Myrs ago (Bohaty and Zachos, 2003; Bohaty et al., 2009; Rivero-Cuesta et al., 2019; Edgar et al., 2020). The requirement for large numbers of individuals means fossilised planktonic foraminifera are an ideal candidate for Hill numbers (Yasuhara et al. (2020). In the modern oceans, planktonic foraminifera are represented by ~ 50 species (Kucera, 2007; Schiebel and Hemleben, 2017), which upon death are deposited on the sea floor in vast quantities. Accumulation of planktonic foraminifera has occurred near continuously since their evolution ~ 200 Ma in the Jurassic period (Fraass, Kelly and Peters, 2015), and foraminifera-rich sediments have been recovered around the globe by the coring efforts of the International Ocean Discovery Program (IODP) and its predecessors. Since planktonic foraminifera diversity shows a strong affinity to climatic fluctuations (Ezard et al., 2011; Fraass, Kelly and Peters, 2015; Fenton et al., 2016b) with a highly temporal and spatially resolved record (Fenton et al., 2021), this is an ideal study system to investigate ecosystem responses to transient and rapid climatic perturbations. In turn, Hill numbers represent an ideal tool to extract biologically meaningful signals.

Here we apply Hill numbers to understand planktonic foraminifera community response through the MECO. The middle-to-late Eocene encapsulates the long-term cooling from the Eocene "Hothouse" of the Early Eocene Climatic Optimum (EECO, 53 - 48 Ma; (Westerhold et al. 2018, 2020)) through to the "Icehouse" of the Oligocene that started at the Eocene-Oligocene Transition (EOT, 34 Ma; (Westerhold et al., 2020; Hutchinson et al., 2021)) with the establishment of permanent Antarctic glaciation (Zachos, Quinn and Salamy, 1996; Coxall et al., 2005). The cooling trend in global temperature through this interval was interrupted by a transient (~ 270 – 500 Kyr) warming event between ~ 40.6 and 40 Ma known as the MECO (Bohaty and Zachos, 2003; Bohaty et al., 2009; Rivero-Cuesta et al., 2019; Edgar et al., 2020). During the MECO there was a ~3 - 6 °C rise in surface and deep-water temperatures (Bohaty and Zachos, 2003; Bohaty et al., 2009; Bijl et al., 2010; Galazzo et al., 2014; Cramwinckel et al., 2019; Henehan et al., 2020), reduced surface ocean pH (Henehan et al., 2020), and a shoaling of the calcium carbonate compensation depth (CCD; Bohaty and Zachos 2003; Bohaty et al. 2009). The MECO was terminated by a rapid return to pre-MECO conditions (Bohaty et al., 2009).

Accompanying the Eocene transition from greenhouse to icehouse conditions, there were also profound changes in in planktonic foraminifera diversity (Steineck, 1971; Boersma and Premoli Silva, 1986; Boersma and Silva, 1991; Keller, MacLeod and Barrera, 1992; Wade, 2004; Sexton,

Wilson and Pearson, 2006b; Wade and Pearson, 2008; Luciani et al., 2010; Ezard et al., 2011; Galazzo et al., 2014; Fenton et al., 2016b). Middle Eocene biotic changes in planktonic foraminifera include: (i) the progressive extinction of surface dwelling symbiont bearing taxa (Boersma and Premoli Silva 1986; Boersma and Silva 1991; Keller et al. 1992; Wade 2004; Wade and Pearson 2008), (ii) a reduction in test size (Schmidt, Thierstein and Bollmann, 2004; Wade and Pearson, 2008; Wade and Olsson, 2009), (iii) development of latitudinal size (Schmidt, Thierstein and Bollmann, 2004) and diversity (Fenton et al., 2016b) gradients alongside major assemblage fluctuations (Steineck, 1971; Keller, 1983; Boersma and Premoli Silva, 1986; Boersma, Silva and Shackleton, 1987; Hallock, Silva and Boersma, 1991; Keller, MacLeod and Barrera, 1992; Sexton, Wilson and Pearson, 2006b; Luciani et al., 2010; Galazzo et al., 2014), and (iv) changes in ecology, e.g., loss or inhibition of algal photosymbionts from hosting taxa (Wade et al., 2008; Edgar et al., 2013) and shallowing depth habitat of *Hantkenina* (Coxall et al., 2000).

Yet, our understanding of planktonic foraminifera ecosystem dynamics across the MECO remain relatively understudied (Pearson et al., 2008; Wade and Pearson, 2008; Pearson and Wade, 2015). The MECO resulted in a global crisis for muricate taxa (Luciani et al., 2010; Edgar et al., 2013), varying symbiotic taxa responses (Luciani et al., 2010; Edgar et al., 2013; Gebhardt et al., 2013; Arimoto et al., 2020; Kearns et al., 2021), increased abundance in ecologically flexible (Galazzo et al., 2015; Kearns et al., 2021) and small opportunistic taxa (Luciani et al., 2010). What we lack is an integrated assemblage perspective on these idiosyncratic changes, pieced together from different sampling localities. Here, using Hill numbers, we generate the first mid-latitude diversity record of planktonic foraminifera at North Atlantic sites through the MECO to investigate how planktonic foraminifera communities responded to the MECO and how this event may have influenced subsequent extinction events observed in the late Eocene. Furthermore, we analyse diversity at two size fractions (> 63 μm and > 180 μm) to understand the effects of sampling bias on diversity and its implications for our understanding of biotic responses to climatic perturbations.

2.3 Material and Methods

2.3.1 Material

IODP Expedition 342 targeted clay rich Palaeogene sediment drifts ~ 700 km east-southeast of Newfoundland in the Northwest Atlantic Ocean (Norris et al., 2014), which were deposited at a palaeolatitude of ~ 32.5 ° N. Exp. 342 Sites U1406 (40°21.0'N, 51°39.0'W), U1408 (41°26.3'N, 49°47.1'W) and U1410 (41°19.6993'N, 49°10.1847'W) recovered clay-rich nannofossil ooze drift deposits well above the late Paleogene CCD, providing a near-continuous record of well-preserved

microfossils from ~ 47 Ma through the Eocene and into the Oligocene (Norris et al., 2014; Boyle et al., 2017). Using low-resolution bulk stable isotope data (unpub. Data), cores from Sites U1406, U1408 and U1410 were sampled to capture a 7-Myr interval of the middle Eocene spanning the MECO. In total, 33 samples of 25 cc between 38 and 45 Ma were studied. Due to increased sediment accumulation rates during parts of the MECO, sampling resolution ranges from ~ 20 kyr during the MECO to ~ 900 kyr outside of the MECO.

Sample ages from Sites U1408 and U1410 were calculated based on age-depth models constructed using available biostratigraphy and magnetostratigraphy (Norris et al., 2014). The 2012 geological timescale was then used for age calibrations for the middle Eocene geomagnetic reversals (GTS2012; (Gradstein et al., 2012)). Samples ages for Site U1406 are based upon shipboard biostratigraphic and magnetostratigraphic data (Norris et al., 2014; Van Peer, 2017). Sample information, including calculated ages, are presented in Table A.1.

2.3.2 Sample preparation

The sample material was disaggregated in a sodium hexametaphosphate solution and then washed over a 36 μm sieve with milli-Q water until the water ran clear. Following 24-hours of drying in a low temperature oven (< 50 °C), samples were weighed to determine the weight percent coarse fraction (> 38 μm). Subsequently each sample was split, using a micro splitter, providing two representative halves: one for diversity analysis (this study) and the other for geochemical analysis (Kearns et al., 2021). The sample half reserved for diversity analysis in this study was then split again to allow analyses at two different size fractions. Planktonic foraminiferal assemblage studies have primarily analyzed size fractions >150 μm (Kucera et al., 2005) to avoid sampling juvenile specimens as well as making species level identification easier (Al-Sabouni, Kucera and Schmidt, 2007; Al-Sabouni et al., 2018). This, by definition, biases assemblages towards larger forms despite suggestions that analyzing > 63 μm size fraction especially in polar regions, where species are generally smaller, is more representative of true diversity (Al-Sabouni, Kucera and Schmidt, 2007). To test whether a smaller size fraction is more characteristic of diversity at mid latitude, non-polar sites like IODP Expedition 342, we determine diversity in two size fractions: > 63 μm and > 180 μm. To avoid juveniles in the smaller size fractions, only individuals showing adult characteristics related to aperture position, keels, and fully developed pore structure in macroperforate forms were picked for analysis (Brummer, Hemlebent and Spindlert, 1986).

2.3.3 Diversity analysis

300 individuals is considered sufficient to estimate diversity in foraminifera assemblages (Al-Sabouni et al. 2007) despite the potential of missing rare specimens due to low abundances (Jost, 2010b). For this study, each sample in both size fractions (> 63 µm and > 180 µm) was further split using a micro splitter until approximately 300 individuals were present on the picking tray, with a minimum cut off of 200 specimens. All individuals in the subsample were then picked to avoid bias as a result of uneven distribution on the tray and identified to genus level (Table A.2 – A.4) based on published taxonomy (Pearson et al., 2006; Wade et al., 2018). Whilst we acknowledge the lower resolution of genera-based studies (Hendricks et al., 2014), we focus on genera rather than species in this study, as genera represent a biological reality (Mayr, 1942) and share phenotypic and ecological traits (Aze et al. 2011). Genera-based diversity is less prone to error and more repeatable amongst different workers and ultimately gives more ecologically informative record of diversity in deep time.

To understand diversity changes further, and move away from merely counting things, we then classified each genus into morphogroups (Table A.5 – A.6) adapted from previous classifications (Aze et al., 2011) and depth habitats (Table A.7 – A.8). We based morphogroup classifications on morphological traits (Table A.9) and depth habitats (Table A.10) on published ecological inferences obtained from stable isotope measurements (summarized in Pearson et al. 2006; Wade et al. 2018). Relative abundances and effective diversity curves were than calculated for each genus, morphogroup and depth habitats.

We calculate diversity as a curve using Hill numbers (Hill, 1973):

$$ {}^{q}D = \left(\sum_{i=1}^{S} p_i^q\right)^{1/(1-q)} \quad (1) $$

where S is the number of taxa and pi the frequency of the ith taxa. The value of D is dependent on the order, q, which determines how rarity is weighted in relation to abundance. At ^{0}D taxic richness is measured such that abundance is ignored as rare taxa are weighted more heavily than common taxa compared to higher powers of q (Figure 2.1). As q gets larger, the weighting towards rare taxa is reduced and relative abundance is considered. At ^{1}D, rare and common taxa are equally weighted, which equates to the exponential of Shannon's index (Figure 2.1, (Chao and Jost, 2012)). At ^{2}D, only relative abundance is accounted for, removing the influence of rare taxa so this measure is equivalent to the inverse of Simpson's index (Figure 2.1, (Chao and Jost, 2012). While these integer values are useful reference points, the strength of the Hill number approach is how the continuum of q values (the slope of the effective diversity curve) can be used to understand the evenness of the assemblage. If an assemblage is made up of equal numbers of represented taxa, then the diversity curve will be flat as abundance does not vary among between

groups and no taxon is rare (Figure 2.1). In contrast, if the curve has a high gradient and plummets into a plateau, then the assemblage can be interpreted as uneven with lots of rare taxa and a few dominant groups (Figure 2.1).

We outline the workflow for calculating our diversity curves (^{q}D) in Appendix A that follows Chao and Jost (2015). $^{0\text{-}2}D$ was calculated at the default 0.1 intervals for *q* between 0 and 2 (Table A.11, (Chao and Jost, 2015)). 95 % confidence intervals were generated for each diversity curve by bootstrapping 1000 times.

2.3.4 Fragmentation

A challenge to using paleoecological data is the inevitable influence of taphonomic bias. Assemblage data of planktonic foraminifera can be heavily influenced by the taphonomic physio-chemical process of dissolution as a result of their shell (test) composition (Berger, 1971; Malmgren, 1987; Nguyen, Petrizzo and Speijer, 2009). The susceptibility of foraminifera to dissolution is both strongly species-specific based on the physical structure of the test wall (e.g., relative porosity and thickness (Nguyen, Petrizzo and Speijer, 2009; Nguyen et al., 2011; Nguyen and Speijer, 2014)) as well as the microenvironment of the individual which influences test chemistry and causes interspecific differences in dissolution susceptibility (Berger, 1970; Nguyen et al., 2011; Petro, Pivel and Coimbra, 2018). To account for this variability, we use an accepted fragmentation proxy to estimate the dissolution levels (Le and Shackleton, 1992) using the proportion of planktonic foraminiferal test fragments (Frag) and whole specimens:

$$Fragmentation\ (\%) = [(Frag/8)\ /\ (((Frag)\ /\ (8) + Whole))]\ \times\ 100 \qquad (2)$$

We classify a fragment as anything < 75 % of a whole specimen (more conservative than the < 50 % previously used, (Malmgren, 1987)). Foraminifera have a tendency to break into multiple pieces therefore the percentage of fragments in a sample varies non-linearly with dissolution (Le and Shackleton, 1992). To account for this, a divisor is used, and we follow previous work and set the divisor as 8 (Le and Shackleton 1992; Leon-Rodriguez and Dickens 2010). We use a baseline of 20 % fragmentation to indicate normal levels of fragmentation and dissolution (Pfuhl and Shackleton, 2004). Samples sieved at 63 μm are expected to have higher fragmentation than samples sieved at a larger size fraction as fragments progressively break into smaller pieces and smaller individuals are less robust. Therefore, we also use the bulk sediment weights to assess potential dissolution effects on the assemblage as dissolution reduces the absolute abundance of planktonic foraminifera in a sample whilst ecological change causes taxa relative abundance fluctuations. Fragmentation was calculated twice on 18 samples (10 samples from the > 180 μm and 9 samples from the > 63 μm) with high repeatability (92%, Table A.12).

2.3.5 Statistical methods

2.3.5.1 Generalized additive models

Diversity has a non-linear relationship with time. To assess the impact of sample age and size fraction on diversity, we applied non-parametric generalized additive models (GAMs) using the R package mgcv (version 1.8.33; (Wood 2017)) in the R environment (version 4.0.3; R Core Team 2020). Prior to model fitting, integer values of Hill numbers were back transformed to genus richness, Shannon's index (H_S) and Simpson's index (H_{GS}) and used as response variables. Models were constructed with a smooth (non-parametric, non-linear) function of age and a linear predictor of fragmentation to control for the impact on dissolution on diversity. Models were fitted using a Gaussian distribution with an identity link using generalized cross validation model (GCV) method. A GCV method was used instead of restricted maximum likelihood estimation (REML) due to the small number of samples through time (Wood, 2011).

Model selection amongst a relevant model set including a null model (Table 2-1) was based on Akaike Information Criterion corrected for small sample size (AICc) and diagnostic plots. The Supporting Information provides further detail on back transformation, models fitted (including all annotated code) and model selection information. Model results are presented as with significance of smoothing parameters with effective degrees of freedom (edf), F-statistics (F) and *p*-value (*p*). The edf indicates the complexity of the curve; an edf of 1 it indicates a straight line whilst and edf of 2 indicates a quadratic curve and so on. In addition, where appropriate, parametric coefficients will be presented with the coefficient (β), t-value (t), standard error (se) and *p*-value (*p*).

2.3.5.2 Kruskall-Wallis and Dunn test

To investigate differences in Hill numbers in response to palaeoclimatic and palaeoceanographic changes, samples were divided into groups representing different climate phases (pre-MECO; > 41.94 Ma, MECO; 40.14 – 41.09 Ma, post-MECO; < 40.14 Ma). The difference between these intervals was assessed when $q < 1$ (weighted towards rarity) and $q > 1$ (relative abundance taken into account) using a Kruksall-Wallis test. A Kruskall-Wallis test was used to investigate whether a difference was present between intervals, and additionally the effect size of the intervals was calculated based on the H statistic from the Kruskall-Wallis test. Following detection of a statistically significant impact of interval in the Kruskall-Wallis test ($p < 0.01$), a *post-hoc* Dunn test using the R package "FIA" (Ogle, Wheeler and Dinno, 2021) was applied, due to unequal observations in each interval (Zar, 2010), to identify intervals which were significantly different from each other.

2.4 Results

2.4.1 Fragmentation

The degree of fragmentation varies across our record from 1.34% to 30.80% (Figure A.1, Table A.11), with generally increased fragmentation in the smaller size fraction as expected. In total, seven samples were above the baseline "normal" fragmentation of 20 % (Pfuhl and Shackleton, 2004), of which six were in the > 63 µm size fraction. These were primarily within the MECO interval (~ 40–41 Ma) and at ~ 38 Ma.

2.4.2 Traditional diversity indices

To understand how commonly used diversity indices changed through time, we back-transformed calculated Hill numbers into genus richness, H_S and H_{GS} index for genera, morphogroup and ecogroup, and fitted GAMs (Figure 2.2, Table 2-1). For all diversity indices, based on AICc, the best fitting GAMs (Table 2-1, Table A.13 – A.21, Figure A.2-A.10) suggest a change in diversity as a function of size fraction, with varying intercepts for size fraction (with the smaller size fraction giving consistently higher values), during the Eocene for richness, H_S and H_{GS}. We concentrate here on genera and morphogroup changes in terms of richness, H_S and H_{GS} (Depth habitat effect diversity changes are discussed in Section 2.4.3.3). Depth habitat analysis showed similar patterns; however, as depth habitat is only represented by three groups, the changes observed are inessential in terms of H_S and H_{GS} and are therefore provided in the supplement (Figure A.8-A.11; Table A.21 – A.23). The ΔAICc between the best fitting models for genera and morphogroup and the next best models ranged from 11.595 to 71.331 (Table A.14-A.18), implying that the second ranked models had "essentially no" support (Burnham and Anderson, 2002).

Following model selection discussed above, we used the best fitting model (Table 2-1) to predict diversity values across our study interval at a mean fragmentation of 10 % to produce diversity curves and 95 % confidence intervals (Figure 2.2). The code to obtain predictions based on observed and defined fragmentation can be found in Appendix A.

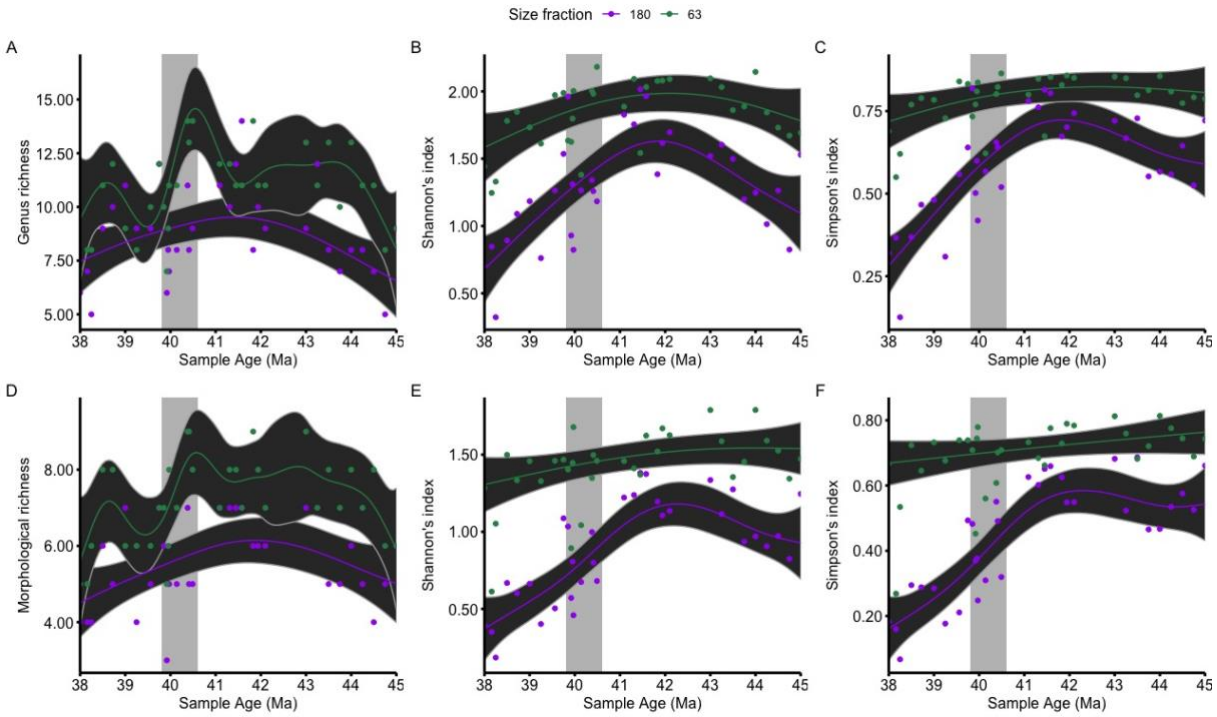

Figure 2.2 North Atlantic predicted diversity from Exp. 342 (Sites U1406, U1408 and U1410) as a function of time at > 63 µm (green) and > 180 µm (purple) size fractions with a constant fragmentation of 10 % through time. Raw data is shown as filled circles. Dark grey shaded area represents 95 % confidence intervals around the central predicted response. A-C show genus diversity indices: D-F show morphological diversity indices. The light grey box represents the MECO interval.

Table 2-1 Table showing the structure of all models fitted. Diversity is replaced by Genus and Morphogroup for each set of models and AIC weights are presented. The smooth term is denoted by s(). [1]Null model, [2]Best fitting model. All other statistical output including df and AIC are provided in Table A.14 – A.18.

	Genera AIC Weight			Morphogroup AIC Weight		
Model Structure	Richness	Shannon's index	Simpson's index	Richness	Shannon's index	Simpson's index
[1]Diversity ~ s(Age)	0.0030	0.0000	0.0000	0.0000	0.0000	0.0000
Diversity ~ s(Age) + Frag	0.0010	0.0000	0.0000	0.0000	0.0000	0.0000
Diversity ~ s(Age, by =size) + Frag	0.0002	0.0000	0.0000	0.0000	0.0000	0.0000
[2]Diversity ~ s(Age, by =size) + size + Frag	0.9959	1.0000	1.0000	0.9999	1.0000	1.0000

2.4.2.1 Richness

Smooth complexity (wigglyness) for genera differed between size fractions with a more complex smooth predicted for the > 63 µm size fraction (edf = 8.54, F = 3.10, $p < 0.01$) compared to the > 180 µm size fraction (edf = 2.65, F = 4.27, $p < 0.01$) (Figure 2.2A). A similar pattern was observed in the morphogroup models where the predicted smooth for > 63 µm size fraction is more complex (edf = 8.26, F = 2.16, $p < 0.05$) than >180 µm (edf = 2.38, F = 3.10, $p < 0.05$) (Figure 2.2D). The complex nature of the > 63 µm size fractions smooth illustrates inter-sample variability represented in the larger confidence intervals compared to > 180 µm (Figure 2.2A, D).

Morphological and genera richness profiles generally follow a similar pattern with increasing richness initially between 45 and 44 Ma, followed by a period of relative stasis until ~ 41.5 Ma (Figure 2.2A, D). In the > 63 µm size fraction, genera and morphological richness peaked at ~ 40.55 Ma, coinciding with the early stages of the MECO (Genera: 14.71 ± 0.98, Morphological: 8.45 ± 0.55; Figure 2.2A, D). In the > 180 µm size fraction, the peak in richness is much less pronounced and ~ 1 Myr prior to the MECO at 41.54 Ma (Genera: 9.52 ± 0.47; Figure 2.2A) and

41.89 Ma (Morphological: 6.14 ± 0.30; Figure 2.2D). Peaks in morphological and genera richness in the > 180 μm are followed by a decline of 1.64 morphogroups and 2.06 genera by the end of our record at 38.00 Ma (Figure 2.2A, D). The wide 95 % confidence intervals around the diversity declines in the (Figure 2.2A, D) suggest these declines are negligible as the confidence intervals could encapsulate a straight line. In contrast, the > 63 μm size fraction shows a greater degree of intrasample variability resulting in more complex GAMs that predict a large decline in morphological (- 2.17 morphogroups) and genera (- 5.62 genera) richness following the MECO at ~ 40.5 Ma (Figure 2.2A, D).

The most influential predictor of genera and morphological richness was size with a predicted reduction in overall richness of 2.537 genera (β = -2.537, se = 0.468, t = -5.423, $p < 0.001$) and 1.728 morphogroups (β = -1.728 se = 0.277, t = -6.235, $p < 0.001$), calculated in assemblages from the > 180 μm fraction rather than > 63 μm fraction (Table A.19). This means that 2.537 genera and 1.728 morphogroups represented in the > 63 μm size fraction are not present in the > 180 μm size fraction. Fragmentation was also a significant predictor for genera richness with a predicted 0.14 decrease in richness per 1% increase in fragmentation (β = -0.14, se = 0.048, t = -13.16, $p <$ 0.001; Table A.19).

2.4.2.2 Shannon's Index

The predicted curves for H_S are smoother than those for richness (Figure 2.2). However, unlike richness, the model predicted a more complex age smooth for genera H_S in the > 180 μm size fraction (edf = 3.06, F = 11.65, $p < 0.001$) than > 63 μm (edf = 2.18, F = 2.73, $p > 0.05$, B, Table A.20). Amongst genera, size is the only significant predictor of diversity (β = -0.58, se = 0.10, t = -8.68, $p < 0.001$; Table A.20), with the > 180 μm size fraction predicted to increase to a peak of 1.64 ± 0.08 at 41.89 Ma followed by a steep decline until 38.00 Ma (Figure 2.2B). In contrast, the > 63 μm size fraction gradually increases reaching a maximum H_S of 1.99 ± 0.07 at 42.10 Ma (Figure 2.2B).

For morphological H_S, the age smooth for the > 63 μm fraction does not differ detectably from a straight line (edf = 1.62, F = 2.28, $p > 0.05$; Table A.20), contrasting the wiggly smooth for >180 μm (edf = 3.47, F = 13.67, $p < 0.001$; Figure 2.2E, Table A.20),. Both fragmentation and size fraction are significant predictors (fragmentation: β = - 0.011, se = 0.004, t = - 2.74, $p < 0.01$; size fraction: β = -0.61, se = 0.05, t = -11.61, $p < 0.001$, Table A.19), but size fraction had a larger, more meaningful impact on diversity with a reduction of 0.61 morphogroups in the >180 μm size fraction compared to the > 63 μm size fraction. The peak in > 180 μm morphological H_S (1.18 ± 0.07) is predicted at 42.40 Ma, 0.50 Ma prior to the peak in genera H_S in the same size fraction (Figure 2.2B, E).

2.4.2.3 Simpson's Index

The narrow range of values allowed for available values for H_{GS} (between 0 and 1), inter sample variation was high (Figure 2.2C, F), and the predicted smooth follows a similar pattern to that in H_S (Figure 2.2B, E). The GAMs predicted a complex age smooth for both genera (edf = 3.31, F = 19.11, $p < 0.001$; Table A.20) and morphogroup (edf = 3.64, F = 17.94, $p < 0.001$; Table A.20) H_{GS} in the > 180 µm size fraction. Both smooths reach peaks prior to the MECO at 41.82 Ma (Figure 2.2C) and 42.31 Ma (Figure 2.2F) for morphogroup and genera H_{GS}, respectively. The age smooth for the smaller size fractions are close to straight lines (Figure 2.2C, E; genera: edf = 1.88, F = 2.01, $p > 0.05$; Morphogroup: edf = 1.06, F = 2.24, $p > 0.05$; Table A.20). In genera, only fragmentation is a significant predictor equating to a predicted 0.21 ± 0.02 reduction in genera Simpson's index per 1% increase in fragmentation (β = -0.21, se = 0.02, t = - 9.40, $p < 0.001$; Table A.19) whilst for morphogroup both fragmentation (β = - 0.01, se = 0.002, t = - 3.06, $p < 0.01$; Table A.19) and size fraction (β = - 0.28, se = 0.02, t = - 11.62, $p < 0.001$; Table A.19) are significant predictors of H_{GS}.

2.4.3 Hill Numbers and Relative Abundance Fluctuations

2.4.3.1 Genera

When relative abundance is not considered (q <1), pre-MECO (> 41.09 Ma), MECO (40.14 – 41.09 Ma) and post-MECO (< 40.14 Ma) intervals are all different to each other (Figure 2.3A, D; $p <$ 0.001), but the effect of size (eta2[H] = 0.18) and magnitude of differences between intervals (pre-MECO, MECO and post-MECO) is only large (defined in the statistical test as eta2[H] > 0.14) in the > 63 µm size fraction (Table A.24). This suggests substantial differences in absolute numbers of genera through the middle Eocene with highest values in the MECO (40.14 – 41.09 Ma) followed by a decline into post-MECO (< 40.14 Ma) assemblages below pre-event levels (Figure 2.3A and D).

When relative genera abundance is considered (q >1), the effect size of time interval is only large (eta2[H] = 0.25) and significant ($p < 0.01$) in the > 180 µm size fraction (Table A.23). A Dunn's test shows that a significant difference exists between the post-MECO interval (< 40.14 Ma) and the other intervals ($p < 0.01$; Table A.24) with the MECO (40.14 – 41.09 Ma) and pre–MECO interval (> 41.09 Ma), showing no significant differences.

2.4.3.2 Morphogroup

In the > 63 µm size fraction, the effective diversity curves show only subtle separation between assemblages because of palaeoceanographic changes (interval) (Figure 2.3B). A Kruskall-Wallis test revealed morphological effective diversity was only significantly different ($p < 0.01$) between

time intervals, with a large effect size of interval (eta2[H] = 0.25) when relative abundance was considered (q >1, Figure 2.3B; Table A.24). Based on a Dunn's test, the significant interval differences are between the MECO (40.14 – 41.09 Ma) and pre-MECO (p < 0.05; (> 41.09 Ma), as well as between the post-MECO (< 40.14 Ma) and pre-MECO (> 41.09 Ma) (p < 0.05; Table A.25).

In the > 180 µm size fraction, the effect size of time interval is large and significant when rare morphologies are influential (q < 1) and when they are discounted (q = 1 - 2) (Table A.24). A Dunn test showed that there is no significant difference between pre-MECO and MECO (40.14 – 41.09 Ma) samples (p > 0.1) at any level of q (Table A.25), resulting in overlapping effective diversity curves except for those assemblages grouped in the post-MECO (< 40.14 Ma) assemblages coloured green (Figure 2.3E). Additionally, the post-MECO (< 40.14 Ma) assemblages show a decrease in evenness compared to the preceding intervals (Figure 2.3E).

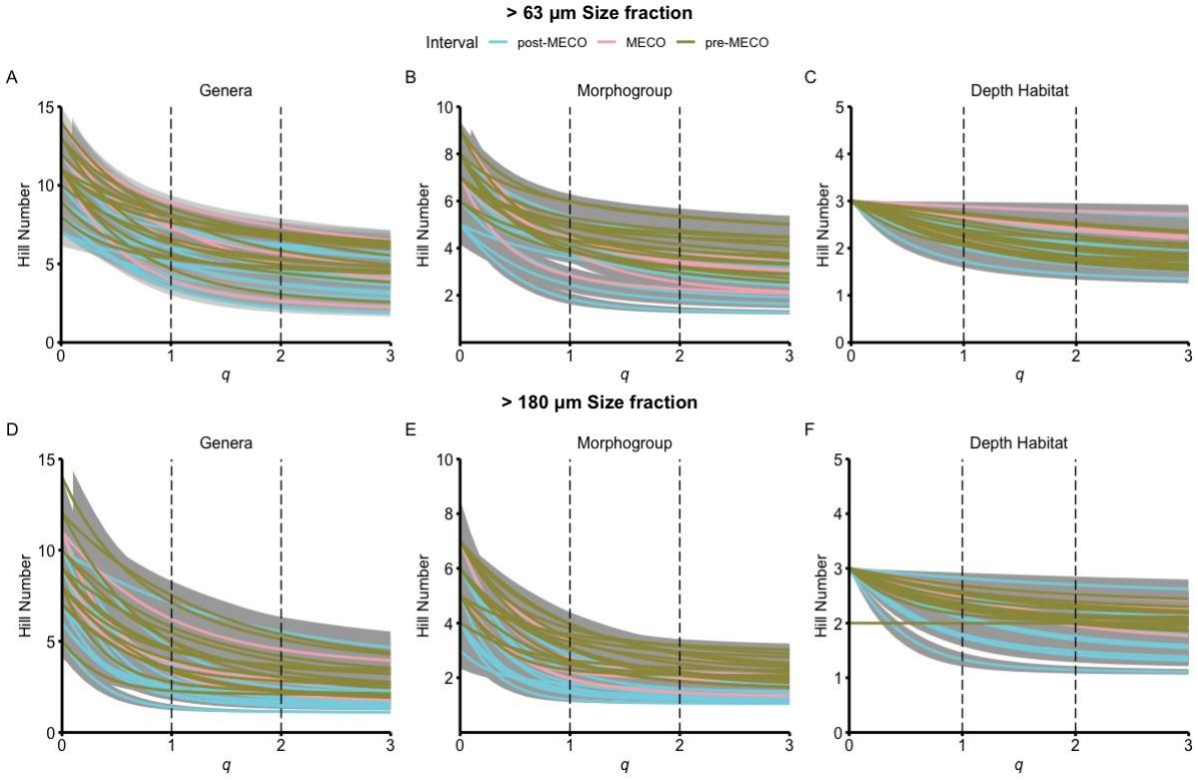

Figure 2.3 North Atlantic diversity curves presenting results of hill number calculations based on abundance counts presented in Table A.3 – A.8. Morphogroup and depth habitat follow the classification outlined in Table A.9-A.10. A-C reflect diversity changes at the > 63 µm size fraction whilst D-F reflect changes at the > 180 µm size fraction. Vertical dotted lines are present where q=1 and q=2 as these correlate to the exponential of Shannon's index (q=1) and the inverse of Simpson's index (q=2) presented in Figure 2.2. Lines are coloured to represent palaeoceanographic interval. Note one horizontal green line in F illustrating a perfectly even assemblage. The grey bands represent 95% confidence intervals.

2.4.3.3 Depth Habitat

Compared to the genera and morphogroup analyses, effective depth habitat richness (^0D) in assemblages is the same in both size fractions ($^0D = 3$; Figure 2.3C, F) with no differences in depth habitat ^0D as a function of size fraction or sample age. A Kruskall-Wallis test showed no difference in effective diversity between palaeoceanographic intervals in the > 63 µm size fraction which is illustrated by the overlap of effective diversity curves (Figure 2.3C). This implies that there was no change in depth habitat evenness through the middle Eocene, meaning no organisms of a certain depth habitat were dominating assemblages.

In comparison, the depth habitat effective number curves show separation in the post-MECO (< 40.14 Ma) samples of the > 180 µm size fraction (Figure 2.3F). A Kruskall-Wallis test showed that the interval had a large effect size (eta[H]=0.262) and was significant ($p < 0.01$) when q is between 1 and 2 in the > 180 µm size fraction (Table A.24). A Dunn test show that the significant differences are between the post-MECO (< 40.14 Ma) interval and both preceding intervals ($p < 0.01$; Table A.25). The gradient change of the effective diversity curves also shows that the post-MECO (< 40.14 Ma) samples are uneven compared to the other intervals.

2.5 Discussion

Understanding biodiversity responses to climate change is challenging, particularly in deep time. A focus on relative abundance changes and biogeographical comparisons can complicate broader interpretations because of the idiosyncratic responses of taxa to environmental change. By using Hill numbers, we have been able to generalise and assess the biodiversity response of planktonic foraminifera temporally to transient warming (Figure 2.3) at mid-latitudes, whilst maintaining the ability to investigate more specific biodiversity measures such as richness (Figure 2.2) and relative abundance changes (Figure 2.4).

Using this approach, we show increases in morphological and generic richness coincident with the early stages of MECO warming in the > 63 µm size fraction (Figure 2.2A and D) which is reflected in our count data with ~ 70 – 72 % of all genera and morphogroups recorded in this study present at ~ 40.5 Ma (Table A.2 – A.8). In addition, we found that analytical choice of size fraction resulted in apparent differences in planktonic foraminifera response to both MECO warming and post-MECO cooling (Figure 2.2;Figure 2.3). Furthermore, we find that the loss of symbiont bearing foraminifera only changes depth habitat diversity in the > 180 µm size fraction (Figure 2.3F), since in the > 63 µm size fraction these genera are replaced in the mixed layer by increased numbers of non-symbiotic *Chiloguembelina* and *Planorotalites* (Figure 2.4).

2.5.1 Influence of dissolution on diversity analysis

In planktonic foraminifera dissolution has the potential to shift assemblages from representing environmentally shaped life assemblages to taphonomically shaped death assemblages (Berger, 1971; Thunell, 1976), biasing climatic and biotic interpretations from those assemblages (Berger, 1973). Dissolution can be morphologically selective (Berger 1970; Boltovskoy and Totah 1992; Petrizzo et al. 2008; Nguyen et al. 2009, 2011, but see Petro et al. 2018) with species specific tendencies (Nguyen et al., 2011). Across the MECO, extensive dissolution as a result of shoaling carbonate compensation depth (CCD), has been recorded in the Pacific, Indian and Atlantic Oceans (Lyle et al., 2005; Bohaty et al., 2009; Pälike et al., 2012). Despite our study sites sitting well above the known late Paleogene CCD (Norris et al., 2014), we still find that ~ 11 % of our samples (7 out of 66) had fragmentation above levels considered normal for a well-preserved sample (Pfuhl and Shackleton, 2004; Table A.12). Whilst this indicates some degree of dissolution, there was no observable drop in overall planktonic foraminifera abundances, which would indicate dissolution impacted assemblages (Malmgren, 1987). We do detect a statistically significant effect of dissolution in our statistical models, and recommend accounting for it in statistical analyses, but the small effect sizes (up to 55 times smaller than the effect of size fraction choice, for example) suggest that dissolution is not a strong driver of the diversity dynamics we report (Figure 2.2-Figure 2.4).

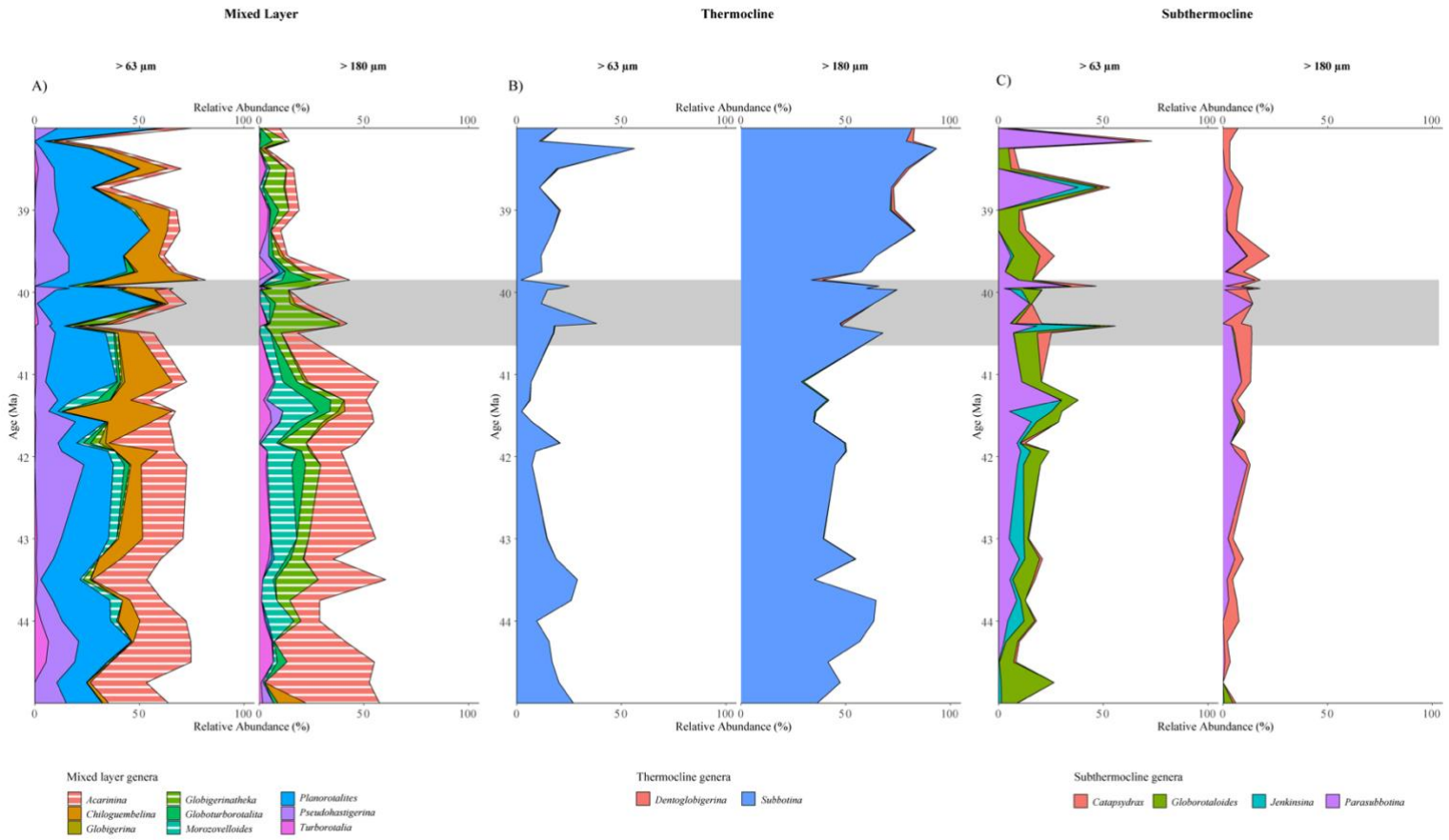

Figure 2.4 Relative abundance plots of genera across the North Atlantic middle Eocene from Expedition 342 Sites U1406, U1408 and U1410 separated by depth habitat and size fraction. A depicts the surface dwellers with symbiont bearing taxa filled with a pattern, (B) represents the thermocline dwellers whilst (C) represents subthermocline dwellers. Note different colour schemes are used per depth habitat for ease of viewing. Symbiont bearing foraminifera: *Acarinina, Morozovelloides* and *Globigerinatheka* are indicated by a striped pattern. The grey box represents the MECO interval. *Turborotalita*, *Orbulinoides* and *Hantkenin*a are not included in this plot as they occurred in such low numbers (1-5 absolute abundance).

2.5.2 Transient climate impacts on specialist feeding ecologies

Our samples are the first mid-latitude samples analysed for assemblages across the middle Eocene to date. Therefore, our results give a unique insight into the impacts of the MECO on symbiont bearing foraminifera and motivate for further studies at high latitude sites.

We observe abundance decreases of symbiont bearing planktonic foraminifera on the Newfoundland margin prior to the MECO at ~ 40.50 Ma in the > 180 µm size fraction and at ~ 41.31 Ma in the > 63 µm size fraction that persist post-MECO (Figure 2.4, Table A.3-A.4). At the lower latitude Ocean Drilling Program Site 1051 in the North Atlantic Ocean (~25°N, Blake Nose), large *Acarinina* (> 300 µm) abundance only temporarily decreases during peak warming of the MECO (Edgar et al., 2013); in the sub-tropical Alano section, the abundance of *Acarinina* is high pre- and during the MECO, but then abruptly decreases post-MECO and remains low (Luciani et al., 2010). Our reported decline in abundance is notably smaller in the high North Atlantic (~ 20 % reduction in *Acarinina*) compared to the sub-tropics (Luciani et al., 2010). *Acarinina* relative abundance never recovers following the decline in our record, instead staying consistently low as in the Tethys (Luciani et al., 2010);Figure 2.4), unlike the lower latitude Blake Nose (~ 25° N) where *Acarinina* recovers in both abundance and test size (Edgar et al., 2013). Though not as abundant as *Acarinina, Morozovelloides* is present in our samples with a peak relative abundance in both size fractions at 41.31 Ma prior to the MECO (~ 20 % in > 180 µm and ~ 11 % in > 63 µm, Figure 2.4), followed by a decline in relative abundance through the MECO and to the end of our record (Figure 2.4). The general trend of post-MECO reduction in relative abundance of *Morozovelloides* is observed at other localities (Wade et al., 2008; Luciani et al., 2010; Edgar et al., 2013) though in the Tethys *Morozovelloides* is scarcely abundant throughout the Middle Eocene (Luciani et al., 2010; Gebhardt et al., 2013). The low relative abundances observed in *Morozovelloides* here and at Tethys sites (Luciani et al., 2010; Gebhardt et al., 2013) are therefore likely a result of these subtropical sites being at the ecological limit for the thermophilic *Morozovelloides*. The biogeographical differences in population dynamics between these two ecologically similar species emphasises the need for spatially replicated ecological sampling.

Stable isotope data, though limited, show that *Acarinina* and *Morozovelloides* at Site U1408 had the expected size-$\delta^{13}C$ relationship of symbiont bearers during the MECO (Henehan et al., 2020). Mixotrophy, or the harbouring of photosymbiotic algae, is relatively common in modern planktonic foraminifera (Takagi et al., 2019) and has been a key component for shaping spatial and temporal diversity patterns (Ezard et al., 2011; Fenton et al., 2016a; Hannisdal et al., 2017). Despite its continual occurrence throughout geological time in this study we classify mixotrophy as a specialist, adaptive ecological feeding strategy as it limits the planktonic foraminifer to a

narrow ecological niche (Raia et al., 2016; Rolland and Salamin, 2016). During the middle Eocene, mixotrophic foraminifera included *Acarinina, Morozovelloides, Globigerinatheka* and *Orbulinoides,* all of which experience major global changes in their relative abundance and ecology as a result of transient climate change (Keller, 1983; Boersma and Silva, 1991; Wade, 2004; Wade and Pearson, 2008; Wade and Olsson, 2009; Luciani et al., 2010; Boscolo Galazzo et al., 2013; Edgar et al., 2013) with *Morozovelloides*, large *Acarinina, Globigerinatheka* and *Orbulinoides* becoming extinct before the end of the Eocene (Wade, 2004; Wade and Pearson, 2008).

Based on a shared ecological strategy one conclusion may be that the reduction of *Acarinina* and *Morozovelloides* at our site was a result of their specialist ecology and changes to their symbiotic relationship (Wade, 2004; Wade et al., 2008; Edgar et al., 2013) as shown by reduction in test size-$\delta^{13}C$ value relationship following the MECO at Blake Nose, Site 1051, in the Northwest Atlantic (Edgar et al., 2013), that occurred as non-symbiont bearing surface layer dwellers continued to thrive (Figure 2.4). Yet, despite sharing a similar specialist mixotrophic ecology, *Globigerinatheka* shows a peak in relative abundance of ~ 33 - 34 % in the > 180 µm size fraction and 11 % in the > 63 µm size fraction at ~ 40.40 Ma coincident with peak MECO warming (Figure 2.4). In addition, other global records record dominance or relative abundance increases of *Globigerinatheka* through the MECO (Boersma and Premoli Silva, 1986; Boersma, Silva and Shackleton, 1987; Edgar et al., 2013; Galazzo et al., 2014).

Specialist feeding ecologies have been cited as the reason for extinction in deep time of herbivorous sea urchins (Smith and Jeffery, 1998), herbivorous insects (Labandeira, Johnson and Wilf, 2002), hypercarnivorous canids (Van Valkenburgh, 2004) and crinoids (Baumiller, 1993). A similar pattern of feeding specialist extinction has also been documented in planktonic foraminifera (Norris, 1992), but Norris' defined a specialist as foraminifera that can has limited food sources. The success of *Globigerinatheka* and persistence of *Acarinina* and *Morozovelloides* suggests that specialisation is not always entirely detrimental for organisms during transient climatic changes even with large fluctuations in climate state. The decline in symbiont bearing planktonic foraminifera across the middle Eocene does suggest the climatic fluctuations pushed these genera to their ecological limits (Edgar et al., 2013), which was a process exaggerated at our sites due to the relatively high latitude locality near the species' biogeographical range limits.

2.5.3 Divergent response of size fraction to the Middle Eocene

Size bias occurs frequently in research, whether as a result of taphonomic or sampling bias (Brown et al., 2013a, 2013b). Independent of the causes of this bias, only sampling certain sizes in nature impacts our understanding and public perception of biodiversity (Rillo et al., 2017).

Assemblage studies are often conducted at size fractions above > 150 µm to avoid juvenile specimens (Al-Sabouni et al. 2007), yet this coarse filter can remove large amounts of diversity and bias studies towards larger individuals particularly at higher latitudes where taxa are known to be smaller (Schmidt et al. 2004). In addition, sampling at a biotically uninformative size fraction can impact inferences on how communities respond to background, transient and rapid environmental fluctuations. In this study, we found different timings of assemblage responses to middle Eocene climate as a result of size fraction choice (Figure 2.2-Figure 2.3).

At the relatively high latitude position of our site, water column heterogeneity is already low due to the lack of a substantial thermocline (Al-Sabouni et al. 2007). Background Eocene cooling (Westerhold et al. 2020) would have increased water column stratification allowing for an increase in relative abundance of genera as a result of widening ecological niches (Whittaker et al. 2001; Al-Sabouni et al. 2007). We see the effects of increasing thermal stratification in the larger size fraction (> 180 µm) where genera and morphological H_S and H_{GS} increase at 42.20 Ma (Figure 2.2B - C, E - F). The positives of cooling seem to be short-lived, however. Thermal stratification and cooling increases prior to the MECO (Arimoto et al. 2020; Kearns et al. 2021), which results in the removal of larger symbiont bearing foraminifera (*Acarinina* and *Morozovelloides*) and a decline in genera and morphological H_S and H_{GS} (Figure 2.3). These results imply that amplitude and intensity of environmental change has a major role on how ecosystems respond, possibly larger than the direction of change (Gibbs et al. 2012; Garcia et al. 2014; Mayfield et al. 2021).

In contrast, we do not see any consistent changes in effective diversity at multiple levels of *q* (Figure 2.3) and no substantive differences between pre-MECO and MECO intervals (Figure 2.3; Table A.25). Instead, effective diversity shows significant change in the post-MECO interval (Figure 2.3; Table A.25) with a decrease in morphological, genera and depth habitat effective diversity at all levels ($^{0\text{-}2}$D) and decreasing assemblage evenness. This trend to less even communities follows the removal of large symbiont-bearing forms (Figure 2.4) and an increase in thermocline dwellers at the expense of mixed layer species (Figure 2.4)

Compared to the > 180 µm size fraction, we observe no impact of general Eocene cooling or enhanced pre-MECO cooling on traditional diversity measures in the smaller size fraction (Figure 2.2). In addition, we see no impact of pre-MECO cooling on effective diversity (Figure 2.3; Table A.25). Instead, we observe peaks on morphological and genera richness coinciding with peak MECO warming (Figure 2.2A, D). Though the magnitude of warming experienced during the MECO at the sites drilled on IODP Expedition 342 is debated (Arimoto et al. 2020; Kearns et al. 2021), a global surface ocean temperature increase, alongside the removal of key large symbiont bearing planktonic foraminifera, may have increased the number of vacant ecological niches leading to increases in rare, small, microperforate surface-dwelling taxa alongside increases in thermocline

dwellers. As a result of the transient nature of the MECO, ~ 270 - 500 kyr (Bohaty and Zachos 2003; Bohaty et al. 2009; Rivero-Cuesta et al. 2019; Edgar et al. 2020), test size increases in response to increasing warmth, and thus emergence of potentially ecologically optimum conditions, are not observed like at other periods in geological history (Schmidt et al. 2003; Al-Sabouni et al. 2007; Todd et al. 2020). A lack of size response as a result of decreasing thermal stratification across the MECO at this site (Arimoto et al. 2020; Kearns et al. 2021), was a driver of globally small test sizes in the middle Eocene (Schmidt et al. 2004) and responsible for the emergence of latitudinal size gradient at ~ 42 Ma which still persists today (Schmidt et al. 2004). The brevity of the MECO also meant increasing diversity in the > 63 µm size fraction was short lived and followed by a dramatic decline in genera and morphological richness (Figure 2.3A, D) and effective diversity ($^{<1}$D;Figure 2.3). Post-MECO cooling had little other effect on effective diversity except a reduction in $^{1\text{-}2}$D morphological diversity as a result of the decline in morphologically distinct *Chiloguembelina* and *Jenkinsina*.

2.5.4 Insights into palaeoceanographic changes across the MECO from "rare" taxa

In our record we have numerous rare taxa that resulted large fluctuations in genera and morphogroup effective diversity, ^{0}D, at both size fraction (Figure 2.2-Figure 2.3). Although rarity in itself is potentially an important measure (e.g., acting as canaries for early warning signals Doncaster et al. (2016)) being rare is common with the majority of taxa represented by only a few individuals (Gaston 2008). Microperforate biserial and triserial taxa, such as *Chiloguembelina* and *Jenkinsina*, are rare in many records as they occur in highest abundance in the not often studied > 63 µm size fraction despite being omnipresent throughout the Cenozoic (Li and Radford 1991), with approximately 20 species occurring in the Eocene alone (Huber et al. 2006). In addition, these taxa have sporadic geographic and biostratigraphic records (Kroon and Nederbragt 1990; Darling et al. 2009), often increasing to noticeable abundances during periods of environmental stress such as ocean acidification events (Nederbragt et al. 1998; Coccioni et al. 2006), periods of background climatic instability (Kroon and Nederbragt 1990; Li and Radford 1991; Luciani et al. 2007, 2010; D'Haenens et al. 2012) and following mass extinction events (Keller 1993; Luciani 1997, 2002; Keller et al. 2002). The lack of changes at the > 63 µm size fraction for most diversity measures compared to the > 180 µm size fraction supports these results that smaller taxa are more resilient to both background (i.e., Eocene cooling) and transient perturbations (MECO) compared to large taxa.

In our record, both *Chiloguembelina* and *Jenkinsina* are only substantive components of assemblages in the > 63 µm size fraction (Figure 2.4A-C), not > 180 µm. Two noticeable peaks in *Chiloguembelina* (43.24 % at 39.85 Ma and 52.27 % at 41.45 Ma) and *Jenkinsina* (30.42 % at 40.41 Ma and 20.05 % at 41.45 Ma), coinciding with palaeoceanographic instability across the MECO,

interrupt relatively low abundance percentages (Figure 2.4A-C). Similar peaks in abundance of *Chiloguembelina* and *Jenkinsina* have been observed in the Tethys Ocean (Alano section; (Luciani et al. 2010) and at other high latitude sites (Li and Radford 1991). Though there is no evidence of upwelling or low oxygen conditions at our study site (Arimoto et al. 2020; Kearns et al. 2021), these peaks in abundance support arguments that these taxa thrive transient climate events.

One hypothesis as to why rare taxa flourish during environmental perturbations is that they replace superior predators or dominant taxa that are lost in order to maintain ecological function (Walker et al. 1999). Both *Chiloguembelina* relative abundance peaks occurs synchronously with troughs in *Acarinina* relative abundance (Figure 2.4). As all three genera are surface-dwelling this rise in abundance may be a response to the vacant ecological niche left by the removal of a large proportion of *Acarinina* and *Morozovelloides*. This synchronicity may reflect changes to productivity as *Chiloguembelina* has been shown to be opportunist eutrophic genera (Luciani et al. 2020). Coincidental changes in relative abundance also occur in the thermocline and subthermocline where *Jenkinsina* peaks at the same time as *Subbotina* (Figure 2.4). Whilst no taxa are being removed from the thermocline during the MECO, *Subbotina* has a wide and plastic ecological niche (Kearns et al. 2021) and it may be that *Jenkinsina* prospered for a short interval due to temporary availability of the thermocline ecological niche. Stable isotope studies of *Chiloguembelina* and *Jenkinsina* across the Middle Eocene would be one route to rigorously testing this hypothesis. Our observations do however suggest that these rara taxa are useful when looking at palaeoceanographic changes to identify periods of environmental instability and therefore should be measured instead of being dismissed for their small size and sporadic geographic and biostratigraphic records (Kroon and Nederbragt 1990; Darling et al. 2009).

2.6 Conclusion

Our analysis of planktonic foraminifera assemblages within the middle Eocene at sites on the Newfoundland margin demonstrate that complex diversity dynamics follow transient environmental changes. We show that transient events are not necessarily terminal for specialist taxa but can push these taxa to their ecological limit, which potentially influences their abundance and community composition for millions of years. Rather than complicating our understanding of planktonic foraminifera responses in the middle Eocene, we argue that measuring at two size fractions illuminates size dynamics more fuly to enhance our understanding of palaeooceanographic drivers of biotic turnover. In particular, by documenting the smaller size fraction, we were able to record smaller and more microperforate taxa, not normally measured, to show how rare taxa can provide equivalent ecological function to those taxa that are lost and

inform our understanding of environmental perturbations and how communities to persist through climate fluctuations.

Chapter 3 Searching for function: Reconstructing adaptive niche changes using geochemical and morphological data in planktonic Foraminifera

3.1 Abstract

Dead species remain dead. The diversity record of life is littered with examples of declines and radiations, yet no species has ever re-evolved following its true extinction. In contrast, functional traits can transcend diversity declines, often develop iteratively and are taxon-free allowing application across taxa, environments, and time. Planktonic foraminifera have an unrivalled, near continuous fossil record for the past 200 million years making them a perfect test organism to understand trait changes through time, but the functional role of morphology in determining habitat occupation has been questioned. Here, we use single specimen stable isotopes to reconstruct the water depth habitat of individual planktonic foraminifera in the genus *Subbotina* alongside morphological measurements of the tests to understand trait changes through the Middle Eocene Climatic Optimum (MECO: ~40 Myr ago (mega annum, Ma)). The MECO is a geologically transient global warming interval that marks the beginning of widespread biotic reorganizations in marine organisms spanning a size spectrum from diatoms to whales. In contrast to other planktonic foraminiferal genera, the subbotinids flourished through this interval despite multiple climatic perturbations superimposed on a changing background climate. Through coupled trait and geochemical analysis, we show that *Subbotina* survival through this climatically dynamic interval was aided by trait plasticity and a wider ecological niche than previously thought for a subthermocline dwelling genus supporting a generalist life strategy. We also show how individually resolved oxygen isotopes can track shifts in depth occupancy through climatic upheaval. During and following the MECO, temperature changes were substantial in the thermocline and subthermocline in comparison to the muted responses of the surface ocean. In our post-MECO samples, we observe restoration of planktonic foraminifera depth stratification. Despite these changing temperatures and occupied depths, we do not detect a contemporaneous morphological response implying that readily available traits such as test size and shape do not have a clear functional role in this generalist genus. Modern imaging measurement technologies offer a promising route to gather more informative morphological traits for functional analysis, rather than the traditional candidates that are most easily measured.

3.2 Introduction

Existence in an ecosystem implies importance. Abundance estimates and extinction rates are key measures used to monitor efforts to conserve species but counting alone cannot accurately demonstrate the health of an ecosystem and the species within it (Akçakaya et al., 2020). To be present in an ecosystem an organism must have a role, and thus a function (Jax, 2005), which is fluid through time, space and biota (Akçakaya et al., 2020). The key is therefore not to merely note an organism's presence but to understand the traits that allows it to function within an ecosystem such as pollinator body and face hairiness which aids pollination (Stavert et al., 2016) or wing length which influences foraging distance (Brousseau, Gravel and Handa, 2018). Functional loss through species extinction can be undetectable, if another species has the same or a similar function, or non-linear and saturating (Cardinale et al., 2012), with the smallest of functions having large impacts on ecosystem health (Akçakaya et al., 2020). But function is not yet used effectively in conservation. For example, functional rarity is highest for species not identified at risk on the IUCN red list in global coral reefs (Grenié et al., 2018) and simulations based on Californian bee populations show the most functionally efficient and important bees (from an analysis of 12 species/genera) are most at risk of extinction (Larsen, Williams and Kremen, 2005). Therefore, identifying and understanding function is of paramount importance.

Simply described, a function typically describes some form of ecological process (Farnsworth, Albantakis and Caruso, 2017) yet applying this definition in ecology has led to much ambiguity (Farnsworth, Albantakis and Caruso, 2017; Jax, 2005). In modern ecosystems, assigning function to a trait can be done through observation and experiments with direct reference to human requirements and usefulness (Mace et al., 2014). In-situ observations are one dimensional, however, and if the past is the key to predicting the future (Tierney et al., 2020), then we need to test modes of inference of how organisms lived thousands to millions of years ago and we need to be able to integrate modern and fossil functional indices. In the fossil record, direct observations of physiology and ecological function are typically not possible, so we are often left instead to infer an organism's functional role in its community from the preserved morphological traits. Such traits may therefore be a viable currency to "bind the past and present together" (Eronen et al., 2010). Here, we relate morphological traits in fossilized planktonic foraminifera to inferred depth habitats, derived from geochemical measurements, through climatic change during the middle Eocene (~48 to 38 Ma).

We define a trait as any morphological, physiological, phenological or behavioural feature measurable at the individual level (Violle et al., 2007). Traits are the avenue through which an organism interacts with its environment (biotic and abiotic) (Lacourse, 2009; Oksanen et al., 2019) and determine whether an organism survives or meets its demise in a changing environment

(McGuire and Lauer, 2020). Thus, traits capture the most important aspects of the environment, and consequently it is the trait and not taxonomic identity that is crucial (Lacourse, 2009). For a trait to be classed as functional, it must, directly or indirectly, impact individual performance and fitness of species (McGill et al., 2006).

Taxon-free traits are a specific class of traits that transcend taxonomic classification and provide a commonality to allow comparisons across communities in different climatic and geographical settings (McGill et al., 2006). Often these traits are phenotypic such as dental morphology (e.g McGuire and Lauer 2020; Renaud et al. 2005; Oksanen et al. 2019; Žliobaitė et al. 2016), overall body geometry (Antczak-Orlewska et al., 2021; Di Martino and Liow, 2021; Bregman, Sekercioglu and Tobias, 2014; Macumber et al., 2020; Pimiento et al., 2017) and, in our study system planktonic foraminifera, test morphology (Schmidt et al., 2004; Rego et al., 2012; Payne et al., 2012; Schmidt et al., 2006; Brombacher et al., 2017; Baumfalk et al., 1987; Huber, Bijma and Darling, 1997; Kucera et al., 2017; Renaud and Schmidt, 2003; Weiner et al., 2015; Weinkauf et al., 2014, 2019). Traits can also include ecological traits like habitat (Bregman, Sekercioglu and Tobias, 2014; Pimiento et al., 2017) and feeding behaviour (Bregman, Sekercioglu and Tobias, 2014). Despite morphological traits being collected in abundance (Parr et al., 2012), trait-based research on fauna is reduced compared to flora (Lacourse, 2009; Steinthorsdottir et al., 2016; Lavorel and Garnier, 2002; Fried et al., 2019; Birks, 2020), which has resulted in a plethora of plant-based data bases (e.g. TRY (Kattge et al. 2020); LEDA (Kleyer et al. 2008) and BIEN (Enquist et al. 2016)). One reason for this discrepancy, is that faunal morphological traits were collected before the birth of trait-based ecology and are therefore not located in easy-to-access databases and require advancements and applications of text mining tools (Parr et al., 2012). Another fundamental issue is that plants make up 81% of global biomass compared to the 0.73% made up by protists (including planktonic foraminifera) and 0.37% made up by animals (Bar-On, Phillips and Milo, 2018), meaning flora is more accessible for research. One promising approach then is to apply trait-based methods in the geological record to understand faunal responses to environmental change.

We have the clearest indication of the impact of extinction on species richness/taxon counts in the deep time fossil record, but assignment of a functional trait in extinct species implies some knowledge of the environment (Violle et al., 2007), as well as an observation of how the trait reacts to climatic fluctuations (Eronen et al., 2010). This correlative or causal relationship allows us to infer the (biotic and abiotic) environment from the traits observed, or vice versa if we wish (Eronen et al., 2010). If function only exists within the context of the broader community, then this inference is particularly challenging and prone to inconsistent extrapolation. Ideally, we should measure traits with an inferred ecological function alongside an environmental indicator that indicates habitat, and then seek to match the two signals.

Our goal in this study is to understand trait changes within the context of a broader community undergoing large-scale abiotically induced change. We present new morphological and geochemical data on planktonic foraminifera. Planktonic foraminifera are extant, holoplanktonic, single celled organisms that build calcite shells (tests) that, upon death, rain down in abundance to the seafloor contributing significantly to deep-sea biogenic carbonate (Vincent and Berger, 1981). Foraminifera tests provide a near continuous, spatially and temporally high-resolution fossil record dating back ~ 200 Myrs to the Jurassic (Fraass, Kelly and Peters, 2015). Additionally, planktonic foraminifera are currently represented by ~ 50 extant species (Kucera, 2007) meaning specimens can be cultured in the lab (e.g., Bé, Caron, and Anderson 1981; Bé, Spero, and Anderson 1982; Bijma, Faber, and Hemleben 1990; Spero and Lea 1993; Fehrenbacher et al. 2018; Holland et al. 2020; Henehan et al. 2017; Burke et al. 2018), yielding an ever-growing knowledge of micro and macroscale influences on foraminifera life-history. In addition, our understanding of what are functional traits in foraminifera is increasing. Some traits have obvious function such as spines for feeding (Hemleben et al., 1991) or the presence of symbionts (Takagi et al., 2019; Bé, Caron and Anderson, 1981; Bé et al., 1977; Bé, Spero and Anderson, 1982). Recent studies, building on previous hypotheses, have shown that pores on foraminifera tests may be functionally linked to gas exchange (Bé, 1968; Baumfalk et al., 1987; Burke et al., 2018) but are only measured reliably from the inside of the test requiring scanning electron microscope (SEM) images or micro-CT scanning (Constandache, Yerly and Spezzaferri, 2013; Burke et al., 2018). In contrast, traits such as test shape and size must have a function, but what those functions are remain highly debated (Caromel et al., 2014; Renaud and Schmidt, 2003; Burke and Hull, 2017).

A high-resolution fossil record, advances in morphological measurements and increasing knowledge of function mean planktonic foraminifera are an ideal candidate to investigate trait-based responses to environmental change in the geological record. Furthermore, geochemical methods are advancing at an astounding rate making ecological inferences such as life history, metabolic rate, gene flow and geolocations accessible in deep time (Trueman, Chung and Shores, 2016). In planktonic foraminifera these advances have allowed geochemical measurements to be taken at the level of the individual, enhancing our knowledge of palaeoclimate (Schmitt et al., 2019a; Thirumalai et al., 2013; Glaubke et al., 2021) and the impact of individual planktonic foraminifera ecology on geochemical signatures (Fehrenbacher et al. 2018; Eggins, De Deckker, and Marshall 2003; Groeneveld, Ho, and Mohtadi 2019; Eggins, Sadekov, and De Deckker 2004; Friedrich et al. 2012; Weinkauf et al. 2020). We leverage these advances in analytical techniques alongside the exemplary evolutionary record of planktonic foraminifera to investigate trait, organismal and community responses to climatic change on geological timescales. Here, we focus on planktonic foraminifera trait changes across a transient warming event known as the Middle Eocene Climatic Optimum (MECO).

The Eocene was a time of global climatic and biotic restructuring. Following the "Hothouse" interval from the Paleocene-Eocene Thermal Maximum (PETM; 56 Ma (Westerhold et al., 2020)) through the Early Eocene Climatic Optimum (EECO; 48 Ma (Westerhold et al., 2020, 2018)), global climate gradually cooled (Cramer et al., 2009; Zachos et al., 2001; Zachos, Dickens and Zeebe, 2008). This long-term cooling trend culminated at the Eocene-Oligocene Climatic Transition (EOT; 34 Ma, (Westerhold et al., 2020; Hutchinson et al., 2021)) with the onset of large-scale glaciation on Antarctica (Coxall et al., 2005; Zachos, Quinn and Salamy, 1996). The early to middle Eocene is punctuated by multiple short-lived (~40–200 kyrs) transient global warming events or "hyperthermals" (Westerhold et al., 2020). During the middle Eocene there was a ~270–500-kyr transient warming event known as the Middle Eocene Climatic Optimum that interrupted the long-term cooling trend (Bohaty et al., 2009; Bohaty and Zachos, 2003; Edgar et al., 2020; Rivero-Cuesta et al., 2019). The MECO was recognised by a progressive shift to lower deep-sea $\delta^{18}O$ values records between ~40.6 Ma and 40 Ma followed by an abrupt return to higher $\delta^{18}O$ values (Bohaty et al., 2009). Interpretations of this shift suggest a gradual ~ 3 – 6 °C increase in surface and deep waters (Bohaty and Zachos, 2003; Cramwinckel et al., 2019; Bijl et al., 2010; Henehan et al., 2020; Bohaty et al., 2009) followed by a rapid 200-kyr cooling to pre-excursion temperatures (Bohaty et al., 2009). This upheaval is the pre-cursor to the restructuring of planktonic foraminifera communities in the proceeding 6 Myrs, which included the progressive loss of characteristic Eocene surface dwellers that were host to algal photosymbionts (Wade, 2004; Ezard et al., 2011; Fraass, Kelly and Peters, 2015), a reduction in morphological (Schmidt, 2004) and assemblage complexity (Schmidt, 2004; Wade and Pearson, 2008). We use the MECO as an exemplar to test for functional shifts amongst the contemporaneous planktonic foraminifera community.

3.3 Materials and Methods

3.3.1 Material and sample preparation

Samples were taken from two scientific drillholes on the North Atlantic Southeast Newfoundland Ridge in the northwest Atlantic Ocean, ~700 km east-southeast of Newfoundland, which were cored during International Ocean Discovery Program (IODP) Expedition 342 at Sites U1408 (41°26.3'N, 49°47.1'W) and U1410 (41°19.6993'N, 49°10.1847'W) (Norris et al., 2014). The material collected from these sites is dominated by clay-rich drift sediments that were deposited at seafloor depths well above the average late Paleogene carbonate compensation depth (CCD) (Norris et al., 2014; Boyle et al., 2017). The clay-rich lithology resulted in good to excellent preservation of carbonate microfossils including foraminifera (Boyle et al., 2017; Norris et al., 2014), with most specimens appearing "glassy" under light microscope observations indicating

little or no diagenetic alteration of the calcite (Sexton, Wilson and Pearson, 2006a). Sample ages were calculated based on an age–depth model constructed using available biostratigraphic and magnetostratigraphic data for Sites U1408 and U1410 (Norris et al., 2014; Yamamoto et al., 2018; Cappelli et al., 2019). Age calibrations from the 2012 geologic timescale were used for middle Eocene geomagnetic polarity reversals (GTS2012;(Gradstein et al., 2012). Six samples that span the MECO (~38.50 to 43.50 Ma) were selected with a ~0.5–1-Myr sample spacing (Table B.1).

Each sample was dried at 40°C for four days and then soaked in sodium hexametaphosphate for a minimum of four days on a shaker table to disaggregate the sediment. Samples were then washed over a 38 µm sieve using deionized water until the water ran clear and then dried overnight in a 40°C oven overnight before being transferred to vials. Each sample was subsequently dry sieved to allow picking of individual specimens under the light microscope. For multi-specimen analysis (Section 3.3.2) foraminifera were picked from a narrow sieve size fraction of 250–315 µm to avoid the effects of foraminifera size on geochemical analysis. For the individual foraminifera analysis (Section 3.3.3.2) we picked from the >180 µm size fraction to capture the widest range of morphological variation from the adult population.

3.3.2 Stable isotope analysis

Planktonic foraminifera occupy different depth niches within the water column creating an ecologically stratified community. As a result of isotopic fractionation in the water column, the stable isotopic signature of planktonic foraminifera tests reflects the depth habitat in which they live. The fractionation of oxygen into foraminifera calcite is temperature dependent, resulting in increasing foraminifera test $\delta^{18}O$ values with increasing depth paralleling the trend of decreasing temperature with depth in the oceans (Fairbanks, Wiebe and Bé, 1980; Fairbanks et al., 1982). The opposite depth dependent trend is seen in carbon isotopes with foraminifera calcite $\delta^{13}C$ values decreasing with depth. This relationship is due to the preferential uptake of ^{12}C during photosynthesis at shallow water depths and the export of particulate organic carbon from the upper water column. Remineralization of particulate organic carbon at depth then releases isotopically light carbon back into the dissolved inorganic carbon (DIC) pool. Thus, surface ocean symbiont-hosting foraminifera have relatively low $\delta^{18}O$ values and high $\delta^{13}C$ values relative to non-symbiont subthermocline dwellers with thermocline dwelling sitting somewhere in-between (Figure 3.1). These relationships do assume isotopic equilibrium between the foraminifera test and seawater. However, this equilibrium is offset by a number of physical parameters such as salinity, carbonate ion concentration (Epstein et al., 1953; Epstein and Lowenstam, 1954; Pearson, 2012a; Spero et al., 1997; Urey, 1947; Urey et al., 1951) as well as foraminifera biology and ecology often referred to as “vital effects” (Bemis, Spero and Bijma, 1998a; Birch et al., 2013; Erez, 1978; Friedrich et al., 2012a; Spero, Lerche and Williams, 1991; Spero and Williams, 1989).

These factors, especially foraminifera biology (Edgar, Hull and Ezard, 2017), tend to impact test $\delta^{13}C$ values more than $\delta^{18}O$ values and can be minimized, for example, by picking foraminifera within a narrow size fraction. Nevertheless, the broad patterns of depth ranking using $\delta^{18}O$ values and $\delta^{13}C$ values (Figure 3.1) remains true and can be used to reconstruct foraminifera depth habitats through geological time (Birch et al., 2013; Coxall et al., 2007; Pearson, 1998; Pearson et al., 2001; Sexton, Wilson and Pearson, 2006, 2006; Spero, 1998). To investigate water column structure across our study interval, planktonic foraminifera from genera representing three depth ecologies were picked: *Globigerinatheka* (mixed layer), *Subbotina* (thermocline) and *Catapsydrax* (sub-thermocline) (Figure 3.1).

We use the symbiont bearing, deep mixed layer dwelling *Globigerinatheka* (Edgar et al., 2013; Sexton, Wilson and Pearson, 2006b) to represent the mixed layer (Figure 3.1) rather than other commonly used shallower mixed layer inhabitants *Acarinina* or *Morozovelloides*. *Morozovelloides* which were not abundant enough in our samples for statistically robust isotope or morphological analyses, whilst *Acarinina* were abundant but showed signs of reworking (stained and heavily fragmented) and recrystallisation. We made every effort to pick individuals with no visible signs of either gametogenic calcite or recrystallized wall textures and were mindful of the caveats during interpretation. To represent the thermocline and subthermocline we used asymbiotic *Subbotina* and *Catapsydrax,* respectively (Figure 3.1).

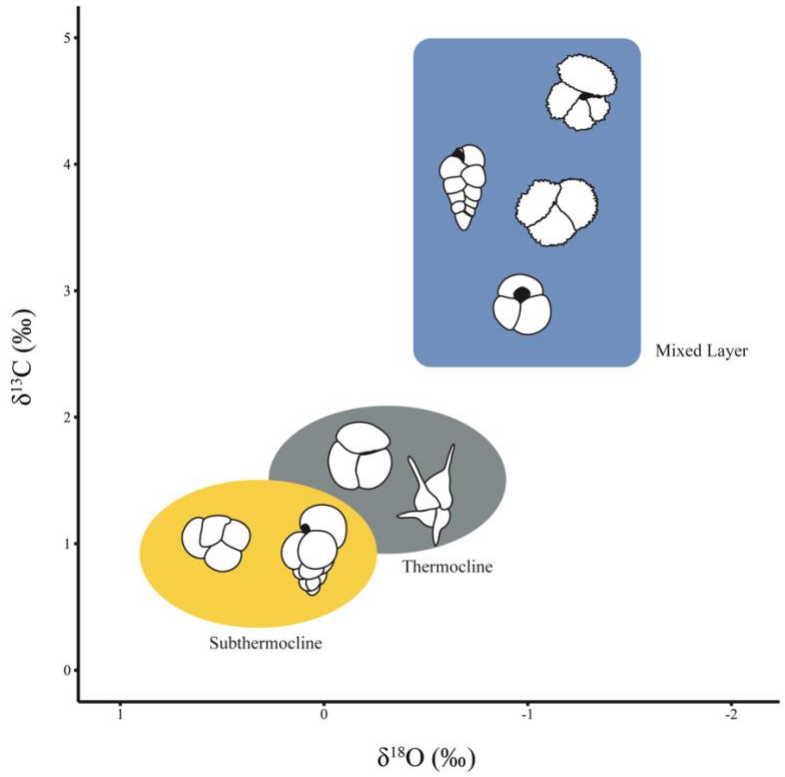

Figure 3.1 Schematic figure showing the three main ecogroups as defined in Aze et al (2011) based on stable isotope measurements. This figure is illustrative and does not represent absolute values for each ecogroup. Top to bottom the mixed layer is represented by schematic outlines of *Acaranina spp.*, *Chiloguembelina spp.*, *Morozovelloides spp.* and *Globigerinatheka spp.* Left to right the thermocline is represented by *Subbotina* spp. and *Hantkenina* spp. and the subthermocline represented by *Catapsydrax* spp. and *Jenkinsina* spp. Note the reversed scale on the x-axis. Modified from Pearson (1998).

Approximately 20 individuals from each of *Globigerinatheka* spp., *Subbotina* spp. *(S. utilisindex, S. eoceana, S. projecta and S. linaperta)* and *Catapsydrax unicavus* were picked from each of the 6 samples following the taxonomy of Pearson et al. (2006). The 18 subsamples, each of 20 individuals, were then crushed, homogenised and weighed into vials. Each subsample weighed between 50 µg and 60 µg and was then cleaned by ultrasonification in ethanol for 3–5 seconds, rinsed in deionized water and then placed in a 40 °C oven for 1–2 hours to dry. Coupled $\delta^{18}O$ and $\delta^{13}C$ measurements (Table B.2) were analysed in the Stable Isotope Mass Spectrometry Laboratory at the National Oceanographic Centre, University of Southampton, using a Thermo Fisher Scientific Kiel IV carbonate device coupled to a MAT253 stable isotope ratio mass spectrometer. All samples were measured against the reference standards NBS19 and NBS18, as well as an in-house quality control standard (GS1) and then standardised using a two-point

calibration between NBS19 and NBS18 to Vienna Pee Dee Belemnite (VPDB). Long-term analytical precision based on repeat analysis of GS1 is estimated as ±0.09 ‰ for $\delta^{18}O$ values and ±0.05 ‰ $\delta^{13}C$ values for bulk analysis.

3.3.3 Individual foraminifera analysis

To investigate the link between functional traits and environmental change in deep time we use individual foraminifera analysis (IFA) on the extinct, thermocline dwelling, asymbiotic planktonic foraminifera genus *Subbotina* (Edgar et al., 2013). *Subbotina* was present globally in Earth's oceans from the early Paleocene through to the end of the Oligocene (~65-23 Ma) (Aze et al., 2011; Wade et al., 2011). During the middle Eocene, Subbotinids increased in abundance at multiple sites across the globe flourishing over a period detrimental to many other groups (Luciani et al., 2010; Macleod et al., 1990). A possible reason for this survival is a hypothesized adaptable depth ecology, which is suggested in various intervals of the Eocene based on stable isotope measurements (Arimoto et al., 2020; Bralower et al., 1995; Dutton et al., 2005; Macleod et al., 1990; Stap et al., 2010; Wade, 2004; Wade & Pearson, 2008). Their ecology, diversity fluctuations and depth habitat make *Subbotina* a versatile group to investigate the link between functional traits and the environment.

3.3.3.1 Individual morphological analysis

To collect morphological traits, 50 individuals of *Subbotina* were picked from each of the six sample residues (discarding specimens showing gametogenic overgrowth and evidence of reworking) resulting in 300 individuals in total. To obtain 50 *Subbotina* individuals per sample, each sample was split using a microsplitter until approximately 300 foraminifera remained, shown to represent the diversity of a sample (Al-Sabouni, Kucera and Schmidt, 2007). *Subbotina* were then picked from this 'split'. To avoid biasing because of an uneven distribution of individuals on the picking tray, individuals were picked from square cells on the picking tray chosen by a random number generator until 50 well-preserved *Subbotina* were picked per sample. *Subbotina* individuals were mounted on glass slides with the aperture facing upwards (umbilical view) using double sided sticky tape in groups of up to 20 for morphological analysis (Brombacher et al., 2017). Images of each block of 20 individuals were taken using a Leica M205C stereo microscope with IC90HD camera illuminated from above and then processed using Image Pro 9.1 Software. Automatic measurements of test area (size) and aspect ratio (shape) (Figure B.1) were taken using the automated image macro in Image Pro (Table B.3), which have high reproducibility (Brombacher et al., 2017). To maintain a similar scale across all analyses, size was log transformed and mean-centred around 0.

3.3.3.2 Single-specimen stable isotope analysis

In addition to the 18 multi-specimen foraminifera samples analysed, oxygen and carbon stable isotope ratios were determined for 120 *Subbotina* individuals. During the morphological analysis, described above, each individual from each sample was assigned a number from one to fifty. For each sample 20 individuals were chosen through computer generated random numbers with no replacement. Samples were cleaned in the same manner as the multi-specimen analysis described in section 3.3.2. Weights of individuals ranged from 13 µg to 21 µg with an average weight of 14 µg (Table B.4). To account for the range of weights, vials were loaded into the Kiel in batches, with each batch consisting of vials of individuals with similar weights so that the settings across the whole batch were optimised for a narrower size fraction. Eight samples out of the analysed 120 failed to record a measurement due to insufficient weight. Long term analytical precision based on GS1 for lower weights used in individual analysis are not available however the short-term analytical precision across runs was 0.14 ‰ for $\delta^{13}C$ values and 0.22 ‰ for $\delta^{18}O$ values.

3.3.4 Statistical methods

Ordinary least squares linear models constructed in the R environment (version 4.0.3; R Core Team 2020) were applied to investigate the drivers of planktonic foraminifera $\delta^{18}O$ values and $\delta^{13}C$ values. Separate models were built with $\delta^{18}O$ values and $\delta^{13}C$ values as the dependent variable and a combination of environmental ($\delta^{18}O$ values and Age), ecological ($\delta^{13}C$ values) and morphological (test area and test aspect ratio) traits as the independent variables. Numerous models were constructed with varying degrees of interaction. Models were compared using analysis of variance and the best model chosen based on likelihood ratio tests and Akaike Information Criterion (AIC). Clustering analysis was conducted with a Gaussian finite mixture model using the mclust package (Scrucca et al., 2016) with the best model and thus number of clusters chosen using the Bayesian Information Criterion (BIC). The influence of sample age on morphological and stable isotope variables was tested using one-way analysis of variance (ANOVA).

3.4 Results

3.4.1 Palaeoceanographic changes based on multi-specimen analyses

To analyse our trait data in the context of local MECO palaeoceanographic changes, we generated stable isotope records from three genera at each of the sites each with different depth habitats (Figure 3.2, Table B.2). *Globigerinatheka* show the lowest $\delta^{18}O$ values across the interval compared to *Catapsydrax* and *Subbotina* (Figure 3.2A). Between 43.50 and 41.31 Myrs

Globigerinatheka $\delta^{18}O$ values increased by 0.25 ‰, over the same interval *Subbotina* $\delta^{18}O$ values increased by 0.72 ‰ whilst *Catapsydrax* increased by 1.03 ‰ (Figure 3.2A). Then at 40.14 Ma all genera show a decrease in $\delta^{18}O$ values with *Globigerinatheka* decreasing by 0.21 ‰, *Subbotina* by 0.64 ‰ and *Catapsydrax* by 1.50 ‰ (Figure 3.2A). Following the MECO to the end of our record at 38.50 Ma both *Globigerinatheka* and *Catapsydrax* show gradual increases in $\delta^{18}O$ values (0.41 ‰ and 1.40 ‰ respectively; Figure 3.2A). In contrast *Subbotina* shows an increase in $\delta^{18}O$ values of 0.89 ‰ at 39.56 Ma followed by a decrease of 0.17 ‰ at 38.50 Ma (Figure 3.2A).

The vertical thermal structure of the water column can be assessed by calculating the difference in $\delta^{18}O$ values between surface water dwellers (*Globigerinatheka*) and deeper dwellers (*Subbotina* (thermocline) and *Catapsydrax* (subthermocline): $\Delta\delta^{18}O_{surface\text{-}deep} = \delta^{18}O_{Catapsydrax\text{-}Subbotina} - \delta^{18}O_{Globigerinatheka}$ (Figure 3.3A, Table B.5). A multiple linear regression using the $\delta^{18}O$ difference between *Globigerinatheka* and the two deeper dwelling genera (*Subbotina* and *Catapsydrax*) as the response variable showed a significant impact on the habitat differences in oxygen isotope space ($p < 0.001$) and in the MECO ($p < 0.01$) interval (Table B.6). There was a predicted 0.71 ± 0.11 ‰ overall decrease in the $\delta^{18}O$ gradient between *Globigerinatheka* and the deeper dwelling genera (*Subbotina* and *Catapsydrax*) across the study interval compared to the gradient change observed in $\delta^{13}C$ values (Figure 3.3, Table B.6). Additionally, there was a predicted 0.56 ± 0.15 ‰ decrease in overall isotopic gradient (both $\delta^{18}O$ values and $\delta^{13}C$ values) during the MECO interval compared to the other time slices, which was primarily due to a reduction $\delta^{18}O$ gradient between all genera (Figure 3.3, Table B.6). An adjusted R^2 of 0.69 shows that 69 % of variation in isotopic differences in Figure 3.3 can be explained by a model that includes isotope grouping (carbon and oxygen) and interval grouping (MECO or not). The $\Delta\delta^{18}O_{surface\text{-}Catapsydrax}$ is between 0.52 ‰ and 1.30 ‰ for most of the interval except at 40.14 Ma where $\Delta\delta^{18}O$ is 0.01 (Figure 3.3A). At this time, both *Globigerinatheka* and *Catapsydrax* have $\delta^{18}O$ values of -1.31 ‰ and -1.30 ‰, respectively. *Subbotina*, with an inferred intermediate depth habitat, records a $\delta^{18}O$ value of -1.12 ‰ (Figure 3.2A).

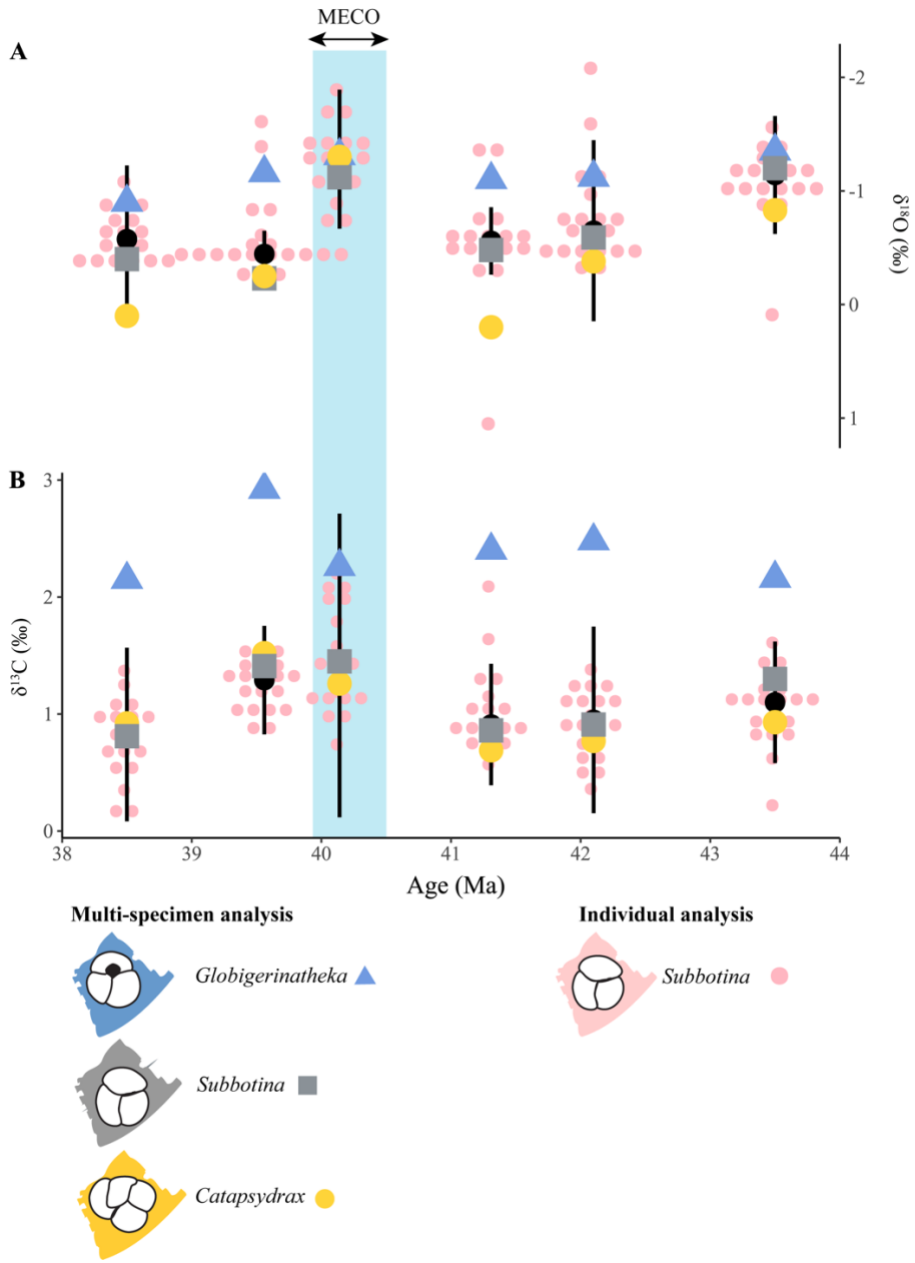

Figure 3.2 Oxygen (A) and carbon (B) stable isotope results from individual foraminifera analysis (IFA) and batch multi-specimen analysis. Small pink circles show IFA of Subbotina, where circles are stacked horizontally multiple individuals have the same measurement. The genera used in batch analysis are represented by consistent colouring and shapes across each time slice: Globigerinatheka = blue triangles, Subbotina = grey squares and Catapsydrax = yellow circles. The black circle and vertical lines represent summary statistics from IFA with the circle representing the median and vertical line indicating 2.5 absolute standard deviations of the median (MAD). Note the reversed y- axis on panel A. The vertical blue box indicates the position of the MECO.

Globigerinatheka consistently show the highest $\delta^{13}C$ values of the measured genera throughout the study interval, and their values stay within a narrow $\delta^{13}C$ value range throughout (between 2.15 ‰ and 2.92 ‰; Figure 3.2B) with the highest $\delta^{13}C$ value recorded immediately after the MECO. *Subbotina* and *Catapsydrax* consistently yield $\delta^{13}C$ values > 1.00 ‰ lower than *Globigerinatheka* and show their highest $\delta^{13}C$ values in the MECO and immediately after. *Subbotina* sits slightly above *Catapsydrax* in $\delta^{13}C$ space as expected based on their recorded depth habitat but following the MECO this relationship is reversed (Figure 3.2B).

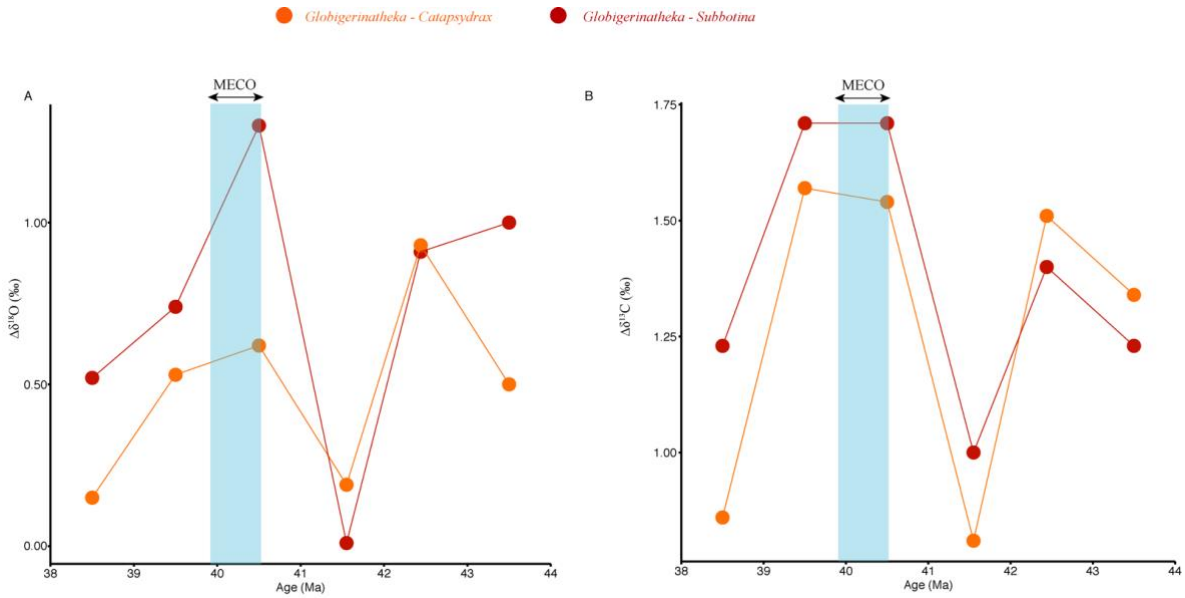

Figure 3.3 Stable oxygen (A) and carbon (B) isotope gradients between Globigerinatheka (surface) and Subbotina (thermocline) and Catapsydrax (subthermocline) across the MECO interval. As the line approaches zero the isotopic gradient between the different genera is reduced, with 0 indicating no difference in isotopic signature between the different depth habitats. The vertical blue box indicates the MECO.

3.4.2 Individual geochemical analysis of *Subbotina*

Individuals of *Subbotina* show variation around "batch" *Subbotina* measurements in both $\delta^{18}O$ and $\delta^{13}C$ space (Figure 3.2). However, the batch *Subbotina* measurements plot within 1 standard deviation of the median of the individual foraminifera analyses (IFA; black circle, Figure 3.2) in each time slice. This is expected and indicates that IFA analysis draws out intraindividual variation within a genus. The range in IFA $\delta^{18}O$ values at each time slice, apart from at 38.5 Ma, is consistently > 1 ‰, with the widest ranges observed prior to the MECO where one to three analyses sit outside of two absolute deviations of the median (Figure 3.2A). These "extreme" values sit apart from the rest of the measurements in each sample. For example, at 41.31 Ma one

positive $\delta^{18}O$ value leads to the largest range across the interval of 2.44 ‰ (Figure 3.2A). Only at 40.14 and 38.50 Ma do all measurements sit within 2.5 absolute deviations of the median. Although these points are more "extreme" there is no reason that they should be excluded. In all samples some individual *Subbotina* measurements plot within the same space or above that of the *Globigerinatheka* batch measurements (Figure 3.2A). In contrast to $\delta^{18}O$, individual measurements of *Subbotina* in $\delta^{13}C$ space are overall more spaced out with limited or no clusters. The range of $\delta^{13}C$ values in each time slice is >1.00 ‰ throughout with the largest range seen between 40.14–41.31Ma around the MECO. The exception is at 39.56 Ma where it is 0.70 ‰ (Figure 3.2B). Unlike $\delta^{18}O$, *Subbotina* individuals are consistently below and separated from batch *Globigerinatheka* $\delta^{13}C$ values albeit with a reduction in this separation at the MECO (Figure 3.2B).

Cross plots of the individual *Subbotina* $\delta^{13}C$ values and $\delta^{18}O$ values measurements shows an apparent cluster of points in the middle of the plot (0.50–1.25 ‰ in $\delta^{13}C$ and -0.2– -1.2 ‰ in $\delta^{18}O$ space) with higher $\delta^{13}C$ values primarily from the MECO plotting to the side (Figure 3.4). To determine whether the MECO data genuinely represent a separate cluster of points, a clustering analysis was conducted using a Gaussian finite mixture model. The analysis revealed a spherical, varying volume model with two clusters fitted the data best with a BIC of -255 (Figure B.2). This model split the 112 data points into two relatively even clusters (Cluster 1: n=53, Cluster 2: n=59, Table B.7). The cluster classification does not cleanly follow the boundaries of our pre-defined time slices (Figure 3.4), with all but three data points from the MECO time slice and one from 43.50 Ma within a separate cluster (Cluster 1) along with some individuals from each other time slice. The MECO and oldest time slice cluster together as these two samples are climatically similar, as indicated by $\delta^{18}O$ values, thus the cluster captures the transient warming interval and the earliest stage of the global cooling trend, respectively.

Although clustering analysis identifies two clusters from the data, there is uncertainty particularly where the clusters are in close contact when the $\delta^{18}O$ value is around -1.00 ‰ (Figure 3.4). To investigate this signal further, one-way ANOVAs were fitted on carbon and oxygen separately with age as the groups. There was a statistically detectable difference between time slices in both $\delta^{18}O$ values ($F(5,106) = 11.84$, $p < 0.001$) (Table B.10) and $\delta^{13}C$ values ($F(5,106) = 9.84$, $p < 0.001$) (Table B.12). A post-hoc TUKEY HSD test showed this difference to only be significant in $\delta^{18}O$ values between the MECO sample (40.14 Ma) and all other samples except for 43.50 Ma at the beginning of the record ($p < 0.001$) supporting the clustering analysis (Table B.11). In $\delta^{13}C$ values, the same post-hoc test showed no detectable difference between the start (43.50 Ma) and end (38.50 Ma) of the record, but a supported a difference between the MECO and all pre-MECO samples ($p < 0.05$) (Table B.13). This, along with the clustering analysis, strengthens the inference that *Subbotina* isotopic variation is more nuanced in $\delta^{13}C$ values than $\delta^{18}O$ values, likely through the increased role of biological "vital effects".

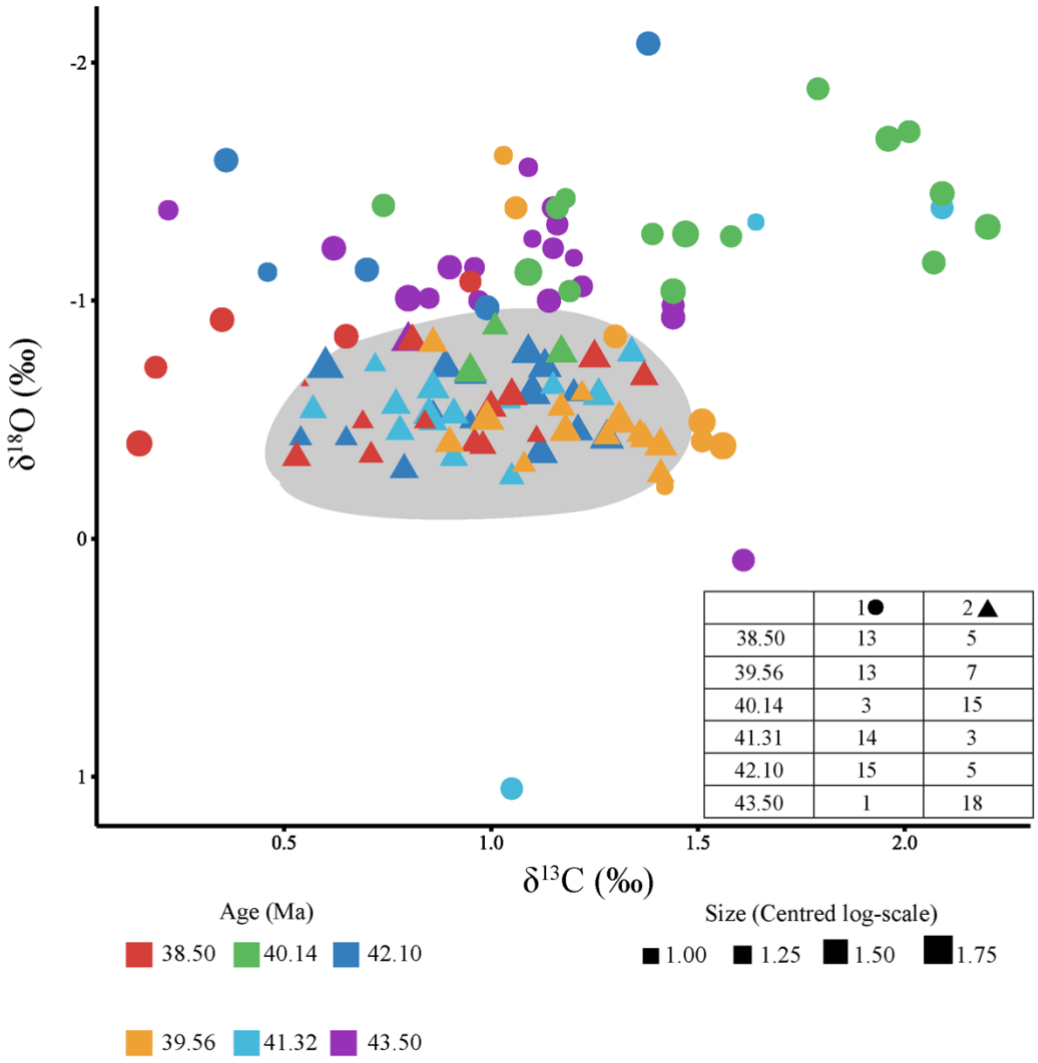

	1●	2▲
38.50	13	5
39.56	13	7
40.14	3	15
41.31	14	3
42.10	15	5
43.50	1	18

Figure 3.4 Cross plot of carbon versus oxygen isotope values for individual Subbotina analysis. Individual point size represents the size (area) of each individual on a log scale. The symbol (triangle vs circle) indicates the cluster that each individual was assigned to following cluster analysis. Circles represent cluster 1 and consist primarily of individuals from 40.14 and 43.50 Ma as highlighted in the table inset into the figure, while triangles represent cluster 2. The number of individuals in each time slice assigned to each cluster is shown in the inset table. The grey area visually represents cluster 2 as identified by the model.

3.4.3 Understanding drivers of individual foraminifera analysis

Morphological traits of test shape (test aspect ratio) and size (mean-cantered test area on log scale) were also made on 300 *Subbotina* individuals including the 120 individuals that were used for geochemical analysis. Considering the full morphological dataset, both size and shape show large ranges in all samples with no clear trend with sample age (Figure 3.5). A one-way ANOVA showed detectable differences between time slices in both mean shape ($F_{(5,294)}=3.171$, $p < 0.01$) (Table B.14) and size ($F_{(5,294)}=3.185$, $p < 0.01$) (Table B.15). Used in isolation these traits give us little information, so we integrated the 120 individuals that had both morphological (size) and stable isotope measurements (Table B.4) into multiple linear regression models because size has an impact on stable isotope and trace element expression in planktonic foraminifera (Friedrich et al., 2012; Elderfield, Vautravers and Cooper, 2002).

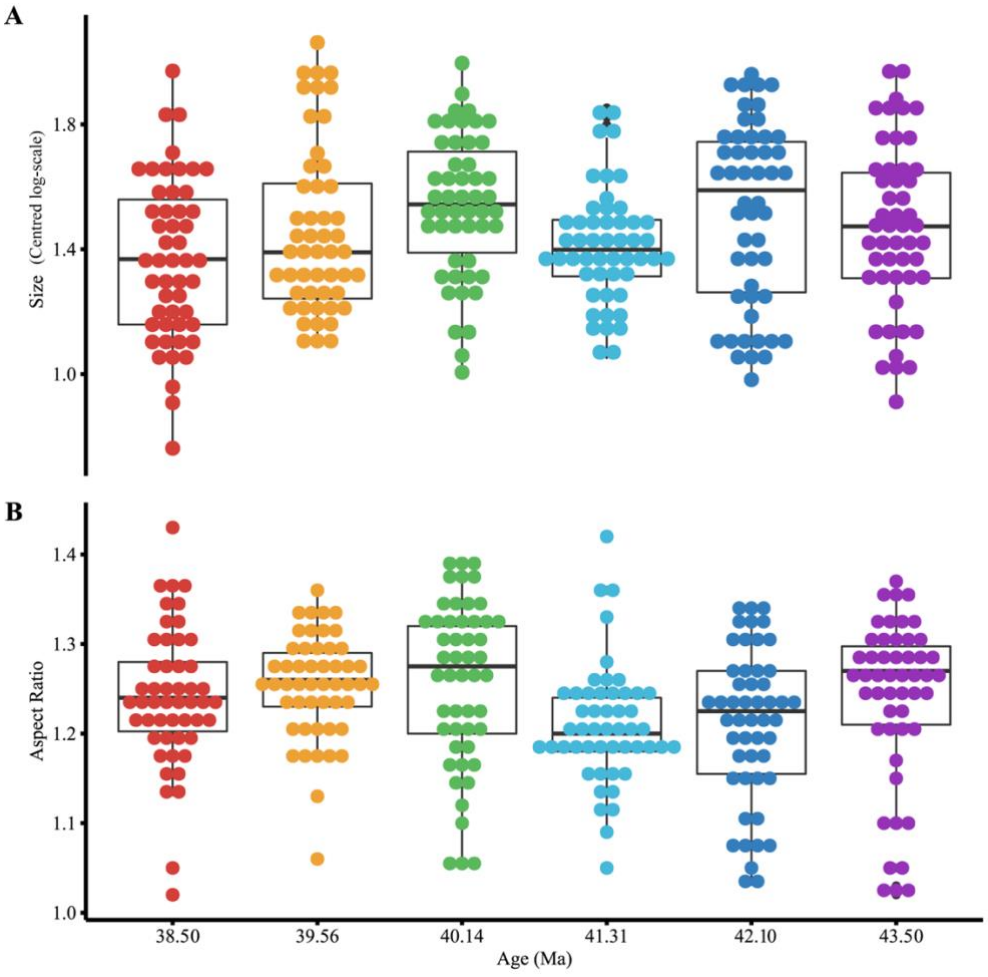

Figure 3.5 Morphological (test size (A) and test aspect ratio (B)) variation of all Subbotina measured in this study (n=300). Size is on a log scale so has no unit of measure. The box represents the interquartile range whilst the whiskers show 1.5*interquartile range. The black line represents the median. Individual filled symbols represent all individual specimens sampled.

The best supported carbon isotope model included an interaction between $\delta^{18}O$ values and size with an adjusted R^2 of 0.28 (Table B.16). Of the predictors included, only age at 40.14 Ma and 39.56 Ma differed detectably from the baseline $\delta^{13}C$ value at 38.50 Ma ($p < 0.001$) (Table B.17). At 39.56 and 40.14 Ma (MECO) $\delta^{13}C$ value is predicted to increase by 0.46 ± 0.11 ‰ and 0.60 ± 0.13 ‰, respectively, compared to $\delta^{13}C$ value at 38.50 Ma (Table B.17). Our models predict a 0.10 ‰ decrease in Subbotina $\delta^{13}C$ value per log size unit increase, although this relationship is not significant (Table B.17). Removal of sample age and oxygen isotopes leaves size as the only explanatory variable results in a positive relationship between $\delta^{13}C$ values and size (0.29 ± 0.15 ‰ increase per log(size) increase), but not one that is detectably different from 0 (Table B.18). For oxygen isotopes a similar model with an interaction between $\delta^{13}C$ values and size was the most supported to explain individual *Subbotina* $\delta^{18}O$ values (Table B.19). Of the predictors $\delta^{13}C$ values, size and sample age, sample age was the main driver of individual Subbotina $\delta^{18}O$ values ($p < 0.001$). At 40.13 Ma (MECO) and 43.50 Ma, $\delta^{18}O$ values are predicted to decrease by 0.61 ± 0.15 ‰ and 0.44 ± 0.13 ‰ respectively compared to $\delta^{18}O$ values at 38.50 Ma (Table B.20). Replacing foraminifer size with weight yielded qualitatively similar results with best fitting model structure remaining the same (Tables B.21-B.24). The positive $\delta^{13}C$ value– weight relationship ($p < 0.05$) was qualitatively consistent with the inferred $\delta^{13}C$ value – size relationship, but weight explained more variation (lower residual sum of squares, Tables B.17 and B.22) than size.

Since we measured batch isotopes on foraminifera with three typically distinct depth ecologies (surface, thermocline and subthermocline), we can use the batch $\delta^{18}O$ values to understand the impact of water-depth temperature changes on *Subbotina* $\delta^{18}O$ values, a proposed thermocline dweller. We used the same model as above but with the age predictor replaced by surface, thermocline and subthermocline $\delta^{18}O$ measurements as a proxy for water depth temperature. It is the deeper ocean temperatures (thermocline and subthermocline), rather than surface ocean, that drive the individual foraminifera measurement of *Subbotina* $\delta^{18}O$ values ($p < 0.05$) (Table B.25). A subthermocline and thermocline oxygen isotope composition increase of 1.00 ‰ is predicted to increase *Subbotina* $\delta^{18}O$ values by 0.34 ± 0.16 ‰ and 0.44 ± 0.19 ‰, respectively, translating to a deepening depth habitat for *Subbotina* as the deeper ocean cools at a faster rate than the surface waters (Table B.25).

3.5 Discussion

Unpicking ecological signals from palaeoceanographic signals is difficult, but worthwhile because of the ability to study transient climatic events in deep time. The most common way to infer functionality in deep time is to look for a correlation between a morphological trait and ecological differences (Eronen et al., 2010). We show complicated morphological and geochemical

responses to the Middle Eocene Climatic Optimum (MECO, Figure 3.2 - Figure 3.5). The reduction of surface-deep $\delta^{18}O$ values and $\delta^{13}C$ value gradients in our study at the MECO (Figure 3.5) could be explained by: (i) hydrological changes causing the changes in "batch" isotopes observed but depth habitat of foraminifera remaining constant through the interval (Figure 3.6) discussed in Section 3.5.1.1; or (ii) ecological changes, with deeper dwelling foraminifera (*Catapsydrax* and *Subbotina*) migrating upwards in the water column to occupy a similar thermal habitat to that of *Globigerinatheka* (Figure 3.6) discussed in Section 3.5.2.1.

The carbon isotope signature ($\delta^{13}C$) of planktonic foraminifera is controlled by biology (Edgar, Hull and Ezard, 2017) and there are long established relationships between test size and $\delta^{13}C$ signal in planktonic foraminifera (Berger, Killingley and Vincent, 1978; Elderfield, Vautravers and Cooper, 2002; Friedrich et al., 2012; Oppo and Fairbanks, 1989; Spero, Lerche and Williams, 1991). The $\delta^{13}C$-test size relationship is commonly controlled in stable isotope analysis by using narrow size fractions intended to remove the relationship between $\delta^{13}C$ values and size. Unfortunately, this pre-emptive censoring also removes the correlation needed to infer functionality. In this study, we use a wide size fraction (>180 µm) and detect no relationship between *Subbotina* $\delta^{13}C$ and size (~47219 - 173204 μm^2) in either multivariate or univariate models when the presence of explanatory variables that track climatic fluctuations are removed ($\delta^{18}O$ values and sample age). Although only a single case study, the lack of size-$\delta^{13}C$ value relationship here has implications for studying functional traits in deep time where vast climatic changes can occur instantaneously in geological terms. Our discussion focusses on the challenges of interpreting these biologically driven isotopic signatures through periods of substantive environmental change.

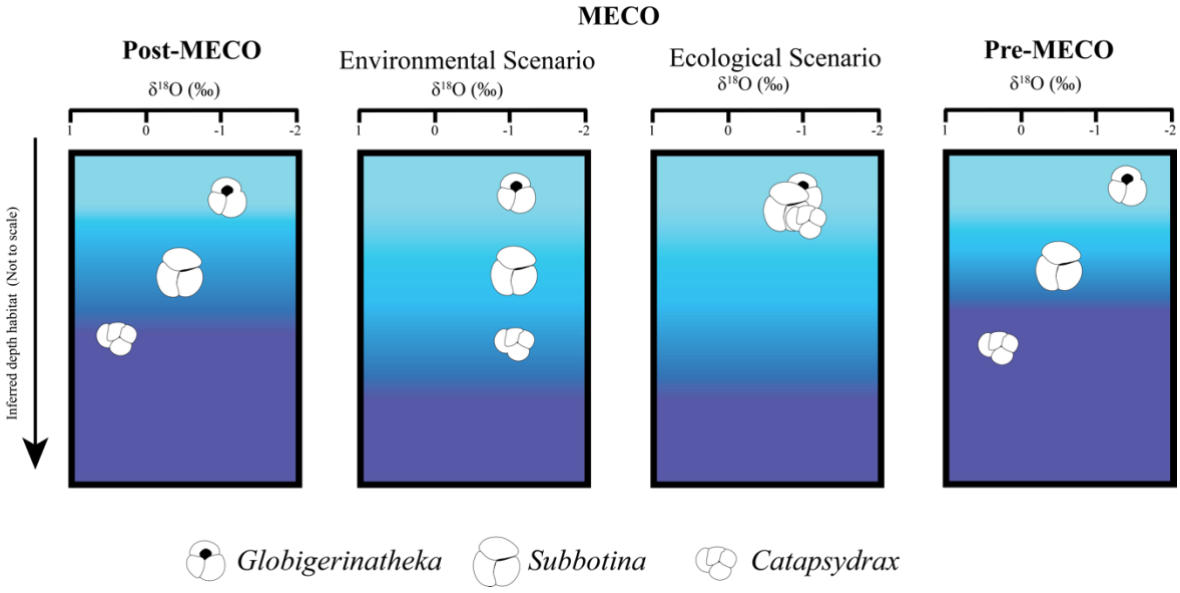

Figure 3.6 Schematic illustration of environmental versus ecological scenarios to explain the $\delta^{18}O$ isotopic gradient changes between genera. Colour gradient in all panels represents temperature change from warm (light blue) to cool (darker blue) temperatures.

3.5.1 Palaeoenvironmental changes

Applying trait-based studies on thousand-to-million-year time scales requires a thorough understanding of climatic and environmental variables. To provide an environmental dimension to our study, we will focus on palaeoenvironmental changes (Figure 3.6) across the 6 Myr focal interval using the inferred depth ecology of individual planktonic foraminifera alongside the measured $\delta^{13}C$ values and $\delta^{18}O$ values of the genera level isotopes. Through this comparison, we can infer potential water column thermal and trophic state changes across the MECO, which in concert with more temporally resolved studies can provide important climatic and environmental context for our trait-based analysis.

3.5.1.1 Water column thermal structure changes across the middle Eocene ($\delta^{18}O$ values)

The Eocene saw a gradual change from hothouse to icehouse climate punctuated by short-lived global warming events, the final globally recognized of which is the MECO (Cappelli et al., 2019). Prior to the MECO, a positive shift in benthic foraminifera $\delta^{18}O$ values at ~42 Ma in the Atlantic Ocean and other ocean basins (Coxall et al., 2000; Westerhold et al., 2020; Edgar et al., 2007; Cramwinckel et al., 2018) as well as nannofossil assemblage composition changes towards cool water taxa in the Southern Ocean at ~ 41.60 Ma (Villa et al., 2008, 2013) indicate that global temperatures were lower than in the early Eocene and that the transition from a hothouse to icehouse was already underway. Water column cooling resulted in increasing planktonic foraminifera depth habitat stratification (Figure 3.2 - Figure 3.3).

In our record from the Newfoundland margin, *Catapsydrax* and *Subbotina* show progressive $\delta^{18}O$ increases of 0.45 ‰ and 0.61 ‰, respectively, suggesting up to 2 ºC cooling of deep-water temperatures in comparison to the surface ocean by 41.44 Ma (Figure 3.2A). Thermal decoupling of the water column due to global cooling would result in the development of a strong, shallow thermocline and more thermally stratified water column prior to the MECO (43.50 Ma to 41.44 Ma; Figure 3.2A), as suggested in previous research at this locality (Arimoto et al., 2020). In contrast, sea surface temperature change in the subtropical North Atlantic Ocean appear to be relatively minimal with *Globigerinatheka* $\Delta\delta^{18}O$ of ~0.23 ‰ across the same interval (Figure 3.2A) supported by minimal surface ocean changes in the South East Atlantic (Galazzo et al., 2014).

Our record indicates that decoupled water column responses to environmental changes continued during the MECO. We see a reduction in $\delta^{18}O$ gradients between surface and deep-water dwellers ($\Delta\delta^{18}O_{Globigerinatheka\text{-}Catapsydrax}$: 0.01 ‰; Figure 3.3) driven by large decreases in *Subbotina* and *Catapsydrax* $\delta^{18}O$ values ($\Delta\delta^{18}O$: 0.64 ‰ and 1.50 ‰, respectively) and only small decreases in *Globigerinatheka* $\delta^{18}O$ values ($\Delta\delta^{18}O$: 0.21 ‰ compared to pre-MECO levels (Figure 3.2A). This suggests that warming was concentrated at thermocline and subthermocline depths

(increasing by ~ 7 °C) compared to the surface ocean (~ 1 °C increase). This muted surface ocean response is not supported by high resolution stable isotope records at this locality that suggest a 4 °C increase in surface ocean temperature (Arimoto et al., 2020) or most other global studies using various geochemical proxies which suggest between 3 - 6 °C warming of sea surface temperatures across the MECO (Cramwinckel et al., 2018, 2019; Bijl et al., 2010; Bohaty and Zachos, 2003; Bohaty et al., 2009). Additional sites in the north Atlantic alongside temperature estimates from a greater range of proxies such as Mg/Ca values and clumped isotopes are needed to understand the mismatch between this dataset and that of Arimoto et al (2020) and any site-specific changes in the thermal structure of the water column.

Peak warming in the MECO was followed by globally rapid cooling (Arimoto et al., 2020; Bohaty et al., 2009; Villa et al., 2008) accompanied by increases in cool water taxa (Luciani et al., 2010; Villa et al., 2013), reduced abundances and eventual extinctions of oligotrophic, shallow mixed layer planktonic foraminifera *Acarinina* and *Morozovelloides* (Wade, 2004) and calcareous nannofossils discoasters (Villa et al., 2008). In our record, global cooling is represented by an increase in $\Delta\delta^{18}O_{\textit{Globigerinatheka-Catapsydrax}}$ of ~1.00 ‰ (Figure 3.3) re-establishing the pre-MECO planktonic foraminifera depth stratification in $\delta^{18}O$ values seen at 43.50 Ma by 38.50 Ma, indicating abrupt cooling of the thermocline following the MECO. Surprisingly, despite such rapid cooling, *Catapsydrax* takes ~2 Myrs to reappear below *Subbotina* in the water column (Figure 3.2A), possibly not returning to its position below *Subbotina* in $\delta^{18}O$ space until thermocline conditions became more stable at 38.50 Ma (Figure 3.2A). *Globigerinatheka* shows a slight increase of 0.15 ‰ in $\delta^{18}O$ values post-MECO, returning to pre-MECO values (Figure 3.2A) indicating only minor cooling of the surface ocean.

3.5.1.2 Trophic state changes across the Middle Eocene Climatic Optimum ($\delta^{13}C$ values)

Inferred trophic state changes are highly site specific (Witkowski et al., 2014, 2012; Moebius et al., 2015; Cramwinckel et al., 2019). Our study shows that, in tandem with the increased $\delta^{18}O$ value depth stratification between 43.50 and 41.31 Ma (described in section 3.4.1), the $\delta^{13}C$ values stratification also increased over the same pre-MECO period by 0.48 ‰ ($\Delta\delta^{13}C_{\textit{Globigerinatheka-Catapsydrax}}$). This increasing separation between genera is interrupted by a transient reduction in $\Delta\delta^{13}C_{\textit{Globigerinatheka-Catapsydrax}}$ to 1.00 ‰ and $\Delta\delta^{13}C_{\textit{Globigerinatheka-Subbotina}}$ to 0.81 ‰ at 40.15 Ma. These $\Delta\delta^{13}C$ values during the peak of the MECO represent the lowest $\delta^{13}C$ gradients between the surface and deep-water dwellers recorded in our samples (Figure 3.3B). The decreasing gradient is a result of increasing *Subbotina* and *Catapsydrax* $\delta^{13}C$ values, coupled with a slight decline in *Globigerinatheka* of ~0.14 ‰ (Figure 3.2B) suggesting a possible decrease in water column primary productivity at Sites U1408 and U1410.

The interpreted reduction in primary productivity from our record during the peak of the MECO event at 40.15 Ma is supported by another study at the same locality (Arimoto et al., 2020) that observed weakened depth stratification between planktic foraminifera and interpreted a large reduction in planktonic foraminifera accumulation rates as an indicator of primary productivity reduction (Arimoto et al., 2020). In addition, decreased productivity during the MECO has been observed in the Southeast Atlantic (Galazzo et al., 2014). Open ocean mid latitude south Atlantic (Galazzo et al., 2014) and north Atlantic (Arimoto et al., 2020) locations are therefore recording a different trophic signal than observed at other sites across the MECO where primary productivity increases have been proposed based on benthic foraminifera accumulation rates and assemblage structure (Moebius et al., 2015; Boscolo Galazzo et al., 2013), increased deposition of organic rich layers in the Tethys ocean (Luciani et al., 2010; Spofforth et al., 2010), increased diatom flux in the Southern Ocean (Witkowski et al., 2012) and North Atlantic Ocean (Witkowski et al., 2014), as well as shifts in planktonic foraminifera communities towards more eutrophic, opportunists (Luciani et al., 2010). At continental margin sites, these changes are attributed to increased weathering and terrestrial input as a result of global warming across the MECO (Moebius et al., 2015). The open ocean setting of our study sites (Sites U1408 and U1410) mean a similar terrestrial input of nutrients is not plausible, which potentially explains the decreased $\delta^{13}C$ gradient and inferred productivity decrease we observe. Further studies combining micropalaeontological methods and geochemistry are needed in the North Atlantic to understand whether our results represent a local or regional signal. The described thermal and trophic state fluctuations above show the importance of including environmental change in functional trait-based studies. Whilst our study period and data reflect the globally observed rapid changes of the MECO, we also capture global background cooling (Figure 3.2). While background climatic changes are not often the focus of palaeoecological studies, our low-resolution record shows how major changes to water column structure occur before and after large climatic fluctuations. These changes will have an impact on ecosystems and, as we have shown, on traits in planktonic foraminifera.

3.5.2 Functional traits in foraminifera in deep time

3.5.2.1 What does “functional” mean for foraminifera?

This study demonstrates that measurable morphological and ecological traits can be used to infer responses to abiotic forcing in palaeoceanographically dynamic environments. However, inferring the functionality of measurable morphological traits is much harder for extinct than for extant species. Further, assigning functions to traits in deep time is often based on observations of extant taxa and the assumption that the observed functional relationship has not changed.

Several studies indicate that this approach may be too simplistic (Eronen et al., 2010; Wade et al., 2008; Edgar et al., 2013). Presence of algal photosymbionts has been shown to be functional (Bé, Spero and Anderson, 1982; Bé, Caron and Anderson, 1981; Bé et al., 1977) in some modern planktonic foraminifera species (obligate symbiosis) (Takagi et al., 2019), with the only way of determining obligate symbiosis through direct observation. Other functional traits such as spines are not readily preserved in-situ and require SEM images to identify. However, more complex morphological traits that are more tightly related to biogeochemical function (such as pore density) can now be easily measured through technological advances (Bé, 1968; Burke et al., 2018; Constandache, Yerly and Spezzaferri, 2013).While gross morphology has been hypothesized to control buoyancy (Caromel et al., 2014), mathematical models suggest any potential relationship is weak at best (Caromel, Schmidt, and Rayfield 2017) and such features are variable even within a constant laboratory environment (Davis et al., 2020). One clear conclusion from this is that simple measures of gross test morphology are not primary controls on organismal function, and that interdisciplinary developments offer promising avenues to extract potentially more biogeochemically relevant signals.

3.5.2.2 Measuring functionality in foraminifera traits

Implying functionality of foraminifera traits is further complicated by foraminifera trait diversity, analytical protocols, and trait plasticity. The genus-based approach used in this study likely expands the range of morphological or geochemical values compared to species level analyses. Genera have long been argued to represent biological reality (Mayr, 1942) and analysis at the generic level has advantages and disadvantages (Hendricks et al., 2014). Despite their highly resolved, species-level record, a genera-based approach is appropriate for planktonic foraminifera as phenotypic and ecological traits are shared across species and genera resulting in morphogroup and ecogroup classifications (Aze et al., 2011).

Despite increasing morphological and geochemical niche breadth by measuring genera rather than species and measuring almost 8 times as many individuals for morphological as geochemical analysis, we do not detect a morphological response in terms of either test size or shape to either the long-term Eocene cooling trend or the transient MECO. In addition, our analysis found no detectable relationship between size and $\delta^{13}C$ values in *Subbotina* as expected for an asymbiotic foraminifera. Note though that we obtained statistical significance between specimen weight and $\delta^{13}C$ values (Table B.22), re-emphasizing the importance of measuring the most relevant trait rather than the easiest to measure. This implies that either size is not a functional trait (assuming a $\delta^{13}C$-size correlation infers functionality) or plasticity of *Subbotina* traits is sufficient to mask any functional relationship.

In contrast, to the lack of $\delta^{13}C$-size relationship in adult *Subbotina*, species hosting dinoflagellate algal photosymbionts do have a positive test size-$\delta^{13}C$ value relationship implying functionality (Berger, Killingley and Vincent, 1978; Elderfield, Vautravers and Cooper, 2002; Friedrich et al., 2012; Oppo and Fairbanks, 1989; Spero, Lerche and Williams, 1991; Edgar, Hull and Ezard, 2017). The $\delta^{13}C$-size relationship in symbiont bearers is a result of algal preferential uptake of isotopically light carbon. If a correlation implies functionality, size is functional in at least symbiont bearing planktonic foraminifera. To understand this relationship further we propose the need for investigations at the individual level outside of analytical size constraints in symbiotic genera and additional research on whether this relationship extends to asymbiotic genera at the individual level.

Individual analysis will also further our ability to constrain the degree of plasticity in planktonic foraminifera traits and therefore better infer their functionality. The discussions in section 3.5.1.2 focus on linking $\delta^{13}C$ value changes in planktonic foraminifera to trophic changes in the water column. This one-dimensional view of $\delta^{13}C$ values assumes that the depth ecology of planktonic foraminifera does not change and therefore palaeohydrological changes drive stable isotope variations. Yet, studies based on extant foraminifera indicate that depth habitat can vary as a result of season, biogeography and environment (e.g Chernihovsky et al., 2020; Jonkers & Kučera, 2017; Kretschmer et al., 2018; Taylor et al., 2018) as well as changes in life strategy (Darling et al., 2009). Additionally, studies of foraminifera species and across evolutionary lineages have shown changing depth habitats through evolutionary history (Coxall et al., 2000; Norris, Corfield and Cartlidge, 1993; Stewart et al., 2012). The increase in $\delta^{13}C$ values in *Subbotina* and *Catapsydrax* ($\Delta\delta^{13}C$: 0.57–0.59 ‰, respectively) across the MECO compared to pre-MECO (Figure 3.2B), reducing the overall surface-deep $\delta^{13}C$ depth gradient, suggests these genera could have migrated up in the water column during the MECO supporting an ecological scenario (Figure 3.6).

An adaptable depth ecology and generalist life strategy has been suggested to explain batch *Subbotina* variation in $\delta^{18}O$ values and $\delta^{13}C$ values at several points through the Eocene (Arimoto et al., 2020; Bralower et al., 1995; Dutton, Lohmann and Leckie, 2005; Macleod, Keller and Kitchell, 1990; Stap et al., 2010; Wade, 2004; Wade and Pearson, 2008). In other studies, these changes are most often associated with cooling of surface waters and/or increases in productivity (Macleod, Keller and Kitchell, 1990). However, with no symbionts and a preference for cooler thermocline waters it is hard to envisage this genus moving to a warmer (=shallower) part of the water column.

Utilizing single specimen analysis, we can explore this conundrum further. Depth habitat hypotheses of *Subbotina* through the Eocene have previously been based on multi-specimen (batch) isotope analyses hiding any interindividual variation (Arimoto et al., 2020; Bralower et al.,

1995; Dutton, Lohmann and Leckie, 2005; Macleod, Keller and Kitchell, 1990; Stap et al., 2010; Wade, 2004; Wade and Pearson, 2008). Assuming that our new individual isotopic measurements reflect a genuine isotopic signature of *Subbotina*, the wide range of individual isotopic values (Figure 3.2, Figure 3.4) with some individuals plotting in the same space as both *Globigerinatheka* (mixed layer) and *Catapsydrax* (subthermocline) suggests that *Subbotina* had a large ecological niche extending from the surface ocean to the subthermocline during the middle Eocene (Figure 3.2). It is this wide ecological niche that may have aided species' resilience through the MECO, multiple early Paleogene hyperthermal events and long-term Eocene cooling. More stable isotope studies of *Subbotina* at the individual level are needed to understand how the width of the *Subbotina* ecological niche changed through time and space during the Eocene and through to their demise in the Oligocene.

In this study, we have demonstrated that planktonic foraminifera are an ideal study organism for trait-based studies and can be integrated with palaeoceanographic changes to investigate functional trait changes through climatic perturbations. Using an integrated approach with individual based analyses, we have demonstrated profound changes to ecosystems undergoing a transient global warming event. We did however detect no evidence that the measured morphological traits, and their relationship to stable isotopes, imply altered functionality across our time period. Further research is needed to reconcile the true meaning of which traits are functional for planktonic foraminifera in deep time, and how we can detect functional relationships statistically in "go-to" morphological traits such as size. We suggest that to truly investigate functionality in planktonic foraminifera we need to be measuring outside of size fractions, using the whole spectrum of genera diversity that planktonic foraminifera offer and leveraging developments in imaging techniques.

Chapter 4 The influence of geochemical variation among *Globigerinoides ruber* individuals on paleoceanographic reconstructions

4.1 Abstract

Variation among individuals within species is a biological precondition for co-existence, but, geochemically, is often considered unimportant. Traditional geochemical analysis based on averages facilitates rapid data gathering but necessarily means the loss of large amounts of potentially crucial information into variability within a given sample. As the sensitivity of geochemical analysis improves, it is now feasible to build sufficiently powerful datasets to investigate the extent of paleoclimatic variation at an individual level. Here, we investigate geochemical and morphological variation among the sensu stricto, sensu lato and sensu lato extreme subspecies of the workhorse extant planktic foraminifera *Globigerinoides ruber*. Our experimental design distinguishes between inter- and intraspecific variability as well as the repeatability of laser ablation inductively coupled plasma mass spectrometry (LA-ICP-MS). We show that geochemical variability in Mg/Ca values is driven by subspecies classification and that ontogenetic trends in Mg/Ca values are observable in all subspecies with the final chamber consistently showing depleted Mg/Ca. Furthermore, we show that whilst there is no detectable impact of test or chamber size on Mg/Ca, relationships between size and stable isotopes do exist even within a narrow size fraction. In addition, the variance we found among individuals in Mg/Ca values is two hundred and fifty times higher than the variance among repeated laser spot analyses, which should direct laboratory protocols towards generating as ecologically and environmentally homogeneous samples as possible. Our results emphasize we can use LA-ICP-MS to quantify how individual variability aggregates to bulk results, and highlights that with sufficient sample size it is possible to reveal how intraspecific variability impacts geochemical inference.

4.2 Introduction

Many palaeoceanographic studies rely on the accurate identification of foraminifera and these organisms form a key archive of oceanic conditions. Despite genetic advances (Morard et al., 2015, 2019; André et al., 2014), foraminiferal taxonomy remains reliant on morphological comparisons. Palaeoceanographic studies ubiquitously use geochemical proxies on

morphologically identified species to infer the ambient environment (Zachos et al., 2001). While the environmental controls of geochemical variance such as temperature and salinity are well studied (Epstein et al., 1951; Urey et al., 1951; Bijma, Spero and Lea, 1999; Pearson, 2012; Bemis et al., 2000), variation as a result of biological factors including physiology and life history (Ezard, Edgar and Hull, 2015) are commonly grouped in the catch-all term "vital effects" (Urey et al., 1951; Epstein et al., 1951). These "vital effects" have been increasingly well documented (Bemis et al., 1998, 2000; Birch et al., 2013; Hönisch et al., 2003; Spero & Williams, 1989; Spero et al., 1991) and understood in an evolutionary context (Edgar, Hull and Ezard, 2017). Yet, many studies still assume that variability among individuals is statistical noise to be averaged away. To demonstrate that there is oceanographic, biological, and climatic meaning in this noise, we designed experimental protocols to deconstruct intraspecific (within-species) variability of laser ablation inductively coupled plasma mass spectrometry (LA-ICP-MS) measurements into meaningful differences among subspecies, size classes and repeated LA-ICP-MS measurements. Our goal is to ascertain the magnitude of variation among individuals relative to the analytical uncertainty of single-specimen LA-ICP-MS analyses.

The dismissal of intraspecific variation is a common thread in paleoecology. The mean of a population is habitually used as a sufficient descriptor of the whole population contrary to mounting evidence that intraspecific variability impacts community stability through resource partitioning (Jung et al., 2010), competition (Bolnick et al., 2011; Hart, Schreiber and Levine, 2016) and abiotic tolerances (Bolnick et al., 2011). Applying a mean-field approximation to foraminifera might be sufficient for biological factors common among individuals such as seasonality resulting from synchronous reproduction (Bijma, Erez and Hemleben, 1990). For many other stratified factors however, the evidence for commonality among individuals is not robust due to the structure of variation among individuals.

Within-species variation can be apportioned into systemic and non-systemic variation. The latter encompasses random noise; there may be mechanistic reasons why two individuals express a different geochemical signature, but these reasons are often not detectable at the given scale of analysis and are prone to random variation during the measurement process. The systemic reasons could be continuous, such as geographical space (Darling and Wade, 2008) or vertical depth habitat (Norris, 2000) or discrete, such as the presence/absence of symbionts (Ezard et al. 2015; Spero and Lea 1993). Sub-species form a supposedly discrete taxonomic rank below the species whose utility in evolutionary biology remains contentious (Phillimore and Owens, 2006). Subspecies' existence could potentially bias paleoceanographic studies in systemic ways if the subspecies are genetically, vertically, seasonally or geographically distinct (Lazarus, 1983; Mayr, 1942b; Norris, 2000; Seears, Darling and Wade, 2012). Co-existence of subspecies at a given location obviates traditional geographical criteria for subspecies delimitation (Mayr and Ashlock,

1991) and makes nuanced recognition increasingly important. Measuring, understanding, and accounting for systemic subspecies variability should be a priority to reduce errors and reveal potential bias in geochemical proxies (Antonarakou et al., 2015; Sadekov et al., 2008).

Technological advances have popularized high-resolution, single specimen measurements and intra-test analysis, previously thought impossible (Emiliani, 1954). Single specimen analysis has revealed size dependent trends in stable isotopes (Kelly, Bralower and Zachos, 1997), unlocked the ability to circumvent post depositional diagenetic issues for palaeotemperature reconstructions (Aze et al., 2014), further constrained seasonal palaeoclimate variability (Metcalfe et al., 2019), revealed the presence of intra-individual chamber difference in biomineralization-related Mg-banding (Eggins, De Deckker and Marshall, 2003a; Sadekov et al., 2008, 2009) and, through an innovative use of culturing experiments, begun to illuminate the physiological drivers of such banding (Fehrenbacher et al., 2017; Spero et al., 2015). Despite instrumental improvements, our understanding of intraspecific variation has not progressed substantially because the few studies that have investigated these issues often display conflicting results, and these results are impacted by our understanding of the drivers of geochemical proxies.

The most widely applied proxies for reconstructing past ocean temperatures from planktonic foraminifera are the oxygen isotope composition ($\delta^{18}O$) and Mg/Ca values of the foraminiferal test. The Mg/Ca proxy is based on the temperature sensitive substitution of Mg^{2+} into the foraminiferal test which increases exponentially with temperature (Lea, Mashiotta and Spero, 1999; Holland *et al.*, 2020). In the case of a thermodynamically ideal calcite the Mg/Ca ratio will increase by 1-3% per °C increase (Lea, Mashiotta and Spero, 1999; Holland *et al.*, 2020). However, in foraminiferal calcite this increase has been shown to be much higher at around 9 % per °C (Lea, Mashiotta and Spero, 1999; Anand and Elderfield, 2005). This difference in thermodynamic response of foraminiferal calcite demonstrates that temperature is not the sole control in foraminiferal Mg^{2+} uptake. These other factors can be divided into two groups: biological and environmental. Biologically Mg^{2+} uptake in planktonic foraminifera is thought to be controlled by symbiotic activity through the alteration of the foraminifer's microenvironment (Eggins, Sadekov and De Deckker, 2004; Sadekov, Eggins and Deckker, 2005; Bentov and Erez, 2006). Additionally, foraminifera can biologically alter their Mg^{2+} by utilizing different biomineralization pathways (Bentov and Erez, 2006). Despite these advances in our understanding of biological controls on Mg^{2+} uptake there is still a lot we do not know.

Culturing experiments have been able to isolate the effects of environmental parameters that control Mg/Ca values. Such experiments have demonstrated a linear relationship between foraminiferal Mg/Ca and salinity (Kisakürek *et al.*, 2008; Hönisch *et al.*, 2013), a negative relationship with pH and/or $[CO_3^{2-}]_{sw}$ (Lea, Mashiotta and Spero, 1999; Kisakürek *et al.*, 2008) as

well as a positive non-linear relationship with Mg/Ca_{sw} when Mg/Ca_{sw} differs from modern values (Evans and Mller, 2012; Evans *et al.*, 2016). Recent modelling has shown that the main factors that modulate the sensitivity of Mg/Ca to temperature are Mg/Ca_{sw}, $[Ca]_{sw}$ and carbon chemistry (DIC, $[CO_3^{2-}]_{sw}$ or pH) (Holland *et al.*, 2020). Over longer time periods Mg/Ca_{sw} and $[Ca]_{sw}$ will be more influential whilst over short time scales seawater carbon chemistry will influence Mg/Ca derived temperatures (Holland *et al.*, 2020).

In contrast to the relative infancy of the Mg/Ca-temperature proxy the use of $\delta^{18}O$ values of foraminiferal calcite as a proxy has been well studied and applied to many different intervals and species since its conception (Urey, 1947). Due to the proxy's longevity a lot more is known about the controlling factors of $\delta^{18}O$ values in foraminiferal calcite. These factors are the oxygen isotope composition of seawater ($\delta^{18}O_{sw}$) which changes as through time and space, seawater carbonate chemistry (pH and $[CO_3^{2-}]$) which in turn can be biologically altered by the foraminifera (Spero and Lea, 1993; Spero *et al.*, 1997) and so called biological "vital effects" (Erez, 1978). Some of these "vital effects" can be controlled for in studies by controlling for size, depth habitat and feeding ecology however other "vital effects" such as metabolism cannot be easily measured or controlled for.

One of the most studied and contentious species in this field is *Globigerinoides ruber* (*G. ruber*), one of the workhorses of palaeoceanography. Despite numerous studies across all the major ocean basins (Antonarakou et al., 2015; Aurahs et al., 2011; Kawahata, 2005; Kuroyanagi et al., 2008; Kuroyanagi and Kawahata, 2004; Lynch-stieglitz et al., 2015; Mohtadi et al., 2009; Naik, 2016; Numberger et al., 2009; Sadekov et al., 2008; Steinke et al., 2010; Thirumalai et al., 2014; Wang, 2000), the degree of intraspecific variation in geochemical and morphological space, and its consequent impact of variation on paleoceanographic reconstructions, is still disputed. The main issues include insufficient sample size (Löwemark et al., 2005; Lynch-stieglitz et al., 2015; Wang, 2000) and a focus on bulk morphotype analysis that averages away individual variability (Antonarakou et al., 2015; Löwemark et al., 2005; Lynch-stieglitz et al., 2015; Mohtadi et al., 2009; Wang, 2000). One potential reason for this ambiguity is the existence of subspecies variation. *G. ruber* has seven identified morphological variants (Kontakiotis et al., 2017; Robbins and Healy-Williams, 1991), with the two most abundant and morphologically distinct (sensu stricto, sensu lato) commonly separated with the more compressed sensu lato extreme additionally separated in some other studies (Antonarakou et al., 2015; Carter et al., 2017; Kontakiotis et al., 2017; Löwemark et al., 2005; Lynch-stieglitz et al., 2015; Mohtadi et al., 2009; Wang, 2000). If geochemical variation is systemic across these subspecies because they inhabit different depth habitats for example, then any cross-study comparisons may not be starting from common units of reference.

Here, we use a combination of morphological, trace element and stable isotope measurements on 264 *G*. *ruber* individuals classified by subspecies identification. Groeneveld et al (2019) studied 451 individuals in 4 species, the largest single-specimen isotope study to date, but their investigations of *G. ruber* analysed these individuals in pairs. The largest *G. ruber* single-specimen LA-ICP-MS investigation to date analysed 60 individuals (Naik, 2016). Our experimental design includes 2087 LA-ICP-MS measurements, with an attempted 9 repeated shots on each of our 264 individuals with statistical replication at the chamber, individual and shot levels. We aim to tease apart the ecological affinity of these subspecies and the repeatability of the geochemical measures. We demonstrate that: (i) intraspecific variability in geochemical space is structured around subspecies classification; (ii) there is a no detectable impact of specimen size on Mg/Ca, even within restricted size fractions; and (iii) Mg/Ca values are a reliable and repeatable measurement when determined using LA-ICP-MS.

4.3 Materials and methods

4.3.1 Material and regional setting

This study uses material collected during the Paleogene GLObal Warming events, 'GLOW' cruise offshore Tanzania in the Western Indian Ocean (Kroon and the Shipboard Scientific Party, 2010). All sites on the cruise collected material that sat well above the carbonate compensation depth (CCD) and lysocline (3,330m; (Belyaeva and Burmistrova, 1984; Ivanova, 2009) and was composed of more than 30% clay leading to excellent well preserved planktic foraminifera (Kroon and the Shipboard Scientific Party, 2010). For this study we focus on box core material collected at GLOW station 8 (from here on referred to as GLOW 8 (9 21' 25.20" S; 40 35' 27.60" E) with a box corer with a diameter of 30cm and height of 55cm. GLOW 8 was located in the Southern Seagap, a topographic high between the Davis ridge and the Tanzanian coastline at a depth of 2420m. The box corer penetrated to a depth of 47cm; for this study we use the top 1cm of the box core sample which was separated whilst onboard (Kroon and the Shipboard Scientific Party, 2010). The estimated sedimentation rate in this area is ~ 2cm/kyr (Kroon and the Shipboard Scientific Party, 2010) which alongside the presence of living benthic foraminifera at the sediment water interface in other cores in the area (Birch et al., 2013) we have a planktonic foraminifera assemblage that is 0 to 65 Ma (Birch et al., 2013).

The Western Indian Ocean is influenced by the Northeast Madagascan Current (NEMC) and movement of the Inter Tropical Convergence Zone (ITCZ). In Northern Tanzania the seasonal shifts of the ITCZ creates two monsoonal periods with heavy, prolonged rains from March to May

(south-east monsoon) and shorter rains between October and December (McClanahan, 1988). The coastal waters of Northeast Africa experience different hydrographic changes through the seasons which lead to different ecosystems from North to South (McClanahan, 1988). Above 4°S ecosystems benefit from cooler, nutrient rich waters as a result of seasonal reversals in the wind and current direction and subsequent variability in thermocline depth and nutrient availability resulting in high planktonic productivity (McClanahan, 1988). In contrast, the GLOW 8 material used in this study sits at ~ 9°S where waters are warm and low in nutrients resulting in a predominance of coral reefs and high benthic productivity (McClanahan, 1988). Today the study area consists of warm surface waters with a max seasonal surface temperature (SST) variation of 5°C (August (~ 25-26 °C); February (30 °C) (McClanahan, 1988; Damassa et al., 2006; Birch et al., 2013)) that remain stratified all year round (Birch et al., 2013). Full Conductivity, Temperature, and Depth (CTD) profiles collected at GLOW 5 (8 54' 6.01" S; 41 29' 42.25" E) ~111 km southwest and GLOW 2 (10 54' 6.01" S; 41 29' 42.25" E) ~198 km southeast of GLOW 8 show that the thermocline sits at ~40m with the turbidity maximum at ~137m indicating a maximum depth for symbiont hosting foraminifera (Supplementary material in Birch et al, (2013)). In addition, CTD data shows that salinity varies between ~34.8 and ~35.4 PSU in the upper 200m of the two GLOW sites.

4.3.2 Morphological Analysis

The material was sieved to 230-355 μm size fraction and the first 150 individuals of each *Globigerinoides ruber* morphotype (Figure 4.1a) were picked for analyses and given an individual ID including a number 1-150 and letters referring to morphotype (sensu stricto: SS, sensu lato: SL and sensu lato extreme SLE). The specimens were mounted on glass slides (Brombacher, Wilson and Ezard, 2017) and orientated with the aperture facing upwards. Images of the final whorl of each sample were captured using an Infinity 3 Lumenera camera mounted on an Olympus SZX10 microscope, illuminated from above (Brombacher, Wilson and Ezard, 2017). Pre-selected traits (Figure 4.1b) were measured using automated image analysis macro within Image Pro 9.1 Premier software. Ontogenetic traits (Figure 4.1c), beyond the scope of the imaging macro, were measured manually in the same software.

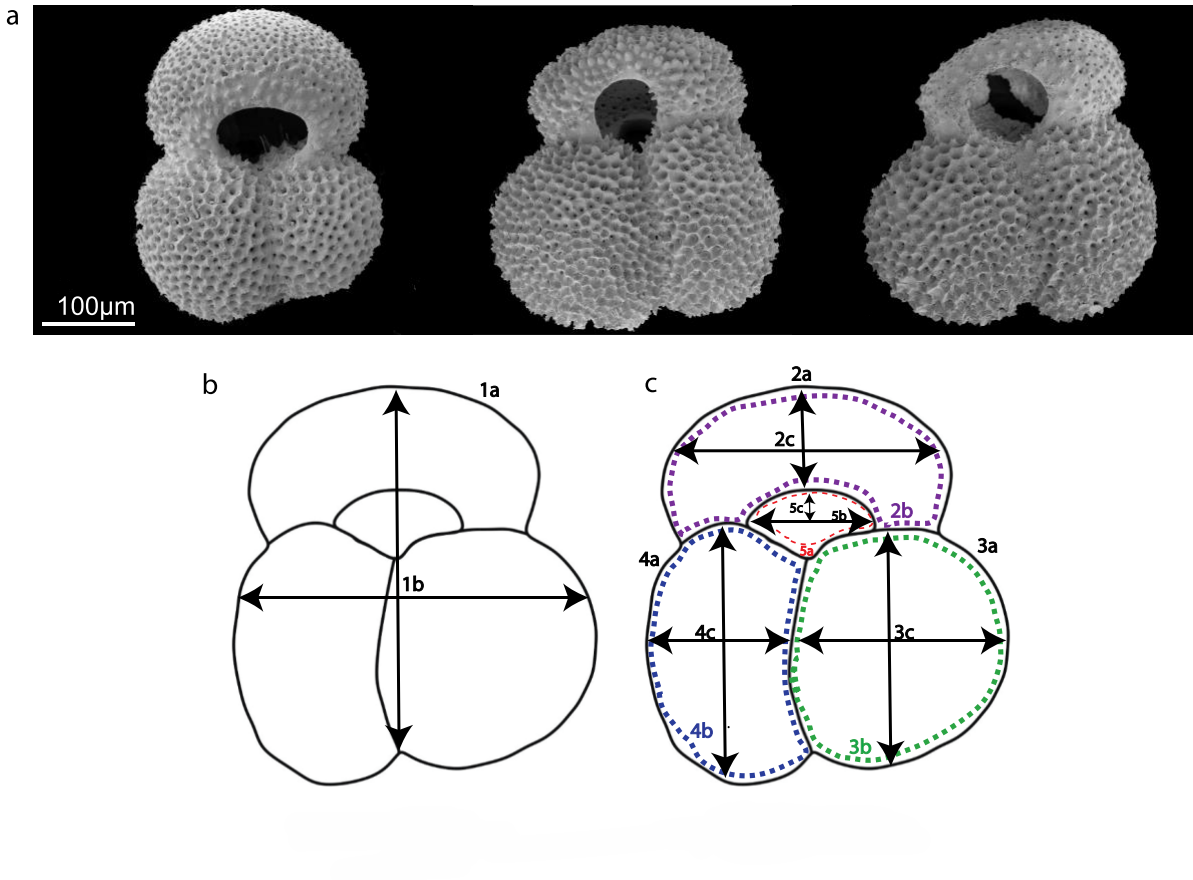

Figure 4.1 (a) Scanning electron microscope images of the morphotypes of Globigerinoides ruber used in this study. Left to right: sensu stricto, sensu lato and sensu lato extreme. (b) Pre-selected traits measured automatically: 1a- test area, 1b- test aspect ratio. (c) Ontogenetic traits measured manually: 2a- final chamber area, 2b- final chamber perimeter, 2c- final chamber aspect ratio, 3a- penultimate chamber area, 3b- penultimate chamber perimeter, 3c- penultimate chamber aspect ratio, 4a- antepenultimate chamber area, 4b- antepenultimate chamber perimeter, 4c- antepenultimate aspect ratio, 5a- aperture perimeter, 5b- aperture width, 5c- aperture height

4.3.3 Geochemical Analysis

4.3.3.1 LA-ICP-MS Trace element analysis

For LA-ICP-MS analysis, 100 individuals from each subspecies already measured morphologically were selected. For each subspecies 100 unique random numbers, relating to the previously assigned morphological ID, were sampled without replacement using a random number function in the R environment (Version 4.0.3; R Core Team 2020). The corresponding individuals were then removed from the slides and placed into separate vials. Individuals were then cleaned by ultrasonification in methanol for 5-6 seconds followed by two washes in Milli-Q water (Eggins, De Deckker and Marshall, 2003). The samples were then dried overnight in a 50°C oven before being remounted as described previously.

Trace element/Ca (TE/Ca) ratios were analysed using a New Wave UP193 laser ablation system coupled to a Thermo Fisher Scientific X-Series II inductively coupled plasma mass spectrometer (LA-ICP-MS) at the University of Southampton. During analysis the isotopes ^{24}Mg, ^{43}Ca, ^{44}Ca, ^{55}Mn, ^{88}Sr, ^{66}Zn and ^{137}Ba were measured as a time resolved acquisition. Individual chambers in the final whorl were ablated in triplicate with each time resolved analysis set to 60s; wall penetration was achieved prior to the end of each analysis to ensure that the full wall thickness was sampled. Each analysis was performed using a 30 µm spot and 3 mJ/cm^3 fluence and followed by a 30s wash to remove the residual sample from the laser system which is followed by a 13s gas blank. Although chamber profiles were obtained, instrument settings were not optimized to generate high-resolution time-resolved profiles through the chamber wall (e.g. (Sadekov, Eggins and Deckker, 2005). For internal calibration and data processing, NIST references glasses 610 and 612 were analysed for ten separate ablation periods of 60s each, every 80-100 ablation spots.

Data processing was done using an automated script generated in the R environment (Version 4.0.3; R Core Team 2020). Each analytical session was processed separately using the same methods to ensure the calibrations and blank values were reflective of the instrument conditions for that day. Firstly, each laser profile was automatically trimmed removing the first 100ms to purge any residual sample from the system. Next each profile was cut off at 2500ms to prevent interference from rates of change at the end of the run which are not of interest (Figure C.1). Each gas blank value that was recorded after every shot was then subtracted from the recorded shot throughout the analytical session. These blanks were then collated and the median for each isotope within these blanks was calculated to remove background noise, gas flow contributions to the recorded mass signal and to minimize analytical drift. Background corrected NIST 610 and 612 were collated and corrected for instrument drift throughout the session. Influential outlier values were detected using Cook's distance and anomalous values beyond a threshold of 0.0001 were

removed. A calibration curve for each elemental isotope was constructed using the cleaned NIST 610 signal and published isotope concentrations (Jochum et al., 2011). Raw sample data were background corrected using the mean background count of each element of interest (in this study just Ca and Mg data are presented) with ratios quantified using ^{43}Ca as an internal standard and NIST 610 glass standard reference material (Eggins, De Deckker and Marshall, 2003). Full quantification was achieved using a three-point calibration based on the NIST standards using the 'preferred' concentration values in the GeoREM database (Jochum et al., 2007).

For each foraminifer, the processing algorithm used the ^{43}Ca signal of each profile to detect when the laser fully penetrates the chamber wall by taking a rolling average of 20 data points and calculating when the largest signal drop occurs. When this signal drop is detected, the script finds the corresponding timestamp and removes all data thereafter. A short laser profile and a low number of data points can be caused by a false positive detection where the laser has encountered a contaminant i.e., clay or something that is not calcite that causes the ^{43}Ca signal to decrease rapidly and trigger the end point detection algorithm. Following this step each individual profile consisted of 1 to 47 data points. 195 out of 2113 profiles with fewer than 4 data points was either flagged as an N/A in data reduction and removed or removed manually as they are unsuitable for obtaining a representative Mg/Ca signal of the test. The mean number of data points per profile was 29.

Amounts of each element (in mmol) in the foraminifera test were calculated for each isotope signal using the NIST 610 and NIST 612 calibration curves previously made. Trace element ratios, including ^{24}Mg/^{43}Ca (mmol/mol), were calculated for every data point and a median taken for subsequent use. We measured the variance in trace element ratios (^{24}Mg/^{43}Ca) calculated using the observed signal and the NIST 610 and NIST 612 published values in Jochum et al (2011), with low variance as an indication of reliable analytical sessions and sensible data processing. Following background correction element/^{43}Ca was then averaged for each ablation location creating a value of spot-average element/^{43}Ca. To manually screen for contaminants, we looked at other indicative element/Ca values against Mg/Ca. Only 8 profiles were removed using Mn/Ca and a cut off at 1 mmol/mol (Figure C.2a). For further contamination control, we also remove 26 additional spots with an unrealistic mean Mg/Ca>10 mmol/mol. Due to low-sensitivity, Al was not recorded, so could not be used to identify further contamination. In total we present results from 2087 analyses of 262 individuals which represents 6384.86 um^3 of material ablated which is the largest study on *G. ruber* to date. The mean spot-average across all analyses was 4.49 mmol/mol with a back-transformed 95% confidence interval of (4.43, 4.55).

Based on the exponential relationship between Mg/Ca values and temperature (Lea et al., 1999; Rosenthal et al., 1997) and excellent preservation of the foraminifera, temperatures were

calculated using Equation 1 where T is temperature, *b*= 0.38 and m= 0.09 based on core top calibrations using *G. ruber* (Dekens et al., 2002).

$$Mg/Ca = b \exp(m(T)) \quad (3)$$

4.3.3.2 Stable Isotope analysis

Stable isotope measurements were obtained from 98 individuals (SS n= 38, SL n=26, SLE n=34), previously measured for trace elements by laser ablation, using a Thermo Fisher Scientific Kiel IV carbonate device coupled to a MAT253 stable isotope ratio mass spectrometer at the SEAPORT Stable Isotope Laboratory, University of Southampton. Samples were placed into individual vials and measured against the global reference standards NBS19 and NBS18 as well as an in-house quality control standard (GS1). Long-term analytical precision (1σ) was based on the repeat analysis of GS1 and estimated as ± 0.09 ‰ for $\delta^{18}O$ and ± 0.05 ‰ for $\delta^{13}C$. The previously stated long-term analytical precision is based on weights of GS1 used to balance multi-specimen analysis which are much heavier than what we used in this study for single specimen analysis. Whilst we have no data for long-term analytical precision on lower weights due to the relative novelty of this method the short-term analytical precision across sessions based on individual specimen weights of GS1 are ± 0.05 ‰ for $\delta^{18}O$ and ± 0.06 ‰ for $\delta^{13}C$. All results were standardized to Vienna Pee Dee Belemnite (VPDB) using a two-point calibration between NBS19 and NBS18. Calcification temperature in degrees Celsius was calculated using the general calibration of (Erez and Luz, 1983):

$$T = 16.998 - 4.52\,(\delta c - \delta w) + 0.028\,(\delta c - \delta w)^2 \quad (4)$$

with a "δw" of 0.47 ‰ (Birch et al., 2013b). Although this conversion was calibrated using *Globigerinoides sacculifer,* we employ it here to allow direct comparisons to other studies based on this material.

4.3.4 Statistical analysis

The raw calculations of Mg/Ca values exaggerate the precision achievable because each analysis is not independent due to nested pseudoreplication at spot, individual and subspecies levels. To remove this pseudoreplication, understand the influence of subspecies and morphological variation on Mg/Ca values and ascertain the relative amounts of variance explained by spot, individual and subspecies levels, we used generalised linear mixed effect models implemented in the lme4 package (Bates et al., 2015). Mixed effects models comprise random and fixed effects. Fixed effects are experimentally determined and of direct interest in hypothesis testing (Bolker et al., 2009) for patterns of variation common to all experimental units; random effects are selected

from a larger population but thought of as uncontrollable "nuisance" parameters systematically obscuring the signal held by the fixed effects (Bolker et al., 2009; Gillies et al., 2006). The "vital effects" that alter each individual's geochemical composition are examples of random effects, while an overall temperature gradient would be a fixed effect. Variation among individuals means we cannot assume each ablation represents an independent sample: as an example, the Mg/Ca value difference from penultimate to final chamber is likely to be more similar in a single individual than from one individual to another. Our experimental design is stratified random sampling because we targeted sufficient numbers of individuals in each subspecies (strata). We do assume that individuals were sampled independently within their subspecies. In all models individual ID, repeat laser spot number (Spot) and analysis batch (Batch) were classified as random effects (Bates, 2005) because, while we know that individuals, batches and spots could differ amongst each other, we do not have a systemic hypothesis for how they differ; chamber and morphotypes were categorized as fixed effects and Mg/Ca values as the dependent response variable because we expect certain relationships with increasing chamber size through ontogeny and because we anticipate that subspecies-specific offsets are possible. The different models were compared using Analysis of Variance to test model fit assuming a Gamma error distribution for the generalised linear model (inverse link function to transform the mean of the data; variance increases as a quadratic function of the mean). The best fit model was decided by likelihood ratio tests and the Akaike Information Criterion (AIC, Burnham & Anderson, 2002), which summarises model fit as a compromise between variance explained and parameters used. All statistical analysis was carried out in the R environment (Version 4.0.3; R Core Team 2020). Scripts are provided in Appendix C.

4.4 Results

4.4.1 Morphological analysis

To test the null hypothesis that the morphotypes of G. *ruber* are morphologically indistinguishable, a principal component analysis (PCA) was conducted using all traits in Figure 4.1b-c. To reduce the number of components, a Horn's Parallel analysis was conducted (Peres-Neto, Jackson and Somers, 2005) using the "paran" package (Dinno, 2018). This analysis indicated the first 3 principal components explaining ~71 % of cumulative variance should be retained (Figure 4.2, Table C.4). When these components are plotted against each other, the sensu stricto and sensu lato subspecies occupy a homogenous morphospace (Figure 4.2). Sensu lato extreme shows a degree of offset in principal component 2 (Figure 4.2), which is loaded highly by the aspect ratio of the final chamber and the whole test (Table C.5).

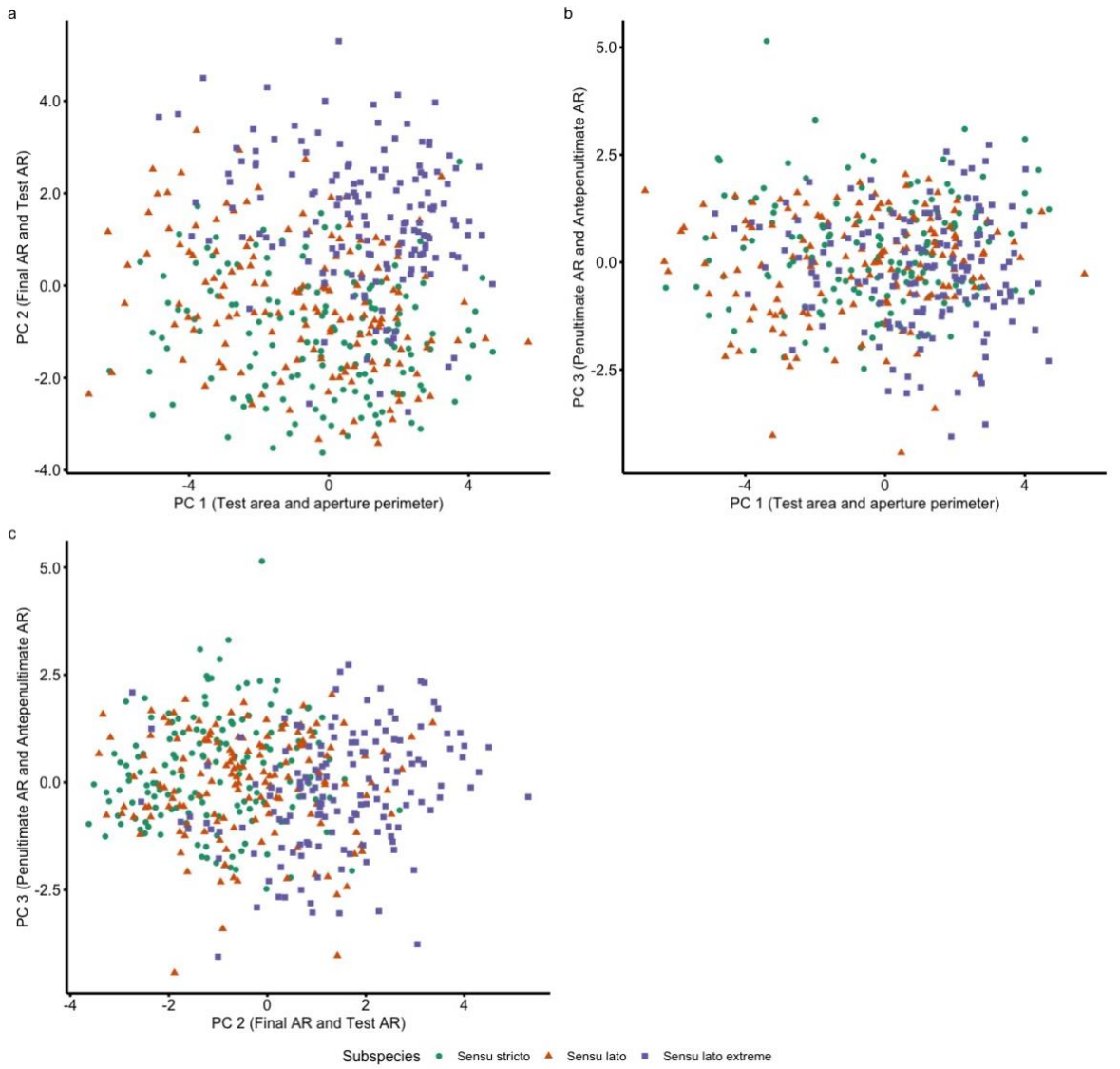

Figure 4.2 Scatter plot of PCA results showing the first 3 principal components that make explain 71 % of the cumulative variance. Principal component 1 (PC1) is loaded highly by test area and perimeter aperture, principal component 2 (PC2) is loaded highly by final chamber aspect ratio and test aspect ratio and principal component 3 (PC3) is loaded highly by penultimate and antepenultimate aspect ratios. a) PC1 vs PC2, b) PC1 vs. PC3 and c) PC2 vs. PC3. Loadings of principal components can be found in Table C.5.

Following the PCA, a cluster analysis was conducted using the package "mclust" (Scrucca et al., 2016) on the three retained principal components. This package tests a finite number of models to determine the most supported statistical model among those considered and identifies the optimal number, size and shape of clusters needed to explain the data using Schwarz's Bayesian information criterion (BIC) (Schwarz, 1978). The BIC takes into account the statistical fit of a model as well as the number of parameters the model has to determine the posterior model probability (Wintle et al., 2003); in the "mclust" package a larger BIC value indicates a better model fit (Fraley and Raftery, 1996). To reject our null hypothesis of no sub-species variability, the "mclust"

analysis must indicate the data is better represented by more than one cluster and thus the morphotypes must occupy statistically different clusters within the plotted morphospace. Clustering analysis shows that the morphospace within PC1 and PC2 is best represented by two clusters (Figure C.3-4), though these do not correspond tightly to our morphological units (Table C.6). When the method is forced to identify three groups (Figure 4.3) subspecies are split across all three groups (Table C.7) and do not correspond to morphologically meaningful units. Therefore, we reject the null hypothesis of no morphological variability in *G. ruber*, but conclude the variability identified is not taxonomically informative.

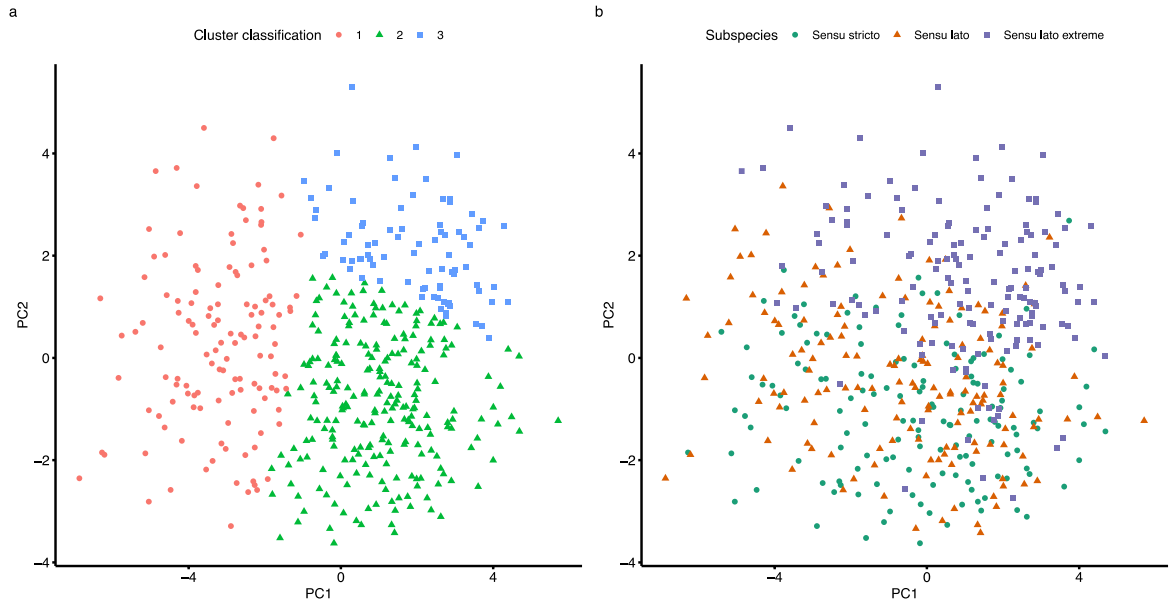

Figure 4.3 Clustering analysis results when the analysis is forced to identify 3 clusters (a) compared to the actual PCA results (b). Subspecies classification within clusters can be found in Table C.7.

4.4.2 Trace element subspecies variability

To investigate subspecies trace element variability, we conducted a one-way Analysis of Variance (ANOVA) on the Mg/Ca dataset. The ANOVA found a statistical difference between subspecies ($F(2,1855) = 149$, $p < 0.01$). A subsequent post-hoc TUKEY HSD test revealed a detectable significant ($p < 0.01$) difference in Mg/Ca values between all subspecies. The SL and SLE morphotypes are depleted by 0.44 mmol/mol and 1.28 mmol/mol respectively when compared to SS. In addition, SLE is depleted in Mg/Ca value compared to SL by 0.83 mmol/mol. To investigate factors driving Mg/Ca value separation between *G. ruber* subspecies, generalized linear mixed effect models were constructed with a gamma link function to account for the positively skewed distribution of the response variable Mg/Ca. The best fitting model assumed a constant test size-subspecies relationship alongside a variable chamber position subspecies relationship. As morphological analysis revealed no detectable separation in morphospace among the three subspecies (Table

C.4-7,Figure 4.2), we constructed models that controlled for test area (Figure 4.1B) to investigate whole test impacts on Mg/Ca value and chamber size (chamber area labelled 2a,3a,4a in Figure 4.1C) to investigate ontogenetic impacts on Mg/Ca.

4.4.2.1 Modelled drivers of Mg/Ca values

We built models separately for test size and chamber size effects. The best model, chosen through AIC, retained both whole test and chamber size effects. Results are reported here with a coefficient (β), standard error (s.e.), t statistic (t) and p value (p) associated with these coefficients; full model outputs are available in Appendix C. The generalized linear mixed model found significant evidence that chamber position (Final, Antepenultimate and Penultimate) and subspecies impacted spot-averaged Mg/Ca values (Table C.8). We find no detectable evidence that test size (Figure 4.4) impacted Mg/Ca values (Table C.8). In addition, when test size was exchanged for chamber size, we found no detectable evidence of chamber size influence on Mg/Ca values even following model reduction, but still found significant influences of chamber position and subspecies (Table C.9). Subsequent discussions of results will focus on the model including test area as this was the highest loading morphological trait from principal component analysis (Figure 4.2). We detected a strong impact of chamber position where the Mg/Ca values differed between the final and penultimate chamber (β=-0.043, s.e. = 0.004, t=-10.111, $p < 0.001$; the coefficients is on the scale of the inverse link function, hence a negative value means a positive relationship through the untransformed data) and between the final and antepenultimate chamber (β=-0.050, s.e. = 0.004, t=-11.711, $p < 0.001$), i.e. a mean enrichment of 0.042 and 0.050 mmol/mol, respectively, in the penultimate and antepenultimate chamber compared to the final chamber (Figure 4.4, Table C.8). This enrichment differs amongst subspecies such that depletion in the penultimate and antepenultimate chamber is stronger in sensu lato than sensu stricto (penultimate: β=-0.035, s.e. = 0.006, t=-5.531, $p < 0.001$, antepenultimate: β=-0.036, s.e. =0.006, t=-5.571, $p < 0.001$; Appendix C). This pattern of depletion is stronger still in sensu lato extreme (penultimate: β= -0.043, s.e. = 00.007, t= -6.018, $p < 0.001$, antepenultimate: β=-0.044, s.e. =0.007, t=-6.214, $p < 0.001$; Appendix C). This interaction supports the conclusion that chamber position is differentially influential amongst the subspecies in driving Mg/Ca value trends, while these are not consistent amongst the subspecies, they are most visible when comparing at chamber resolution rather than the whole specimen (Figure 4.2).

These interdependent relationships among chamber position and subspecies are present after controlling for so-called “random effects”. We included individual test ID, batch, and spot number as random effects to test the repeatability of the LA-ICP-MS method on repeated measurements of the same chamber (Spot) in the same individual (test ID) across two days (batch). Compared to residual standard deviation of 0.047, the variance explained by individual, batch and shot were

0.001, 0.0001 and 0.000004, respectively (Figure C.5). This means that, on top of the systemic "fixed effect" variation explained in the previous paragraph, 250 times more variation (0.001/0.000004) can be explained by intraspecific variability among individuals than by variability among repeated laser shots or by batches run on different days (Figure C.5). Multi-shot chamber ablation is therefore a highly repeatable technique for extracting trace element signatures given that shot-average Mg/Ca value does not vary substantially within a given chamber.

4.4.2.2 What is the optimum number of individuals to detect subspecies variability?

To understand the optimum number of individuals needed to detect subspecies differences we conducted a rarefaction subsampling experiment using the best supported model from the previous subsection, and a simplified model without the subspecies effect. The difference in AIC scores between these two models indicates the improvement in model fit by considering systemic variation amongst subspecies. Each subspecies was subsampled at random in increments of 5 up to a maximum of 80. The process was repeated 50 times to create 800 model comparisons in total. We either record the ΔAIC values for the two models with and without subspecies, or N/A if a model failed to converge due to insufficient sampling coverage. As subsample size increased, so too did the ΔAIC (Figure 4.5A) while the percentage of models failing to converge decreased (Figure 4.5B). Once ~50 individuals from each subspecies were sampled (Figure 4.3B), the ΔAIC was consistently sufficiently large to infer statistical support for systemic subspecies variation with most models converging. This finding illustrates that a focus for palaeoceanography and palaeoclimate research must be on increasing sample sizes for LA-ICP-MS work to achieve representative sample sizes as used here. Representaive sample sizes will vary between species and system investigated, particularly the homogeneity of the material being sampled.

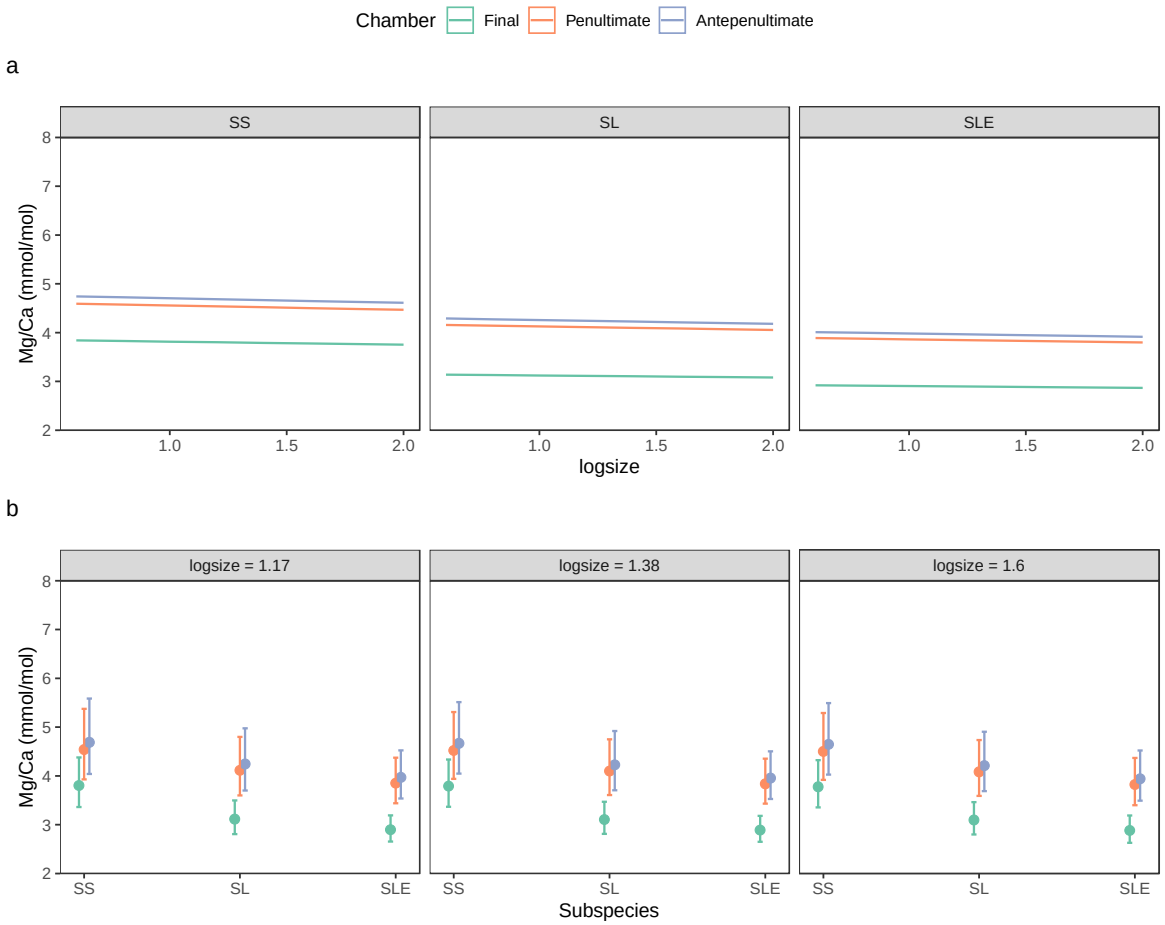

Figure 4.4 Model predictions of the relationship between Mg/Ca values, Subspecies classification (SS= Sensu stricto, SL=Sensu lato and SLE=Sensu lato extreme) and test size separated by chamber position represented by the colour of dot/line with 95% confidence intervals. Panel (a) presents predictions against log transformed test size separated by sub-species and panel (b) separated by mean-centred log test size. Note particularly how test size has no relationship with Mg/Ca.

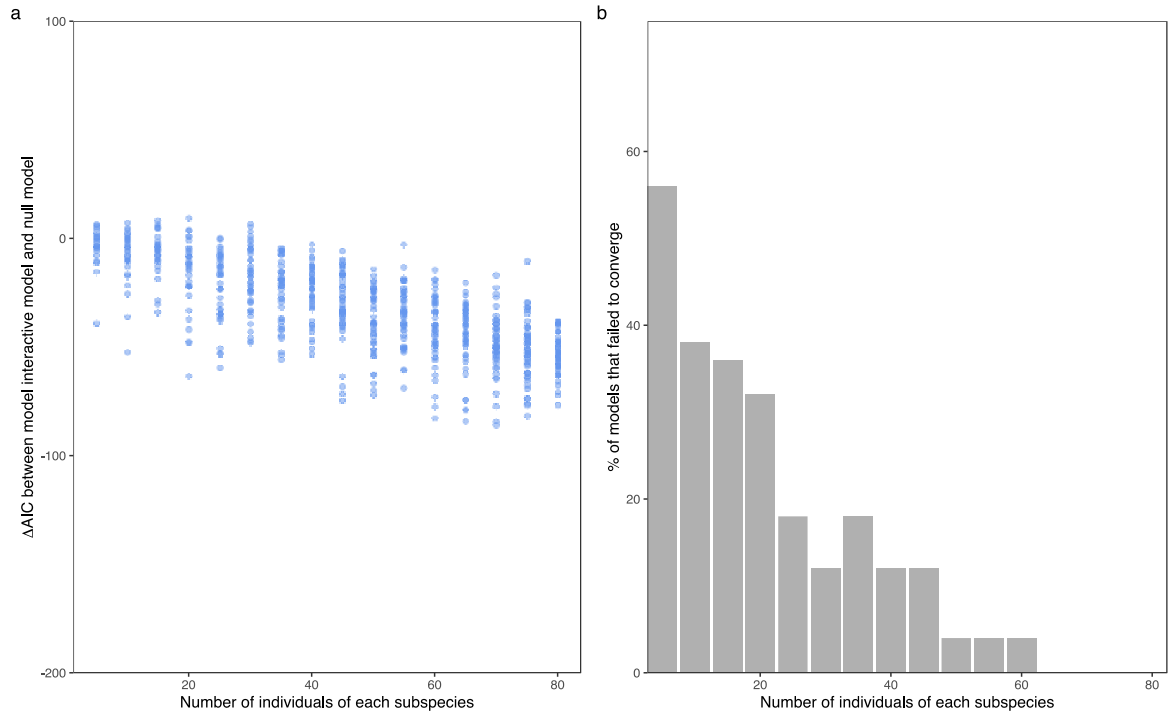

Figure 4.5 Results from rarefaction subsampling experiment. (a) The change in AIC between the fully interactive model which included subspecies as a fixed effect and the null model which did not include subspecies (Appendix C). Each subspecies sample size underwent 50 iterations. The larger the value on the y-axis the more support is given to the interactive model, note that as the number of individuals from each subspecies increases so does the support for the interactive model. (b) The percentage of models that failed to converge due to insufficient sample size and/or anomalously high values of Mg/Ca.

4.4.3 Stable Isotope variability

Stable isotope analysis was conducted on a subset of 104 individual specimens that had previously undergone LA-ICP-MS analysis using the methods described in Section 4.3.3.2. In contrast to trace element analysis, no detectable difference was found between subspecies in carbon or oxygen isotopes (ANOVA: Carbon $F(2,101) = 0.724$, $p = 0.487$, Oxygen $F(2,101) = 0.724$, $p = 0.487$) (Figure 4.6a-b). A conversion of oxygen isotope values to temperature using Eq. (2) shows the small difference between the mean for each subspecies equates to < 1°C. The range of calculated temperatures within each subspecies is however large, with sensu stricto and sensu lato extreme showing intraspecific variation of ~ 9 °C, whilst sensu lato show a difference of ~ 11°C between the highest and lowest calculated temperatures. The relationship between size and stable isotopes differs amongst subspecies (Figure 4.6c-d, Table C.10-C.11). Sensu stricto and sensu lato extreme show large variation with size in both oxygen and carbon; sensu lato shows a positive relationship, clearest in carbon isotopes, between stable isotopes and test area (Figure 4.6c-d).

4.4.3.1 Stable isotope values vs. Mg/Ca values

Using only the penultimate chamber Mg/Ca values (Figure 4.4), we plot $\delta^{18}O$ values and $\delta^{13}C$ values against Mg/Ca values (Figure 4.7). There is no detectable correlation between stable isotope values and Mg/Ca values (Figure 4.7; Table C.12-C.17) in all subspecies apart from $\delta^{18}O$ values and Mg/Ca values in SL (Table C.13; $p < 0.05$). In oxygen isotopes we observe that as $\delta^{18}O$ values become more negative Mg/Ca increase in SS and SL which would be expected (Figure 4.7a), however this relationship is much weaker in SLE. In carbon isotopes there is no observable pattern between $\delta^{13}C$ values and Mg/Ca, most likely because of a narrow range of $\delta^{13}C$ values.

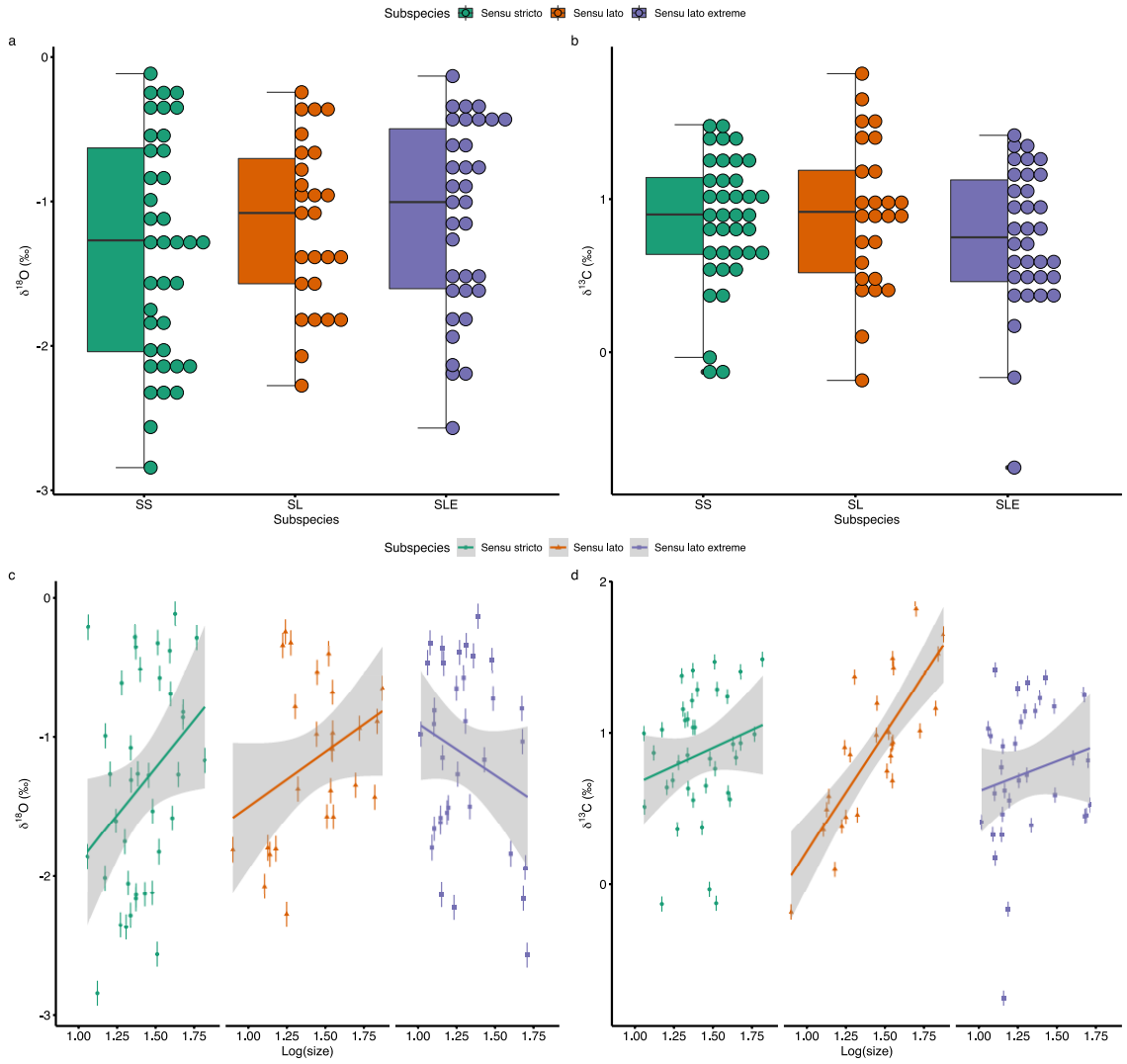

Figure 4.6 Stable oxygen (a, c) and carbon (b, d) isotope composition from analysis of 98 individuals, sample numbers differ between subspecies with SS=38, SL=26, SLE=34. In panels (a)-(b) the box represents the interquartile range whilst the whiskers show 1.5*interquartile range. Black circles represent outliers exceeding the 1.5*interquartile range. Black line represents the mean. Individual dots represent all individual specimens sampled. The among-individual distribution of stable isotope measurements reinforces the importance of considering sufficient sample sizes for intraspecific variability. Panels c-d show oxygen and carbon isotopes of individual foraminifera versus test area (size) separated into subspecies. Bars represent 0.09 ‰ analytical precision of oxygen measurements (c) and 0.05 ‰ of carbon measurements (d) . The lines show linear regression of isotope value against log(size) with grey representing 95 % confidence intervals.

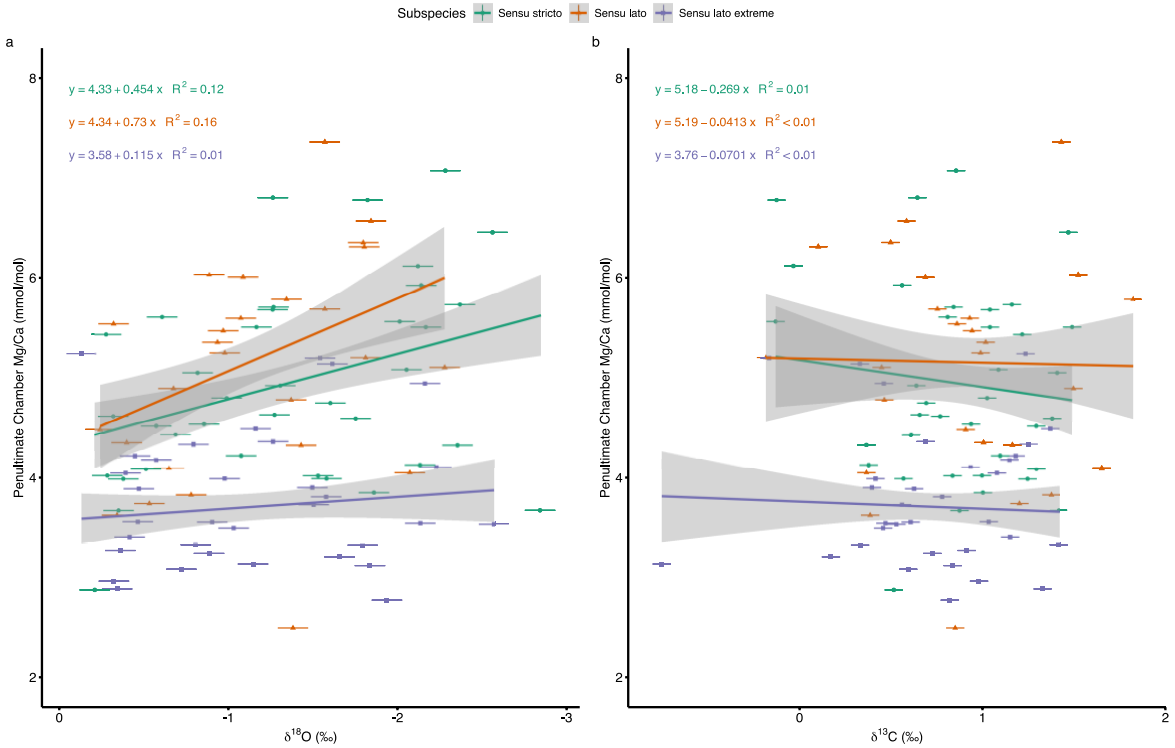

Figure 4.7 Stable isotopes oxygen (a) and carbon (b) values plotted against the penultimate chamber Mg/Ca values. Each point represents a spot value in the y-axis against whole specimen $\delta^{18}O$ and $\delta^{13}C$ values with error bars representing 0.09 ‰ analytical precision in oxygen isotopes (a) and 0.05 ‰ analytical precision in carbon isotopes (b).

4.5 Discussion

We show substantial variability in *Globigerinoides ruber* Mg/Ca values are partially explained by the presence of subspecies. In addition, we found differential Mg/Ca signatures through the ontogeny of those subspecies with the final chamber consistently depleted in Mg/Ca value compared to the other chambers. However, we found no difference between stable isotopes as a result of subspecies classification. Furthermore, we find no relationship between morphological traits and subspecies identification. Nevertheless, we calculate that within-specimen variation through ontogeny explains more variation in Mg/Ca values than differences among subspecies and thus argue for larger sample sizes when performing LA-ICP-MS.

4.5.1 Morphological variability in *G. ruber* subspecies

Morphological variation between subspecies is present, and can be used for identification, yet the degree of morphological separation and its potential taxonomic importance is disputed (Phillimore and Owens, 2006). The number of distinct morphological groups identified in *G. ruber* ranges from three (Parker, 1962) to eight (Robbins and Healy-Williams, 1991) along a morphocline. In this study we found that morphological variation does exist but does not correspond to taxonomically informative units (Figure 4.2, Table C.4), similar to other studies that used a greater range of morphological measurements (Numberger et al., 2009). We observed some separation in the aspect ratio of the final chamber and test that separated a large proportion of the sensu lato extreme morphotype (PC2 - Figure 4.2). Further separation was observed due to test and final chamber aspect ratio which corresponds to test and chamber compression, which is commonly used for morphotype identification (Aurahs et al., 2011; Carter et al., 2017; Kontakiotis et al., 2017; Kuroyanagi et al., 2008; Lin, Wang and Hung, 2004; Löwemark et al., 2005; Steinke et al., 2010; Wang, 2000). Future morphological studies should focus on measuring traits that have a known functional role and can be linked to the environment such as pore size which is linked to gas exchange (Bé, 1968; Burke et al., 2018; Constandache, Yerly and Spezzaferri, 2013; Kearns et al., 2021).

4.5.2 Geochemical variability

Variability in the geochemistry of subspecies does exist in *Globigerinoides ruber* at this Indian Ocean site. *G. ruber* sensu stricto shows systematically higher Mg/Ca values at the mean specimen size compared to sensu lato and sensu lato extreme of 0.44 ± 0.18 and 1.28 ± 0.17 mmol/mol respectively based on test-averaged Mg/Ca values (Table C.7). The depletion of SL and SLE in comparison to SS is in agreement with other trace element studies (Antonarakou et al., 2015; Sadekov et al., 2008; Schmitt et al., 2019). However, as we will discuss, the final chamber in

all subspecies is depleted in comparison to the other chambers (Figure 4.4) and therefore may not represent true water column temperature. Re-calculating this depletion based on the penultimate chamber suggests that sensu stricto is enriched compared to sensu lato and sensu lato extreme by 0.21 ± 0.26 and 1.23 ± 0.27 mmol/mol, respectively. The main subspecies difference exists between SS and SLE and is larger when calculated on the penultimate rather than final chamber. When penultimate chamber specific Mg/Ca values are converted to temperature using Eq. (1) this equates to a 0.56°C difference between sensu stricto and sensu lato and a 3.11°C difference between sensu stricto and sensu lato extreme. The temperature differences we find between SS and SL is similar to that found in the Indian Ocean of 0.5-1°C (Steinke et al., 2005) and correspond well to our $\delta^{18}O$ value derived temperature difference between SS and SL of 0.83 °C. Our Mg/Ca derived temperature difference is smaller than previously found in the Gulf of Mexico (~ 3°C; (Antonarakou et al., 2015), but the SL morphological concept used by Antonarakou et al (2015) is similar to our SLE in this study (Figure 4.1). Based on this observation, our 3.11°C difference between SS and SLE in this study is within the range of that between SS and SL in the Gulf of Mexico (Antonarakou et al., 2015). Detailed morphological work is clearly fundamental for unbiased geochemical inference.

Despite our trace element results, stable isotopes do not show detectable differences amongst subspecies in $\delta^{13}C$ or $\delta^{18}O$ values (Figure 4.6) with SS having a lower $\delta^{18}O$ value by 0.179 ‰ and 0.2 ‰ compared to SL and SLE respectively (Figure 4.6). In $\delta^{13}C$ values this difference is smaller with a maximum separation of 0.144 ‰ between SS and SLE (Figure 4.6). The lack of isotopic differences among subspecies (Section 4.4.3) is similar to some studies (Lynch-stieglitz et al., 2015; Mohtadi et al., 2009; Thirumalai et al., 2014) but in disagreement with others (Antonarakou et al., 2015; Carter et al., 2017; Löwemark et al., 2005; Steinke et al., 2010; Wang, 2000). Research that disagrees with our findings was primarily conducted over glacial-interglacial cycles where the magnitude of subspecies differences varied through time (Antonarakou et al., 2015; Carter et al., 2017; Steinke et al., 2010; Wang, 2000) with the smallest subspecies differences often similar to the mean ~0.2 ‰ difference between SS and SLE samples we observed (Carter et al., 2017; Steinke et al., 2010; Wang, 2000). Only one study conducted over glacial cycles agreed with our failure to detect differences among subspecies (Lynch-stieglitz et al., 2015).

When converted to temperature using Eq. (2), our results suggest a mean 0.83 °C difference between SS and SL and a 0.99°C difference between SS and SLE. Therefore, the penultimate chamber Mg/Ca temperature derived differences between SS and SLE we find are higher than those recorded by our oxygen isotope analysis. The lack of detectable differences in $\delta^{18}O$ and $\delta^{13}C$ values between subspecies is likely in part due to the different number of specimens analysed in each analysis (Trace element n=262; Stable isotopes n=98). Indeed, our Mg/Ca analysis suggested ~ 50 individuals from each subspecies were needed to unpick subspecies difference (Figure 4.5).

Additionally, our results and those discussed (Antonarakou et al., 2015; Carter et al., 2017; Steinke et al., 2010; Wang, 2000) may show that differences in the stable isotopes of subspecies are only revealed over longer time periods such as glacial cycles where subspecies differences are at their peak. More studies, with more individuals over climatic transitions, are needed to understand the sensitivity of stable isotope and trace element analysis to both time and analytical resolution.

4.5.2.1 Drivers of geochemical variability

G. ruber is restricted to the upper water column (Dekens et al., 2002; Anand and Elderfield, 2005) and is not thought to migrate vertically during life (Aurahs et al., 2011; Tolderlund and Bé, 1971). Despite being used to indicate surface mixed layer (SML) temperatures, *G. ruber* does have a broad ecological niche extending below the base of the SML to the base of the deep chlorophyl maximum (DCM) (Lončarić et al., 2006; Peeters, Brummer and Ganssen, 2002).

Our Mg/Ca results, like others (Antonarakou et al., 2015; Carter et al., 2017; Kawahata, 2005; Kuroyanagi and Kawahata, 2004; Löwemark et al., 2005; Numberger et al., 2009; Steinke et al., 2005; Wang, 2000), suggest subspecies variability in calcification depth with SLE calcifying in a cooler, deeper part of the upper water column compared to SS and SL. Subspecies calcification depth variability would explain the large ecological niche found in other studies (Lončarić et al., 2006; Peeters, Brummer and Ganssen, 2002). Based on CTD profiles from the area (Birch et al., 2013; Kroon and the Shipboard Scientific Party, 2010) our temperature calibrations would place SS slightly above the base of the surface mixed layer (SML) at ~40m (Birch et al., 2013b) with SL and SLE inhabiting the upper thermocline below the SML but well above the deep chlorophyl maximum at ~95m (Birch et al., 2013). Our stable isotope results however do not point towards such a difference in depth habitat (Figure 4.6). Again, based on CTD profiles from the area (Birch et al., 2013; Kroon and the Shipboard Scientific Party, 2010) our $\delta^{18}O$ results suggest all subspecies lived above the base of the SML at ~ 40 m (Birch et al., 2013). The CTD profiles of DIC $\delta^{13}C$ values show that there is a weak $\delta^{13}C$ gradient in the upper 100 m of the water column, potentially explaining the narrow range and lack of statistical significance we observe in our $\delta^{13}C$ values.

Another potential influence subspecies temperature variability is the seasonal preference of subspecies. The annual seasonal SST range in this area is ~ 5°C (Birch et al., 2013; Damassa et al., 2006; McClanahan, 1988), which is larger than 1-2°C range we observe among subspecies. Seasonality would imply that SS and SL preferentially live during the summer months when SST is ~ 30°C whilst SLE lives during the winter when SST decreases to around 25°C (Birch et al., 2013). Preferential seasonality has been proposed as potential driver in other ocean basins (Antonarakou et al., 2015; Sadekov et al., 2008) but sediment trap studies in Java (Mohtadi et al., 2009), South

China Sea (Lin, Wang and Hung, 2004) and the Gulf of Mexico (Thirumalai et al., 2014) as well as plankton tow studies in the Arabian Sea (Peeters, Brummer and Ganssen, 2002) reveal no seasonal or monsoonal preference of *G*. *ruber* subspecies which is supported by our stable isotope results.

The conflicting results between Mg/Ca values and stable isotopes could be the result of multiple phenomena. Individual SS and SL appear to show a linear relationship between $\delta^{18}O$ values and Mg/Ca values (Figure 4.7a), indicating similar depth habitat or seasonality controls on both proxies. However, this relationship is not perfect, which implies other controls acting on one or both proxies. In comparison, SLE shows little to no relationship between $\delta^{18}O$ values and Mg/Ca values, suggesting there is another factor driving $\delta^{18}O$ values and/or Mg/Ca values aside from depth habitat/seasonality in this subspecies. We find a negative correlation between individual specimen $\delta^{18}O$ and $\delta^{13}C$ values (Figure 4.8). Similar correlations have been observed in culturing experiments from changes to seawater [CO_3^{2-}] (Spero et al., 1997), which is also known to influence Mg/Ca values (Evans et al., 2016; Gray et al., 2018; Kisakürek et al., 2008; Lea, Mashiotta and Spero, 1999; Russell et al., 2004) and implies some influence of the carbonate system on our stable isotope and Mg/Ca values. In addition, we see a large degree of intraspecific variability in both $\delta^{13}C$ and $\delta^{18}O$ values (Figure 4.6 - Figure 4.8) alongside a relationship between stable isotopes and size (Figure 4.6). Together these observations are consistent with the larger foraminifera having on average higher rates of respiration and calcification thus adding proportionally more CO_2 into the foraminifera microenvironment (Zeebe and Wolf-Gladrow, 2001). This would in turn cause the pH of the microenvironment to decrease, increasing $\delta^{13}C$ values and reducing $\delta^{18}O$ values (Bijma et al., 1998; Spero et al., 1997) and increasing Mg/Ca values (Evans et al., 2016). Variations in the fluxes of calcification and respiration at an individual level could then be a significant contributor to the large intraspecific variance we observe (Figure 4.6 - Figure 4.8).

In summary, whilst we cannot dismiss potential impacts of seasonality, we think a major impact is unlikely based on our Mg/Ca values and $\delta^{18}O$ values and other studies (Lin, Wang and Hung, 2004; Mohtadi et al., 2009; Peeters, Brummer and Ganssen, 2002; Thirumalai et al., 2014). We instead hypothesize that the geochemical variability we observe is a combined result of physiological mediated differences in the carbonate system experienced and depth habitat variability in the upper water column, with SLE on average living at a greater depth than SS and SL.

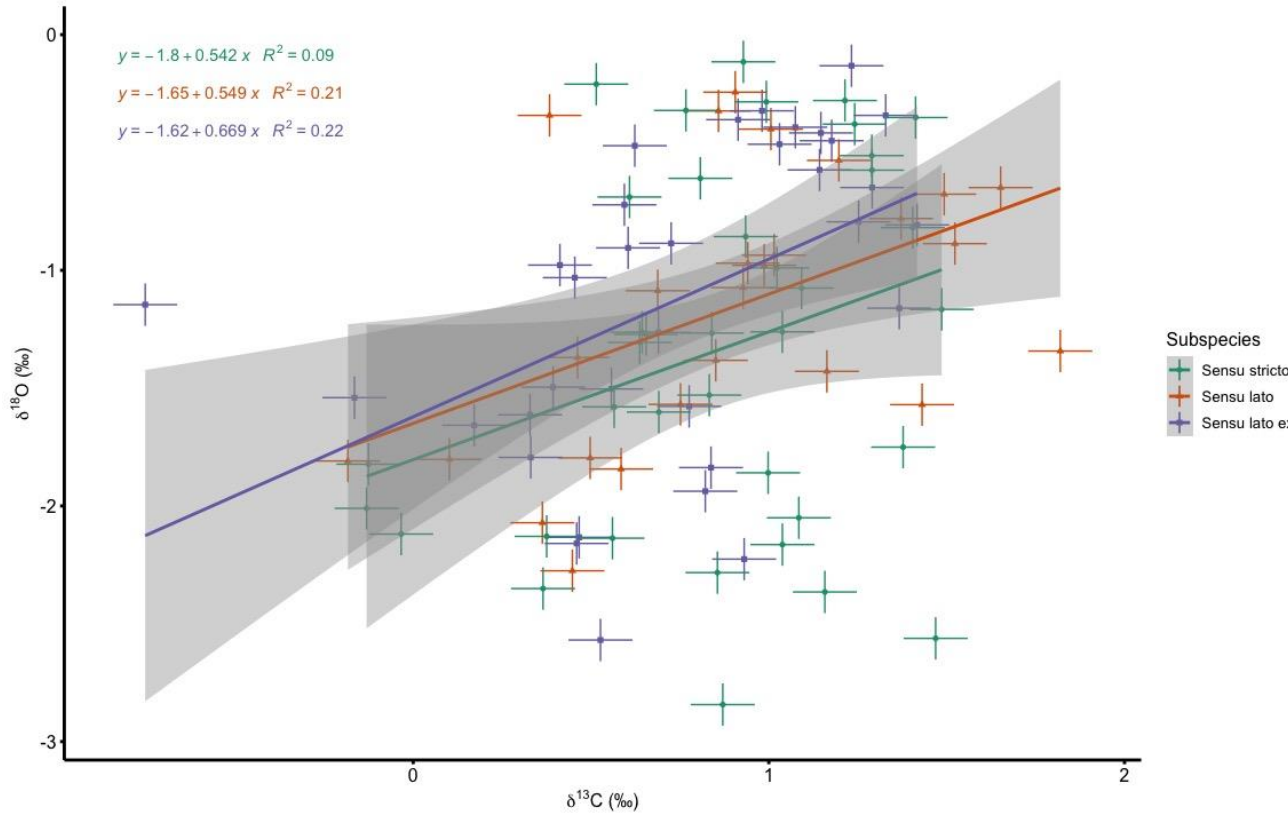

Figure 4.8 – Stable isotope $\delta^{13}C$ values plotted against $\delta^{18}O$ values. Line and point colour represent subspecies. Error bars represent 0.09 ‰ analytical precision. Each point represents an individual foraminifer.

4.5.2.2 Ontogenetic variability

Subspecies variability, discussed in Section 4.5.2, is complicated by ontogenetic changes (Figure 4.4). Test heterogeneity of Mg is present in all species of foraminifera and is thought to be at least partly decoupled from temperature (Spero et al., 2015). Variability between chambers is not unexpected, given the nature of the water column and planktonic lifestyle of these foraminifera (Pracht, Metcalfe and Peeters, 2019). Ontogenetic variability has been observed in other studies of planktonic foraminifera (Anand and Elderfield, 2005b; Bolton et al., 2011; Dueñas-Bohórquez et al., 2011; Sadekov et al., 2008). Here, we have shown for the first time that chamber variation in *G. ruber* Mg/Ca values is systematic at the subspecies level with different Mg/Ca values through the final whorl. We observed an overall pattern of final chamber depletion in all subspecies (Figure 4.4) with the antepenultimate and penultimate chambers showing similar values though the antepenultimate chamber tends to be enriched in comparison (Figure 4.4). The subspecies grouping of these patterns suggests they are ecologically or biologically driven geochemical signatures.

Final chamber depletion is a pattern observed in various planktonic foraminifera (*G. sacculifer* (Dueñas-Bohórquez et al., 2011; Hemleben, Spindler and Anderson, 1989); *G. bulloides* (Anand and Elderfield, 2005; Marr et al., 2011) and *G. ruber* (Bolton et al., 2011; Sadekov et al., 2008)). This pattern is often thought to be a byproduct of the life cycle of planktonic foraminifera and the deepening depth habitat during the terminal growth stages (Bijma, Erez and Hemleben, 1990; Pracht, Metcalfe and Peeters, 2019) and therefore linked to temperature changes in the water column. However, observations of final chamber depletion in cultured, lab grown *G. sacculifer* (Dueñas-Bohórquez et al., 2011) and plankton tow samples (Bolton et al., 2011) suggest that this pattern may not be environmentally linked. Furthermore *G. ruber,* as previously noted, is not thought to migrate vertically during life (Aurahs et al., 2011; Meilland et al., 2019; Tolderlund and Bé, 1971).

Chamber heterogeneity between subspecies could be a result of the biomineralization process. In symbiont bearing planktonic foraminifera, like *G. ruber*, diurnal changes in the biological activity of algal symbionts have been hypothesized to contribute to Mg/Ca banding within the chamber walls (Eggins, Sadekov and De Deckker, 2004a; Fehrenbacher et al., 2017a; Sadekov, Eggins and Deckker, 2005). As foraminifera grow, older chambers are overprinted with the calcite of newly formed chambers (Hemleben, Spindler and Anderson, 1989) increasing chamber thickness and adding new Mg/Ca bands. Variability in high and low Mg bands between chambers may explain the variation we see if such banding was subspecies specific and a geochemical “vital effect”. The

number of high Mg bands diminishes through the final whorl of *G*. *ruber* with the final chamber made up of only low Mg bands (Sadekov, Eggins and Deckker, 2005). Although this banding is not thought to impact overall test signal (Holland et al., 2020b), it could influence chamber specific signals. The observed absence of high Mg bands in the final chamber of *G*. *ruber* specimens (Sadekov, Eggins and Deckker, 2005) may also explain the apparent depletion of the final chamber in this study and others (Anand and Elderfield, 2005b; Bolton et al., 2011; Dueñas-Bohórquez et al., 2011; Sadekov et al., 2008). The experimental design of our study meant that an investigation of banding differences between subspecies or chamber, while of fundamental interest, is not possible given the nature of our data collection. Though the reasons behind chamber heterogeneity are unknown in our dataset, we can conclude that the final chamber does not reflect SST and therefore should not be used for SST reconstructions. Instead, we recommend the use of the penultimate chamber for all subspecies.

4.5.2.3 Influence of chamber and test size

Test size is recognized as an influential driver of stable isotope variability in foraminifera (Elderfield et al., 2002; Ezard et al., 2015; Friedrich et al., 2012; Spero, 1998; Spero & Lea, 1996). To minimize such effects, stable isotope analyses are typically conducted on narrow size fractions. A similar practice has been applied to trace elements (Cléroux et al., 2008; Elderfield, Vautravers and Cooper, 2002; Friedrich et al., 2012; McConnell and Thunell, 2005; Ni et al., 2007) with the larger size fraction often recommended (Elderfield et al., 2002). In this study we picked individuals from a narrow size fraction (250-355 µm) and found no significant impact on Mg/Ca values of individual test size (Figure 4.4; Table C.7). Although size does have an impact on Mg/Ca, the use of narrow size fractions remains a good mitigation technique in trace element analysis to avoid test size effects.

The effects of individual chamber size on Mg/Ca values have never been investigated until now. We found no detectable impact of chamber size on chamber Mg/Ca values (Section 4.4.2.1; Table C.8). This demonstrates that the final chamber depletion we observe in all subspecies is not, in our dataset, the result of smaller final chambers which are often found in “kummerform” individuals (Berger, 1969; Olsson, 1973). This contrasts with our stable isotope results which show a correlation with size (Figure 4.7). We suggest that the differing relationships between Mg/Ca values, $\delta^{13}C$ values, $\delta^{18}O$ values and size should be investigated further to understand the implications and drivers of these discrepancies.

4.6 Conclusions and palaeoceanographic implications

We have shown that using LA-ICP-MS at chamber-by-chamber resolution is a repeatable, reliable method to measure ontogenetic variability in planktic foraminifera that is lost when using bulk sampling methods. Although such fine scale measurements do generate statistical noise, meaningful patterns can still be found when sufficient samples of individuals are used and interpreted as members of a wider homogeneous population. By applying this approach, we detected subspecies differences in *G. ruber* from the Indian Ocean. To avoid signal mixing, we recommend palaeoceanographic studies should favor using *G. ruber* sensu stricto as the subspecies that best represents the surface mixed layer. We recommend for the continued selection of the narrowest size fraction LA-ICP-MS analysis of Mg/Ca until other studies find a qualitatively similar result. In addition, recommend for the continued sampling from the narrowest size fraction possible for stable isotope analysis. When measuring intra-individual variation using LA-ICP-MS, the penultimate chamber provides a more reliable signal for the overall individual than the depleted final stage. Through this analysis we have also demonstrated and discussed how more work is needed to understand the drivers of Mg incorporation and how this signal is influenced by environmental and biological variables. Better understanding of the biological, ecological, and environmental causes of intraspecific variability would unlock the full potential of Mg/Ca measurements, integrating single-specimen and time-averaged bulk measurements, to reveal past climate change at all levels of temporal granularity from days to millions of years.

Chapter 5 Conclusion

The work presented in this thesis applies novel approaches to understand planktonic foraminifera on an individual scale in both deep and shallow time. I use effective diversity to understand community-level ecosystem responses to transient climatic perturbations (Chapter 2). Subsequently, I dive deeper into those effective diversity curves (Hill numbers) to probe two emergent problems from a high taxonomic level approach. Then, I investigate the feasibility of applying ecometric, trait-based approaches to planktonic foraminifera in deep time(Chapter 3). Finally, I present and analyse a large-scale relational data set combing morphological and geochemical data to understand the correspondence between genetics, morphology and geochemistry, the role of cryptic diversity within species and the potential implications for palaeoceanographic studies (Chapter 4). The results of these chapters are outlined below in response to the research questions presented in Chapter 1. I make recommendations for future studies.

5.1 Chapter 2

5.1.1 How did planktonic foraminifera diversity respond to transient warming during the Middle Eocene Climatic Optimum (MECO) in the mid-latitude North Atlantic?

The Middle Eocene was a period of biotic restructuring for planktonic foraminifera that included, but was not limited to, the progressive extinction of key symbiont bearing surface dwellers (Boersma and Premoli Silva 1986; Boersma and Silva 1991; Keller et al. 1992; Wade 2004; Wade and Pearson 2008), changes to ecology (Coxall et al., 2000; Wade et al., 2008; Edgar et al., 2013) and reduction in test size (Schmidt, Thierstein and Bollmann, 2004; Wade and Pearson, 2008; Wade and Olsson, 2009). Our understanding of how the Middle Eocene Climatic Optimum (MECO) impacted planktonic foraminifera ecosystems, and the relative roles of the constituent functional groups, is lacking, however.

In Chapter 2, I presented calculated diversity changes across the MECO using Hill numbers on 22,830 individual tests separated into two size fractions. I presented diversity analysis for the first time at a mid-latitude MECO site (IODP Exp. 342) providing a unique insight into this transient interval and our climate system. My results show whilst the MECO did impact diversity dynamics of planktonic foraminifera in the Middle Eocene (Figure 2.2 - Figure 2.4), the millions of years pre- and proceeding the MECO were also influential: rather than an abrupt climate reset, the MECO might be better thought of as a catalyst for changes to the climate system and thus, unsurprisingly, the biota that lived within it. I showed that major changes occurred in depth

habitat occupation resulting from the gradual removal of large symbiotic surface-dwelling taxa because of pre-and post-MECO cooling (Figure 2.4). In addition, my results show that palaeoclimatic and palaeoceanographic changes during the MECO resulted in uneven assemblages that were morphologically less diverse than the period preceding the MECO. Whilst some taxa were losers because of the MECO, generalist and opportunistic taxa were winners.

My results show that biotic responses to transient warming events are dynamic and are driven by site locality and palaeolatitude. To gain a complete global picture of biotic responses to climatic perturbations, more work is need in the high latitudes. My results demonstrate that future diversity studies could utilize effective diversity to permit the inter-site comparisons that are needed to create a global view of ecosystem responses to the MECO and other intervals of climatic upheaval.

5.1.2 How does analytical choice of size fraction impact inferences of diversity change across climatic perturbations?

Size is a broad issue, whether it be as a result of taphonomic or sampling bias (Brown et al., 2013a, 2013b), that impacts our understanding and public perception of biodiversity (Rillo et al., 2017). Diversity analyses in planktonic foraminifera are generally conducted in one size fraction, most often > 150 µm (Kucera et al., 2005) despite the inevitability of removing smaller individuals. In Chapter 2, I conducted diversity analyses at two size fractions (> 63 µm and > 180 µm) and showed that the timing and strength of assemblage responses to the different stages of the MECO varied with size fraction choice Figure 2.2 - Figure 2.4. I showed that for morphological and genera richness, the GAMs for > 63 µm size fraction were more complex compared to > 180 µm size fraction indicating that intra-sample variability was larger in the > 63 µm size fraction (Figure 2.2). In contrast, both Shannon's index and Simpson's index in the > 180 µm size fraction showed more complex responses as a function of age compared to the > 63 µm size fraction (Figure 2.2). In addition, I presented results that showed that size was the most influential predictor for both genera and morphological diversity in terms of richness and Shannon's index.

These results showed that when conducting diversity analysis care should be taken when choosing a size fraction for analysis to gain a representative understanding of diversity changes across climatic transitions. Future studies should choose a size fraction according to the diversity of the individuals present in the assemblages and should strive to use the smallest size fraction possible. Furthermore, my results demonstrate the advantages of using two size fractions to assess diversity which should be implemented into future studies where possible.

5.2 Chapter 3

5.2.1 How consistent are hypothesized functional traits in planktonic foraminifera across the Middle Eocene Climatic Optimum?

The use of ecometrics has been proposed as a way of link the past to the present (Eronen et al., 2010) but requires the identification of a trait-environment relationship. In deep time, such a relationship requires the identification of meaningful correlations between organism and environment through so-called functional traits (Eronen et al., 2010). Examples of functional traits in planktonic foraminifera are spines (Hemleben et al., 1991) and pore size (Bé, 1968; Baumfalk et al., 1987; Burke et al., 2018), which are difficult to measure easily and in the potentially high numbers required to investigate functionality. In Chapter 3, I present results of combined geochemical and morphological analysis of the Eocene genera *Subbotina* to investigate functionality of test size and shape in foraminifera.

In symbiont-bearing foraminifera, a positive $\delta^{13}C$ value size relationship is present, which suggests that size is functional because a correlation between environment and organism is observable (Eronen et al., 2010). I found no detectable relationship between $\delta^{13}C$ values and test size in *Subbotina* (Figure 3.4). Whilst this was expected in a non-symbiont bearing foraminifera, I showed for the first time that either test size is not functional in *Subbotina* or that trait plasticity can mask functionality during climatic perturbations. Furthermore, my results indicate that test weight, rather than test size, may be functional in *Subbotina* as there is a detectable correlation between $\delta^{13}C$ values and test weight. These results imply that functionality of traits in planktonic foraminifera can vary between different ecological strategies, that more involved measuring technologies might provide better inference of trait function and that more work is needed to identify the strength of functionality in multiple traits across all planktonic foraminifera for ecometrics to be applied effectively.

5.2.2 How did the planktonic foraminifera genus *Subbotina* rise to dominance through the middle Eocene despite substantial thermal changes in its depth habitat?

Subbotina is a key, thermocline dwelling planktonic foraminifera of Paleogene assemblages as a result of its global occurrence throughout the Eocene and into the late Oligocene (~65 - 23 Ma; (Aze et al., 2011; Wade et al., 2011)), thus persisting through numerous climatic fluctuations. Additionally, *Subbotina* has been shown to have a variable depth habitat across the Eocene based on bulk isotopes (Macleod, Keller and Kitchell, 1990; Bralower et al., 1995; Wade, 2004; Dutton, Lohmann and Leckie, 2005; Wade and Pearson, 2008; Stap et al., 2010; Arimoto et al., 2020) and showed global increases in abundance in the Middle Eocene which was a period detrimental to

other groups (Macleod, Keller and Kitchell, 1990; Luciani et al., 2010). The drivers of such a variable habitat and increasing abundances were unknown, however. To better understand this, I measured $\delta^{18}O$ values and $\delta^{13}C$ values of 120 *Subbotina* individuals and compared them to bulk stable isotopes of planktonic foraminifera from different depth habitats (Figure 3.2). The results presented in Chapter 3 show that, whilst *Subbotina* bulk isotopes do a good job of representing the mean isotopic value of individuals, intraindividual variability is high in both $\delta^{13}C$ and $\delta^{18}O$ values (Figure 3.2). This variability implies *Subbotina* individuals existed in a broad isotopic space overlapping bulk measurements that indicate the location of the mixed layer and subthermocline. These results indicate that *Subbotina* had a wide ecological niche, and it is this wide niche that aided its survival through a climatic transition (MECO), that we showed warmed its favoured depth habitat (thermocline) and allowed it to dominate assemblages as shown in Figure 2.4.

These results support arguments that intraindividual variability can provide insights into ecological responses. Given their abundance as fossils, future foraminifera studies should focus on generating individual based records to further both palaeoecological and palaeoceanographic research.

5.2.3 How did the thermal and trophic structure of the upper water column respond to palaeoceanographic changes in Northwest Atlantic during the Middle Eocene?

The MECO is a globally recognized event (Bohaty and Zachos, 2003; Bohaty et al., 2009; Rivero-Cuesta et al., 2019; Edgar et al., 2020). Our understanding of the palaeoceanographic changes in the upper water column across the MECO relies on spatially diverse planktonic foraminifera $\delta^{18}O$ and $\delta^{13}C$ data. The restricted number of IODP sites that capture the MECO with sufficient resolution and fossil preservation is therefore hindering progress. My work adds the most northerly site to date to this spatial record.

Upper water column thermal change were decoupled from those in the thermocline and subthermocline in response to the MECO (Galazzo et al., 2014; Arimoto et al., 2020). In Chapter 3, I presented results from low resolution bulk stable isotopes that support this decoupled response in the North Atlantic at Exp. 342 (Sites U1408 and U1410). My results show that the thermocline and subthermocline experienced much more warming (~7°C) than the mixed layer (~1 °C) through to the MECO. In Chapter 3, I show abrupt cooling after the MECO occurred at the thermocline, whilst the surface ocean experienced only minor cooling. These results contrast with others that found a larger thermal response in the surface ocean in the southern high latitudes (Bijl et al., 2010; Bohaty and Zachos, 2003; Bohaty et al., 2009), tropics (Cramwinckel et al., 2018, 2019) and northern mid-latitudes (Arimoto et al., 2020). My results do show a reduction in primary productivity coincident with peak MECO warming, which has also been observed in the South

Atlantic (Galazzo et al., 2014), which implies that the mid latitude South and North Atlantic experienced similar productivity declines, unlike the other MECO sites cited previously. My results reinforce the need for geographical coverage among IODP sites to understand geographical differences in palaeoceanographic responses to the MECO and that future drilling expeditions should focus on the northern mid and high latitudes.

5.3 Chapter 4

5.3.1 Does intraspecific variability in *Globigerinoides ruber* match the definition of genetically inferred subspecies?

Globigerinoides ruber is the workhorse planktonic foraminifera for palaeoceanographic studies. Yet, the water column signal it represents is debated due to the presence of cryptic diversity and genetic subspecies that some researchers have argued live in different parts of the water column (Antonarakou et al., 2015; Aurahs et al., 2011; Kawahata, 2005; Kuroyanagi et al., 2008; Kuroyanagi and Kawahata, 2004; Lynch-stieglitz et al., 2015; Mohtadi et al., 2009; Naik, 2016; Numberger et al., 2009; Sadekov et al., 2008; Steinke et al., 2010; Thirumalai et al., 2014; Wang, 2000). The depth disparity between subspecies is highly debated, however. None of these studies have taken a high-resolution individual based analysis integrating morphological, stable isotope and Mg/Ca data. In Chapter 4 I present morphological data on 450 *G. ruber* individuals, paired with 98 individually analysed tests for stable isotopes and 262 individuals analysed for Mg/Ca values using LA-ICP-MS (Laser Ablation Inductively Coupled Plasma Mass Spectrometry) at the chamber level. This is the largest dataset on *Globigerinoides ruber* produced to date.

The results I presented showed that substantial variability in Mg/Ca values exists, which is driven by subspecies classification: SLE (sensu lato extreme) subspecies lives at a greater depth than SS (sensu stricto) and SL (sensu lato) as inferred by Mg/Ca LA-ICP-MS (Figure 4.4). This separation is not expressed morphologically or through stable isotopes. These results demonstrate that the morphological traits measured in my study were not sufficient to unpick genetically inferred subspecies; future studies could focus on different morphological traits, perhaps those hypothesized in Chapter 3 to be more likely to have a functional role. Furthermore, rarefaction analysis suggests that subspecies identification requires > 50 individuals to be analysed to stand a reasonable chance of detecting differences amongst geochemically inferred niches. Part of the controversy surrounding such cryptic diversity is thus likely due to the vagaries of random sampling on small sample sizes. Though I did present results that find evidence for trace element separation among *G. ruber* subspecies, stable isotope results did not show a corresponding separation (Figure 4.6). As multiple LA-ICP-MS shots were taken per individual, and this

pseudoreplication was accounted for in my statistical models, this reinforces the need that larger datasets are required for sample sufficiency. I conclude that future studies should only pick SS for surface water reconstructions and should focus on the more reliable penultimate chamber. More work is needed to understand the driving factors of Mg/Ca values and $\delta^{18}O$ values for more reliable temperature reconstructions.

5.3.2 What are the impacts of intraspecific and intra-chamber size variation on Mg/Ca values in *Globigerinoides ruber?*

The picking within size fractions is a commonly practiced protocol in studies based on planktonic foraminifera to reduce the impact of test size on geochemical results. The impact of individual test size alongside the impact of chamber size on Mg/Ca values is understudied, however. In Chapter 4 I combine morphological, and chamber resolved Mg/Ca measurements of 262 individuals of *G. ruber* to investigate the role of test and chamber size on Mg/Ca, but found no detectable effect on Mg/Ca values (Figure 4.4). If other studies find a qualitatively similar result, this implies that the protocol of picking within narrow size fractions is sufficient to reduce the impacts of size in trace element studies and should be continued in future studies. In contrast, stable isotopes showed a detectable relationship between both $\delta^{18}O$ values and $\delta^{13}C$ values and size implying that future studies should endeavour to sample from the narrowest possible size fraction to control for the effects of size.

5.4 Future work

The planktonic foraminifera fossil record is an outstanding tool for investigating macroevolutionary responses to abiotic forcings. Its high spatial and temporal resolution allows for the generation of integrated morphological, ecological, and climatic datasets that can be used to answer questions related to the impacts of current and future anthropogenic climate change. For these records to be as biologically meaningful and useful as possible it is important that we as researchers focus on measuring the correct variables. A major focus of my thesis has been to integrate different layers of data, whether those metrics are genetic, geochemical, morphological, taxonomic or community.

The research I presented in Chapter 2 and Chapter 3 focused on one locality at one point in time. To increase our understanding, more work is needed to generate similar records across time and space to understand the geographical nature of ecosystem responses and the consistency across different magnitudes and/or directions of abiotic change. I show that effective diversity is an appropriate and informative tool for investigating diversity changes in deep time with the capacity to provide a “common currency” of ecosystem functioning across samples. Further work should

be undertaken to use newly published species occurrence datasets (e.g., Triton, (Fenton et al., 2021)) to generate effective diversity records that can then be compared across time and space.

The work I presented in Chapter 2 focused on planktonic foraminifera morphological traits that can be reliably and repeatedly measured with ease (test area and test shape). As I demonstrated these traits have no detectable functional role across the planktonic foraminifera in my work, and therefore not suitable for ecometric analysis. Future work should use more refined morphological measurements from technological advancements such as micro-CT scanning to investigate other assumed functional traits such as pore size (Burke et al., 2018; Bé, 1968).

The results presented in Chapter 4 show that more work is needed to understand the drivers of Mg/Ca values and $\delta^{18}O$ values to generate reliable temperature records. Future research should focus on high resolution individual scale planktonic foraminifera analysis to further understand so called “vital effects” and how they influence generated temperature records. Vital effects are hard to quantify but using the approaches I advocate and explore in this thesis we can being to unpick them.

Appendix A Supplementary information for Chapter 2

The following supplement provides tables of all data produced. Where data is not provided this is because it is too large and be made available upon request. The following document is included to enable the reproducibility of the results in Chapter 2 and upon publication of this manuscript will be made publicly available along with the data.

1 Introduction to Appendix A

This appendix is intended to provide reproducible code for the results presented in the manuscript. All analyses were performed in the freely distributed R environment (R Core Team (2020)). This supporting information was written using knitr (Xie (2020)) and kableExtra (Zhu (2019)). The code uses the tidyverse (Wickham (2019)) , readxl (Wickham and Bryan (2019)) and mgcv (Wood (2017)) and packages within as well as dependencies (Aze et al. (2011)). Here we provide the sample information for all samples included in our analysis as well as morphological and ecological classification of identified genera which are all referenced within the manuscript.

```
library(readxl)
library(tidyverse)
library(knitr)
library(kableExtra)
library(mgcv)
library(FSA)
library(broom)
library(itsadug)
library(xtable)
library(formatR)
library(MuMIn)
library(rstatix)
library(ggpubr)
```

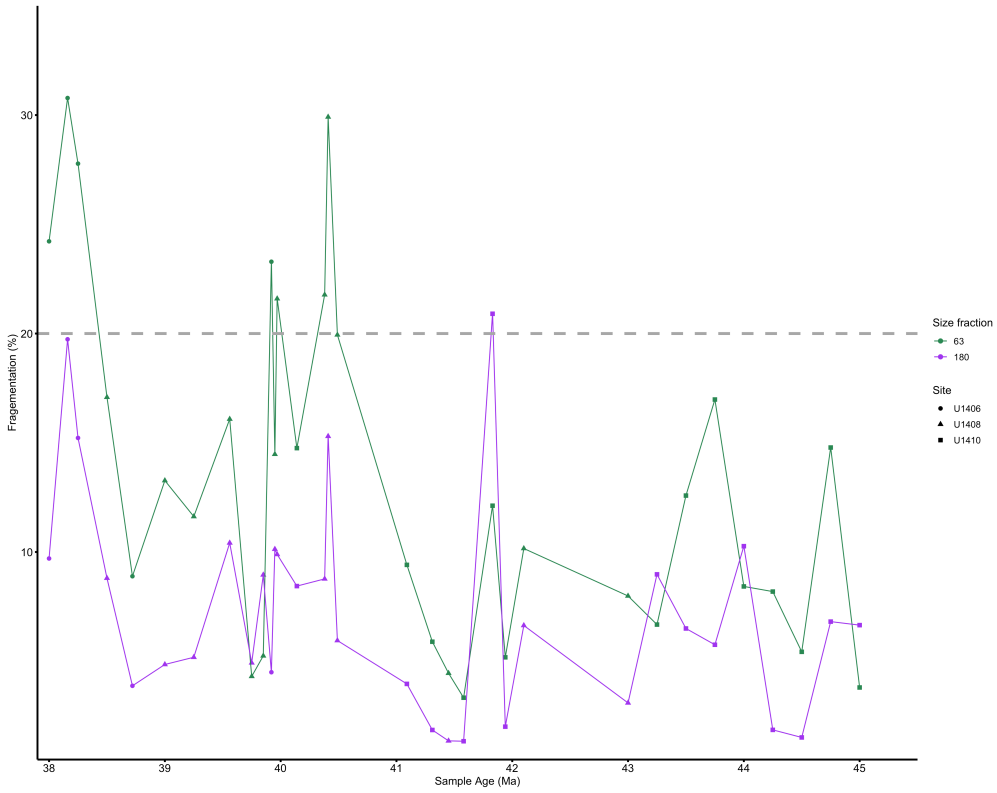

Figure A.1: Fragmentation across samples from Expedition 342 at both size fractions. Symbols indicate site, whilst colour indicates size fraction.

Table A.1: IODP Expedition 342 samples used in this study. Lab ID= Study specific sample ID, Expedition = IODP expedition number, Top Int = Top interval (m), Bottom Int = Bottom interval (m), Sample ages were calculated based on an age depth model constructed using available biostratigraphic and magnetostratigraphic data for Sites U1408 and U1410 (Norris et al (2012), Yamamoto et al (2018) and Cappelli et al (2019)). Age calibrations from the 2012 geologic timescale were used for middle Eocene geomagnetic polarity reversals (GTS2012; Gradstein et al (2012), Ogg et al (2012))

LAB ID	EXPEDITION	SITE	HOLE	CORE	SECTION	TOP_DEPTH	BOTTOM_DEPTH	Depth (CCSF-A, m)	U1408 Mapped Depth (CCSF-M, m)	Inter-site Mapped Depth (CCSF-X)	Age (GTS_2012)
67	342	1406	A	27	3	88	90				38.00
7	342	1406	A	27	4	137.5	139				38.16
68	342	1406	A	27	5	100	102				38.25
80	342	1408	B	5	2	60	62				38.50
8	342	1406	A	27	6	62	63.5				38.72
74	342	1408	A	5	2	38	40				39.00
75	342	1408	A	5	5	30	32				39.25
82	342	1408	B	7	1	98	100	49.08	49.08	49.76	39.56
96	342	1408	C	7	2	58	60	54.19	54.26	54.94	39.68
34	342	1408	B	8	1	120	121.5	60.11	60.13	60.81	39.85
20	342	1406	B	28	5	1.5	3				39.92
83	342	1408	B	8	4	28	30	63.69	63.69	64.32	39.95
35	342	1408	B	8	4	106.5	108	64.47	64.47	64.89	39.97
59	342	1410	B	10	5	117	118.5	90.04	90.04	70.64	40.14
76	342	1408	A	8	2	117	118	71.57	71.57	78.89	40.38
30	342	1408	A	8	3	69	71	72.59	72.59	79.91	40.41
98	342	1408	C	9	2	98	100	75.28	75.46	82.78	40.49
51	342	1410	A	11	1	97	98.5	102.20	101.93	102.98	41.09
53	342	1410	A	11	5	129.5	131	108.53	108.53	109.79	41.31
48	342	1408	C	11	5	137	139	99.33	99.33	113.51	41.45
54	342	1410	A	12	2	64	65.5	115.07	115.07	116.66	41.58
61	342	1410	B	14	2	79	80.5	121.82	121.56	122.99	41.83
62	342	1410	B	14	3	92.5	94	123.46	124.05	125.48	41.94
49	342	1408	C	13	1	142	144	114.37	114.37	129.48	42.10
78	342	1408	A	13	1	140	142				43.00
114	342	1410	A	15	7	49.5	51				43.25
115	342	1410	A	16	4	120	121.5				43.50
116	342	1410	A	17	1	2	3.5				43.75
117	342	1410	A	17	4	56	57.5				44.00
118	342	1410	A	18	1	67	68.5				44.25
119	342	1410	A	18	4	122	123.5				44.50
120	342	1410	A	19	1	114	115.5				44.75
121	342	1410	A	19	5	18	19.5				45.00

Table A.2: Genera found in this study and there morphogroup and depth habitat based on Table S2 and Table S3 below, which are updated from those published by Aze et al. (2011)

Genera	Morphogroup	Depth Habitat
Acarinina	7	Mixed layer
Catapsydrax	2	Subthermocline
Chiloguembelina	9	Mixed layer
Dentoglobigerina	2	Thermocline
Globigerina	2	Mixed layer
Globigerinatheka	3	Mixed layer
Globorotaloides	2	Subthermocline
Globoturborotalita	2	Mixed layer
Hantkinena	5	Thermocline
Jenkinsina	10	Subthermocline
Morozovelloides	8	Mixed layer
Orbulinoides	11	Mixed layer
Parasubbotina	2	Subthermocline
Planorotalites	8	Mixed layer
Pseudohastigerina	4	Mixed layer
Subbotina	2	Thermocline
Turborotalita	1	Mixed layer
Turborotalia	6	Mixed layer

1.1 Data preparation and processing

Here we will show how we processed our data from raw abundance plots to data sets suitable for Hill number analysis. We only present the process for genera here for simplicity but morphogroup and ecogroup data sets were prepared in the same manner. Firstly, we import the data selecting only one sheet from the data set provided, the first two lines are skipped to remove surplus information then only the column containing abundance counts:*Turborotalita* to *Orbulinoides.* We then select only rows 1 to 33 so that any blank space in the datasheet is removed.

We then create a function so that all abundance data is transformed into the structure needed to Hill number analysis with the code provided in Chao and Jost (2015) (Appendix S8 of Chao and Jost (2015)). The data we import is structured so that each column is a genera whilst each row is a sample. The function transforms this in the following steps:

STEP 1. Transposes the data so that each column is now sample and each row is the genera STEP 2. Removes all row names STEP 3. Reorders each column into ascending order. For this analysis the name of genera does not matter, the analysis is based purely on counts STEP 4. Creates a dataframe fo easy export

We then run the function on the data frame and we recommend saving the restructured data as a separate .csv file for future reference.

```
genus_63 <- read_excel("Data/Final_Abundance.xlsx", sheet = "Genus_>63_abs", skip=2) %>%
  select(Turborotalita:Orbulinoides) %>%
  slice(1:33) #18 Columns
```

```
structure_chao <- function(x){
  x1 <- t(x)
  rownames(x1) <- c()
  ordered <- apply(x1,2,sort)
  data.frame(ordered)
```

Table A.3: Raw counts of genera in the >63μm size fraction

Age (Ma)	Turborotalita	Subbotina	Globigerina	Catapsydrax	Globoturborotalita	Parasubbotina	Dentoglobigerina	Globorotaloides	Globigerinatheka	Pseudohastigerina	Hantkinena	Turborotalia	Acarinina	Morozovelloides	Chiloguembelina	Jenkinsina	Planorotalites	Orbulinoides	Total
38.00	0	73	0	5	0	0	0	15	0	41	0	0	48	0	8	0	184	0	374
38.16	0	30	0	22	0	180	3	0	4	0	0	0	15	0	9	0	13	0	276
38.25	0	152	0	7	0	0	0	13	3	8	0	0	8	0	16	0	63	0	270
38.50	0	64	0	13	0	0	2	20	3	25	1	6	22	0	44	0	134	0	334
38.72	1	35	0	10	0	122	0	9	1	29	0	1	26	2	0	30	56	0	322
39.00	0	64	0	4	0	0	2	31	5	36	0	0	11	0	51	0	111	0	315
39.25	0	89	0	17	0	0	0	50	0	43	0	2	31	0	43	0	235	0	510
39.56	0	37	0	22	0	19	0	40	0	52	0	0	8	1	53	4	83	0	319
39.75	0	41	4	6	12	11	0	49	2	53	0	2	9	0	56	0	94	0	339
39.85	0	8	0	0	6	35	0	24	2	32	0	0	14	0	160	1	88	0	370
39.92	0	56	0	27	0	77	0	0	16	0	0	0	9	0	2	0	36	0	223
39.95	0	51	0	5	0	7	0	23	0	41	0	1	6	0	50	0	69	0	253
39.97	0	53	0	1	0	20	0	35	7	36	0	1	25	0	57	19	105	0	359
40.14	0	37	4	0	0	47	0	3	3	3	0	1	27	4	4	0	182	0	315
40.38	0	128	0	41	4	19	0	8	38	22	0	6	15	3	11	1	38	1	335
40.41	0	43	0	0	1	44	0	17	9	16	1	1	12	1	5	73	17	0	240
40.49	0	109	0	42	4	44	2	70	9	57	0	4	48	24	58	1	150	0	622
41.09	0	20	4	0	4	32	0	27	2	13	0	2	20	1	65	0	98	0	288
41.31	0	18	0	0	18	87	0	23	1	32	1	0	28	35	28	1	20	0	292
41.45	0	19	0	0	0	41	0	38	2	51	0	1	13	15	404	155	34	0	773
41.58	0	23	0	0	2	49	0	33	0	59	0	2	26	2	65	8	45	0	314
41.83	0	74	11	9	12	32	0	0	15	39	1	1	111	12	6	5	32	0	360
41.94	0	34	0	0	0	40	0	33	1	48	0	1	31	13	76	18	84	0	379
42.10	0	21	0	0	7	26	0	23	2	67	0	0	62	15	14	8	40	0	285
43.00	0	74	0	2	0	26	0	10	4	59	1	6	99	20	59	36	116	0	512
43.25	0	74	0	5	0	39	0	28	0	32	0	3	75	2	41	10	83	0	392
43.50	0	90	1	3	0	17	0	30	10	5	0	4	81	5	2	4	58	0	310
43.75	0	84	0	0	0	28	0	7	0	26	0	2	50	19	12	6	88	0	322
44.00	0	56	4	5	0	26	0	30	1	59	0	18	129	17	60	45	135	0	585
44.25	0	59	0	3	0	10	0	21	0	55	0	25	104	1	3	4	96	0	381
44.50	0	47	0	3	0	0	0	19	3	38	0	15	106	1	1	1	43	0	277
44.75	0	67	0	0	0	0	0	84	0	35	0	0	89	1	5	4	47	0	332
45.00	0	99	0	1	0	0	0	27	0	55	0	0	104	2	10	5	62	0	365

Table A.4: Raw counts of genera in the >180μm size fraction

Age (Ma)	Turborotalita	Subbotina	Globigerina	Catapsydrax	Parasubbotina	Dentoglobigerina	Globoturborotalita	Globorotaloides	Globigerinatheka	Pseudohastigerina	Hantkinena	Turborotalia	Acarinina	Morozovelloides	Chiloguembelina	Jenkinsina	Planorotalites	Orbulinoides	Total
38.00	0	238	0	21	0	3	0	0	5	0	0	0	22	2	0	0	0	0	291
38.16	0	285	0	12	0	12	21	0	24	0	0	2	5	0	0	0	0	0	361
38.25	0	298	0	10	0	0	0	0	2	0	0	0	3	0	6	0	0	0	319
38.50	0	291	0	9	3	5	0	0	29	3	0	12	13	4	0	0	0	0	369
38.72	0	220	2	15	14	3	2	0	29	0	0	1	16	4	0	0	0	0	306
39.00	0	220	0	18	5	5	12	0	15	2	2	14	15	1	0	0	0	0	309
39.25	0	192	0	10	4	1	2	1	0	2	0	9	11	0	0	0	0	0	232
39.56	0	209	0	34	37	0	7	1	10	15	0	0	6	0	6	0	0	0	325
39.75	0	157	0	22	3	0	6	2	16	9	0	18	31	1	2	0	6	0	273
39.85	0	94	0	7	43	15	38	0	24	11	0	0	28	17	0	0	0	3	280
39.92	0	209	0	24	4	0	3	0	76	1	0	0	0	0	0	0	0	0	317
39.95	0	159	0	9	38	0	0	0	34	8	0	4	9	4	0	0	0	0	265
39.97	0	281	0	40	3	0	0	0	50	0	1	2	0	1	0	0	0	0	378
40.14	0	192	7	0	43	0	8	0	21	0	0	2	16	14	0	0	0	0	303
40.38	0	145	0	27	0	5	1	0	102	1	1	12	11	1	0	0	1	0	307
40.41	0	139	0	27	12	0	3	0	100	0	0	2	2	5	0	0	0	0	290
40.49	0	257	0	31	18	0	1	3	18	0	0	1	30	20	0	0	0	0	379
41.09	0	81	4	12	25	0	19	0	10	2	3	20	95	10	0	0	0	0	281
41.31	0	152	0	10	15	0	39	0	24	6	3	8	39	73	0	0	0	0	369
41.45	0	99	9	11	16	0	16	2	11	17	2	15	36	47	0	0	0	0	281
41.58	0	131	8	3	30	1	20	5	25	15	0	22	84	32	0	1	1	0	378
41.83	0	207	0	0	15	0	5	0	54	3	2	0	100	32	0	0	0	0	418
41.94	0	125	3	11	15	0	6	0	9	0	1	10	35	35	0	0	0	0	250
42.10	0	167	0	5	43	0	24	0	27	3	0	12	47	43	0	0	0	0	371
43.00	0	148	0	9	9	0	0	0	21	1	1	21	121	46	0	0	0	0	377
43.25	0	174	1	13	18	0	7	0	19	4	1	15	45	18	0	0	4	0	319
43.50	0	124	0	9	7	0	4	0	72	0	0	6	114	18	0	0	0	0	354
43.75	0	167	0	10	7	0	0	0	16	0	0	3	37	19	0	0	0	0	259
44.00	0	191	0	23	0	0	0	0	10	2	0	8	27	37	0	0	3	0	301
44.25	0	244	0	7	2	0	0	0	0	1	0	26	146	2	0	0	2	0	430
44.50	0	147	0	9	3	0	16	0	0	0	0	24	148	7	0	0	0	0	354
44.75	0	198	0	0	0	0	0	0	0	4	0	4	209	3	0	0	0	0	418
45.00	0	154	0	6	0	0	9	18	0	22	0	7	148	0	57	2	0	0	423

Table A.5: Raw counts of morphogroups in the >63μm size fraction

Age (Ma)	1	2	3	4	5	6	7	8	9	10	11	Total
38.00	0	93	0	41	0	0	48	184	8	0	0	374
38.16	0	235	4	0	0	0	15	13	9	0	0	276
38.25	0	172	3	8	0	0	8	63	16	0	0	270
38.50	0	99	3	25	1	6	22	134	44	0	0	334
38.72	1	176	1	29	0	1	26	58	0	30	0	322
39.00	0	101	5	36	0	0	11	111	51	0	0	315
39.25	0	156	0	43	0	2	31	235	43	0	0	510
39.56	0	118	0	52	0	0	8	84	53	4	0	319
39.75	0	123	2	53	0	2	9	94	56	0	0	339
39.85	0	73	2	32	0	0	14	88	160	1	0	370
39.92	0	160	16	0	0	0	9	36	2	0	0	223
39.95	0	86	0	41	0	1	6	69	50	0	0	253
39.97	0	109	7	36	0	1	25	105	57	19	0	359
40.14	0	91	3	3	0	1	27	186	4	0	0	315
40.38	0	200	38	22	0	6	15	41	11	1	1	335
40.41	0	105	9	16	1	1	12	18	5	73	0	240
40.49	0	271	9	57	0	4	48	174	58	1	0	622
41.09	0	87	2	13	0	2	20	99	65	0	0	288
41.31	0	146	1	32	1	0	28	55	28	1	0	292
41.45	0	98	2	51	0	1	13	49	404	155	0	773
41.58	0	107	0	59	0	2	26	47	65	8	0	314
41.83	0	138	15	39	1	1	111	44	6	5	0	360
41.94	0	107	1	48	0	1	31	97	76	18	0	379
42.10	0	77	2	67	0	0	62	55	14	8	0	285
43.00	0	112	4	59	1	6	99	136	59	36	0	512
43.25	0	146	0	32	0	3	75	85	41	10	0	392
43.50	0	141	10	5	0	4	81	63	2	4	0	310
43.75	0	119	0	26	0	2	50	107	12	6	0	322
44.00	0	121	1	59	0	18	129	152	60	45	0	585
44.25	0	93	0	55	0	25	104	97	3	4	0	381
44.50	0	69	3	38	0	15	106	44	1	1	0	277
44.75	0	151	0	35	0	0	89	48	5	4	0	332
45.00	0	127	0	55	0	0	104	64	10	5	0	365

Table A.6: Raw counts of morphogroups in the >180μm size fraction

Age (Ma)	1	2	3	4	5	6	7	8	9	10	11	Total
38.00	0	262	5	0	0	0	22	2	0	0	0	291
38.16	0	330	24	0	0	2	5	0	0	0	0	361
38.25	0	308	2	0	0	0	3	0	6	0	0	319
38.50	0	308	29	3	0	12	13	4	0	0	0	369
38.72	0	256	29	0	0	1	16	4	0	0	0	306
39.00	0	260	15	2	2	14	15	1	0	0	0	309
39.25	0	210	0	2	0	9	11	0	0	0	0	232
39.56	0	288	10	15	0	0	6	0	6	0	0	325
39.75	0	190	16	9	0	18	31	7	2	0	0	273
39.85	0	197	24	11	0	0	28	17	0	0	3	280
39.92	0	240	76	1	0	0	0	0	0	0	0	317
39.95	0	206	34	8	0	4	9	4	0	0	0	265
39.97	0	324	50	0	1	2	0	1	0	0	0	378
40.14	0	250	21	0	0	2	16	14	0	0	0	303
40.38	0	178	102	1	1	12	11	2	0	0	0	307
40.41	0	181	100	0	0	2	2	5	0	0	0	290
40.49	0	310	18	0	0	1	30	20	0	0	0	379
41.09	0	141	10	2	3	20	95	10	0	0	0	281
41.31	0	216	24	6	3	8	39	73	0	0	0	369
41.45	0	153	11	17	2	15	36	47	0	0	0	281
41.58	0	198	25	15	0	22	84	33	0	1	0	378
41.83	0	227	54	3	2	0	100	32	0	0	0	418
41.94	0	160	9	0	1	10	35	35	0	0	0	250
42.10	0	239	27	3	0	12	47	43	0	0	0	371
43.00	0	166	21	1	1	21	121	46	0	0	0	377
43.25	0	213	19	4	1	15	45	22	0	0	0	319
43.50	0	144	72	0	0	6	114	18	0	0	0	354
43.75	0	184	16	0	0	3	37	19	0	0	0	259
44.00	0	214	10	2	0	8	27	40	0	0	0	301
44.25	0	253	0	1	0	26	146	4	0	0	0	430
44.50	0	175	0	0	0	24	148	7	0	0	0	354
44.75	0	198	0	4	0	4	209	3	0	0	0	418
45.00	0	187	0	22	0	7	148	0	57	2	0	423

Table A.7: Raw counts of hepth habitats in the >63μm size fraction

Age (Ma)	Mixed_Layer	Thermocline	Subthermocline	Total
38.00	281	73	20	374
38.16	41	33	202	276
38.25	98	152	20	270
38.50	234	67	33	334
38.72	116	35	171	322
39.00	214	66	35	315
39.25	354	89	67	510
39.56	197	37	85	319
39.75	232	41	66	339
39.85	302	8	60	370
39.92	63	56	104	223
39.95	167	51	35	253
39.97	231	53	75	359
40.14	228	37	50	315
40.38	138	128	69	335
40.41	62	44	134	240
40.49	354	111	157	622
41.09	209	20	59	288
41.31	162	19	111	292
41.45	520	19	234	773
41.58	201	23	90	314
41.83	239	75	46	360
41.94	254	34	91	379
42.10	207	21	57	285
43.00	363	75	74	512
43.25	236	74	82	392
43.50	166	90	54	310
43.75	197	84	41	322
44.00	423	56	106	585
44.25	284	59	38	381
44.50	207	47	23	277
44.75	177	67	88	332
45.00	233	99	33	365

Table A.8: Raw counts of depth habitats in the >180μm size fraction

Age (Ma)	Mixed_Layer	Thermocline	Subthermocline	Total
38.00	29	241	21	291
38.16	52	297	12	361
38.25	11	298	10	319
38.50	61	296	12	369
38.72	54	223	29	306
39.00	59	227	23	309
39.25	24	193	15	232
39.56	44	209	72	325
39.75	89	157	27	273
39.85	121	109	50	280
39.92	80	209	28	317
39.95	59	159	47	265
39.97	53	282	43	378
40.14	68	192	43	303
40.38	129	151	27	307
40.41	112	139	39	290
40.49	70	257	52	379
41.09	160	84	37	281
41.31	189	155	25	369
41.45	151	101	29	281
41.58	207	132	39	378
41.83	194	209	15	418
41.94	98	126	26	250
42.10	156	167	48	371
43.00	210	149	18	377
43.25	113	175	31	319
43.50	214	124	16	354
43.75	75	167	17	259
44.00	87	191	23	301
44.25	177	244	9	430
44.50	195	147	12	354
44.75	220	198	0	418
45.00	243	154	26	423

Table A.9: Descriptions of morphological classification applied to genera of this study updated from previous work (Aze et al (2011)) to include microperforate genera

Morphogroup	Description
1	Spinose, flat
2	Spinose, globular
3	Spinose globular with supplementary apertures
4	Non-spinose, planispiral
5	Non-spinose, tubilospinate
6	Non-spinose, turborotaliform, keeled
7	Non-spinose, muricate, acariniform
8	Non-spinose, muriconate, keeled
9	Microperforate, non-spinose, biserial
10	Microperforate, non-spinose,triserial
11	Spinose, spherical, flat

Table A.10: Descriptions of depth habitat classifications applied to genera found in this study updated from previous research (Aze et al (2011)) to include microperforate genera

Depth Habitat	Description
Mixed layer	Heavy 13C, light 18O
Thermocline	Light 13C, relativley heavy 18O
Subthermocline	Very light 13C, very heavy 18O

Table A.11: Calculated hill numbers for genera, morphogroup and depth habitat. Columns relating to different measured diversity are as follows: genera begin with Genus, morphogroup begin with Morph, and depth habitat begin with Eco. Hill refers to calulated hill numbers, UCI is the upper confidence interval, LCI is the lower confidence interval and SD is the standard deviation. Size fraction relates to the size fraction measured whilst Q is the order of q effective diveristy was calculated. This table is too large in its entirety so only the first 11 lines are presented here with the dataset available on request.

Size Fraction	Age	Fragmentation %	Q	Genus_Hill	Genus_UCI	Genus_LCI	Genus_SD	Morph_Hill	Morph_UCI	Morph_LCI	Morph_SD	Eco_Hill	Eco_UCI	Eco_LCI	Eco_SD
180	38	9.7	0.0	6.00	6.19	5.19	0.41	4.00	4.15	3.15	0.36	3.00	3.00	3.00	0.00
180	38	9.7	0.1	5.22	5.51	4.49	0.33	3.43	3.66	2.77	0.28	2.82	2.86	2.78	0.02
180	38	9.7	0.2	4.55	4.89	3.90	0.28	2.97	3.23	2.45	0.22	2.66	2.73	2.58	0.04
180	38	9.7	0.3	3.98	4.35	3.41	0.25	2.60	2.86	2.19	0.18	2.50	2.60	2.40	0.06
180	38	9.7	0.4	3.50	3.87	3.00	0.22	2.30	2.56	1.98	0.15	2.36	2.48	2.23	0.07
180	38	9.7	0.5	3.11	3.47	2.68	0.20	2.07	2.32	1.81	0.13	2.23	2.37	2.09	0.08
180	38	9.7	0.6	2.79	3.13	2.42	0.18	1.89	2.12	1.67	0.11	2.12	2.26	1.96	0.08
180	38	9.7	0.7	2.53	2.85	2.20	0.17	1.75	1.96	1.55	0.10	2.02	2.17	1.86	0.09
180	38	9.7	0.8	2.32	2.62	2.02	0.15	1.64	1.83	1.47	0.09	1.93	2.09	1.76	0.09
180	38	9.7	0.9	2.15	2.43	1.87	0.14	1.55	1.72	1.40	0.08	1.85	2.01	1.68	0.09
180	38	9.7	1.0	2.01	2.28	1.76	0.13	1.48	1.64	1.34	0.08	1.78	1.94	1.62	0.09

Table A.12: Fragmentation of samples at both size fractions including recounts

LAB ID	EXPEDITION	SITE	HOLE	CORE	CORE_TYPE	SECTION	CC	TOP_DEPTH	BOTTOM_DEPTH	Age_2021(Ma)	180_Fragmentation (%)	180_Recount_Fragmentation (%)	63_Fragmentation (%)	63_Recount_Fragmentation (%)
67	342	1406	A	27	X	3	no	88	90	38.00	9.70	9.79	24.22	
7	342	1406	A	27	X	4	no	137.5	139	38.16	19.74		30.78	25.38
68	342	1406	A	27	X	5	no	100	102	38.25	15.22	15.12	27.78	31.02
80	342	1408	B	5	H	2	no	60	62	38.50	8.80		17.08	
8	342	1406	A	27	X	6	no	62	63.5	38.72	3.88		8.89	
74	342	1408	A	5	H	2	no	38	40	39.00	4.85		13.27	
75	342	1408	A	5	H	5	no	30	32	39.25	5.18	4.97	11.62	11.09
82	342	1408	B	7	H	1	no	98	100	39.56	10.42	12.35	16.08	17.14
96	342	1408	C	7	H	2	no	58	60	39.75	4.93		4.31	
20	342	1406	B	28	X	5	no	1.5	3	39.92	4.50	4.67	23.29	
34	342	1408	B	8	H	1	no	120	121.5	39.85	8.95		5.25	
83	342	1408	B	8	H	4	no	28	30	39.95	10.13		14.47	
35	342	1408	B	8	H	4	no	106.5	108	39.97	9.89		21.59	
59	342	1410	B	10	H	5	no	117	118.5	40.14	8.44		14.76	
98	342	1408	C	9	H	2	no	98	100	40.49	5.95		19.94	
76+77	342	1408	A	8	H	2	no	117	118	40.38	8.77		21.77	
30	342	1408	A	8	H	3	no	69	71	40.41	15.30	16.05	29.91	
51	342	1410	A	11	H	1	no	97	98.5	41.09	3.96	2.92	9.41	
53	342	1410	A	11	H	5	no	129.5	131	41.31	1.85		5.89	6.20
54	342	1410	A	12	H	2	no	64	65.5	41.58	1.34		3.33	3.66
48	342	1408	C	11	H	5	no	137	139	41.45	1.36		4.45	3.21
61	342	1410	B	14	H	2	no	79	80.5	41.83	20.91		12.12	
62	342	1410	B	14	H	3	no	92.5	94	41.94	2.01		5.18	
49	342	1408	C	13	H	1	no	142	144	42.10	6.64		10.16	
78	342	1408	A	13	H	1	no	140	142	43.00	3.09		7.99	
114	342	1410	A	15	H	7	no	49.5	51	43.25	8.98		6.68	
115	342	1410	A	16	H	4	no	120	121.5	43.50	6.50	5.26	12.58	
116	342	1410	A	17	X	1	no	2	3.5	43.75	5.76		16.98	
117	342	1410	A	17	X	4	no	56	57.5	44.00	10.27		8.42	
118	342	1410	A	18	X	1	no	67	68.5	44.25	1.86		8.19	8.58
119	342	1410	A	18	X	4	no	122	123.5	44.50	1.51		5.43	
120	342	1410	A	19	X	1	no	114	115.5	44.75	6.81		14.78	14.20
121	342	1410	A	19	X	5	no	18	19.5	45.00	6.65		3.80	

```
}

genus_63_chao <- structure_chao(genus_63)
write_csv(genus_63_chao, "Data/genus_180_chao.csv") #This is for illstration only.
```

Using this data we can then calculate Hill numbers using the code of Chao and Jost (2015) (as shown Appendix S8 Chao and Jost (2015)). You will need to download the code and run it once for the following code to work, without it the following lines of code will not work. If you are not interested in the process of calculating Hill numbers and are instead looking for the statistical analysis presented in the manuscript we recommend you skip to Section 2. As before we only show the process for genera but all data can be processing in the same manner. The data we provide (Supplementary Data 1) contains the combined calculated hill numbers generated following these steps, you do not need to do the following steps if you want replicate our statistical analysis, this is shown for transparency.

- STEP 1 - Read in data and source and the analysis script
- STEP 2 - Create a variable of sample ages
- STEP 3 - Transform the restructured data set into a matrix
- STEP 4 - Create a variable of n which should equal the number of columns in your matrix (i.e the number of samples)
- STEP 5 - Create empty matrix's to put the calculated hill numbers into. The number of rows assumes you're outputting the default Hill numbers from 0 to 3 in steps of 0.1.

```
#STEP 1
source("Scripts/Chao_2014_Script.R")


#Create a variable of age
age <- read_excel("Data/Final_Abundance.xlsx", sheet = "Genus_>63_abs", skip=2) %>%
  select(Age_2021) %>%
  slice(1:33)

#STEP 2
Age <- signif(age$Age_2021, digits=4)

#STEP 3
genus_63_chao <- as.matrix(genus_63_chao)

#STEP 4
## Set the number of columns - this will be the number of samples you want to analyse
###(Should be the same as the number of rows in imported data set)
n <- 33 #Number of columns

#STEP5
# Create matrix for the output
#31 assumes you're outputting the default Hill numbers from 0 to 3 in steps of 0.1
# est = hill number calculated EMPERICAL
# lci = lower confidence interval
# uci = upper confidence interval
# sd = standard deviation ?
# With P e.g estP this is the proposed data using the Chao Estimator
```

```
est <- matrix(0, nrow=31, ncol=n)
lci <- matrix(0,nrow=31, ncol=n)
uci <- matrix(0, nrow=31, ncol=n)
sd <- matrix(0, nrow=31, ncol=n)
estP <- matrix(0, nrow=31, ncol=n)
lciP <- matrix(0,nrow=31, ncol=n)
uciP <- matrix(0, nrow=31, ncol=n)
sdP <- matrix(0, nrow=31, ncol=n)
```

- STEP 6 - Calculate Hill numbers. **WARNING** this calculation will take a long time !

```
#STEP 6 - WARNING this calculation will take a long time !
##Time code
ptm <- proc.time()
# Loop to calculate the above for each sample and extract the calculated values
for(i in 1:n)
{cat(i,"\n")
  tmp <- genus_63_chao[,i]
  mych <- ChaoHill(tmp,"abundance")
  est[,i] <- as.numeric(mych$EST[1,])
  lci[,i] <- as.numeric(mych$LCI[1,])
  uci[,i] <- as.numeric(mych$UCI[1,])
  sd[,i] <- as.numeric(mych$SD[1,])
  estP[,i] <- as.numeric(mych$EST[2,])
  lciP[,i] <- as.numeric(mych$LCI[2,])
  uciP[,i] <- as.numeric(mych$UCI[2,])
  sdP[,i] <- as.numeric(mych$SD[2,])

}
##Stop the Clock
proc.time() - ptm
```

- STEP 7 - Extract information from the matrix's and create a dataframe including sample age, this extracts empirical and predicted values. For the manuscript we only use empirical values.
- STEP 8 - Save your data frames as a .csv.

```
#STEP 7
## EXTRACTING VALUES##
#Reformat empirical values into a data frame
chaolist <- list(est,uci,lci,sd)

df_reform <- lapply(chaolist,   function(x)
{
  x1 <- data.frame(x)
  names(x1) <- Age
  x1$Q <- seq(0,3,0.1)
  x1  %>% gather(Age,Hill,'38':'45', factor_key = TRUE)
})

emp_est <- df_reform[[1]]
emp_uci <- df_reform[[2]] %>% rename(UCI = Hill)
```

```
emp_lci <- df_reform[[3]] %>% rename(LCI = Hill)
emp_sd <- df_reform[[4]] %>% rename(SD= Hill)


emp_full <- list(emp_est, emp_uci,emp_lci, emp_sd) %>% reduce(left_join, by = c("Q","Age"))


##PROPOSED##
chaolistP <- list(estP,uciP,lciP,sdP)

df_reformP <- lapply(chaolistP,   function(x)
{
  x1 <- data.frame(x)
  names(x1) <- Age
  x1$Q <- seq(0,3,0.1)
  x1  %>% gather(Age,Hill,'38':'45', factor_key = TRUE)
})

pred_est <- df_reform[[1]]
pred_uci <- df_reform[[2]] %>% rename(UCI = Hill)
pred_lci <- df_reform[[3]] %>% rename(LCI = Hill)
pred_sd <- df_reform[[4]] %>% rename(SD= Hill)


pred_full <- list(pred_est, pred_uci,pred_lci, pred_sd) %>%
  reduce(left_join, by = c("Q","Age"))

#STEP 8
write_csv(pred_full, "Data/genus_63_Hill_predicted.csv")
write_csv(emp_full, "Data/genus_63_Hill_emperical.csv")
```

2 Generalized additive models (GAMs)

```
full <- read_csv("Data/Hill_Emperical_All_Frag_2021.csv")%>%
  rename(frag=`Fragmentation %`)
Age <- full$Age
full$size <-as.factor(full$size)
```

```
shan <- function(x){
  conv <- log(x)
  return(conv)
}
```

```
simps <- function(x){
  conv <- (x-1)/x
  return(conv)
}
```

Table A.13: AICc Comparison between models of genera richness

		df	AIC	ΔAIC	AICweight	ΔAICc
Genera	s(Age, by=size) +size + Frag	15.18	262.91	272.78	0.9958690567	0.00
Genera	s(Age)	4.61	283.52	284.37	0.0030231261	11.59
Genera	s(Age) + Frag	5.62	285.42	286.68	0.0009554745	13.90
Genera	s(Age, by=size) + Frag	7.72	288.00	290.35	0.0001523427	17.57

2.1 Genera

2.1.1 Richness

```
gh_0null <-gam(Genus_Hill ~ s(Age,k=11),data = full %>% filter(Q==0))
gh0_0 <-gam(Genus_Hill ~ s(Age,k=11)+frag,data = full %>% filter(Q==0))
gh1_0<-update(gh0_0, Genus_Hill ~ s(Age,k=11, by=size) + size + frag)
gh2_0 <-update(gh0_0, Genus_Hill ~ s(Age,k=11,by=size)+frag)
```

```
##
## Method: GCV   Optimizer: magic
## Smoothing parameter selection converged after 6 iterations.
## The RMS GCV score gradient at convergence was 8.146794e-07 .
## The Hessian was positive definite.
## Model rank =  23 / 23
##
## Basis dimension (k) checking results. Low p-value (k-index<1) may
## indicate that k is too low, especially if edf is close to k'.
##
##                   k'   edf k-index p-value
## s(Age):size63  10.00  8.54    0.88    0.17
## s(Age):size180 10.00  2.65    0.88    0.13
```

```
## null device
##           1
```

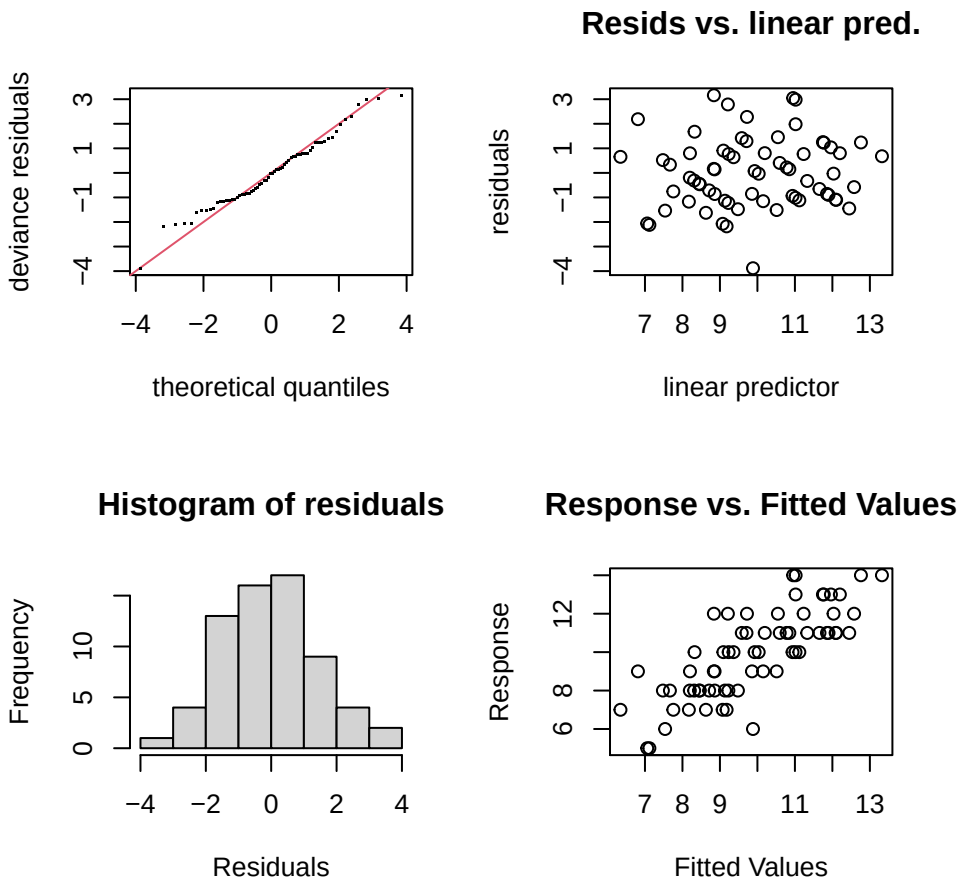

Figure A.2: Diagnostoc plots for best fitting GAM for genera richness

2.1.2 Shannon's index

```
gh_1null <-gam(Genus_Hill ~ s(Age,k=7),data = full %>% filter(Q==1))
gh0_1 <- update(gh0_0, shan(Genus_Hill) ~ s(Age, k=7)+ frag,data = full %>% filter(Q==1))
gh1_1 <- update(gh0_1,shan(Genus_Hill) ~ s(Age, k=7, by=size)+size+ frag )
gh2_1 <-update(gh0_1,  shan(Genus_Hill) ~ s(Age, k=7, by=size)+ frag )
```

```
##
## Method: GCV   Optimizer: magic
## Smoothing parameter selection converged after 6 iterations.
## The RMS GCV score gradient at convergence was 1.328545e-06 .
```

Table A.14: AICc Comparison between models of genera Shannon's index

		df	AIC	ΔAIC	AICweight	ΔAICc
Genera	s(Age, by=size) +size + Frag	9.23	7.48	10.87	1.000000e+00	0.00
Genera	s(Age) + Frag	5.66	56.54	57.81	6.389707e-11	46.95
Genera	s(Age, by=size) + Frag	7.57	59.40	61.66	9.327830e-12	50.80
Genera	s(Age)	4.45	262.98	263.79	1.200397e-55	252.92

```
## The Hessian was positive definite.
## Model rank =  15 / 15
##
## Basis dimension (k) checking results. Low p-value (k-index<1) may
## indicate that k is too low, especially if edf is close to k'.
##
##                   k'  edf k-index p-value
## s(Age):size63  6.00 2.18    1.07    0.67
## s(Age):size180 6.00 3.06    1.07    0.69

## null device
##           1
```

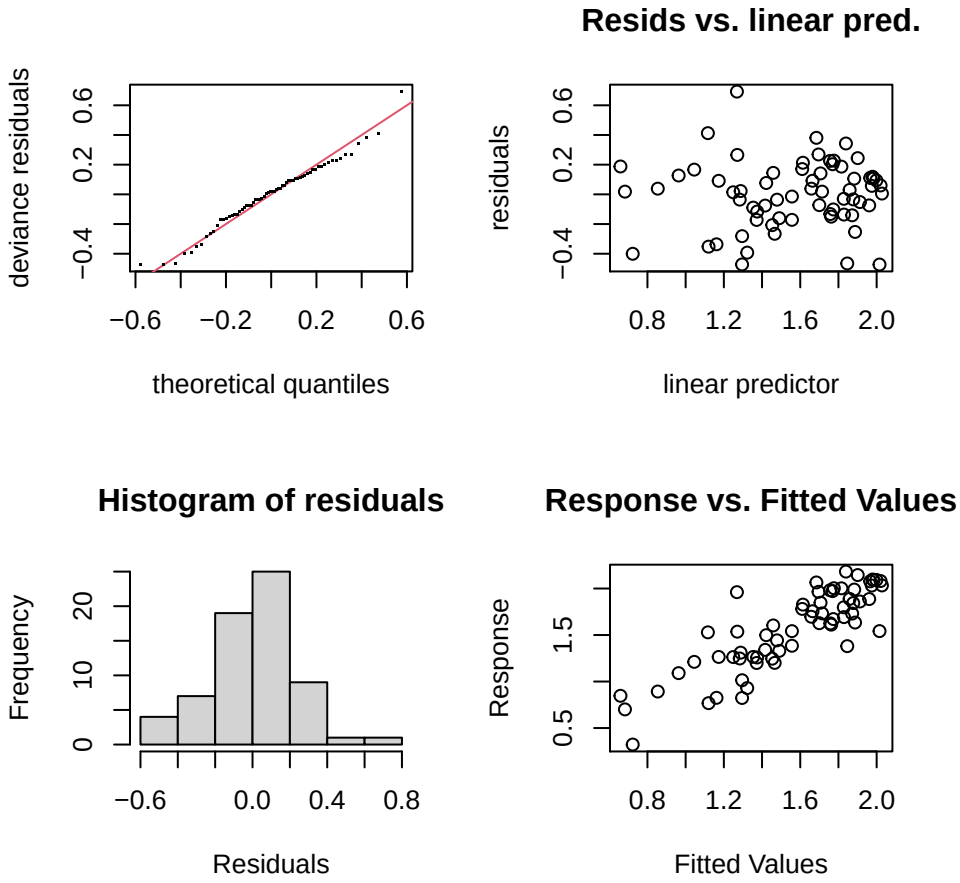

Figure A.3: Diagnostoc plots for best fitting GAM for genera Shannon's index

Table A.15: AICc Comparison between models of genera Simpson's index

		df	AIC	ΔAIC	AICweight	ΔAICc
Genera	s(Age, by=size) +size + Frag	9.57	17.13	20.78	1.000000e+00	0.00
Genera	s(Age) + Frag	5.53	71.65	72.86	4.894746e-12	52.09
Genera	s(Age, by=size) + Frag	7.47	75.15	77.35	5.194793e-13	56.57
Genera	s(Age)	4.27	249.70	250.44	1.343504e-50	229.67

2.1.3 Simpson's index

```
gh_2null <-gam(Genus_Hill ~ s(Age,k=7),data = full %>% filter(Q==2))
gh0_2 <- update(gh0_0, shan(Genus_Hill) ~ s(Age, k=7)+ frag,data = full %>% filter(Q==2))
gh1_2 <- update(gh0_2,shan(Genus_Hill) ~ s(Age, k=7, by=size)+size+ frag )
gh2_2 <-update(gh0_2,  shan(Genus_Hill) ~ s(Age, k=7, by=size)+ frag )
```

```
##
## Method: GCV   Optimizer: magic
## Smoothing parameter selection converged after 5 iterations.
## The RMS GCV score gradient at convergence was 9.147102e-07 .
## The Hessian was positive definite.
## Model rank =  15 / 15
##
## Basis dimension (k) checking results. Low p-value (k-index<1) may
## indicate that k is too low, especially if edf is close to k'.
##
##                  k'  edf k-index p-value
## s(Age):size63  6.00 2.20    1.15    0.90
## s(Age):size180 6.00 3.37    1.15    0.87

## null device
##           1
```

```
gh1_0_para <- summary(gh1_0)$p.table
gh1_1_para <- summary(gh1_1)$p.table
gh1_2_para <- summary(gh1_2)$p.table
genera_para <- rbind(gh1_0_para,gh1_1_para,gh1_2_para)
genera_para<- data.frame(genera_para)
genera_para$q <- c("0","0","0","1","1","1","2","2","2")
genera_para$model <- c("Genera ~ s(Age, by=size) +size + Frag")
genera_para$Parametric_Coefficient <- rep(c("Intercept","Size:180", "Fragmentation"),
                                          times=3)
genera_para <- genera_para[,c(6,5,7,1,2,3,4)]
row.names(genera_para) <- NULL
genera_para$Pr...t.. <- round(genera_para$Pr...t.., digits = 2)
genera_para$Estimate <- round(genera_para$Estimate, digits = 2)
genera_para$Std..Error<- round(genera_para$Std..Error, digits = 2)
genera_para$t.value<- round(genera_para$t.value, digits = 2)
```

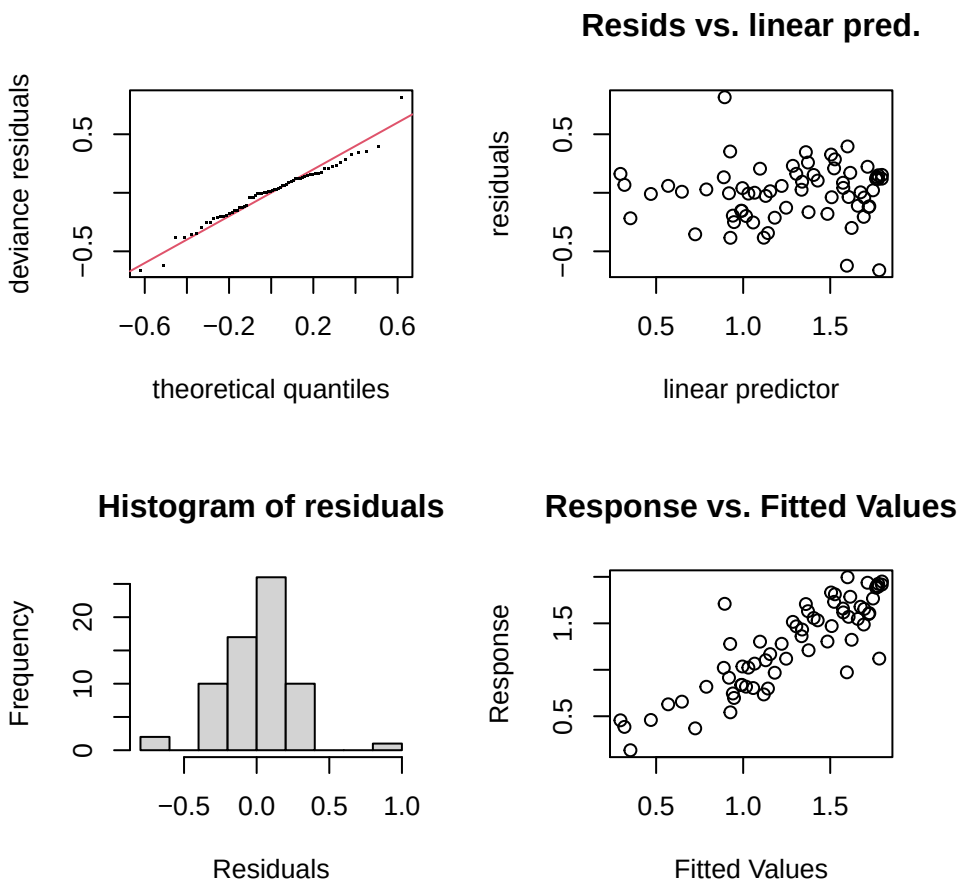

Figure A.4: Diagnostoc plots for best fitting GAM for genera Simpson's index

```
gh1_0_smooth <- summary(gh1_0)$s.table
gh1_1_smooth <- summary(gh1_1)$s.table
gh1_2_smooth <- summary(gh1_2)$s.table
genera_smooth <- rbind(gh1_0_smooth,gh1_1_smooth,gh1_2_smooth)
genera_smooth<- data.frame(genera_smooth)
genera_smooth$q <- c("0","0","1","1","2","2")
genera_smooth$model <- c("Genera ~ s(Age, by=size) +size + Frag")
genera_smooth$Smooth_term <- rep(c("s(Age):Size=63","s(Age):Size=180"), times=3 )
genera_smooth <- genera_smooth[,c(6,5,7,1,3,4)]
row.names(genera_smooth) <- NULL
genera_smooth$p.value <- round(genera_smooth$p.value, digits=2)
genera_smooth$edf<- round(genera_smooth$edf, digits=2)
genera_smooth$F <- round(genera_smooth$F, digits = 2)
```

Table A.16: AICc Comparison between models of morphogroup richness

		df	AIC	ΔAIC	AICweight	ΔAICc
Morphogroup	s(Age, by=size) + size +Frag	14.64	194.26	203.35	9.999426e-01	0.00
Morphogroup	s(Age) + Frag	9.73	220.21	223.99	3.307456e-05	20.63
Morphogroup	s(Age)	4.38	224.30	225.07	1.919572e-05	21.72
Morphogroup	s(Age, by=size) + Frag	7.36	225.57	227.70	5.159959e-06	24.35

2.2 Morphogroup

2.2.1 Richness

```
mh_0null <-gam(Morph_Hill ~ s(Age,k=20),data = full %>% filter(Q==0))
mh0_0 <- gam(Morph_Hill ~ s(Age, k=20)+ frag,data = full %>% filter(Q==0))
mh1_0 <- update(mh0_0, Morph_Hill ~ s(Age, k=20, by=size) + size+ frag)
mh2_0 <- update(mh0_0, Morph_Hill ~ s(Age, k=20, by=size)+ frag)
```

```
##
## Method: GCV   Optimizer: magic
## Smoothing parameter selection converged after 7 iterations.
## The RMS GCV score gradient at convergence was 5.620187e-05 .
## The Hessian was positive definite.
## Model rank =  41 / 41
##
## Basis dimension (k) checking results. Low p-value (k-index<1) may
## indicate that k is too low, especially if edf is close to k'.
##
##                   k'   edf k-index p-value
## s(Age):size63  19.00  8.26    0.97    0.41
## s(Age):size180 19.00  2.38    0.97    0.39

## null device
##           1
```

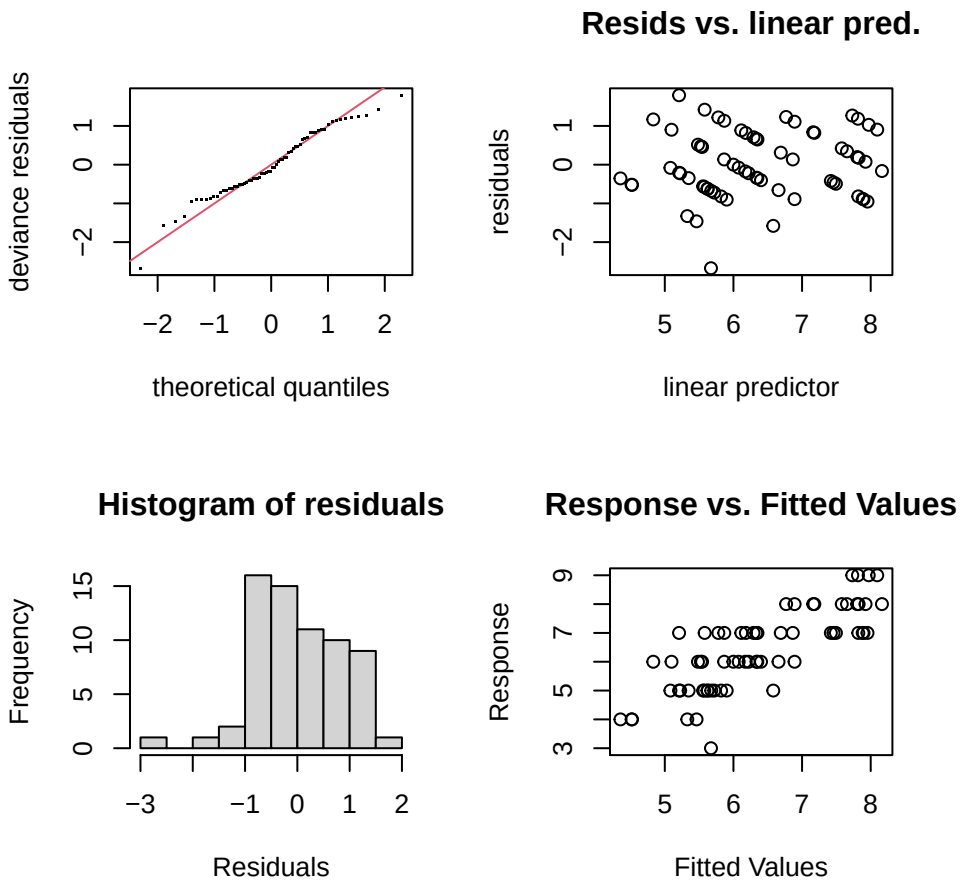

Figure A.5: Diagnostoc plots for best fitting GAM for morphological richness

2.2.2 Shannon's index

```
mh_1null <- gam(Morph_Hill ~ s(Age,k=8),data = full %>% filter(Q==1))
mh0_1 <- update(mh0_0,  shan(Morph_Hill) ~ s(Age, k=8)+ frag,data = full %>%
                  filter(Q==1))
mh1_1 <- update(mh1_0,  shan(Morph_Hill) ~ s(Age, k=8, by=size)+size+ frag,data = full%>%
                  filter(Q==1))
mh2_1 <-update(mh2_0,  shan(Morph_Hill) ~ s(Age, k=8, by=size)+ frag,data = full %>%
                 filter(Q==1))
```

```
##
## Method: GCV   Optimizer: magic
```

Table A.17: AICc Comparison between models of morphogroup Shannon's index

		df	AIC	ΔAIC	AICweight	ΔAICc
Morphogroup	s(Age, by=size) +size + Frag	9.09	-24.63	-21.35	1.000000e+00	0.00
Morphogroup	s(Age) + Frag	5.40	48.84	50.00	3.222099e-16	71.34
Morphogroup	s(Age, by=size) + Frag	6.87	51.18	53.03	7.050141e-17	74.38
Morphogroup	s(Age)	4.16	201.85	202.56	2.395645e-49	223.91

```
## Smoothing parameter selection converged after 5 iterations.
## The RMS GCV score gradient at convergence was 1.076856e-06 .
## The Hessian was positive definite.
## Model rank =  17 / 17
##
## Basis dimension (k) checking results. Low p-value (k-index<1) may
## indicate that k is too low, especially if edf is close to k'.
##
##                   k'  edf k-index p-value
## s(Age):size63  7.00 1.62    1.13    0.84
## s(Age):size180 7.00 3.47    1.13    0.84

## null device
##           1
```

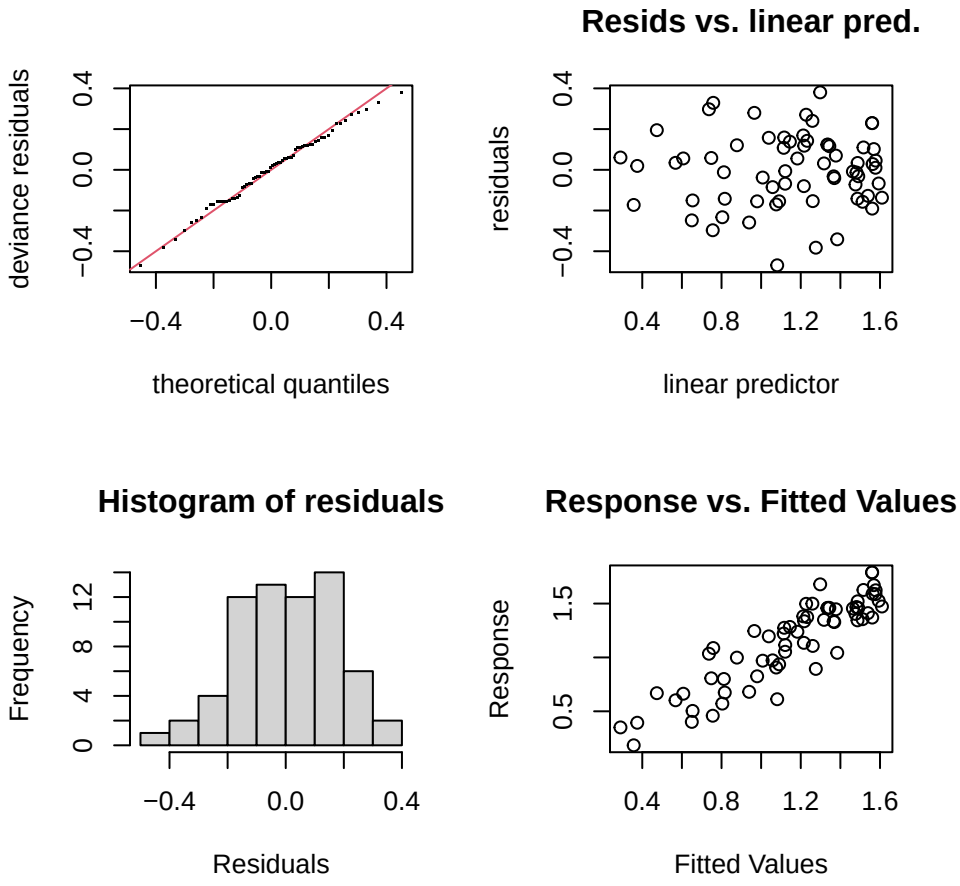

Figure A.6: Diagnostoc plots for best fitting GAM for morphogroup Shannon's index

Table A.18: AICc Comparison between models of morphogroup Simpson's index

		df	AIC	ΔAIC	AICweight	ΔAICc
Morphogroup	s(Age, by=size) +size + Frag	8.70	-124.93	-121.93	1.000000e+00	0.00
Morphogroup	s(Age) + Frag	5.22	-49.04	-47.96	8.653347e-17	73.97
Morphogroup	s(Age, by=size) + Frag	6.60	-49.44	-47.73	7.709662e-17	74.20
Morphogroup	s(Age)	3.77	192.83	193.42	3.342410e-69	315.34

2.2.3 Simpson's index

```
mh_2null <- gam(Morph_Hill ~ s(Age,k=10),data = full %>% filter(Q==2))
mh0_2 <- update(mh0_0,  simps(Morph_Hill) ~ s(Age, k=10)+ frag,data = full %>%
                 filter(Q==2))
mh1_2<- update(mh1_0,  simps(Morph_Hill) ~ s(Age, k=10, by=size)+size+ frag,data = full%>%
                filter(Q==2))
mh2_2 <-update(mh2_0, simps(Morph_Hill) ~ s(Age, k=10, by=size)+ frag,data = full %>%
                filter(Q==2))
```

```
##
## Method: GCV   Optimizer: magic
## Smoothing parameter selection converged after 4 iterations.
## The RMS GCV score gradient at convergence was 2.679448e-06 .
## The Hessian was not positive definite.
## Model rank =  21 / 21
##
## Basis dimension (k) checking results. Low p-value (k-index<1) may
## indicate that k is too low, especially if edf is close to k'.
##
##                   k'  edf k-index p-value
## s(Age):size63  9.00 1.06    1.15    0.86
## s(Age):size180 9.00 3.64    1.15    0.86

## null device
##           1
```

```
mh1_0_para <- summary(mh1_0)$p.table
mh1_1_para <- summary(mh1_1)$p.table
mh1_2_para <- summary(mh1_2)$p.table
morph_para <- rbind(mh1_0_para,mh1_1_para,mh1_2_para)
morph_para<- data.frame(morph_para)
morph_para$q <- c("0","0","0","1","1","1","2","2","2")
morph_para$model <- c("Morphogroup ~ s(Age, by=size) +size + Frag")
morph_para$Parametric_Coefficient <- rep(c("Intercept","Size:180", "Fragmentation"),
                                         times=3)
morph_para <- morph_para[,c(6,5,7,1,2,3,4)]
row.names(morph_para) <- NULL
morph_para$Pr...t.. <- round(morph_para$Pr...t.., digits = 2)
morph_para$Estimate <- round(morph_para$Estimate, digits = 2)
morph_para$Std..Error<- round(morph_para$Std..Error, digits = 2)
morph_para$t.value<- round(morph_para$t.value, digits = 2)
```

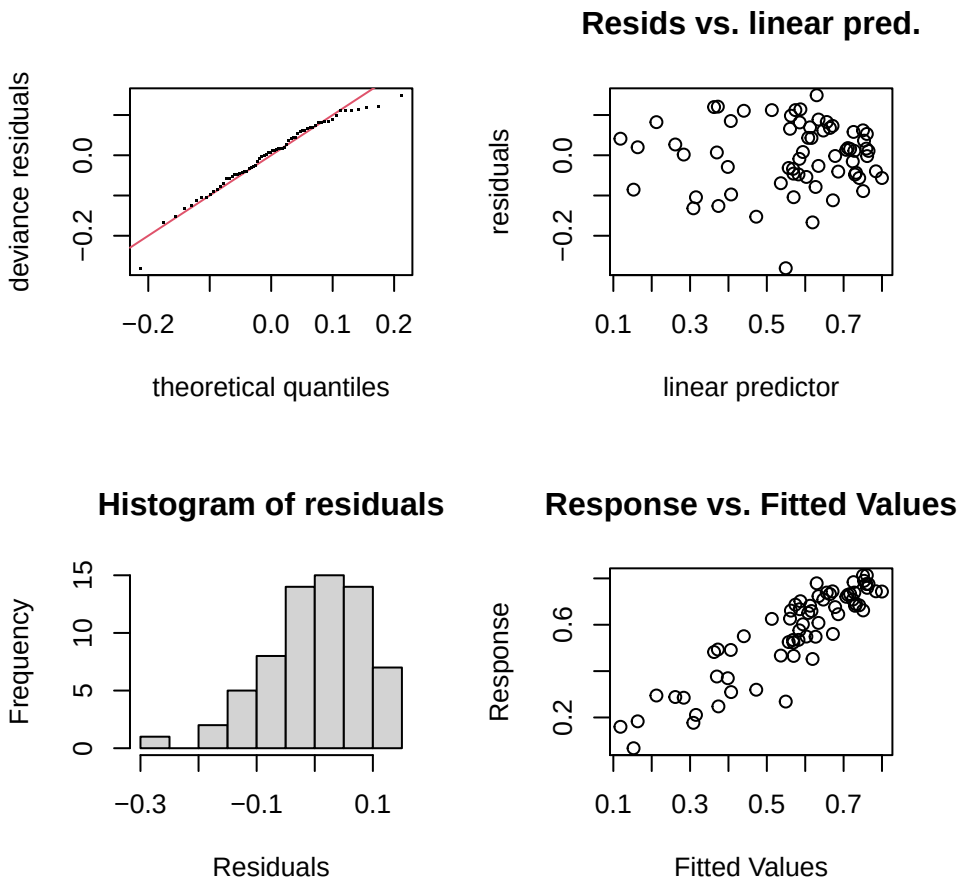

Figure A.7: Diagnostoc plots for best fitting GAM for morphogroup Shannon's index

```
mh1_0_smooth <- summary(mh1_0)$s.table
mh1_1_smooth <- summary(mh1_1)$s.table
mh1_2_smooth <- summary(mh1_2)$s.table
morph_smooth <- rbind(mh1_0_smooth,mh1_1_smooth,mh1_2_smooth)
morph_smooth<- data.frame(morph_smooth)
morph_smooth$q <- c("0","0","1","1","2","2")
morph_smooth$model <- c("Morphogroup ~ s(Age, by=size) +size + Frag")
morph_smooth$Smooth_term <- rep(c("s(Age):Size=63","s(Age):Size=180"), times=3 )
morph_smooth <- morph_smooth[,c(6,5,7,1,3,4)]
row.names(morph_smooth) <- NULL
morph_smooth$p.value <- round(morph_smooth$p.value, digits=2)
morph_smooth$edf<- round(morph_smooth$edf, digits=2)
morph_smooth$F <- round(morph_smooth$F, digits = 2)
```

```
para_tab <- rbind(genera_para,morph_para)
kbl(para_tab, col.names = c("Model", "\\textit{q}","Parametric Coefficient",
                            "Estimate","Std. Error","t.value",
                            "\\textit{p}"),
    escape=FALSE, caption = "Parametric coefficients for best fitting GAM models based on
    AIC difference compared to next best fitting model being more than 2") %>%
  kable_styling(latex_options = "scale_down")
```

Table A.19: Parametric coefficients for best fitting GAM models based on AIC difference compared to next best fitting model being more than 2

Model	q	Parametric Coefficient	Estimate	Std. Error	t.value	p
Genera s(Age, by=size) +size + Frag	0	Intercept	12.58	0.64	19.71	0.00
Genera s(Age, by=size) +size + Frag	0	Size:180	-2.54	0.47	-5.42	0.00
Genera s(Age, by=size) +size + Frag	0	Fragmentation	-0.14	0.04	-3.16	0.00
Genera s(Age, by=size) +size + Frag	1	Intercept	1.93	0.08	23.52	0.00
Genera s(Age, by=size) +size + Frag	1	Size:180	-0.58	0.07	-8.68	0.00
Genera s(Age, by=size) +size + Frag	1	Fragmentation	-0.01	0.01	-1.44	0.16
Genera s(Age, by=size) +size + Frag	2	Intercept	1.68	0.09	19.06	0.00
Genera s(Age, by=size) +size + Frag	2	Size:180	-0.67	0.07	-9.40	0.00
Genera s(Age, by=size) +size + Frag	2	Fragmentation	-0.01	0.01	-1.21	0.23
Morphogroup s(Age, by=size) +size + Frag	0	Intercept	7.49	0.37	20.04	0.00
Morphogroup s(Age, by=size) +size + Frag	0	Size:180	-1.73	0.28	-6.23	0.00
Morphogroup s(Age, by=size) +size + Frag	0	Fragmentation	-0.03	0.03	-1.02	0.31
Morphogroup s(Age, by=size) +size + Frag	1	Intercept	1.57	0.06	24.56	0.00
Morphogroup s(Age, by=size) +size + Frag	1	Size:180	-0.61	0.05	-11.61	0.00
Morphogroup s(Age, by=size) +size + Frag	1	Fragmentation	-0.01	0.00	-2.74	0.01
Morphogroup s(Age, by=size) +size + Frag	2	Intercept	0.77	0.03	25.96	0.00
Morphogroup s(Age, by=size) +size + Frag	2	Size:180	-0.28	0.02	-11.62	0.00
Morphogroup s(Age, by=size) +size + Frag	2	Fragmentation	-0.01	0.00	-3.07	0.00

```
smooth_tab <- rbind(genera_smooth,morph_smooth)
kbl(smooth_tab, col.names = c("Model", "\\textit{q}","Smooth Term", "Estimated d.f",
                              "F statistics", "\\textit{p}"),
    escape=FALSE,
    caption = "Smooth terms for best fitting GAM models")
```

Table A.20: Smooth terms for best fitting GAM models

Model	q	Smooth Term	Estimated d.f	F statistics	p
Genera s(Age, by=size) +size + Frag	0	s(Age):Size=63	8.54	3.10	0.00
Genera s(Age, by=size) +size + Frag	0	s(Age):Size=180	2.65	4.27	0.01
Genera s(Age, by=size) +size + Frag	1	s(Age):Size=63	2.18	2.73	0.05
Genera s(Age, by=size) +size + Frag	1	s(Age):Size=180	3.06	11.65	0.00
Genera s(Age, by=size) +size + Frag	2	s(Age):Size=63	2.20	3.71	0.02
Genera s(Age, by=size) +size + Frag	2	s(Age):Size=180	3.37	10.33	0.00
Morphogroup s(Age, by=size) +size + Frag	0	s(Age):Size=63	8.26	2.16	0.03
Morphogroup s(Age, by=size) +size + Frag	0	s(Age):Size=180	2.38	3.07	0.03
Morphogroup s(Age, by=size) +size + Frag	1	s(Age):Size=63	1.62	2.28	0.11
Morphogroup s(Age, by=size) +size + Frag	1	s(Age):Size=180	3.47	13.68	0.00
Morphogroup s(Age, by=size) +size + Frag	2	s(Age):Size=63	1.06	2.23	0.12
Morphogroup s(Age, by=size) +size + Frag	2	s(Age):Size=180	3.64	17.96	0.00

Table A.21: AICc Comparison between models of depth habitat richness

		df	AIC	ΔAIC	AICweight	ΔAICc
Depth Habitat	s(Age, by=size) + Frag	7.40	-93.38	-91.22	0.5645456	0.00
Depth Habitat	s(Age, by=size) +size + Frag	8.42	-92.76	-89.96	0.2993750	1.27
Depth Habitat	s(Age)	3.97	-88.48	-87.83	0.1034386	3.39
Depth Habitat	s(Age) + Frag	4.94	-86.50	-85.52	0.0326408	5.70

2.3 Depth Habitat

These results are not discussed in the manuscript but are included here for completeness.

2.3.1 Richness

```
eh_0null <-gam(Eco_Hill ~ s(Age),data = full %>% filter(Q==0))
eh0_0 <-gam(Eco_Hill ~ s(Age)+frag,data = full %>% filter(Q==0))
eh1_0<-update(eh0_0, Eco_Hill ~ s(Age, by=size) + size + frag)
eh2_0 <-update(eh0_0, Eco_Hill ~ s(Age,by=size)+frag)
```

```
##
## Method: GCV   Optimizer: magic
## Smoothing parameter selection converged after 9 iterations.
## The RMS GCV score gradient at convergence was 8.004899e-08 .
## The Hessian was positive definite.
## Model rank =  20 / 20
##
## Basis dimension (k) checking results. Low p-value (k-index<1) may
## indicate that k is too low, especially if edf is close to k'.
##
##                 k' edf k-index p-value
## s(Age):size63  9.0 1.0    1.03    0.68
## s(Age):size180 9.0 3.4    1.03    0.70

## null device
##           1
```

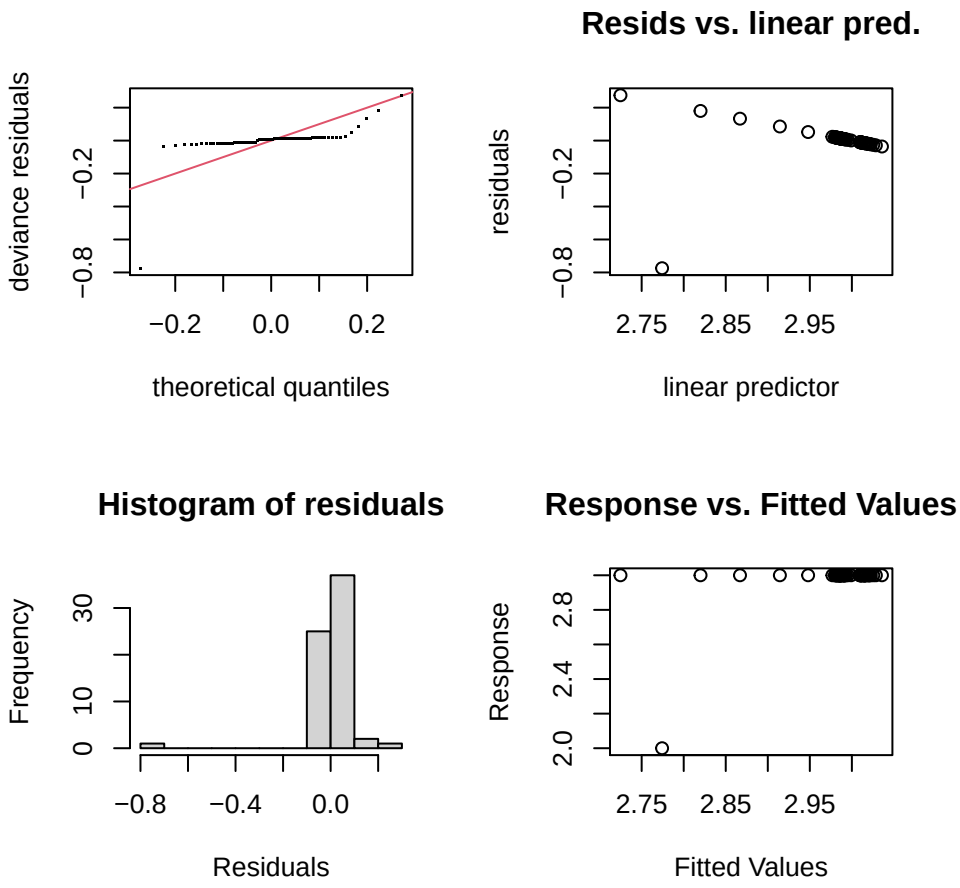

Figure A.8: Diagnostoc plots for best fitting GAM for depth habitat richness

2.3.2 Shannon's index

```
eh_1null <- gam(Eco_Hill ~ s(Age),data = full %>% filter(Q==1))
eh0_1 <- update(eh0_0,  shan(Eco_Hill) ~ s(Age)+ frag,data = full %>%
                  filter(Q==1))
eh1_1 <- update(eh1_0,  shan(Eco_Hill) ~ s(Age, by=size)+size+ frag,data = full %>%
                  filter(Q==1))
eh2_1 <-update(eh2_0,  shan(Eco_Hill) ~ s(Age,by=size)+ frag,data = full %>%
                 filter(Q==1))
```

```
##
## Method: GCV   Optimizer: magic
```

Table A.22: AICc Comparison between models of depth habitat Shannon's index

		df	AIC	ΔAIC	AICweight	ΔAICc
Depth Habitat	s(Age, by=size) + Frag	7.59	-108.01	-105.74	7.843871e-01	0.00
Depth Habitat	s(Age, by=size) +size + Frag	8.54	-106.01	-103.12	2.118117e-01	2.62
Depth Habitat	s(Age) + Frag	6.21	-96.60	-95.08	3.801111e-03	10.66
Depth Habitat	s(Age)	5.05	13.93	14.95	4.859187e-27	120.69

```
## Smoothing parameter selection converged after 4 iterations.
## The RMS GCV score gradient at convergence was 5.380348e-07 .
## The Hessian was positive definite.
## Model rank =  20 / 20
##
## Basis dimension (k) checking results. Low p-value (k-index<1) may
## indicate that k is too low, especially if edf is close to k'.
##
##                  k'  edf k-index p-value
## s(Age):size63  9.00 1.51    0.97    0.34
## s(Age):size180 9.00 3.08    0.97    0.32

## null device
##           1
```

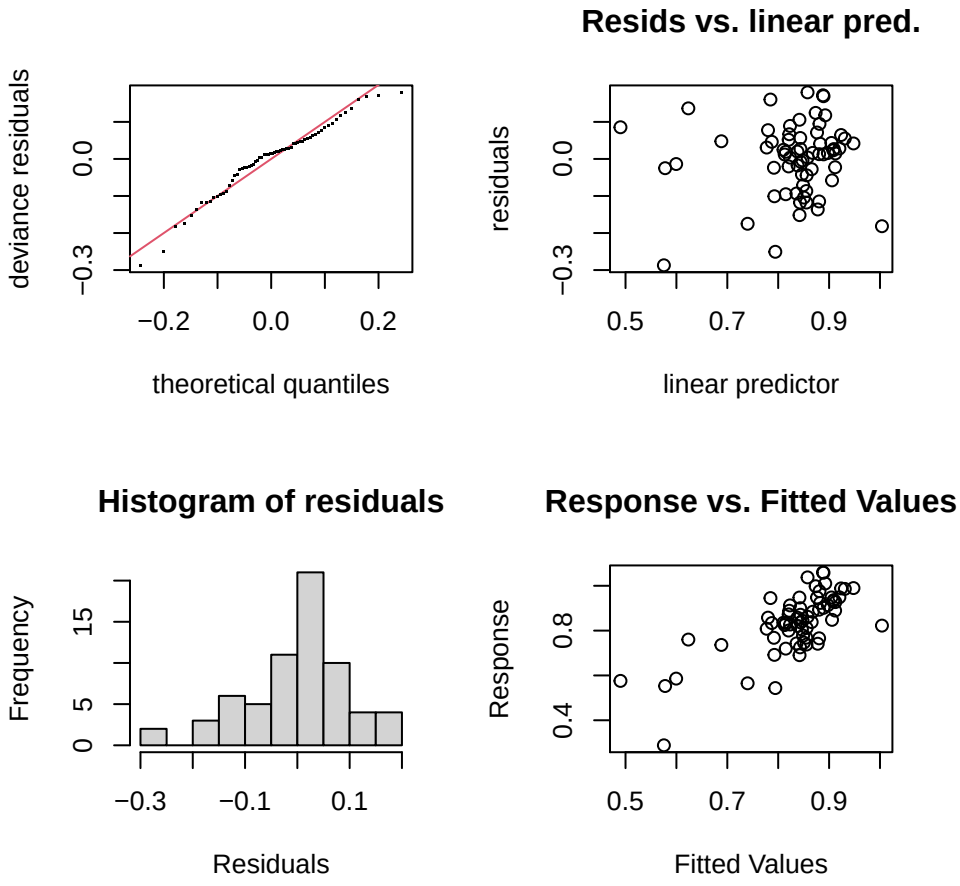

Figure A.9: Diagnostoc plots for best fitting GAM for Depth habitat Shannon's index

Table A.23: AICc Comparison between models of depth habitat Simpson's index

		df	AIC	ΔAIC	AICweight	ΔAICc
Depth Habitat	s(Age, by=size) + Frag	7.52	-160.60	-158.37	7.441301e-01	0.00
Depth Habitat	s(Age, by=size) +size + Frag	8.61	-159.17	-156.23	2.550421e-01	2.14
Depth Habitat	s(Age) + Frag	6.00	-146.19	-144.77	8.277223e-04	13.60
Depth Habitat	s(Age)	4.79	33.54	34.46	9.965258e-43	192.83

2.3.3 Simpson's index

```
eh_2null <- gam(Eco_Hill ~ s(Age),data = full %>% filter(Q==2))
eh0_2 <- update(eh0_0,  simps(Eco_Hill) ~ s(Age)+ frag,data = full %>%
                  filter(Q==2))
eh1_2<- update(eh1_0,  simps(Eco_Hill) ~ s(Age, by=size)+size+ frag,data = full %>%
                 filter(Q==2))
eh2_2 <-update(eh2_0, simps(Eco_Hill) ~ s(Age, by=size)+ frag,data = full %>%
                 filter(Q==2))
```

```
##
## Method: GCV   Optimizer: magic
## Smoothing parameter selection converged after 4 iterations.
## The RMS GCV score gradient at convergence was 2.928622e-06 .
## The Hessian was positive definite.
## Model rank =  20 / 20
##
## Basis dimension (k) checking results. Low p-value (k-index<1) may
## indicate that k is too low, especially if edf is close to k'.
##
##                   k'  edf k-index p-value
## s(Age):size63  9.00 1.50    1.02    0.47
## s(Age):size180 9.00 3.03    1.02    0.50

## null device
##           1
```

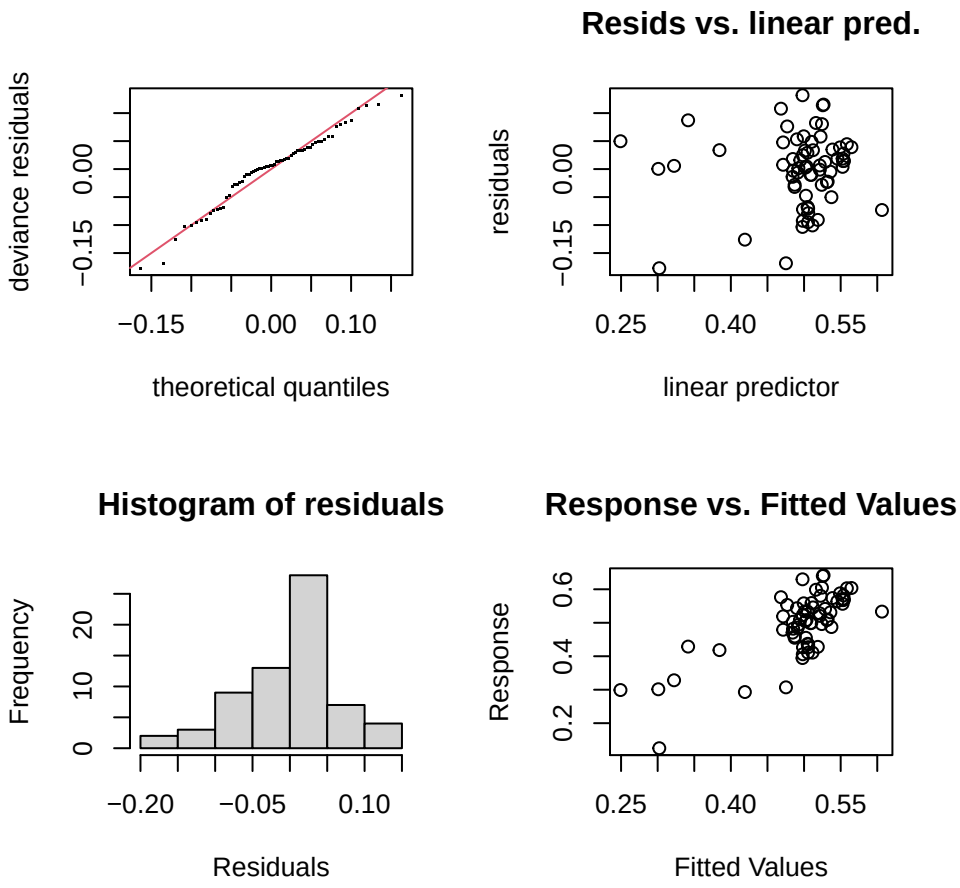

Figure A.10: Diagnostoc plots for best fitting GAM for Depth habitat Simpson's

2.4 Predicting GAMs

```
e_0_plot <- ggplot(predicted_eh2_0, aes(Age,fit, group=size))+
  geom_line(aes(col=size))+
  geom_ribbon(aes(ymax=upper,ymin=lower), col="darkgrey", alpha=0.4)+
  geom_point(data=full%>%filter(Q==0), aes(Age,Eco_Hill, col=size))+
  scale_colour_manual(values=c("purple", "seagreen"))+
  scale_x_continuous(expand = c(0,0), breaks=seq(from=38, to=45,by=1))+
  labs(x="Sample Age (Ma)", y= "Depth habitat richness", col="Size fraction", tag="A")

e_1_plot <- ggplot(predicted_eh2_1, aes(Age,fit, group=size))+
  geom_line(aes(col=size))+
  geom_ribbon(aes(ymax=upper,ymin=lower), col="darkgrey", alpha=0.4)+
  geom_point(data=full%>%filter(Q==1), aes(Age,shan(Eco_Hill), col=size))+
  scale_colour_manual(values=c("purple", "seagreen"))+
  scale_x_continuous(expand = c(0,0), breaks=seq(from=38, to=45,by=1))+
  labs(x="Sample Age (Ma)", y= "Shannon's index", col="Size fraction", tag="B")

e_2_plot <- ggplot(predicted_eh2_2, aes(Age,fit, group=size))+
  geom_line(aes(col=size))+
  geom_ribbon(aes(ymax=upper,ymin=lower), col="darkgrey", alpha=0.4)+
  geom_point(data=full%>%filter(Q==2), aes(Age,simps(Eco_Hill), col=size))+
```

```
scale_colour_manual(values=c("purple", "seagreen"))+
scale_x_continuous(expand = c(0,0), breaks=seq(from=38, to=45,by=1))+
labs(x="Sample Age (Ma)", y= "Simpson's index", col="Size fraction", tag="C")
```

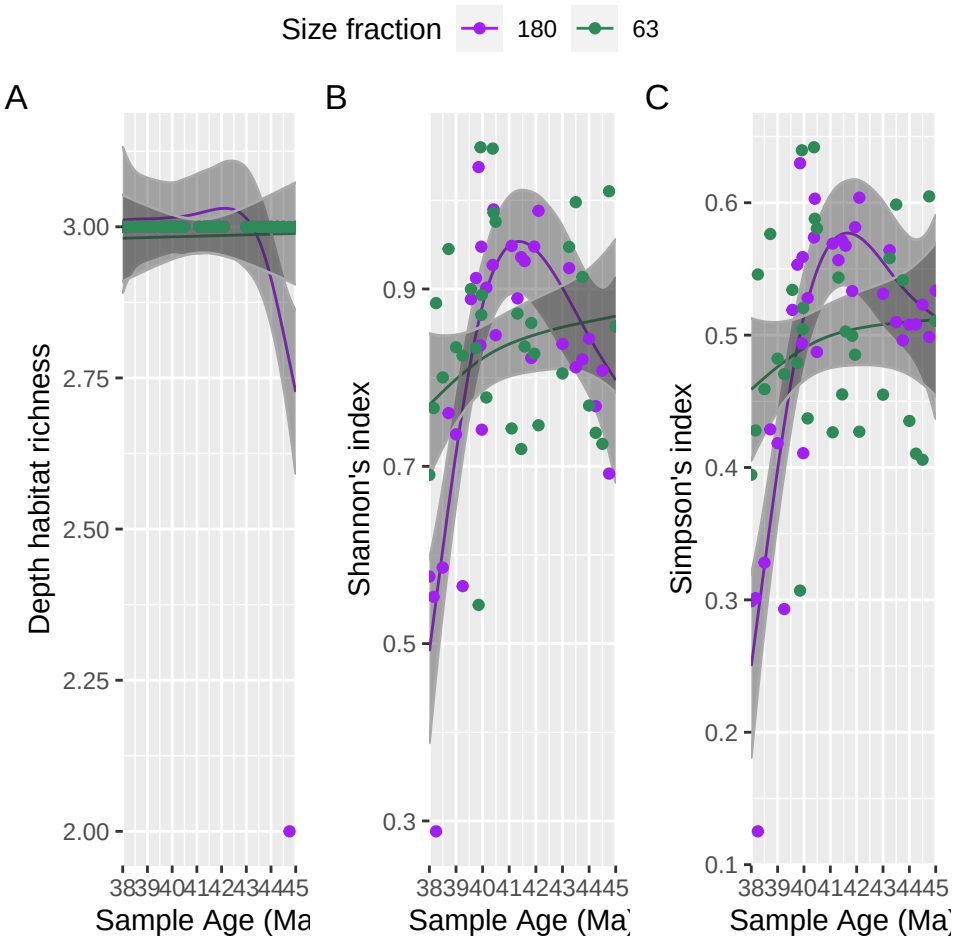

Figure A.11: Depth habitat diversity at integers of q. A - Richness, B - Shannon's index, C - Simpons index

3 Hill Numbers

3.1 Kruskal Test

```
full <- read_csv("Data/Hill_Emperical_All_Frag_2021.csv")
full$interval <- rep(c("postMECO","MECO","preMECO","postMECO","MECO","preMECO"),
                     c(403,155,465,403,155,465))
full$interval <- as.factor(full$interval)
```

```
k1 <- tidy(kruskal.test(Genus_Hill ~ interval,
             data = full %>% filter(Q <1)%>% filter(size==63)))
k2 <-tidy(kruskal.test(Genus_Hill ~ interval,
             data = full %>% filter(Q %in% (1:2))%>% filter(size==63)))
k3<- tidy(kruskal.test(Genus_Hill ~ interval,
             data = full %>% filter(Q <1)%>% filter(size==180)))
k4<- tidy(kruskal.test(Genus_Hill ~ interval,
             data = full %>% filter(Q %in% (1:2))%>% filter(size==180)))
k5<- tidy(kruskal.test(Morph_Hill ~ interval,
             data = full %>% filter(Q <1)%>% filter(size==63)))
k6<- tidy(kruskal.test(Morph_Hill ~ interval,
             data = full %>% filter(Q %in% (1:2))%>% filter(size==63)))
k7<- tidy(kruskal.test(Morph_Hill ~ interval,
             data = full %>% filter(Q <1)%>% filter(size==180)))
k8<- tidy(kruskal.test(Morph_Hill ~ interval,
             data = full %>% filter(Q %in% (1:2))%>% filter(size==180)))
k9<- tidy(kruskal.test(Eco_Hill ~ interval,
             data = full %>% filter(Q <1)%>% filter(size==63)))
k10<- tidy(kruskal.test(Eco_Hill ~ interval,
             data = full %>% filter(Q %in% (1:2))%>% filter(size==63)))
k11<- tidy(kruskal.test(Eco_Hill ~ interval,
             data = full %>% filter(Q <1)%>% filter(size==180)))
k12<- tidy(kruskal.test(Eco_Hill ~ interval,
             data = full %>% filter(Q %in% (1:2))%>% filter(size==180)))
```

```
e1 <- kruskal_effsize( data=full %>% filter(Q <1) %>%
                         filter(size==63),Genus_Hill ~ interval,ci = FALSE,
                       conf.level =0.95,ci.type =
                         "perc",nboot = 1000)

e2<- kruskal_effsize(
  data=full %>% filter(Q%in% (1:2) ) %>% filter(size==63),
  Genus_Hill ~ interval,
  ci = FALSE,
  conf.level = 0.95,
  ci.type = "perc",
  nboot = 1000
)
e3<-kruskal_effsize(
  data=full %>% filter(Q <1) %>% filter(size==180),
  Genus_Hill ~ interval,
  ci = FALSE,
  conf.level = 0.95,
```

```
  ci.type = "perc",
  nboot = 1000
)
e4<- kruskal_effsize(
  data=full %>% filter(Q %in% (1:2)) %>% filter(size==180),
  Genus_Hill ~ interval,
  ci = FALSE,
  conf.level = 0.95,
  ci.type = "perc",
  nboot = 1000
)
e5 <- kruskal_effsize(
  data=full %>% filter(Q <1) %>% filter(size==63),
  Morph_Hill ~ interval,
  ci = FALSE,
  conf.level = 0.95,
  ci.type = "perc",
  nboot = 1000
)
e6 <- kruskal_effsize(
  data=full %>% filter(Q %in% (1:2)) %>% filter(size==63),
  Morph_Hill ~ interval,
  ci = FALSE,
  conf.level = 0.95,
  ci.type = "perc",
  nboot = 1000
)
e7 <- kruskal_effsize(
  data=full %>% filter(Q <1) %>% filter(size==180),
  Morph_Hill ~ interval,
  ci = FALSE,
  conf.level = 0.95,
  ci.type = "perc",
  nboot = 1000
)
e8<- kruskal_effsize(
  data=full %>% filter(Q %in% (1:2)) %>% filter(size==180),
  Morph_Hill ~ interval,
  ci = FALSE,
  conf.level = 0.95,
  ci.type = "perc",
  nboot = 1000
)
e9 <- kruskal_effsize(
  data=full %>% filter(Q <1) %>% filter(size==63),
  Eco_Hill ~ interval,
  ci = FALSE,
  conf.level = 0.95,
  ci.type = "perc",
  nboot = 1000
)
e10<- kruskal_effsize(
  data=full %>% filter(Q %in% (1:2)) %>% filter(size==63),
```

Table A.24: Results from Kruskal test, bold and italic p values show those models that indicate significant differences between intervals. Effect size was calculated usng the eta squared based on the H-statistic (eta2[H]), A large effect size is calssified as a value > 0.14, whilst a small effect size is a valye < 0.06, with a moderate effect size values in between 0.06 and 0.14

Model formula	Size fraction	q	Z-score	p	Effect Size	Magnitude
Genera Interval	63	<1	59.603	***0.000***	0.1644754	large
Genera Interval	63	1-2	10.280	***0.006***	0.1372551	moderate
Genera Interval	180	<1	38.198	***0.000***	0.0590297	small
Genera Interval	180	1-2	17.622	***0.000***	0.2297179	large
Morphogroup Interval	63	<1	42.622	***0.000***	0.1309620	moderate
Morphogroup Interval	63	1-2	11.518	***0.003***	0.1927881	large
Morphogroup Interval	180	<1	56.015	***0.000***	0.1854895	large
Morphogroup Interval	180	1-2	30.581	***0.000***	0.5128037	large
Depth Habitat Interval	63	<1	0.600	0.741	0.0145352	small
Depth Habitat Interval	63	1-2	0.633	0.729	0.0059556	small
Depth Habitat Interval	180	<1	24.967	***0.000***	0.0423392	small
Depth Habitat Interval	180	1-2	18.486	***0.000***	0.1842991	large

```
  Eco_Hill ~ interval,
  ci = FALSE,
  conf.level = 0.95,
  ci.type = "perc",
  nboot = 1000
)
e11<- kruskal_effsize(
  data=full %>% filter(Q <1) %>% filter(size==180),
  Eco_Hill ~ interval,
  ci = FALSE,
  conf.level = 0.95,
  ci.type = "perc",
  nboot = 1000
)
e12<-kruskal_effsize(
  data=full %>% filter(Q %in% (1:2)) %>% filter(size==180),
  Eco_Hill ~ interval,
  ci = FALSE,
  conf.level = 0.95,
  ci.type = "perc",
  nboot = 1000
)
```

3.2 *Post-hoc* Dunn Test

```
d1 <- dunnTest(Genus_Hill ~ interval,
         data = full %>% filter(Q <1) %>% filter(size==63),
         method="none")
d2 <- dunnTest(Genus_Hill ~ interval,
         data = full %>% filter(Q %in% (1:2)) %>% filter(size==63),
         method="none")
d3 <-dunnTest(Genus_Hill ~ interval,
       data = full %>% filter(Q <1) %>% filter(size==180),
         method="none")
d4 <-dunnTest(Genus_Hill ~ interval,
         data = full %>% filter(Q %in% (1:2)) %>% filter(size==180),
         method="none")
d5<- dunnTest(Morph_Hill ~ interval,
         data = full %>% filter(Q <1) %>% filter(size==63),
         method="none")
d6<- dunnTest(Morph_Hill ~ interval,
         data = full %>% filter(Q %in% (1:2)) %>% filter(size==63),
         method="none")
d7 <- dunnTest(Morph_Hill ~ interval,
         data = full %>% filter(Q <1) %>% filter(size==180),
         method="none")
d8<- dunnTest(Morph_Hill ~ interval,
         data = full %>% filter(Q %in% (1:2)) %>% filter(size==180),
         method="none")
d11 <- dunnTest(Eco_Hill ~ interval,
         data = full %>% filter(Q <1) %>% filter(size==180),
         method="none")
d12 <- dunnTest(Eco_Hill ~ interval,
         data = full %>% filter(Q %in% (1:2)) %>% filter(size==180),
         method="none")
```

Table A.25: Results from *post-hoc* Dunn test showing differences between palaeoclimatic intervals, bold and italic p values show significantly different intervals

Model		Size fraction	q	Interval Comparison	Z-score	p
Genera	Interval	63	<1	MECO - postMECO	7.50	***0.00***
Genera	Interval	63	<1	MECO - preMECO	2.42	***0.02***
Genera	Interval	63	<1	postMECO - preMECO	-4.92	***0.00***
Genera	Interval	63	1-2	MECO - postMECO	2.80	***0.01***
Genera	Interval	63	1-2	MECO - preMECO	0.16	0.87
Genera	Interval	63	1-2	postMECO - preMECO	-2.62	***0.01***
Genera	Interval	180	<1	MECO - postMECO	6.08	***0.00***
Genera	Interval	180	<1	MECO - preMECO	4.16	***0.00***
Genera	Interval	180	<1	postMECO - preMECO	-1.66	0.10
Genera	Interval	180	1-2	MECO - postMECO	4.09	***0.00***
Genera	Interval	180	1-2	MECO - preMECO	1.38	0.17
Genera	Interval	180	1-2	postMECO - preMECO	-2.62	***0.01***
Morphogroup	Interval	63	<1	MECO - postMECO	5.24	***0.00***
Morphogroup	Interval	63	<1	MECO - preMECO	-0.51	0.61
Morphogroup	Interval	63	<1	postMECO - preMECO	-5.79	***0.00***
Morphogroup	Interval	63	1-2	MECO - postMECO	1.22	0.22
Morphogroup	Interval	63	1-2	MECO - preMECO	-2.03	***0.04***
Morphogroup	Interval	63	1-2	postMECO - preMECO	-3.38	***0.00***
Morphogroup	Interval	180	<1	MECO - postMECO	6.89	***0.00***
Morphogroup	Interval	180	<1	MECO - preMECO	1.19	0.24
Morphogroup	Interval	180	<1	postMECO - preMECO	-5.63	***0.00***
Morphogroup	Interval	180	1-2	MECO - postMECO	4.55	***0.00***
Morphogroup	Interval	180	1-2	MECO - preMECO	-0.24	0.81
Morphogroup	Interval	180	1-2	postMECO - preMECO	-4.81	***0.00***
Depth Habitat	Interval	180	<1	MECO - postMECO	4.97	***0.00***
Depth Habitat	Interval	180	<1	MECO - preMECO	2.18	***0.03***
Depth Habitat	Interval	180	<1	postMECO - preMECO	-2.65	***0.01***
Depth Habitat	Interval	180	1-2	MECO - postMECO	3.85	***0.00***
Depth Habitat	Interval	180	1-2	MECO - preMECO	0.43	0.67
Depth Habitat	Interval	180	1-2	postMECO - preMECO	-3.40	***0.00***

Bibliography

Aze, Tracy, Thomas H.G. G Ezard, Andy Purvis, Helen K. Coxall, R M Stewart, Bridget S. Wade, Paul N. Pearson, et al. 2011. "A Phylogeny of Cenozoic Macroperforate Planktonic Foraminifera from Fossil Data." *Biological Reviews* 86 (4): 900–927. https://doi.org/10.1111/j.1469-185X.2011.00178.x.

Cappelli, C., P. R. Bown, Thomas Westerhold, S. M. Bohaty, M. de Riu, V. Lobba, Y. Yamamoto, and C. Agnini. 2019. "The Early to Middle Eocene Transition: An Integrated Calcareous Nannofossil and Stable Isotope Record From the Northwest Atlantic Ocean (Integrated Ocean Drilling Program Site U1410)." *Paleoceanography and Paleoclimatology* 34 (12): 1913–30. https://doi.org/10.1029/2019PA003686.

Chao, Anne, and Lou Jost. 2015. "Estimating Diversity and Entropy Profiles via Discovery Rates of New Species." *Methods in Ecology and Evolution* 6 (8): 873–82. https://doi.org/10.1111/2041-210X.12349.

Gradstein, Felix M, James George Ogg, Mark D Schmitz, and Gabi M Ogg. 2012. *The Geologic Time Scale 2012*. elsevier.

Ogg, James G., Linda A. Hinnov, and Chunju Huang. 2012. "Cretaceous." In, 1-2:793–853. Elsevier B.V. https://doi.org/10.1016/B978-0-444-59425-9.00027-5.

R Core Team. 2020. *R: A Language and Environment for Statistical Computing*. Vienna, Austria: R Foundation for Statistical Computing. https://www.R-project.org/.

Wickham, Hadley. 2019. *Tidyverse: Easily Install and Load the 'Tidyverse'*. https://CRAN.R-project.org/package=tidyverse.

Wickham, Hadley, and Jennifer Bryan. 2019. *Readxl: Read Excel Files*. https://CRAN.R-project.org/package=readxl.

Wood, Simon N. 2017. *Generalized Additive Models: An Introduction with R, Second Edition*. 2nd edition. Chapman; Hall/CRC. https://www.routledge.com/Generalized-Additive-Models-An-Introduction-with-R-Second-Edition/Wood/p/book/9781498728331.

Xie, Yihui. 2020. *Knitr: A General-Purpose Package for Dynamic Report Generation in r*. https://CRAN.R-project.org/package=knitr.

Yamamoto, Y., H. Fukami, W. Taniguchi, and P.C. Lippert. 2018. "Data Report: Updated Magnetostratigraphy for IODP Sites U1403, U1408, U1409, and U1410." *Proceedings of the Integrated Ocean Drilling Program,. 342: College Station, TX (Integrated Ocean Drilling Program)*. https://doi.org/10.2204/iodp.proc.342.2014.

Zhu, Hao. 2019. *kableExtra: Construct Complex Table with 'Kable' and Pipe Syntax*. https://CRAN.R-project.org/package=kableExtra.

Appendix B Supplementary information for Chapter 3

The following supplement provides tables of all data produced. Where data is not provided this is because it is too large. The following document is included to enable the reproducibility of the results in Chapter 3. The data and formatted supplement can be found at https://doi.org/10.3389/fevo.2021.679722

1 Introduction to Appendix B

This supplementary material is intended to provide reproducible code for the results presented in the paper. All analyses were performed in the freely distributed R environment (R Core Team 2020). This supporting information was written using knitr (Xie 2021). The code uses the tidyverse (Wickham 2019) and packages within, mclust (Fraley, Raftery, and Scrucca 2020), kableExtra (Zhu 2021), scales (Wickham and Seidel 2020) and broom(Robinson, Hayes, and Couch 2021) packages as well as dependencies:

```
library(tidyverse)
library(mclust)
library(knitr)
library(kableExtra)
library(png)
library(scales)
library(broom)
library(bookdown)
library(xtable)
print(sessionInfo(), local = FALSE)
```

```
## R version 4.0.3 (2020-10-10)
## Platform: x86_64-apple-darwin17.0 (64-bit)
## Running under: macOS Mojave 10.14.6
##
## Matrix products: default
## BLAS:   /Library/Frameworks/R.framework/Versions/4.0/Resources/lib/libRblas.dylib
## LAPACK: /Library/Frameworks/R.framework/Versions/4.0/Resources/lib/libRlapack.dylib
##
## attached base packages:
## [1] stats     graphics  grDevices utils     datasets  methods   base
##
## other attached packages:
##  [1] xtable_1.8-4     bookdown_0.22    broom_0.7.8      scales_1.1.1
##  [5] png_0.1-7        kableExtra_1.3.2 knitr_1.31       mclust_5.4.7
##  [9] forcats_0.5.1    stringr_1.4.0    dplyr_1.0.6      purrr_0.3.4
## [13] readr_1.4.0      tidyr_1.1.3      tibble_3.1.2     ggplot2_3.3.3
## [17] tidyverse_1.3.1
##
## loaded via a namespace (and not attached):
##  [1] tidyselect_1.1.1  xfun_0.22         haven_2.3.1       colorspace_2.0-1
##  [5] vctrs_0.3.8       generics_0.1.0    viridisLite_0.4.0 htmltools_0.5.1.1
##  [9] yaml_2.2.1        utf8_1.2.1        rlang_0.4.11      pillar_1.6.1
## [13] glue_1.4.2        withr_2.4.2       DBI_1.1.1         dbplyr_2.1.1
## [17] modelr_0.1.8      readxl_1.3.1      lifecycle_1.0.0   munsell_0.5.0
## [21] gtable_0.3.0      cellranger_1.1.0  rvest_1.0.0       evaluate_0.14
## [25] fansi_0.5.0       Rcpp_1.0.6        backports_1.2.1   webshot_0.5.2
## [29] jsonlite_1.7.2    fs_1.5.0          hms_1.0.0         digest_0.6.27
## [33] stringi_1.5.3     grid_4.0.3        cli_3.0.0         tools_4.0.3
## [37] magrittr_2.0.1    crayon_1.4.1      pkgconfig_2.0.3   ellipsis_0.3.2
## [41] xml2_1.3.2        reprex_2.0.0      lubridate_1.7.10  assertthat_0.2.1
## [45] rmarkdown_2.6     httr_1.4.2        rstudioapi_0.13   R6_2.5.0
## [49] compiler_4.0.3
```

Table B1: IODP Expedition 342 samples used in this study. ID= Study specific sample ID, Exp. = IODP expedition number, Top Int = Top interval (m), Bottom Int = Bottom interval (m), Sample ages were calculated based on an age depth model constructed using available biostratigraphic and magnetostratigraphic data for Sites U1408 and U1410 (Norris et al (2012), Yamamoto et al (2018) and Cappelli et al (2019)). Age calibrations from the 2012 geologic timescale were used for middle Eocene geomagnetic polarity reversals (GTS2012; Gradstein et al (2012), Ogg et al (2012))

ID	Exp.	Site	Hole	Core	Core Type	Section	Top Int	Bottom Int	Depth (CCSF-A, m)	U1408 Mapped Depth (CCSF-M, m)	Inter-site Mapped Depth (CCSF-X)	Age (Ma, GTS2012)
S80	342	1408	B	5	H	2	60.0	62.0	31.35	N/A	N/A	38.50
S82	342	1408	B	7	H	1	98.0	100.0	49.08	49.08	49.76	39.56
S59	342	1410	B	10	H	5	117.0	118.5	90.04	90.04	70.64	40.14
S49	342	1408	C	13	H	1	142.0	144.0	114.37	114.37	129.48	42.10
S53	342	1410	A	11	H	5	129.5	131.0	108.53	108.53	109.79	41.31
S115	342	1410	A	16	H	4	120.0	121.5	152.59	N/A	N/A	43.50

Table B2: Planktic foraminifera stable carbon and oxygen isotope values based on multi-specimen samples used for palaeoceanographic analysis. Sample ID is the study specific sample ID. Age is presented in millions of years ago (Ma), Depth habitat refers to the inferred depth habitat of the foraminifera in the water column based on stable isotope studies as summarized in the main text, Oxygen = δ^{18}O VPDB (‰) and Carbon = δ^{13}C VPDB (‰)

Sample_ID	Age	Genus	Depth_Habitat	Carbon	Oxygen
S80	38.50	*Globigerinatheka spp.*	Surface	2.15	-0.90
S80	38.50	*Catapsydrax spp.*	Subthermocline	0.92	0.10
S80	38.50	*Subbotina spp.*	Thermocline	0.81	-0.40
S82	39.56	*Globigerinatheka spp.*	Surface	2.92	-1.16
S82	39.56	*Catapsydrax spp.*	Subthermocline	1.52	-0.25
S82	39.56	*Subbotina spp.*	Thermocline	1.41	-0.23
S59	40.14	*Globigerinatheka spp.*	Surface	2.26	-1.31
S59	40.14	*Catapsydrax spp.*	Subthermocline	1.26	-1.30
S59	40.14	*Subbotina spp.*	Thermocline	1.45	-1.12
S53	41.31	*Catapsydrax spp.*	Subthermocline	0.69	0.20
S53	41.31	*Globigerinatheka spp.*	Surface	2.40	-1.10
S53	41.31	*Subbotina spp.*	Thermocline	0.86	-0.48
S49	42.10	*Globigerinatheka spp.*	Surface	2.48	-1.12
S49	42.10	*Catapsydrax spp.*	Subthermocline	0.77	-0.38
S49	42.10	*Subbotina spp.*	Thermocline	0.91	-0.59
S115	43.50	*Globigerinatheka spp.*	Surface	2.16	-1.35
S115	43.50	*Catapsydrax spp.*	Subthermocline	0.93	-0.83
S115	43.50	*Subbotina spp.*	Thermocline	1.30	-1.20

Table B3: Morphological measurements for all 300 *Subbotina* individuals as presented in Figure S1. Sample ID is the study specific sample ID, Age is presented in million of years ago (Ma), Area is presented as μm^2.

Sample_ID	Genus	Age	Aspect_Ratio	Area
S49	*Subbotina spp.*	42.10	1.22	150954.86
S49	*Subbotina spp.*	42.10	1.17	156424.83
S49	*Subbotina spp.*	42.10	1.03	75273.33
S49	*Subbotina spp.*	42.10	1.15	62659.74
S49	*Subbotina spp.*	42.10	1.31	153363.28
S49	*Subbotina spp.*	42.10	1.27	102827.28
S49	*Subbotina spp.*	42.10	1.15	122543.67
S49	*Subbotina spp.*	42.10	1.15	123441.73
S49	*Subbotina spp.*	42.10	1.20	153077.54
S49	*Subbotina spp.*	42.10	1.19	78375.70
S49	*Subbotina spp.*	42.10	1.05	87152.14
S49	*Subbotina spp.*	42.10	1.22	132830.48
S49	*Subbotina spp.*	42.10	1.10	114379.54
S49	*Subbotina spp.*	42.10	1.18	65476.37
S49	*Subbotina spp.*	42.10	1.21	91642.42
S49	*Subbotina spp.*	42.10	1.23	113277.38
S49	*Subbotina spp.*	42.10	1.22	114787.74
S49	*Subbotina spp.*	42.10	1.19	66211.14
S49	*Subbotina spp.*	42.10	1.34	149240.39

Table B3: Morphological measurements for all 300 *Subbotina* individuals as presented in Figure S1. Sample ID is the study specific sample ID, Age is presented in million of years ago (Ma), Area is presented as μm^2. *(continued)*

Sample_ID	Genus	Age	Aspect_Ratio	Area
S49	*Subbotina spp.*	42.10	1.31	65721.29
S49	*Subbotina spp.*	42.10	1.24	63778.34
S49	*Subbotina spp.*	42.10	1.27	86143.94
S49	*Subbotina spp.*	42.10	1.33	130238.73
S49	*Subbotina spp.*	42.10	1.17	113555.45
S49	*Subbotina spp.*	42.10	1.25	66824.06
S49	*Subbotina spp.*	42.10	1.08	125829.25
S49	*Subbotina spp.*	42.10	1.24	119874.18
S49	*Subbotina spp.*	42.10	1.27	77597.74
S49	*Subbotina spp.*	42.10	1.22	144921.84
S49	*Subbotina spp.*	42.10	1.25	126056.55
S49	*Subbotina spp.*	42.10	1.31	67596.86
S49	*Subbotina spp.*	42.10	1.15	98235.92
S49	*Subbotina spp.*	42.10	1.11	62687.33
S49	*Subbotina spp.*	42.10	1.04	139057.69
S49	*Subbotina spp.*	42.10	1.07	128556.77
S49	*Subbotina spp.*	42.10	1.08	58823.36
S49	*Subbotina spp.*	42.10	1.33	102327.19
S49	*Subbotina spp.*	42.10	1.07	126192.92
S49	*Subbotina spp.*	42.10	1.20	101008.89
S49	*Subbotina spp.*	42.10	1.34	123738.16
S49	*Subbotina spp.*	42.10	1.30	92374.86
S49	*Subbotina spp.*	42.10	1.34	116368.33
S49	*Subbotina spp.*	42.10	1.24	111769.59
S49	*Subbotina spp.*	42.10	1.24	138162.40
S49	*Subbotina spp.*	42.10	1.23	122566.65
S49	*Subbotina spp.*	42.10	1.24	72047.06
S49	*Subbotina spp.*	42.10	1.27	104171.65
S49	*Subbotina spp.*	42.10	1.24	87042.98
S49	*Subbotina spp.*	42.10	1.26	65448.86
S49	*Subbotina spp.*	42.10	1.32	79378.40
S53	*Subbotina spp.*	41.31	1.20	92708.11
S53	*Subbotina spp.*	41.31	1.15	133030.47
S53	*Subbotina spp.*	41.31	1.20	83643.91
S53	*Subbotina spp.*	41.31	1.09	96707.02
S53	*Subbotina spp.*	41.31	1.25	92308.21
S53	*Subbotina spp.*	41.31	1.24	81377.86
S53	*Subbotina spp.*	41.31	1.25	99906.15
S53	*Subbotina spp.*	41.31	1.19	127765.23
S53	*Subbotina spp.*	41.31	1.23	114302.23
S53	*Subbotina spp.*	41.31	1.19	72646.90
S53	*Subbotina spp.*	41.31	1.20	90194.65
S53	*Subbotina spp.*	41.31	1.16	62843.39
S53	*Subbotina spp.*	41.31	1.20	71579.91
S53	*Subbotina spp.*	41.31	1.36	75799.25
S53	*Subbotina spp.*	41.31	1.15	87811.97

Table B3: Morphological measurements for all 300 *Subbotina* individuals as presented in Figure S1. Sample ID is the study specific sample ID, Age is presented in million of years ago (Ma), Area is presented as μm^2. *(continued)*

Sample_ID	Genus	Age	Aspect_Ratio	Area
S53	*Subbotina spp.*	41.31	1.05	82599.84
S53	*Subbotina spp.*	41.31	1.18	88159.44
S53	*Subbotina spp.*	41.31	1.18	70537.48
S53	*Subbotina spp.*	41.31	1.16	104044.03
S53	*Subbotina spp.*	41.31	1.26	98534.06
S53	*Subbotina spp.*	41.31	1.26	87563.77
S53	*Subbotina spp.*	41.31	1.26	68105.15
S53	*Subbotina spp.*	41.31	1.36	72920.17
S53	*Subbotina spp.*	41.31	1.20	78330.85
S53	*Subbotina spp.*	41.31	1.23	90343.57
S53	*Subbotina spp.*	41.31	1.23	103349.07
S53	*Subbotina spp.*	41.31	1.13	86124.23
S53	*Subbotina spp.*	41.31	1.42	140479.29
S53	*Subbotina spp.*	41.31	1.21	87315.57
S53	*Subbotina spp.*	41.31	1.24	111688.48
S53	*Subbotina spp.*	41.31	1.24	93701.54
S53	*Subbotina spp.*	41.31	1.11	95537.86
S53	*Subbotina spp.*	41.31	1.22	85065.91
S53	*Subbotina spp.*	41.31	1.19	99210.48
S53	*Subbotina spp.*	41.31	1.12	88242.24
S53	*Subbotina spp.*	41.31	1.19	113801.72
S53	*Subbotina spp.*	41.31	1.19	105116.46
S53	*Subbotina spp.*	41.31	1.18	85562.21
S53	*Subbotina spp.*	41.31	1.24	90723.74
S53	*Subbotina spp.*	41.31	1.33	136284.13
S53	*Subbotina spp.*	41.31	1.19	96083.79
S53	*Subbotina spp.*	41.31	1.28	65610.93
S53	*Subbotina spp.*	41.31	1.14	78415.49
S53	*Subbotina spp.*	41.31	1.22	81641.44
S53	*Subbotina spp.*	41.31	1.19	93254.87
S53	*Subbotina spp.*	41.31	1.18	85959.25
S53	*Subbotina spp.*	41.31	1.25	85165.17
S53	*Subbotina spp.*	41.31	1.25	97026.76
S53	*Subbotina spp.*	41.31	1.19	95934.90
S53	*Subbotina spp.*	41.31	1.21	70127.27
S59	*Subbotina spp.*	40.14	1.32	104714.71
S59	*Subbotina spp.*	40.14	1.33	96468.34
S59	*Subbotina spp.*	40.14	1.12	132652.85
S59	*Subbotina spp.*	40.14	1.15	76207.86
S59	*Subbotina spp.*	40.14	1.17	135496.43
S59	*Subbotina spp.*	40.14	1.35	79122.52
S59	*Subbotina spp.*	40.14	1.32	82605.90
S59	*Subbotina spp.*	40.14	1.14	68174.75
S59	*Subbotina spp.*	40.14	1.06	112321.28
S59	*Subbotina spp.*	40.14	1.05	85662.75
S59	*Subbotina spp.*	40.14	1.38	125543.91

Table B3: Morphological measurements for all 300 *Subbotina* individuals as presented in Figure S1. Sample ID is the study specific sample ID, Age is presented in million of years ago (Ma), Area is presented as μm^2. *(continued)*

Sample_ID	Genus	Age	Aspect_Ratio	Area
S59	*Subbotina spp.*	40.14	1.39	95828.53
S59	*Subbotina spp.*	40.14	1.31	99738.45
S59	*Subbotina spp.*	40.14	1.34	132297.41
S59	*Subbotina spp.*	40.14	1.28	60212.74
S59	*Subbotina spp.*	40.14	1.10	100307.17
S59	*Subbotina spp.*	40.14	1.06	81468.47
S59	*Subbotina spp.*	40.14	1.39	138340.01
S59	*Subbotina spp.*	40.14	1.28	96539.43
S59	*Subbotina spp.*	40.14	1.29	107487.20
S59	*Subbotina spp.*	40.14	1.27	162112.95
S59	*Subbotina spp.*	40.14	1.33	137045.58
S59	*Subbotina spp.*	40.14	1.37	99577.59
S59	*Subbotina spp.*	40.14	1.17	104473.97
S59	*Subbotina spp.*	40.14	1.34	115118.29
S59	*Subbotina spp.*	40.14	1.30	128423.69
S59	*Subbotina spp.*	40.14	1.18	123314.42
S59	*Subbotina spp.*	40.14	1.22	123154.75
S59	*Subbotina spp.*	40.14	1.27	114000.64
S59	*Subbotina spp.*	40.14	1.20	68815.51
S59	*Subbotina spp.*	40.14	1.32	78076.07
S59	*Subbotina spp.*	40.14	1.23	132574.97
S59	*Subbotina spp.*	40.14	1.21	94202.21
S59	*Subbotina spp.*	40.14	1.26	112616.88
S59	*Subbotina spp.*	40.14	1.37	99098.59
S59	*Subbotina spp.*	40.14	1.34	139972.77
S59	*Subbotina spp.*	40.14	1.39	63546.57
S59	*Subbotina spp.*	40.14	1.27	104314.31
S59	*Subbotina spp.*	40.14	1.30	102504.78
S59	*Subbotina spp.*	40.14	1.32	146891.58
S59	*Subbotina spp.*	40.14	1.23	94602.19
S59	*Subbotina spp.*	40.14	1.28	119183.87
S59	*Subbotina spp.*	40.14	1.20	80516.83
S59	*Subbotina spp.*	40.14	1.22	112479.77
S59	*Subbotina spp.*	40.14	1.20	100019.64
S59	*Subbotina spp.*	40.14	1.26	98258.97
S59	*Subbotina spp.*	40.14	1.30	103744.14
S59	*Subbotina spp.*	40.14	1.19	86476.02
S59	*Subbotina spp.*	40.14	1.16	110041.92
S59	*Subbotina spp.*	40.14	1.32	83022.40
S80	*Subbotina spp.*	38.50	1.25	108687.56
S80	*Subbotina spp.*	38.50	1.27	94195.89
S80	*Subbotina spp.*	38.50	1.36	99816.49
S80	*Subbotina spp.*	38.50	1.24	64196.76
S80	*Subbotina spp.*	38.50	1.43	97107.76
S80	*Subbotina spp.*	38.50	1.37	89929.65
S80	*Subbotina spp.*	38.50	1.13	113698.70

Table B3: Morphological measurements for all 300 *Subbotina* individuals as presented in Figure S1. Sample ID is the study specific sample ID, Age is presented in million of years ago (Ma), Area is presented as μm^2. *(continued)*

Sample_ID	Genus	Age	Aspect_Ratio	Area
S80	*Subbotina spp.*	38.50	1.28	81600.32
S80	*Subbotina spp.*	38.50	1.31	100290.52
S80	*Subbotina spp.*	38.50	1.05	137941.78
S80	*Subbotina spp.*	38.50	1.20	66293.11
S80	*Subbotina spp.*	38.50	1.20	65299.03
S80	*Subbotina spp.*	38.50	1.19	71636.32
S80	*Subbotina spp.*	38.50	1.21	106615.73
S80	*Subbotina spp.*	38.50	1.20	54612.60
S80	*Subbotina spp.*	38.50	1.28	74307.93
S80	*Subbotina spp.*	38.50	1.25	79589.01
S80	*Subbotina spp.*	38.50	1.24	78222.14
S80	*Subbotina spp.*	38.50	1.30	100154.17
S80	*Subbotina spp.*	38.50	1.22	62192.51
S80	*Subbotina spp.*	38.50	1.17	71884.85
S80	*Subbotina spp.*	38.50	1.15	136997.48
S80	*Subbotina spp.*	38.50	1.23	67473.59
S80	*Subbotina spp.*	38.50	1.02	113512.20
S80	*Subbotina spp.*	38.50	1.23	47219.09
S80	*Subbotina spp.*	38.50	1.22	86982.53
S80	*Subbotina spp.*	38.50	1.25	101769.56
S80	*Subbotina spp.*	38.50	1.25	117488.54
S80	*Subbotina spp.*	38.50	1.32	81390.79
S80	*Subbotina spp.*	38.50	1.37	115873.15
S80	*Subbotina spp.*	38.50	1.33	98171.36
S80	*Subbotina spp.*	38.50	1.25	121712.45
S80	*Subbotina spp.*	38.50	1.25	115639.35
S80	*Subbotina spp.*	38.50	1.17	69684.13
S80	*Subbotina spp.*	38.50	1.22	68744.99
S80	*Subbotina spp.*	38.50	1.28	85336.45
S80	*Subbotina spp.*	38.50	1.21	86400.81
S80	*Subbotina spp.*	38.50	1.22	79513.79
S80	*Subbotina spp.*	38.50	1.34	105747.08
S80	*Subbotina spp.*	38.50	1.18	92599.13
S80	*Subbotina spp.*	38.50	1.24	117580.23
S80	*Subbotina spp.*	38.50	1.14	57475.32
S80	*Subbotina spp.*	38.50	1.23	75694.62
S80	*Subbotina spp.*	38.50	1.16	62171.02
S80	*Subbotina spp.*	38.50	1.30	158088.44
S80	*Subbotina spp.*	38.50	1.35	87026.90
S80	*Subbotina spp.*	38.50	1.23	69684.13
S80	*Subbotina spp.*	38.50	1.21	86713.86
S80	*Subbotina spp.*	38.50	1.30	72564.16
S80	*Subbotina spp.*	38.50	1.24	67242.37
S82	*Subbotina spp.*	39.56	1.25	159575.80
S82	*Subbotina spp.*	39.56	1.27	87488.69
S82	*Subbotina spp.*	39.56	1.31	97266.47

Table B3: Morphological measurements for all 300 *Subbotina* individuals as presented in Figure S1. Sample ID is the study specific sample ID, Age is presented in million of years ago (Ma), Area is presented as μm^2. *(continued)*

Sample_ID	Genus	Age	Aspect_Ratio	Area
S82	*Subbotina spp.*	39.56	1.26	80522.83
S82	*Subbotina spp.*	39.56	1.28	154782.77
S82	*Subbotina spp.*	39.56	1.24	107299.87
S82	*Subbotina spp.*	39.56	1.17	75090.73
S82	*Subbotina spp.*	39.56	1.33	150692.72
S82	*Subbotina spp.*	39.56	1.26	96563.49
S82	*Subbotina spp.*	39.56	1.24	100781.35
S82	*Subbotina spp.*	39.56	1.34	76049.34
S82	*Subbotina spp.*	39.56	1.28	81417.53
S82	*Subbotina spp.*	39.56	1.23	70425.52
S82	*Subbotina spp.*	39.56	1.18	73429.15
S82	*Subbotina spp.*	39.56	1.30	82184.41
S82	*Subbotina spp.*	39.56	1.26	65824.22
S82	*Subbotina spp.*	39.56	1.36	82631.76
S82	*Subbotina spp.*	39.56	1.17	137847.42
S82	*Subbotina spp.*	39.56	1.06	87169.16
S82	*Subbotina spp.*	39.56	1.18	97458.19
S82	*Subbotina spp.*	39.56	1.18	91625.49
S82	*Subbotina spp.*	39.56	1.25	107267.32
S82	*Subbotina spp.*	39.56	1.24	121510.28
S82	*Subbotina spp.*	39.56	1.32	71723.49
S82	*Subbotina spp.*	39.56	1.29	173204.61
S82	*Subbotina spp.*	39.56	1.23	111273.15
S82	*Subbotina spp.*	39.56	1.29	83995.33
S82	*Subbotina spp.*	39.56	1.27	147579.99
S82	*Subbotina spp.*	39.56	1.27	158898.06
S82	*Subbotina spp.*	39.56	1.26	88255.50
S82	*Subbotina spp.*	39.56	1.26	79290.07
S82	*Subbotina spp.*	39.56	1.26	91879.83
S82	*Subbotina spp.*	39.56	1.29	75474.99
S82	*Subbotina spp.*	39.56	1.32	114961.06
S82	*Subbotina spp.*	39.56	1.21	88637.01
S82	*Subbotina spp.*	39.56	1.28	118140.29
S82	*Subbotina spp.*	39.56	1.21	68862.18
S82	*Subbotina spp.*	39.56	1.26	76110.84
S82	*Subbotina spp.*	39.56	1.33	152539.59
S82	*Subbotina spp.*	39.56	1.20	83486.66
S82	*Subbotina spp.*	39.56	1.30	80528.44
S82	*Subbotina spp.*	39.56	1.34	76714.87
S82	*Subbotina spp.*	39.56	1.26	93299.47
S82	*Subbotina spp.*	39.56	1.27	72457.86
S82	*Subbotina spp.*	39.56	1.32	74320.30
S82	*Subbotina spp.*	39.56	1.13	135603.50
S82	*Subbotina spp.*	39.56	1.20	66604.47
S82	*Subbotina spp.*	39.56	1.28	94807.16
S82	*Subbotina spp.*	39.56	1.23	90106.71

Table B3: Morphological measurements for all 300 *Subbotina* individuals as presented in Figure S1. Sample ID is the study specific sample ID, Age is presented in million of years ago (Ma), Area is presented as μm^2. *(continued)*

Sample_ID	Genus	Age	Aspect_Ratio	Area
S82	*Subbotina spp.*	39.56	1.21	67313.97
S115	*Subbotina spp.*	43.50	1.25	128863.24
S115	*Subbotina spp.*	43.50	1.21	85140.20
S115	*Subbotina spp.*	43.50	1.29	103675.93
S115	*Subbotina spp.*	43.50	1.30	97822.54
S115	*Subbotina spp.*	43.50	1.17	108997.19
S115	*Subbotina spp.*	43.50	1.27	116446.96
S115	*Subbotina spp.*	43.50	1.32	81149.25
S115	*Subbotina spp.*	43.50	1.24	108819.81
S115	*Subbotina spp.*	43.50	1.21	85051.51
S115	*Subbotina spp.*	43.50	1.10	94363.72
S115	*Subbotina spp.*	43.50	1.33	143381.91
S115	*Subbotina spp.*	43.50	1.05	89741.77
S115	*Subbotina spp.*	43.50	1.25	90344.47
S115	*Subbotina spp.*	43.50	1.20	113608.62
S115	*Subbotina spp.*	43.50	1.10	130062.28
S115	*Subbotina spp.*	43.50	1.27	99927.37
S115	*Subbotina spp.*	43.50	1.26	114090.78
S115	*Subbotina spp.*	43.50	1.29	160197.19
S115	*Subbotina spp.*	43.50	1.23	97998.74
S115	*Subbotina spp.*	43.50	1.26	88355.56
S115	*Subbotina spp.*	43.50	1.05	54785.27
S115	*Subbotina spp.*	43.50	1.02	125180.43
S115	*Subbotina spp.*	43.50	1.03	137535.74
S115	*Subbotina spp.*	43.50	1.27	98541.16
S115	*Subbotina spp.*	43.50	1.27	60209.56
S115	*Subbotina spp.*	43.50	1.24	84799.64
S115	*Subbotina spp.*	43.50	1.30	138741.14
S115	*Subbotina spp.*	43.50	1.36	138741.14
S115	*Subbotina spp.*	43.50	1.24	144527.04
S115	*Subbotina spp.*	43.50	1.10	114151.05
S115	*Subbotina spp.*	43.50	1.22	68864.81
S115	*Subbotina spp.*	43.50	1.21	68519.04
S115	*Subbotina spp.*	43.50	1.03	114448.12
S115	*Subbotina spp.*	43.50	1.15	99176.85
S115	*Subbotina spp.*	43.50	1.31	62122.39
S115	*Subbotina spp.*	43.50	1.32	89841.20
S115	*Subbotina spp.*	43.50	1.37	83386.92
S115	*Subbotina spp.*	43.50	1.30	80620.81
S115	*Subbotina spp.*	43.50	1.35	91973.42
S115	*Subbotina spp.*	43.50	1.31	61430.87
S115	*Subbotina spp.*	43.50	1.35	106610.79
S115	*Subbotina spp.*	43.50	1.33	99407.36
S115	*Subbotina spp.*	43.50	1.27	82176.75
S115	*Subbotina spp.*	43.50	1.27	63390.20
S115	*Subbotina spp.*	43.50	1.28	92664.94

Table B3: Morphological measurements for all 300 *Subbotina* individuals as presented in Figure S1. Sample ID is the study specific sample ID, Age is presented in million of years ago (Ma), Area is presented as μm^2. *(continued)*

Sample_ID	Genus	Age	Aspect_Ratio	Area
S115	*Subbotina spp.*	43.50	1.29	69441.08
S115	*Subbotina spp.*	43.50	1.29	155651.75
S115	*Subbotina spp.*	43.50	1.24	79929.28
S115	*Subbotina spp.*	43.50	1.29	75434.34
S115	*Subbotina spp.*	43.50	1.28	67712.26

Table B4: Stable isotope and morphological measurements for a subset of 112 *Subbotina* individuals selected from the 300 measured morphologically (Table S4). Sample ID is the study specific sample ID, Age is presented in million of years ago (Ma), Oxygen = δ^{18}O VPDB (‰), Carbon = δ^{13}C VPDB (‰) and Area is presented as μm^2.. Note this table is a subset of those presented in Table B4 and includes species identification

Sample_ID	Age	Genus	Species	Carbon	Oxygen	Aspect Ratio	Area	Weight
S80	38.50	*Subbotina*	*linaperta*	1.05	-0.60	1.25	108687.56	0.031
S80	38.50	*Subbotina*	*eocaena*	0.98	-0.39	1.25	79589.01	0.021
S80	38.50	*Subbotina*	*yeguaensis*	1.00	-0.55	1.30	100154.17	0.019
S80	38.50	*Subbotina*	*eocaena*	0.69	-0.49	1.22	62192.51	0.008
S80	38.50	*Subbotina*	*utilisindex*	0.71	-0.35	1.17	71884.85	0.007
S80	38.50	*Subbotina*	*utilisindex*	0.15	-0.40	1.15	136997.48	0.007
S80	38.50	*Subbotina*	*utilisindex*	0.55	-0.65	1.23	47219.09	0.008
S80	38.50	*Subbotina*	*jacksonensis*	1.37	-0.68	1.22	86982.53	0.022
S80	38.50	*Subbotina*	*eocaena*	0.35	-0.92	1.25	117488.54	0.008
S80	38.50	*Subbotina*	*eocaena*	0.96	-0.40	1.32	81390.79	0.017
S80	38.50	*Subbotina*	*crociapertura*	0.19	-0.72	1.36	99816.49	0.012
S80	38.50	*Subbotina*	*eocaena*	0.81	-0.83	1.33	98171.36	0.006
S80	38.50	*Subbotina*	*crociapertura*	0.95	-1.08	1.18	92599.13	0.008
S80	38.50	*Subbotina*	*crociapertura*	0.65	-0.85	1.24	117580.23	0.013
S80	38.50	*Subbotina*	*utilisindex*	1.11	-0.43	1.14	58289.24	0.019
S80	38.50	*Subbotina*	*eocaena*	0.84	-0.49	1.16	62171.02	0.015
S80	38.50	*Subbotina*	*eocaena*	0.53	-0.34	1.37	89929.65	0.012
S80	38.50	*Subbotina*	*eocaena*	1.25	-0.76	1.13	113698.70	0.019
S82	39.56	*Subbotina*	*yeguaensis*	1.31	-0.49	1.25	159511.89	0.017
S82	39.56	*Subbotina*	*utilisindex*	1.06	-1.39	1.24	100781.35	0.007
S82	39.56	*Subbotina*	*crociapertura*	1.03	-1.61	1.18	73429.15	0.006
S82	39.56	*Subbotina*	*utilisindex*	1.17	-0.55	1.36	82631.76	0.018
S82	39.56	*Subbotina*	*crociapertura*	0.99	-0.50	1.17	137847.42	0.010
S82	39.56	*Subbotina*	*eocaena*	1.37	-0.42	1.27	87616.51	0.019
S82	39.56	*Subbotina*	*eocaena*	1.51	-0.41	1.18	97458.19	0.016
S82	39.56	*Subbotina*	*yeguaensis*	0.86	-0.82	1.18	91625.49	0.007
S82	39.56	*Subbotina*	*crociapertura*	1.30	-0.85	1.25	107267.32	0.007
S82	39.56	*Subbotina*	*utilisindex*	1.41	-0.27	1.29	83995.33	0.015
S82	39.56	*Subbotina*	*utilisindex*	1.41	-0.39	1.32	114961.06	0.014
S82	39.56	*Subbotina*	*crociapertura*	1.08	-0.31	1.21	68862.18	0.017
S82	39.56	*Subbotina*	*utilisindex*	1.36	-0.44	1.26	80522.83	0.015

Table B4: Stable isotope and morphological measurements for a subset of 112 *Subbotina* individuals selected from the 300 measured morphologically (Table S4). Sample ID is the study specific sample ID, Age is presented in million of years ago (Ma), Oxygen = δ^{18}O VPDB (‰), Carbon = δ^{13}C VPDB (‰) and Area is presented as μm^2.. Note this table is a subset of those presented in Table B4 and includes species identification *(continued)*

Sample_ID	Age	Genus	Species	Carbon	Oxygen	Aspect Ratio	Area	Weight
S82	39.56	*Subbotina*	*linaperta*	1.28	-0.43	1.30	80528.44	0.018
S82	39.56	*Subbotina*	*utilisindex*	1.42	-0.22	1.20	66604.47	0.018
S82	39.56	*Subbotina*	*utilisindex*	0.90	-0.40	1.28	94807.16	0.013
S82	39.56	*Subbotina*	*utilisindex*	1.56	-0.39	1.28	154782.77	0.013
S82	39.56	*Subbotina*	*utilisindex*	1.22	-0.61	1.21	67313.97	0.011
S82	39.56	*Subbotina*	*utilisindex*	1.18	-0.45	1.24	107299.87	0.012
S82	39.56	*Subbotina*	*crociapertura*	1.51	-0.49	1.33	150692.72	0.024
S59	40.14	*Subbotina*	*yeguaensis*	2.01	-1.71	1.31	99738.45	0.010
S59	40.14	*Subbotina*	*crociapertura*	1.19	-1.04	1.28	96539.43	0.008
S59	40.14	*Subbotina*	*crociapertura*	1.39	-1.28	1.33	96468.34	0.006
S59	40.14	*Subbotina*	*linaperta*	2.07	-1.16	1.29	107487.20	0.013
S59	40.14	*Subbotina*	*eocaena*	1.09	-1.12	1.27	162112.95	0.018
S59	40.14	*Subbotina*	*eocaena*	1.44	-1.04	1.30	128423.69	0.018
S59	40.14	*Subbotina*	*eocaena*	0.95	-0.70	1.18	123314.42	0.016
S59	40.14	*Subbotina*	*yeguaensis*	2.20	-1.31	1.12	132866.12	0.019
S59	40.14	*Subbotina*	*eocaena*	1.96	-1.68	1.23	132574.97	0.017
S59	40.14	*Subbotina*	*crociapertura*	1.58	-1.27	1.21	94202.21	0.005
S59	40.14	*Subbotina*	*utilisindex*	1.79	-1.89	1.37	99098.59	0.012
S59	40.14	*Subbotina*	*crociapertura*	0.74	-1.40	1.27	104314.31	0.012
S59	40.14	*Subbotina*	*utilisindex*	1.01	-0.89	1.15	76207.86	0.007
S59	40.14	*Subbotina*	*linaperta*	1.47	-1.28	1.32	146891.58	0.020
S59	40.14	*Subbotina*	*eocaena*	2.09	-1.45	1.28	119183.87	0.008
S59	40.14	*Subbotina*	*crociapertura*	1.18	-1.43	1.20	80516.83	0.006
S59	40.14	*Subbotina*	*crociapertura*	1.16	-1.39	1.20	100019.64	0.006
S59	40.14	*Subbotina*	*jacksonensis*	1.17	-0.78	1.06	112321.28	0.017
S53	41.31	*Subbotina*	*utilisindex*	0.78	-0.45	1.20	90194.65	0.010
S53	41.31	*Subbotina*	*utilisindex*	0.72	-0.73	1.16	62843.39	0.008
S53	41.31	*Subbotina*	*crociapertura*	1.15	-0.64	1.36	75799.25	0.016
S53	41.31	*Subbotina*	*crociapertura*	0.86	-0.49	1.26	87563.77	0.014
S53	41.31	*Subbotina*	*utilisindex*	1.05	-0.26	1.36	73019.45	0.011
S53	41.31	*Subbotina*	*eocaena*	1.04	-0.58	1.20	78330.85	0.016
S53	41.31	*Subbotina*	*linaperta*	1.26	-0.60	1.24	112035.96	0.017
S53	41.31	*Subbotina*	*crociapertura*	0.85	-0.52	1.19	105116.46	0.013
S53	41.31	*Subbotina*	*linaperta*	1.34	-0.78	1.24	90773.37	0.015
S53	41.31	*Subbotina*	*eocaena*	0.91	-0.52	1.09	96707.02	0.017
S53	41.31	*Subbotina*	*yeguaensis*	1.64	-1.33	1.28	65610.93	0.004
S53	41.31	*Subbotina*	*linaperta*	0.57	-0.54	1.22	81641.44	0.008
S53	41.31	*Subbotina*	*linaperta*	0.91	-0.34	1.25	85165.17	0.011
S53	41.31	*Subbotina*	*crociapertura*	1.05	1.05	1.25	97026.76	0.011
S53	41.31	*Subbotina*	*utilisindex*	0.77	-0.56	1.25	92308.21	0.014
S53	41.31	*Subbotina*	*crociapertura*	2.09	-1.39	1.25	99906.15	0.015
S53	41.31	*Subbotina*	*crociapertura*	0.86	-0.63	1.23	114302.23	0.014
S49	42.10	*Subbotina*	*crociapertura*	0.86	-0.52	1.19	78375.70	0.015

Table B4: Stable isotope and morphological measurements for a subset of 112 *Subbotina* individuals selected from the 300 measured morphologically (Table S4). Sample ID is the study specific sample ID, Age is presented in million of years ago (Ma), Oxygen = δ^{18}O VPDB (‰), Carbon = δ^{13}C VPDB (‰) and Area is presented as μm^2.. Note this table is a subset of those presented in Table B4 and includes species identification *(continued)*

Sample_ID	Age	Genus	Species	Carbon	Oxygen	Aspect Ratio	Area	Weight
S49	42.10	*Subbotina*	*eocaena*	0.79	-0.29	1.05	87152.14	0.007
S49	42.10	*Subbotina*	*crociapertura*	0.36	-1.59	1.10	114379.54	0.005
S49	42.10	*Subbotina*	*utilisindex*	0.65	-0.42	1.18	65476.37	0.009
S49	42.10	*Subbotina*	*crociapertura*	1.38	-2.08	1.23	113277.38	0.009
S49	42.10	*Subbotina*	*crociapertura*	0.70	-1.13	1.22	114787.74	0.008
S49	42.10	*Subbotina*	*crociapertura*	0.60	-0.72	1.17	156424.83	0.009
S49	42.10	*Subbotina*	*linaperta*	0.54	-0.42	1.31	65721.29	0.012
S49	42.10	*Subbotina*	*crociapertura*	1.28	-0.42	1.08	125965.63	0.016
S49	42.10	*Subbotina*	*crociapertura*	1.20	-0.61	1.27	77597.74	0.031
S49	42.10	*Subbotina*	*crociapertura*	0.46	-1.12	1.03	75273.33	0.012
S49	42.10	*Subbotina*	*linaperta*	1.12	-0.36	1.07	128556.77	0.016
S49	42.10	*Subbotina*	*crociapertura*	1.21	-0.45	1.20	101008.89	0.031
S49	42.10	*Subbotina*	*utilisindex*	0.95	-0.49	1.15	62823.02	0.008
S49	42.10	*Subbotina*	*crociapertura*	0.89	-0.72	1.34	116368.33	0.009
S49	42.10	*Subbotina*	*crociapertura*	0.95	-0.69	1.24	111769.59	0.007
S49	42.10	*Subbotina*	*crociapertura*	0.99	-0.97	1.23	122566.65	0.010
S49	42.10	*Subbotina*	*crociapertura*	1.10	-0.61	1.31	153363.28	0.030
S49	42.10	*Subbotina*	*utilisindex*	1.13	-0.72	1.15	122543.67	0.015
S49	42.10	*Subbotina*	*crociapertura*	1.09	-0.78	1.15	123441.73	0.025
S115	43.50	*Subbotina*	*eocaena*	0.80	-1.01	1.33	143381.91	0.024
S115	43.50	*Subbotina*	*corpulenta*	1.22	-1.06	1.05	90163.66	0.013
S115	43.50	*Subbotina*	*corpulenta*	0.80	-0.83	1.10	130062.28	0.020
S115	43.50	*Subbotina*	*crociapertura*	1.44	-0.98	1.27	99927.37	0.016
S115	43.50	*Subbotina*	*crociapertura*	1.44	-0.93	1.26	114090.78	0.013
S115	43.50	*Subbotina*	*linaperta*	1.15	-1.22	1.26	88355.56	0.017
S115	43.50	*Subbotina*	*corpulenta*	1.14	-1.00	1.10	114151.05	0.019
S115	43.50	*Subbotina*	*crociapertura*	1.10	-1.26	1.22	68864.81	0.015
S115	43.50	*Subbotina*	*corpulenta*	0.90	-1.14	1.03	114448.12	0.017
S115	43.50	*Subbotina*	*utilisindex*	1.61	0.09	1.15	99176.85	0.018
S115	43.50	*Subbotina*	*crociapertura*	0.97	-1.00	1.37	83386.92	0.012
S115	43.50	*Subbotina*	*linaperta*	0.22	-1.38	1.30	80620.81	0.009
S115	43.50	*Subbotina*	*yeguaensis*	1.16	-1.32	1.35	91973.42	0.017
S115	43.50	*Subbotina*	*crociapertura*	1.15	-1.39	1.30	97822.54	0.020
S115	43.50	*Subbotina*	*linaperta*	0.96	-1.14	1.27	82176.75	0.017
S115	43.50	*Subbotina*	*linaperta*	1.09	-1.56	1.29	75434.34	0.013
S115	43.50	*Subbotina*	*linaperta*	1.20	-1.18	1.28	67712.26	0.014
S115	43.50	*Subbotina*	*corpulenta*	0.62	-1.22	1.27	116446.96	0.021
S115	43.50	*Subbotina*	*utilisindex*	0.85	-1.01	1.21	85051.51	0.017

Table B5: Stable carbon and oxygen isotope differences between *Globigerinatheka* and both *Subbotina* and *Catapsydrax*. Age is presented as millions of years ago (Ma), Difference is in per mille (‰), MECO indicates whether that sample is in the MECO (Y) or not (N)

Gradient	Age	Difference	Stable Isotope	MECO
Globigerinatheka spp.-Catapsydrax spp.	38.50	1.00	oxygen	N
Globigerinatheka spp.-Subbotina spp.	38.50	0.50	oxygen	N
Globigerinatheka spp.-Catapsydrax spp.	38.50	1.23	carbon	N
Globigerinatheka spp.-Subbotina spp.	38.50	1.34	carbon	N
Globigerinatheka spp.-Catapsydrax spp.	39.56	0.91	oxygen	N
Globigerinatheka spp.-Subbotina spp.	39.56	0.93	oxygen	N
Globigerinatheka spp.-Catapsydrax spp.	39.56	1.40	carbon	N
Globigerinatheka spp.-Subbotina spp.	39.56	1.51	carbon	N
Globigerinatheka spp.-Catapsydrax spp.	40.14	0.01	oxygen	Y
Globigerinatheka spp.-Subbotina spp.	40.14	0.19	oxygen	Y
Globigerinatheka spp.-Catapsydrax spp.	40.14	1.00	carbon	Y
Globigerinatheka spp.-Subbotina spp.	40.14	0.81	carbon	Y
Globigerinatheka spp.-Catapsydrax spp.	41.31	1.30	oxygen	N
Globigerinatheka spp.-Subbotina spp.	41.31	0.62	oxygen	N
Globigerinatheka spp.-Catapsydrax spp.	41.31	1.71	carbon	N
Globigerinatheka spp.-Subbotina spp.	41.31	1.54	carbon	N
Globigerinatheka spp.-Catapsydrax spp.	42.10	0.74	oxygen	N
Globigerinatheka spp.-Subbotina spp.	42.10	0.53	oxygen	N
Globigerinatheka spp.-Catapsydrax spp.	42.10	1.71	carbon	N
Globigerinatheka spp.-Subbotina spp.	42.10	1.57	carbon	N
Globigerinatheka spp.-Catapsydrax spp.	43.50	0.52	oxygen	N
Globigerinatheka spp.-Subbotina spp.	43.50	0.15	oxygen	N
Globigerinatheka spp.-Catapsydrax spp.	43.50	1.23	carbon	N
Globigerinatheka spp.-Subbotina spp.	43.50	0.86	carbon	N

1.0.1 Importing of data

Firstly we need to import Table S2-5 to set variables for easy recall. For the following set of analyses the age of the sample (Age) needs to be converted to a factor. Morphological traits shown in Figure S1 need also need to be renamed for easier recall in supplementary table 3-5. Size (Area) is measured on a different scale to stable isotopes therefore needs to be transformed on the log scale to aid model fit and centered in both Table 4 and 5.

```
bulk <- read_csv("Supplementary_Table_S2.csv") #Multispecimen Stable Isotopes
morph <- read_csv("Supplementary_Table_S3.csv") #Subbotina Morphometrics
morph_iso <- read_csv("Supplementary_Table_S4.csv") #Subbotina Stable Isotopes
diff <- read_csv("Supplementary_Table_S5.csv") #Multispecimen Isotope Gradients
```

```
# Supplementary table 5 renaming and factoring
MECO <- as.factor(diff$MECO)
isotope <- as.factor(diff$`Stable Isotope`)

# Supplementary table 4 renaming and factoring
morph$Age <- as.factor(morph$Age)
morph <- morph %>% rename(size = Area)
morph <- morph %>% rename(shape =Aspect_Ratio)
morph$size <- log(morph$size) - 10

# Supplementary table 5 renaming and factoring
morph_iso$Age <- as.factor(morph_iso$Age)
morph_iso <- morph_iso %>% rename(size = Area)
morph_iso <- morph_iso %>% rename(shape = `Aspect Ratio`)
morph_iso$size <- log(morph_iso$size) - 10
```

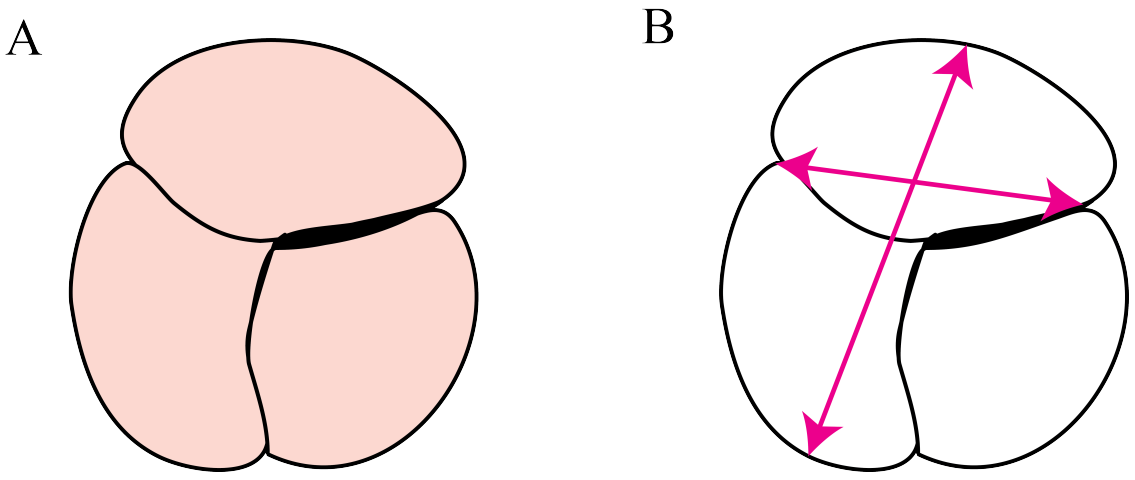

Figure B1: Schematic of the morphological traits used in this study. A) Test area, B) Test aspect (maximum feret diameter/minimum feret diameter).

2 Multi-specimen analysis

2.1 Multiple Linear Regression

To test if the MECO samples are different from the rest of the time slices. Y = MECO (40.1 Ma sample) , N = Not MECO (other 5 samples in analysis).

```
diff_lm <- lm(Difference ~ isotope + MECO, data=diff)
```

Table B6: Coefficient-Level estimates for a model fitted to estimate variation in isotopic differences, model formula: lm(Difference ∼ isotope + MECO, data=diff

Predictor	Coefficient	SE	t	*p*
(Intercept)	1.42	0.08	16.96	<0.001
isotopeoxygen	-0.71	0.11	-6.28	<0.001
MECOY	-0.56	0.15	-3.71	0.001

3 Individual analysis

3.1 Clustering Analysis

Individual *Subbotina* stable isotope measurements used to see if the samples can be separated in stable isotope space.

```
for_clust <- morph_iso %>% dplyr::select(Age, Oxygen,Carbon)
class <- for_clust$Age
X <- for_clust[,-1]
BIC <- mclustBIC(X)
mod1<- Mclust(X, x=BIC)
```

Table B7: Assignment of individuals to either cluster 1 or 2 (columns) in each sample. Rows correspond to the inferred sample ages (Ma). Note there is no strong correlation between sample age and cluster assignment, implying no continuous trend, but that the two warmest samples (the oldest 43.5 Ma and the MECO at 40.14 Ma) both show very different relative frequencies to the cooler samples.

	1	2
38.5	13	5
39.56	13	7
40.14	3	15
41.31	14	3
42.1	15	5
43.5	1	18

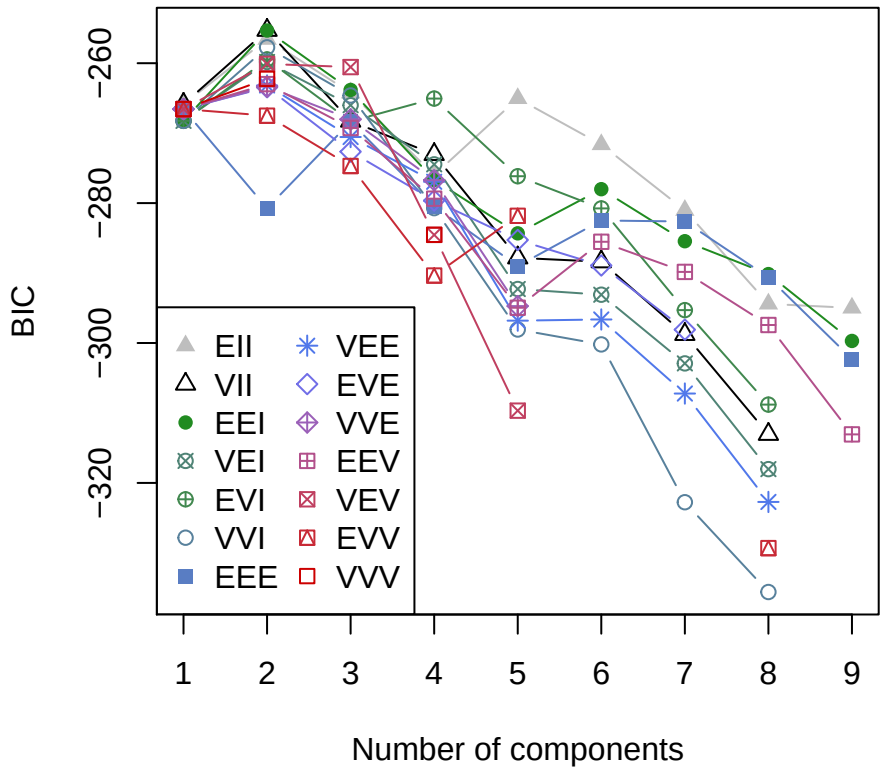

Figure B2: BIC plot from clustering analysis showing the best fitting model is a spherical, variable volume model (VII) with two clusters. Best fitting model in mclust is chosen by the model with the highest BIC, best fitting model in this analysis: BIC = -255

3.2 Analysis of variance

3.2.1 Stable Isotopes using subset of *Subbotina* geochemically analysed (Supplementary table 4)

These analyses also included species to understand whether it has any influence on stable isotopes before carrying species forward into further models. Species was found not to have any detectable impact ($F(6, 100) = 1.62$, $p>0.05$) and is therefore not carried forward.

```
ox1<- aov(Oxygen ~ Age, data = morph_iso)
ox2<- aov(Oxygen ~ Age + Species , data = morph_iso)
#Species has no detectable impact so ox1 is carried forward to post-hoc test.
TUK_o <- TukeyHSD(ox1)

carb1 <- aov(Carbon ~ Age, data = morph_iso)
carb2 <- aov(Carbon ~ Age + Species, data = morph_iso)
#Species has no detectable impact so ox1 is carried forward to post-hoc test.
TUK_c <- TukeyHSD(carb1)
```

3.2.2 Morphology using supplementary table 3 with all 300 *Subbotina* measurements

Table B8: Summary table for one-way ANOVA: Oxygen∼Age + Species

Term	df	Sum of squares	Mean sum of squares	F statistic	*p-value*
Age	5	8.27	1.65	12.26	<0.001
Species	6	1.31	0.22	1.62	0.149
Residuals	100	13.49	0.13		

Table B9: Summary table for one-way ANOVA: Carbon∼Age + Species

Term	df	Sum of squares	Mean sum of squares	F statistic	*p-value*
Age	5	5.48	1.10	9.87	<0.001
Species	6	0.70	0.12	1.05	0.396
Residuals	100	11.10	0.11		

Table B10: Summary table for one-way ANOVA: Oxygen∼Age showing significant differences (p <0.001) between MECO samples (40.14 Ma) and those pre-MECO (bold) except at the beginning of the record 43.5 Ma

Term	df	Sum of squares	Mean sum of squares	F statistic	*p-value*
Age	5	8.27	1.65	11.84	<0.001
Residuals	**106**	**14.80**	**0.14**		

Table B11: Results from TUKEY-HD test following one-way ANOVA with oxygen

Term	Difference	Estimate (ppm)	Lower estimate (ppm)	Upper estimate (ppm)	*p-value*
Age	39.56-38.5	0.04	-0.32	0.39	>0.999
Age	40.14-38.5	-0.66	-1.02	-0.30	<0.001
Age	41.31-38.5	0.06	-0.31	0.43	0.997
Age	42.1-38.5	-0.15	-0.50	0.20	0.826
Age	43.5-38.5	-0.47	-0.83	-0.12	0.003
Age	40.14-39.56	-0.70	-1.05	-0.34	<0.001
Age	41.31-39.56	0.02	-0.33	0.38	>0.999
Age	42.1-39.56	-0.18	-0.53	0.16	0.631
Age	43.5-39.56	-0.51	-0.86	-0.16	<0.001
Age	41.31-40.14	0.72	0.35	1.09	<0.001
Age	42.1-40.14	0.51	0.16	0.86	<0.001
Age	43.5-40.14	0.19	-0.17	0.54	0.653
Age	42.1-41.31	-0.21	-0.57	0.15	0.544
Age	43.5-41.31	-0.53	-0.90	-0.17	<0.001
Age	43.5-42.1	-0.33	-0.67	0.02	0.080

Table B12: Summary table for one-way ANOVA: Carbon∼Age showing significant differences (p <0.005) between MECO samples (40.14 Ma) and pre-MECO samples (bold)

Term	df	Sum of squares	Mean sum of squares	F statistic	*p-value*
Age	5	5.48	1.10	9.84	<0.001
Residuals	106	11.80	0.11		

Table B13: Results from TUKEY-HD test following one-way ANOVA with carbon

Term	Difference	Estimate (ppm)	Lower estimate (ppm)	Upper estimate (ppm)	*p-value*
Age	39.56-38.5	0.46	0.15	0.78	<0.001
Age	40.14-38.5	0.69	0.36	1.01	<0.001
Age	41.31-38.5	0.26	-0.06	0.59	0.186
Age	42.1-38.5	0.13	-0.19	0.44	0.850
Age	43.5-38.5	0.26	-0.06	0.58	0.185
Age	40.14-39.56	0.23	-0.09	0.54	0.307
Age	41.31-39.56	-0.20	-0.52	0.12	0.480
Age	42.1-39.56	-0.33	-0.64	-0.03	0.024
Age	43.5-39.56	-0.20	-0.51	0.11	0.406
Age	**41.31-40.14**	**-0.42**	**-0.75**	**-0.09**	**0.004**
Age	**42.1-40.14**	**-0.56**	**-0.87**	**-0.24**	**<0.001**
Age	**43.5-40.14**	**-0.43**	**-0.75**	**-0.11**	**0.002**
Age	42.1-41.31	-0.14	-0.46	0.18	0.811
Age	43.5-41.31	-0.01	-0.33	0.32	>0.999
Age	43.5-42.1	0.13	-0.18	0.44	0.825

```
aov_shape <- aov(shape ~ Age, data = morph)
aov_size <- aov(size ~ Age, data = morph)
```

Table B14: Summary table for one-way ANOVA: Shape∼Age

Term	df	Sum of squares	Mean sum of squares	F statistic	*p-value*
Age	5	0.10	0.02	3.25	0.007
Residuals	294	1.84	0.01		

Table B15: Summary table for one-way ANOVA: Size∼Age

Term	df	Sum of squares	Mean sum of squares	F statistic	*p-value*
Age	5	1.02	0.20	3.18	0.008
Residuals	294	18.78	0.06		

3.3 Multiple linear regression

3.3.1 With size

```
c1.s <- lm(Carbon ~ Oxygen + size + Age, data= morph_iso)
c2.s <- lm(Carbon ~ (Oxygen + size + Age)^2, data=morph_iso)
anova(c1.s,c2.s)
```

3.3.1.1 Carbon with size

```
## Analysis of Variance Table
```

```
##
## Model 1: Carbon ~ Oxygen + size + Age
## Model 2: Carbon ~ (Oxygen + size + Age)^2
##   Res.Df     RSS Df Sum of Sq      F  Pr(>F)
## 1    104 11.6425
## 2     93  9.1557 11    2.4868 2.2964 0.01554 *
## ---
## Signif. codes:  0 '***' 0.001 '**' 0.01 '*' 0.05 '.' 0.1 ' ' 1
```

```
# Interactions with age are affecting so assume a constant size with age
c3.s <- lm(Carbon~ (Oxygen+size)^2 + Age, data = morph_iso)
anova(c2.s,c3.s)
```

```
## Analysis of Variance Table
##
## Model 1: Carbon ~ (Oxygen + size + Age)^2
## Model 2: Carbon ~ (Oxygen + size)^2 + Age
##   Res.Df     RSS  Df Sum of Sq      F  Pr(>F)
## 1     93  9.1557
## 2    103 11.5736 -10    -2.418 2.4561 0.01189 *
## ---
## Signif. codes:  0 '***' 0.001 '**' 0.01 '*' 0.05 '.' 0.1 ' ' 1
```

```
## c3 best fitting model that includes in interaction between carbon and size
```

```
## null device
##           1
```

Table B16: Model comparison for carbon linear regression models

	Model	Reisidual df	df	Residual sum of squares	Sum of squares	F statistic	*p*-value	AIC	ΔAIC
1	$(\text{Oxygen+size+Age})^2$	93	9.16					77.38	0.00
2	Oxygen+size+Age	104	11.64	-11	-2.49	2.3	0.016	82.29	4.91
3	$(\text{Oxygen+size})^2$+Age	103	11.57	1	0.07	0.7	0.405	83.63	6.25

Table B17: Model summary for best fitting model following model reduction. Model: Carbon ∼ $(\text{Oxygen+size})^2$ + Age

Predictor	Coefficient	SE	t	*p*-value
(Intercept)	0.88	0.43	2.04	0.044
Oxygen	0.36	0.55	0.64	0.522
size	-0.10	0.30	-0.32	0.747
Age39.56	0.46	0.11	4.18	<0.001
Age40.14	0.60	0.13	4.59	<0.001
Age41.31	0.28	0.11	2.43	0.017
Age42.1	0.10	0.11	0.88	0.382
Age43.5	0.23	0.12	1.91	0.059
Oxygen:size	-0.29	0.37	-0.78	0.436

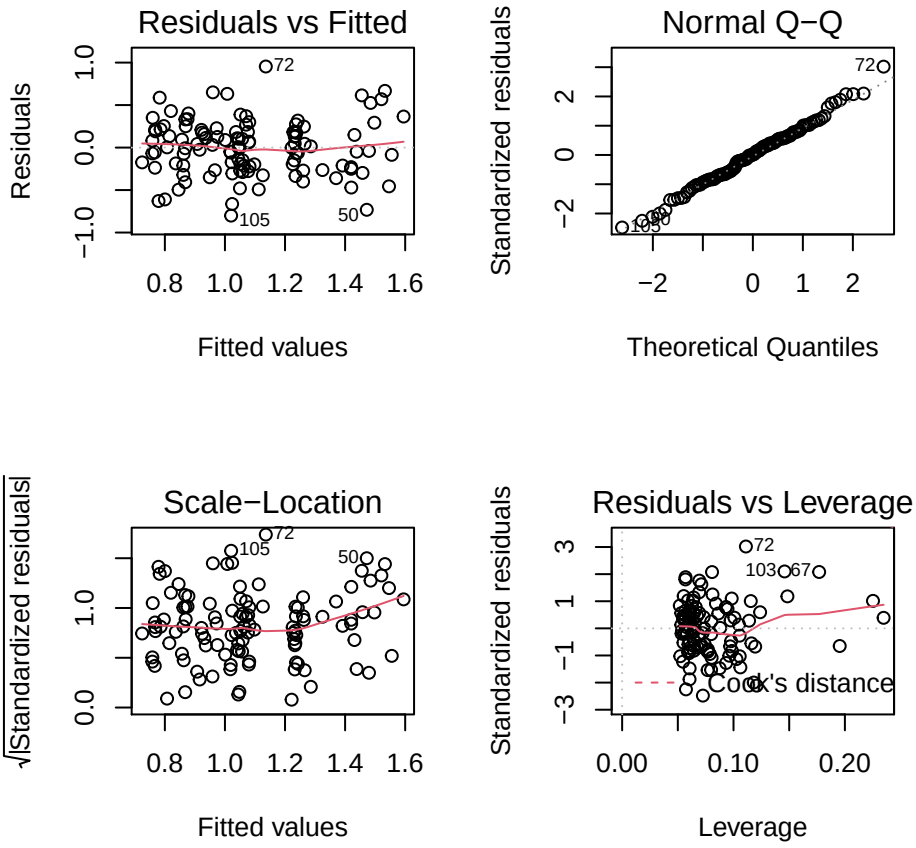

Figure B3: Diagnostic plot for model: Carbon $\sim$ (Oxygen+size)^2 + Age

Remove all other variables to see if size without environmental variables has an impact on carbon

```
c1.s.1 <- lm(Carbon ~ size, data =morph_iso)
```

Table B18: Univariate model summary. Model: Carbon$\sim$size

Predictor	Coefficient	SE	t	p-value
(Intercept)	0.65	0.22	2.95	0.004
size	0.29	0.15	1.99	0.050

```
o1 <- lm(Oxygen ~ Carbon + size + Age, data=morph_iso)
o2 <- lm(Oxygen ~ (Carbon + size + Age)^2 , data= morph_iso)
anova(o1,o2)
```

3.3.1.2 Oxygen with size

```
## Analysis of Variance Table
##
## Model 1: Oxygen ~ Carbon + size + Age
```

```
## Model 2: Oxygen ~ (Carbon + size + Age)^2
##   Res.Df    RSS Df Sum of Sq      F  Pr(>F)
## 1    104 14.705
## 2     93 11.582 11    3.1228 2.2795 0.01634 *
## ---
## Signif. codes:  0 '***' 0.001 '**' 0.01 '*' 0.05 '.' 0.1 ' ' 1
```

```
o3 <- lm(Oxygen ~ (Carbon*size)^2  + Age, data = morph_iso)
anova(o2,o3)
```

```
## Analysis of Variance Table
##
## Model 1: Oxygen ~ (Carbon + size + Age)^2
## Model 2: Oxygen ~ (Carbon * size)^2 + Age
##   Res.Df    RSS  Df Sum of Sq      F  Pr(>F)
## 1     93 11.582
## 2    103 14.643 -10   -3.0603 2.4573 0.01185 *
## ---
## Signif. codes:  0 '***' 0.001 '**' 0.01 '*' 0.05 '.' 0.1 ' ' 1

## null device
##           1
```

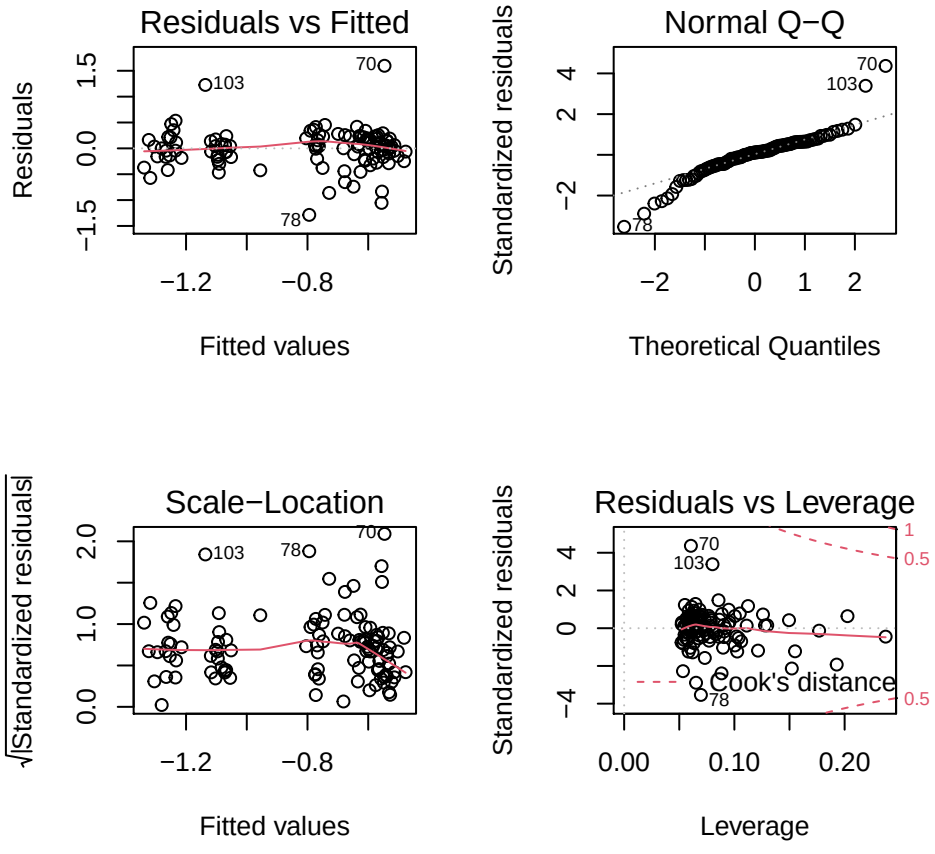

Figure B4: Diagnostic plot for model: Oxygen $\sim$ (Carbon+size)^2 + Age

Table B19: Model comparison for oxygen linear regression models

	Model	Reisidual df	df	Residual sum of squares	Sum of squares	F statistic	*p*-value	AIC	ΔAIC
1	(Carbon+size+Age)^2	93	11.58					103.71	0.00
2	Carbon+size+Age	104	14.71	-11	-3.12	2.28	0.016	108.45	4.74
3	(Carbon+size)^2+Age	103	14.64	1	0.06	0.50	0.480	109.97	6.26

Table B20: Model summary for best fitting model following mdoel reduction. Model: Oxygen ~ (Carbon+size)^2 + Age

Predictor	Coefficient	SE	t	*p*-value
(Intercept)	-0.15	0.64	-0.23	0.821
Carbon	-0.49	0.62	-0.80	0.426
size	-0.26	0.42	-0.61	0.546
Age39.56	0.08	0.13	0.61	0.540
Age40.14	-0.61	0.15	-4.05	<0.001
Age41.31	0.09	0.13	0.69	0.494
Age42.1	-0.14	0.13	-1.11	0.270
Age43.5	-0.44	0.13	-3.47	<0.001
Carbon:size	0.26	0.39	0.66	0.509

3.3.2 With weight

Now we replace size with weight to see if weight has any influence on the stable isotopes we measured. The best fitting models are similar for both size and weight. Where size was not detectable in either carbon (Table S17) or oxygen (Table S20) regressions, weight was detectable in carbon (Table S22). Furthermore, the model including weight for carbon explains more variation (lower residual sum of squares; 9.9264) than the model containing size (11.5736) . We include only size in the manuscript as this is a more commonly used measure.

```
c1.w <- lm(Carbon ~ Oxygen + Age, data= morph_iso)
c2.w <- lm(Carbon ~ (Oxygen + Weight + Age)^2, data=morph_iso)
anova(c1.w,c2.w)
```

3.3.2.1 Carbon with weight

```
## Analysis of Variance Table
##
## Model 1: Carbon ~ Oxygen + Age
## Model 2: Carbon ~ (Oxygen + Weight + Age)^2
##   Res.Df     RSS Df Sum of Sq     F    Pr(>F)
## 1    105 11.7216
## 2     93  8.0079 12    3.7137 3.594 0.0002031 ***
## ---
## Signif. codes:  0 '***' 0.001 '**' 0.01 '*' 0.05 '.' 0.1 ' ' 1
```

```
# Interactions with age are affecting so assume a constant size with age
c3.w <- lm(Carbon~ (Oxygen+Weight)^2 + Age, data = morph_iso)
anova(c2.w,c3.w)
```

```
## Analysis of Variance Table
##
## Model 1: Carbon ~ (Oxygen + Weight + Age)^2
## Model 2: Carbon ~ (Oxygen + Weight)^2 + Age
##   Res.Df    RSS  Df Sum of Sq     F  Pr(>F)
## 1     93 8.0079
## 2    103 9.9264 -10   -1.9184 2.228 0.02248 *
## ---
## Signif. codes:  0 '***' 0.001 '**' 0.01 '*' 0.05 '.' 0.1 ' ' 1
```

```
## c3.w best fitting model that includes in interaction between carbon and weight
```

Table B21: Model comparison for carbon linear regression models

	Model	Reisidual df	df	Residual sum of squares	Sum of squares	F statistic	*p*-value	AIC	ΔAIC
1	(Oxygen+weight+Age)^2	93	8.01					62.38	0.00
2	Oxygen+weight+Age	105	11.72	-12	-3.71	3.59	0	81.05	18.67
3	(Oxygen+weight)^2+Age	103	9.93	2	1.80	10.42	0	66.43	4.05

```
o1.w <- lm(Oxygen ~ Carbon + Age , data=morph_iso)
o2.w <- lm(Oxygen ~ (Carbon + Weight + Age)^2 , data= morph_iso)
anova(o1.w,o2.w)
```

3.3.2.2 Oxygen with weight

```
## Analysis of Variance Table
```

Table B22: Model summary for best fitting model following mdoel reduction. Model: Carbon ∼ (Oxygen+weight)^2 + Age

Predictor	Coefficient	SE	t	*p*-value
(Intercept)	0.23	0.19	1.21	0.229
Oxygen	-0.33	0.19	-1.71	0.089
Weight	34.07	12.84	2.65	0.009
Age39.56	0.46	0.10	4.48	<0.001
Age40.14	0.63	0.12	5.40	<0.001
Age41.31	0.31	0.11	2.95	0.004
Age42.1	0.09	0.10	0.90	0.368
Age43.5	0.16	0.12	1.34	0.184
Oxygen:Weight	14.84	15.46	0.96	0.339

```
##
## Model 1: Oxygen ~ Carbon + Age
## Model 2: Oxygen ~ (Carbon + Weight + Age)^2
##   Res.Df    RSS Df Sum of Sq      F   Pr(>F)
## 1    105 14.705
## 2     93 11.116 12    3.5891 2.5022 0.006829 **
## ---
## Signif. codes:  0 '***' 0.001 '**' 0.01 '*' 0.05 '.' 0.1 ' ' 1
```

```
o3.w <- lm(Oxygen ~ (Carbon*Weight)^2  + Age, data = morph_iso)
```

Table B23: Model comparison for oxygen linear regression models

	Model	Reisidual df	df	Residual sum of squares	Sum of squares	F statistic	*p*-value	AIC	ΔAIC
1	$(\text{CarbonWeighte+Age})^2$	103	13.27					98.97	0.00
2	Carbon+Age	93	11.12	10	2.16	1.8	0.070	99.11	0.14
3	$(\text{Carbon+Weight})^2$+Age	105	14.71	-12	-3.59	2.5	0.007	106.45	7.48

Table B24: Model summary for best fitting model following model reduction. Model: Oxygen ~ $(\text{Carbon+Weight})^2$ + Age

Predictor	Coefficient	SE	t	*p*-value
(Intercept)	-0.64	0.29	-2.24	0.027
Carbon	-0.31	0.27	-1.15	0.254
Weight	13.24	23.05	0.57	0.567
Age39.56	0.14	0.13	1.10	0.275
Age40.14	-0.47	0.15	-3.20	0.002
Age41.31	0.15	0.13	1.21	0.230
Age42.1	-0.12	0.12	-1.06	0.291
Age43.5	-0.46	0.12	-3.73	<0.001
Carbon:Weight	7.38	19.91	0.37	0.711

3.3.3 Including climate

With bulk oxygen isotopes to represent temperature changes at different water depths. First rename the variables for easier recall and select only oxygen isotopes before combining the datasets.

```
bulk$Age <- as.factor(bulk$Age)
bulk_oxygen <- bulk %>% dplyr::select(Genus, Oxygen, Age) %>% spread(Genus,Oxygen)
with_bulk <- merge(bulk_oxygen,morph_iso, by="Age")
subthermocline <- with_bulk$Catapsydrax
thermocline <- with_bulk$Subbotina
surface <- with_bulk$Globigerinatheka
```

```
bulk_o <- lm(Oxygen ~ (Carbon*size)^2 + subthermocline + thermocline + surface, data=with_bulk)
```

Table B25: Model summary for linear regression including multi-specimen analysis. Model: Oxygen ~(Carbon*size)^2 + subtherm + therm + surface

Predictor	Coefficient	SE	t	*p*-value
(Intercept)	-0.46	0.74	-0.63	0.529
Carbon	-0.49	0.61	-0.81	0.420
size	-0.25	0.42	-0.60	0.547
subthermocline	0.35	0.16	2.21	0.029
thermocline	0.44	0.19	2.30	0.024
surface	-0.51	0.47	-1.08	0.281
Carbon:size	0.26	0.39	0.66	0.509

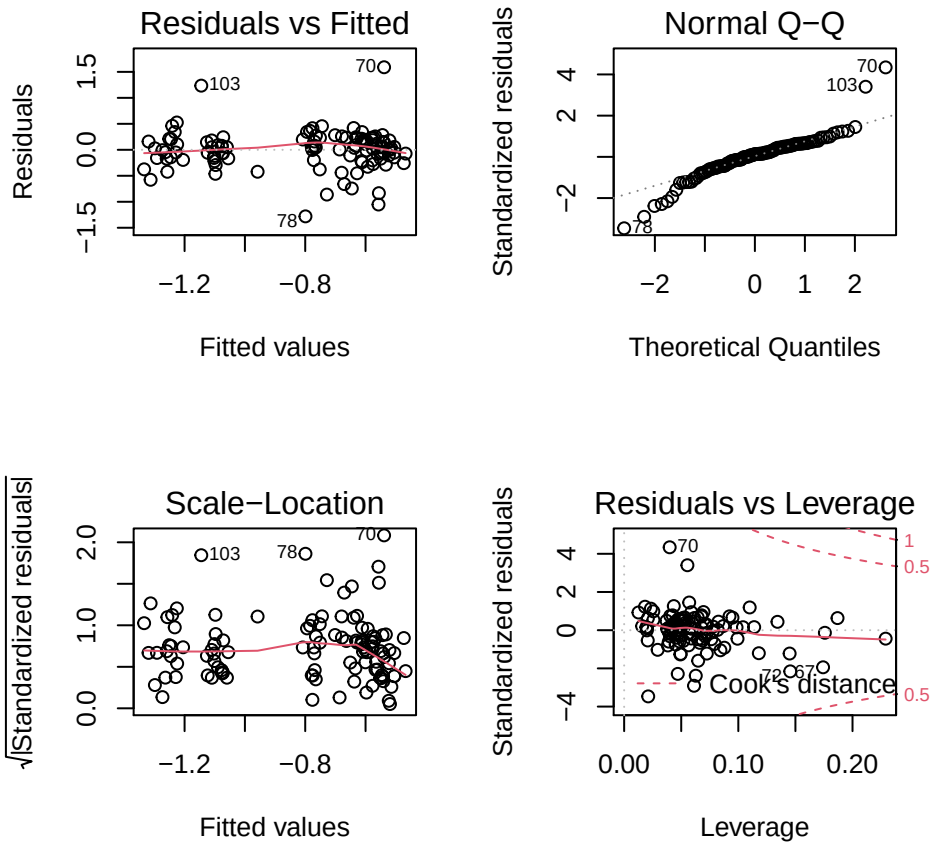

Figure B5: Diagnostic plot for model: Oxygen ~ (Carbon*size)^2 + subthermocline + thermocline + surface

Bibliography

Cappelli, C., P. R. Bown, Thomas Westerhold, S. M. Bohaty, M. de Riu, V. Lobba, Y. Yamamoto, and C. Agnini. 2019. "The Early to Middle Eocene Transition: An Integrated Calcareous Nannofossil and Stable Isotope Record From the Northwest Atlantic Ocean (Integrated Ocean Drilling Program Site U1410)." *Paleoceanography and Paleoclimatology* 34 (12): 1913–30. https://doi.org/10.1029/2019PA003686.

Fraley, Chris, Adrian E. Raftery, and Luca Scrucca. 2020. *Mclust: Gaussian Mixture Modelling for Model-Based Clustering, Classification, and Density Estimation*. https://mclust-org.github.io/mclust/.

Gradstein, Felix M, James George Ogg, Mark D Schmitz, and Gabi M Ogg. 2012. *The Geologic Time Scale 2012*. elsevier.

Norris, Richard D., P. A. Wilson, P. Blum, A. Fehr, C. Agnini, A. Bornemann, S. Boulila, et al. 2014. "Proceedings of the Integrated Ocean Drilling Program; Paleogene Newfoundland Sediment Drifts and MDHDS Test; Expedition 342 of the Riserless Drilling Platform, St. George, Bermuda, to St. John's, Newfoundland (Canada); Sites U1402-U1411, 2 June-1 August 2."

Ogg, James G., Linda A. Hinnov, and Chunju Huang. 2012. "Cretaceous." In, 1-2:793–853. Elsevier B.V. https://doi.org/10.1016/B978-0-444-59425-9.00027-5.

R Core Team. 2020. *R: A Language and Environment for Statistical Computing*. Vienna, Austria: R Foundation for Statistical Computing. https://www.R-project.org/.

Robinson, David, Alex Hayes, and Simon Couch. 2021. *Broom: Convert Statistical Objects into Tidy Tibbles*. https://CRAN.R-project.org/package=broom.

Wickham, Hadley. 2019. *Tidyverse: Easily Install and Load the Tidyverse*. https://CRAN.R-project.org/package=tidyverse.

Wickham, Hadley, and Dana Seidel. 2020. *Scales: Scale Functions for Visualization*. https://CRAN.R-project.org/package=scales.

Xie, Yihui. 2021. *Knitr: A General-Purpose Package for Dynamic Report Generation in r*. https://yihui.org/knitr/.

Yamamoto, Y., H. Fukami, W. Taniguchi, and P.C. Lippert. 2018. "Data Report: Updated Magnetostratigraphy for IODP Sites U1403, U1408, U1409, and U1410." *Proceedings of the Integrated Ocean Drilling Program,. 342: College Station, TX (Integrated Ocean Drilling Program).* https://doi.org/10.2204/iodp.proc.342.2014.

Zhu, Hao. 2021. *kableExtra: Construct Complex Table with Kable and Pipe Syntax*. https://CRAN.R-project.org/package=kableExtra.

Appendix C Supplementary information for Chapter 4

The following supplement provides tables of all data produced. Where data is not provided this is because it is too large. The following document is included to enable the reproducibility of the results in Chapter 4 and all data plus this supplement will be made publicly available upon acceptance of this manuscript.

1 Introduction to Appendix C

All analyses were performed in the freely distributed R environment (R Core Team 2019). This supporting information was written using knitr (Xie 2020) . The code uses the tidyverse (Wickham 2019) and packages within, lme4 (Bates et al. 2019), mclust (Fraley, Raftery, and Scrucca 2019), ggpubr (Kassambara 2020), kableExtra (Zhu 2019) and paran (Dinno 2018) packages :

```
library(tidyverse)
library(mclust)
library(ggpubr)
library(knitr)
library(kableExtra)
library(lme4)
library(paran)
library(png)
library(sjPlot)
library(tinytex)
library(tidyverse)
library(mclust)
library(knitr)
library(kableExtra)
library(png)
library(scales)
library(broom)
library(bookdown)
library(xtable)
opts_chunk$set(fig.align = "center", fig.show = "hold", tidy = FALSE, fig.width = 5,
    fig.height = 5, cache = FALSE, par = TRUE)
pdf.options(encoding = "CP1251")
options(replace.assign = TRUE, width = 80)
sessionInfo()
```

```
## R version 4.0.3 (2020-10-10)
## Platform: x86_64-apple-darwin17.0 (64-bit)
## Running under: macOS Mojave 10.14.6
##
## Matrix products: default
## BLAS:   /Library/Frameworks/R.framework/Versions/4.0/Resources/lib/libRblas.dylib
## LAPACK: /Library/Frameworks/R.framework/Versions/4.0/Resources/lib/libRlapack.dylib
##
## locale:
## [1] en_GB.UTF-8/en_GB.UTF-8/en_GB.UTF-8/C/en_GB.UTF-8/en_GB.UTF-8
##
## attached base packages:
## [1] stats     graphics  grDevices utils     datasets  methods   base
##
## other attached packages:
##  [1] xtable_1.8-4     bookdown_0.22    broom_0.7.8      scales_1.1.1
##  [5] tinytex_0.31     sjPlot_2.8.7     png_0.1-7        paran_1.5.2
##  [9] MASS_7.3-53      lme4_1.1-26      Matrix_1.2-18    kableExtra_1.3.2
## [13] knitr_1.31       ggpubr_0.4.0     mclust_5.4.7     forcats_0.5.1
## [17] stringr_1.4.0    dplyr_1.0.6      purrr_0.3.4      readr_1.4.0
## [21] tidyr_1.1.3      tibble_3.1.2     ggplot2_3.3.3    tidyverse_1.3.1
```

Table C.1: Morphological measurements of 450 G. ruber individuals.This table is large so is provided at the end of the thesis. Column headers are as follows: AR = Aspect Ratio, ap = aperture, Final/F = Final Chamber, F-1 = Penultimate chamber and F-2 = Antepenultimate chamber, AH= Aperture height, AW= Aperture width

Subspecies	ID	testArea	testAR	FinalArea	FinalAR	f-1Area	f-1AR	f-2Area	f-2AR	apArea	AH	AW	PerimeterAp	PerimeterF-1	PerimeterF-2	PerimeterF
SS	1	123264.52	1.326308	49430.66	1.606793	37642.54	1.229748	28870.36	1.355055	9218.084	38.97194	151.92237	413.2665	700.7762	659.2872	1019.3880
SS	2	123961.75	1.312882	37180.42	1.477390	41696.22	1.538520	38493.81	1.216631	7685.791	39.69539	122.40052	330.7471	802.0246	710.4390	948.7622
SS	3	79354.98	1.323753	30889.10	1.748839	24078.90	1.400407	19368.52	1.337320	4564.452	39.20004	72.41012	251.4720	568.5338	517.8772	894.1571
SS	4	114168.04	1.330035	44687.85	1.743729	38639.74	1.055892	25684.16	1.887590	6194.034	43.33494	93.60137	285.6436	697.1046	685.7106	970.7465
SS	5	106133.63	1.160780	24184.30	1.787768	42061.06	1.354638	35923.77	1.291116	4799.565	24.06195	86.43809	271.7040	755.1648	705.4060	746.9104
SS	6	75398.58	1.359571	28651.46	1.593582	25530.12	1.303716	17836.22	1.234209	4329.338	26.29406	101.02408	262.6157	584.5671	491.3635	727.1137
SS	7	62661.89	1.309115	22027.74	1.661556	21371.04	1.170797	18825.32	1.697740	1483.649	19.17342	40.94860	139.6414	520.1319	562.5430	643.6877
SS	8	78090.23	1.327570	31772.80	1.720160	29429.77	1.274363	16782.26	1.570452	2278.172	17.76081	69.90873	199.2941	615.6960	507.2203	743.2611
SS	9	86854.30	1.218444	29770.28	1.731684	29608.13	1.350227	22960.08	1.262151	5723.806	35.80639	95.98966	286.8928	627.3203	566.2732	753.4808
SS	10	76063.38	1.300490	30621.55	1.563399	28635.25	1.227591	16206.64	1.623931	1978.199	19.32650	50.00078	179.8620	607.5344	539.4991	807.5747

```
##
## loaded via a namespace (and not attached):
##  [1] TH.data_1.0-10    minqa_1.2.4       colorspace_2.0-1  ggsignif_0.6.0
##  [5] ellipsis_0.3.2    rio_0.5.16        sjlabelled_1.1.7  estimability_1.3
##  [9] parameters_0.12.0 fs_1.5.0          rstudioapi_0.13   fansi_0.5.0
## [13] mvtnorm_1.1-1     lubridate_1.7.10  xml2_1.3.2        codetools_0.2-16
## [17] splines_4.0.3     sjmisc_2.8.6      jsonlite_1.7.2    nloptr_1.2.2.2
## [21] ggeffects_1.0.1   dbplyr_2.1.1      effectsize_0.4.3  compiler_4.0.3
## [25] httr_1.4.2        sjstats_0.18.1    emmeans_1.5.4     backports_1.2.1
## [29] assertthat_0.2.1  cli_3.0.0         formatR_1.7       htmltools_0.5.1.1
## [33] tools_4.0.3       coda_0.19-4       gtable_0.3.0      glue_1.4.2
## [37] Rcpp_1.0.6        carData_3.0-4     cellranger_1.1.0  vctrs_0.3.8
## [41] nlme_3.1-149      insight_0.13.1    xfun_0.22         openxlsx_4.2.3
## [45] rvest_1.0.0       lifecycle_1.0.0   statmod_1.4.35    rstatix_0.7.0
## [49] zoo_1.8-9         hms_1.0.0         sandwich_3.0-0    yaml_2.2.1
## [53] curl_4.3          stringi_1.5.3     bayestestR_0.8.2  boot_1.3-25
## [57] zip_2.1.1         rlang_0.4.11      pkgconfig_2.0.3   evaluate_0.14
## [61] lattice_0.20-41   tidyselect_1.1.1  magrittr_2.0.1    R6_2.5.0
## [65] generics_0.1.0    multcomp_1.4-16   DBI_1.1.1         pillar_1.6.1
## [69] haven_2.3.1       foreign_0.8-80    withr_2.4.2       survival_3.2-7
## [73] abind_1.4-5       performance_0.7.0 modelr_0.1.8      crayon_1.4.1
## [77] car_3.0-10        utf8_1.2.1        rmarkdown_2.6     grid_4.0.3
## [81] readxl_1.3.1      data.table_1.13.6 reprex_2.0.0      digest_0.6.27
## [85] webshot_0.5.2     munsell_0.5.0     viridisLite_0.4.0
```

The aim of this supplement is to aid in the reproduction of our analyses, on the data from this paper and from subsequently collected data by other researchers. The emphasis of this supplement is on reproducible analysis and not formatted end-product, therefore the images in this document are not formatted to the standard found in the manuscript. This document supplies both the code and the output for the analysis presented in the manuscript, it should be noted that sometimes different operating systems will result in slightly different numbers. Where text is not provided to support the figure/table the information can be found in the manuscript itself where these figures/tables are referenced.

#Introduction to data

Table C.3: Stable Isotope measurements. Oxygen = δ^{18}O VPDB (‰), Carbon = δ^{13}C VPDB (‰). testArea= Test Area and is measured in μm^2

Subspecies	ID	Carbon	Oxygen	testArea	Run
SL	10	1.3715672	-0.7802817	81145.94	1

Table C.3: Stable Isotope measurements. Oxygen = δ^{18}O VPDB (‰), Carbon = δ^{13}C VPDB (‰). testArea= Test Area and is measured in μm^2 *(continued)*

Subspecies	ID	Carbon	Oxygen	testArea	Run
SL	101	0.6876677	-1.0867566	103124.83	1
SL	104	0.3632976	-2.0712644	66567.82	1
SL	107	1.1632331	-1.4287300	135722.24	1
SL	111	1.0148622	-0.9358961	122856.06	1
SL	126	0.8584712	-0.3236177	78883.76	1
SL	13	0.5846690	-1.8433602	68896.50	1
SL	130	1.4309023	-1.5702566	103860.19	1
SL	135	1.0058396	-0.4009053	100774.78	1
SL	16	1.1969931	-0.5336036	93520.24	1
SL	18	0.4622042	-1.3699179	82594.97	1
SL	19	0.4976279	-1.7961165	67983.05	1
SL	31	-0.1835195	-1.8091839	54222.15	1
SL	48	0.3834536	-0.3425978	74836.73	1
SL	51	0.7516665	-1.5689446	99628.03	1
SL	53	0.8508529	-1.3819801	102065.51	1
SL	61	0.1018944	-1.8021476	71607.33	1
SL	62	0.9055066	-0.2441102	76194.31	1
SL	66	0.9277729	-1.0733882	102821.43	1
SL	75	0.9407367	-0.9698151	103412.81	1
SL	78	0.9869319	-0.9788106	93153.80	1
SL	79	1.8194485	-1.3426287	119878.63	1
SL	82	1.4930699	-0.6769615	103289.39	1
SL	83	1.6517401	-0.6489755	142715.84	1
SL	84	1.5231971	-0.8868566	137871.74	1
SL	97	0.4476539	-2.2751624	76770.25	1
SLE	1	0.3286062	-1.6131728	69221.80	1
SLE	101	0.9306516	-2.2256956	75587.51	2
SLE	102	0.3933083	-1.4959802	83676.21	2
SLE	103	1.2524561	-0.7943694	117070.48	2
SLE	105	1.3667419	-1.1607327	91897.09	2
SLE	109	1.2905514	-0.6488278	76729.83	2
SLE	115	0.8374185	-1.8372502	108987.43	2
SLE	119	0.8213784	-1.9376237	119891.85	2
SLE	12	0.3306304	-1.7941061	65531.85	1
SLE	120	0.5938095	-0.7221005	97256.06	2
SLE	13	0.9136034	-0.3607117	69875.67	1
SLE	137	1.4168672	-0.8074180	66547.25	2
SLE	15	0.5573421	-1.5036076	72809.88	1
SLE	18	0.6231290	-0.4712821	70690.55	1
SLE	19	0.4126110	-0.9778956	61033.60	1
SLE	21	1.3285669	-0.3426184	81842.53	1
SLE	38	1.1767510	-0.4501733	96768.88	1
SLE	45	1.0745283	-0.3928777	78395.24	1
SLE	46	1.1463878	-0.4170021	85795.09	1
SLE	48	0.6896762	-1.2636682	77330.77	1
SLE	5	0.7253517	-0.8854185	81343.09	1
SLE	51	0.7760410	-1.5775112	69262.41	1

Table C.3: Stable Isotope measurements. Oxygen = δ^{18}O VPDB (‰), Carbon = δ^{13}C VPDB (‰). testArea= Test Area and is measured in μm^2 *(continued)*

Subspecies	ID	Carbon	Oxygen	testArea	Run
SLE	55	-0.1649338	-1.5405297	72224.41	1
SLE	56	0.4597048	-2.1592204	118613.61	1
SLE	65	1.0301143	-0.4650675	63682.95	1
SLE	66	0.9809064	-0.3231384	64711.42	1
SLE	67	0.6043156	-0.9048476	66336.41	1
SLE	69	1.1425894	-0.5740130	80400.76	1
SLE	71	1.2324060	-0.1319043	88340.56	2
SLE	82	0.4667345	-2.1332334	69730.37	2
SLE	85	0.1714873	-1.6574713	66506.11	2
SLE	88	0.4544612	-1.0312509	117508.01	2
SLE	9	-0.7533352	-1.1457615	70161.53	1
SLE	94	0.5266416	-2.5689730	121529.33	2
SS	111	-0.0337594	-2.1192997	96522.05	3
SS	112	0.8554637	-2.2829085	83907.84	3
SS	113	0.6439348	-1.2631137	73545.99	3
SS	118	0.8073434	-0.6096822	79238.58	3
SS	121	1.4860401	-1.1657514	135490.83	3
SS	125	1.0379198	-1.2611062	87918.88	3
SS	13	0.7668481	-0.3215095	99972.03	2
SS	130	1.2414453	-0.3796557	108082.07	3
SS	140	-0.1258519	-1.8229108	100805.63	3
SS	143	-0.1309348	-2.0102034	71154.80	3
SS	145	1.2139977	-0.2794992	86365.89	3
SS	146	0.9283393	-0.1152426	112067.39	3
SS	147	1.2902410	-0.5749609	101222.16	3
SS	148	0.3651552	-2.3507355	78621.50	3
SS	19	1.4125717	-0.3516651	86805.65	2
SS	23	0.8326350	-1.5297424	96732.88	2
SS	28	1.1575210	-2.3650514	81532.08	2
SS	33	0.5603784	-2.1368744	86952.12	2
SS	36	0.5148337	-0.2099339	63760.09	2
SS	4	0.8397197	-1.2663838	114168.04	2
SS	40	0.6906805	-1.6014993	76353.72	2
SS	41	0.5651502	-1.5795102	109838.70	2
SS	42	0.9979785	-1.8593703	63505.06	2
SS	46	0.6083326	-0.6889555	108598.28	2
SS	48	0.9347113	-0.8568716	117621.78	2
SS	56	1.0843433	-2.0502749	82622.25	2
SS	61	0.3753485	-2.1292354	92048.20	2
SS	62	1.4046966	-0.8188906	117790.84	2
SS	72	0.9929573	-0.2851574	128548.65	2
SS	83	1.3775820	-1.7504248	80873.85	2
SS	84	0.8705013	-2.8429927	67642.57	2
SS	85	1.0228822	-0.9900978	71319.35	2
SS	86	1.0920551	-1.0754152	83995.26	2
SS	87	0.6369173	-1.3062743	84216.39	2
SS	88	1.2895489	-0.5133236	89291.89	2

Table C.3: Stable Isotope measurements. Oxygen = δ^{18}O VPDB (‰), Carbon = δ^{13}C VPDB (‰). testArea= Test Area and is measured in μm^2 *(continued)*

Subspecies	ID	Carbon	Oxygen	testArea	Run
SS	9	1.0380925	-2.1640144	86854.30	2
SS	90	1.4689975	-2.5619469	99756.59	2
SS	96	0.6549624	-1.2721473	94290.26	3

2 Data processing

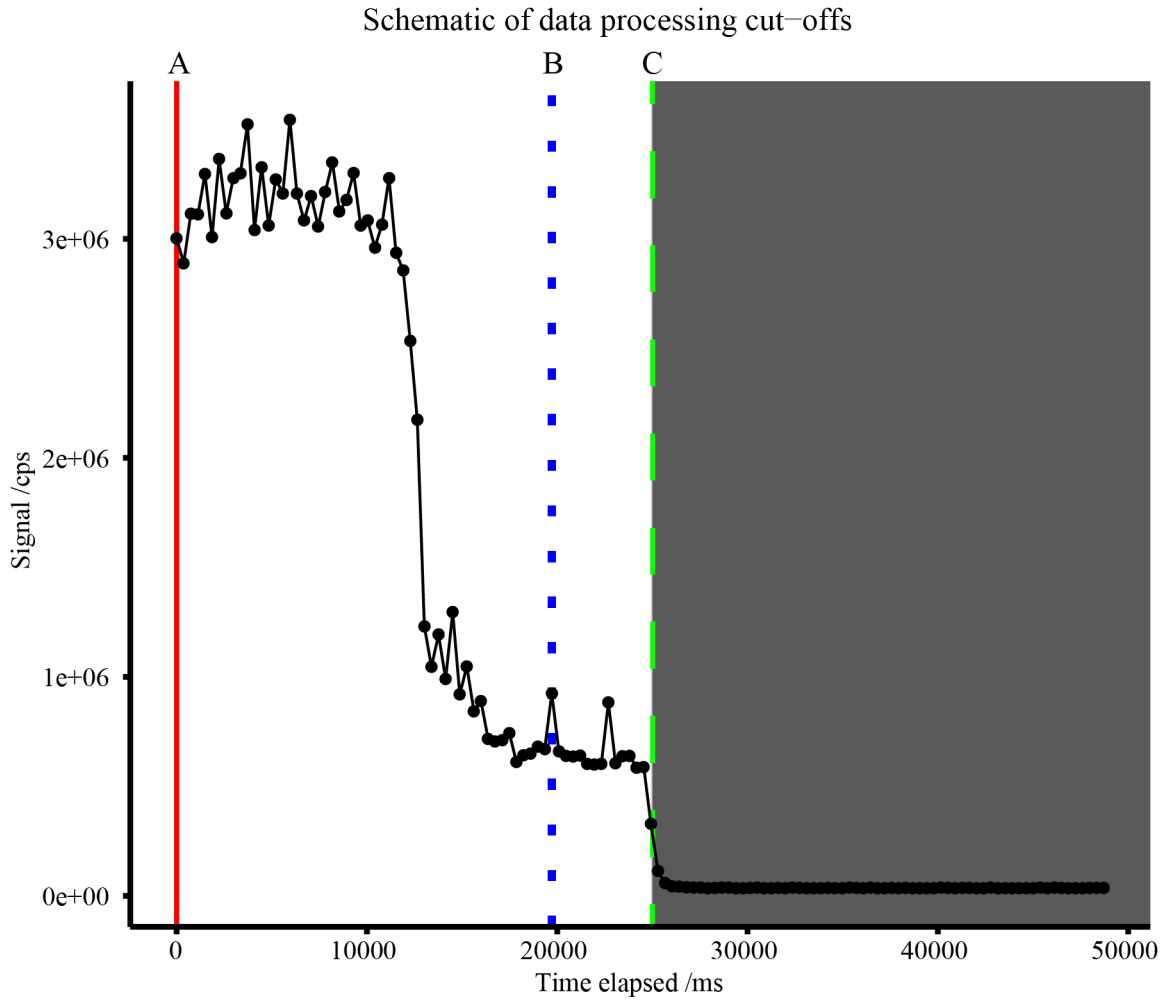

Figure C.1: Schematic of automatic data processing. A indicates the point where analysis is started with the first 100 ms cut off, B is the point on this illustration where the calculated largest signal change occurs which is taken to indicate the point where the laser penetrates the chamber, C is a universal cut off for all samples at 25000 ms any data collected after this point is dismissed

Table C.2: Spot averaged trace element data for 262 inidviduals of G.ruber. This table is large so will provided as a link in the final thesis when this paper is published. Presented here are the row headers and first few lines of data. All elemental ratios are presented in mmol/mol and size data in μm^2

Morphological_ID	Chamber	LabID	Spot	BaCa	MgCa	MnCa	SrCa	ZnCa	Batch	Subspecies	Chamber_Size	TestSize	MgCaTemperature
SL1	Antepenultimate	SL1	1	-0.0061249	3.950835	0.0974259	1.798194	-0.0247389	1.0	SL	20707.07	87595.95	26.01679
SL1	Antepenultimate	SL1	2	-0.0084587	3.904826	0.0783684	1.761066	-0.0375114	1.0	SL	20707.07	87595.95	25.88663
SL1	Antepenultimate	SL1	3	-0.0002580	5.072016	0.1439419	1.679203	-0.0152749	1.0	SL	20707.07	87595.95	28.79247
SL1	Final	SL1	1	-0.0097125	3.949476	0.0917165	1.707941	-0.0308780	1.0	SL	28875.55	87595.95	26.01297
SL1	Final	SL1	2	-0.0090735	3.674736	0.0856113	1.699966	-0.0238796	1.0	SL	28875.55	87595.95	25.21184
SL1	Final	SL1	3	-0.0118904	3.830795	0.0711590	1.723597	-0.0403790	1.0	SL	28875.55	87595.95	25.67396
SL1	Penultimate	SL1	1	-0.0056157	5.306356	0.1825870	1.544188	-0.0192046	1.0	SL	38210.48	87595.95	29.29433
SL1	Penultimate	SL1	2	-0.0081399	4.519170	0.0816787	1.636100	-0.0311133	1.0	SL	38210.48	87595.95	27.51014
SL1	Penultimate	SL1	3	-0.0040551	5.002892	0.1664271	1.687807	-0.0091799	1.0	SL	38210.48	87595.95	28.64000
SL10	Antepenultimate	SL3	1	0.0009660	4.323860	0.0977682	1.955692	0.0095438	3.2	SL	27751.81	81145.94	27.01925

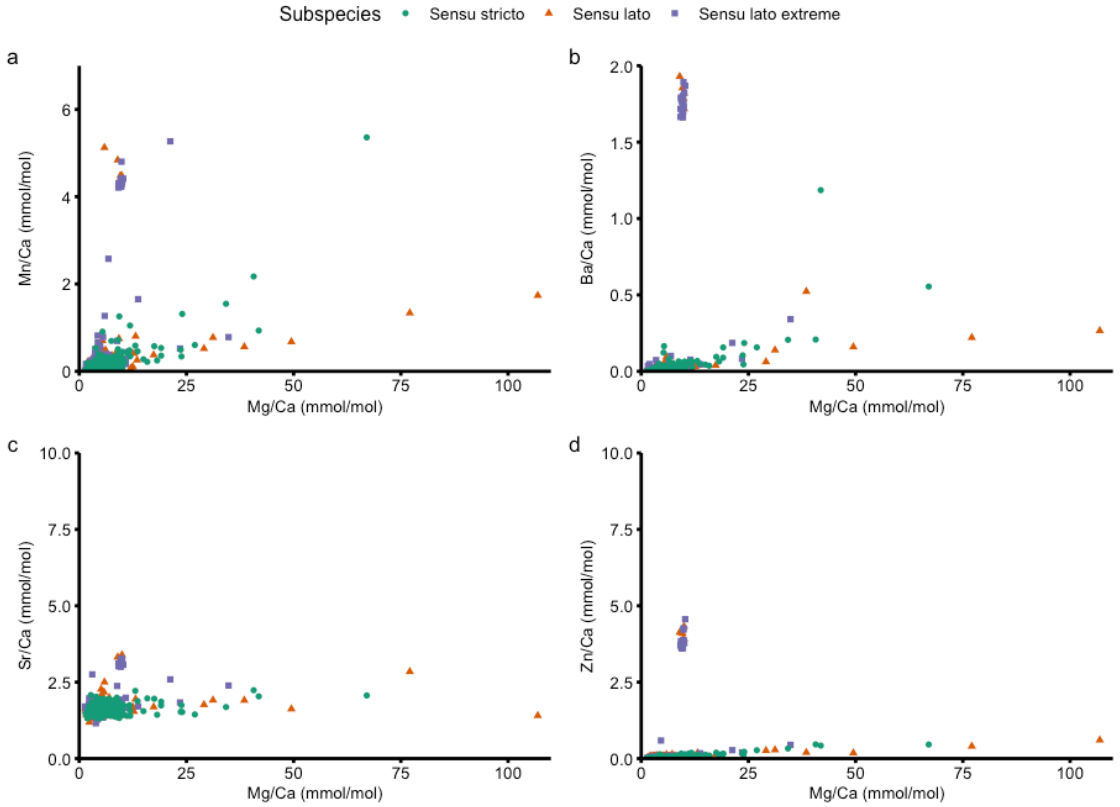

Figure C.2: a-d Cross plot of elemental ratios against Mg/Ca used to identify contaminants.

This section shows how to load the required .csv files for the subsequent analysis, in total three .csv files are used :

```
morph <- read_csv ("Submission /Morphometrics.csv") # Morphological
mgca <- read_csv("mgca_temp.csv") # Trace element
oc <- read_csv("Submission /Stable_Isotope.csv")  #Stable isotope
```

Size is measured on a different scale than mg/ca and stable isotopes therefore needs to be transformed on the log scale to make model fitting simpler across both data sets.

```
mgca$chamberlogsize <- log(mgca$Chamber_Size) - 10
mgca$testlogsize <- log(mgca$TestSize) - 10
oc$logsize <- log(oc$testArea) - 10 #Only test size is used in stable isotope analysis
```

The following lines change the categorical variables in mgca into factors so that there influence on MgCa can be explored. Where levels are specified this makes ordered plotting easier.

```
mgca$Subspecies <- factor(mgca$Subspecies, levels = c("SS","SL","SLE"))
mgca$Chamber <- factor(mgca$Chamber, levels = c("Final","Penultimate","Antepenultimate"))
mgca$ID <- factor(mgca$LabID)
mgca$Spot <- factor(mgca$Spot)
mgca$Batch <- factor(mgca$Batch)
```

Table C.4: Proportional and cumulative variance of retained components

	PC1	PC2	PC3
Standard deviation	2.44035	1.750248	1.285711
Proportion of Variance	0.39702	0.204220	0.110200
Cumulative Proportion	0.39702	0.601250	0.711450

3 Morphological Analysis

3.1 PCA Analysis

```
morph$Subspecies <- factor(morph$Subspecies, levels = c("SS","SL","SLE"))
morph.pca <- prcomp(morph[,3:17], scale. = TRUE, center = TRUE)
morph2 <- morph
morph2$Subspecies <- rep(c(1,2,3), each=150)
#paran only takes numerical values, convert subspecies into numbers 1=ss, 2=sl, 3=sle
#duplicate morph table so plotting codes below work
paranres <- paran(morph2, iterations = 10000, centile = 95, quietly = FALSE, graph = FALSE)
```

```
##
## Using eigendecomposition of correlation matrix.
## Computing: 10%  20%  30%  40%  50%  60%  70%  80%  90%  100%
##
##
## Results of Horn's Parallel Analysis for component retention
## 10000 iterations, using the 95 centile estimate
##
## ------------------------------------------------
## Component   Adjusted    Unadjusted    Estimated
##             Eigenvalue  Eigenvalue    Bias
## ------------------------------------------------
## 1           5.625086    6.043104      0.418017
## 2           3.152239    3.480770      0.328531
## 3           1.420070    1.686560      0.266489
## ------------------------------------------------
##
## Adjusted eigenvalues > 1 indicate dimensions to retain.
## (3 components retained)
```

Table C.5: PCA loadings of measured traits of the retained principal components

	PC1	PC2	PC3
testArea	-0.3920996	-0.0385862	0.0741195
testAR	-0.1252589	-0.4068957	0.2334472
FinalArea	-0.2575113	-0.3719410	0.1801531
FinalAR	0.0768080	0.4558934	-0.1607534
f-1Area	-0.3055993	0.2768017	0.1722870
f-1AR	-0.0131705	-0.1578635	-0.6669414
f-2Area	-0.3183228	0.1172342	-0.2872055
f-2AR	0.0754544	0.3733220	0.5048362
apArea	-0.2279058	0.1123738	-0.1016385
AH	-0.1820518	0.1257996	-0.1712460
AW	-0.2564674	-0.0953733	0.0142084
PerimeterAp	-0.3446416	0.0000608	-0.0864970
PerimeterF-1	-0.3241961	0.2248315	0.0098264
PerimeterF-2	-0.2865821	0.2943482	-0.0056448
PerimeterF	-0.3176472	-0.2395315	0.1496798

3.2 Clustering Analysis

As shown in figure 2 in the main text there appears to be some separation of the SLE morphotype in morphological space. To test this we conduct a clustering analysis. Clustering analysis shows that the morphospace within PC1 and PC2 is best represented by two clusters (Figure S3) which do not correspond to morphologically identified units (Table S3, Figure S4). Therefore, we reject the null hypothesis of no morphological variability in G. ruber but the variability identified is not taxonomically informative. When forced to identity three groups (the number of subspecies identified in this study), a subsequent model identified clusters that visually appear to correspond to subspecies (Figure 3 main text), but a classification table shows the subspecies are split across all three groups (Table S6).

```
class= factor(morph$Subspecies, levels = c("SS","SL", "SLE"))
model1 <- PCA_output[,1:2]
bic_m1 <- mclustBIC(model1)
mod1 <- Mclust(model1,x=bic_m1)
summary(mod1)
```

```
## ----------------------------------------------------
## Gaussian finite mixture model fitted by EM algorithm
## ----------------------------------------------------
##
## Mclust EII (spherical, equal volume) model with 2 components:
##
##  log-likelihood   n df       BIC       ICL
##        -1908.74 450  6 -3854.136 -3949.629
##
## Clustering table:
##   1   2
## 124 326
```

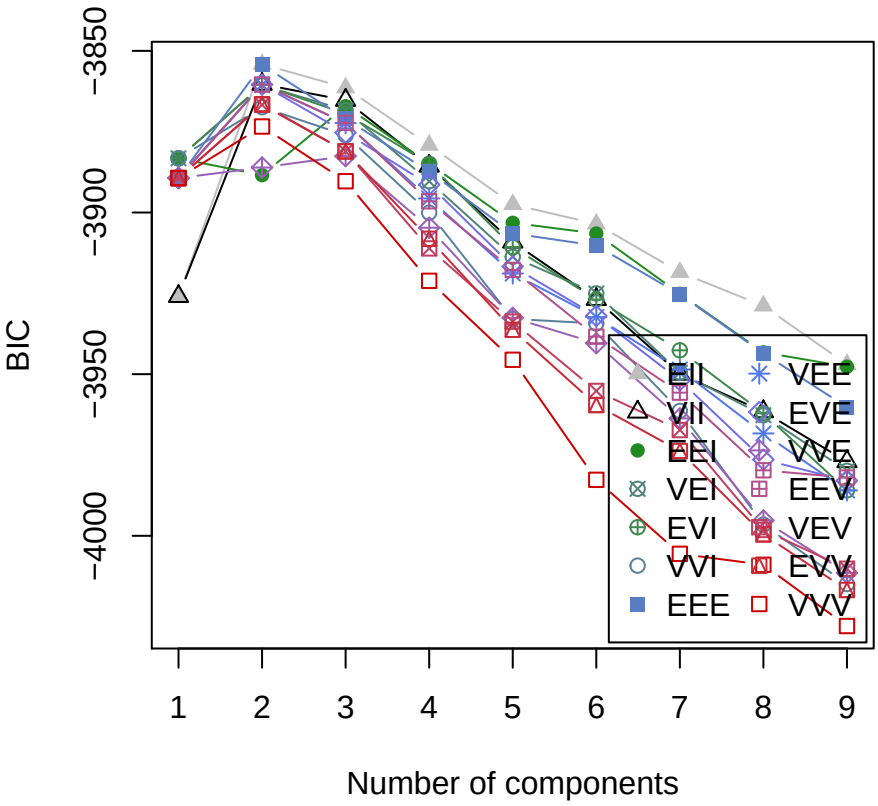

Figure C.3: Model Comparisons when no groups are specififed, BIC indicate that the best fitting model is that with 2 components

Table C.6: Model 1 Classification

	1	2
SS	46	104
SL	55	95
SLE	23	127

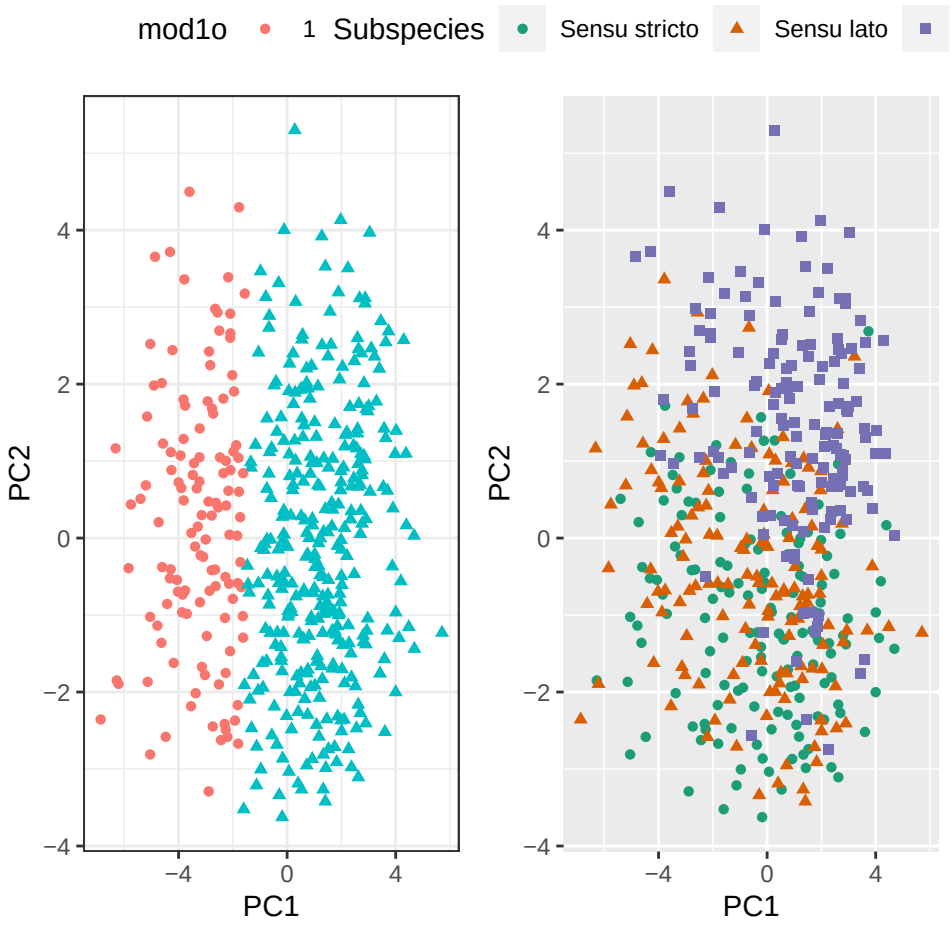

Figure C.4: Model 1 vs Actual Classification

```
model2 <- PCA_output[,1:2]
bic_m2 <- mclustBIC(model2, G=3)
mod2 <- Mclust(model2,x=bic_m2)
summary(mod2)
```

```
## ----------------------------------------------------
## Gaussian finite mixture model fitted by EM algorithm
## ----------------------------------------------------
##
## Mclust EII (spherical, equal volume) model with 3 components:
##
##  log-likelihood   n df       BIC       ICL
##       -1903.208 450  9 -3861.399 -4089.535
```

Table C.7: Model 2 Classification

	1	2	3
SS	46	102	2
SL	57	87	6
SLE	25	50	75

```
##
## Clustering table:
##   1   2   3
## 128 239  83
```

4 Trace element analysis - mixed effect models

Mixed effect models were constructed as outlined in the manuscript. The tolerance of the models was set to 0.01 instead of the default 0.001. Model selection following analysis of variance was based on the lowest AIC score.

4.1 First we try just including test size

```
m1 <- glmer(MgCa ~ (Chamber+Subspecies)^2 + (testlogsize+Subspecies)^2 + (1|Spot) +
              (1|ID) + (1|Batch),data=mgca, family=Gamma,
            control = glmerControl(check.conv.grad=.makeCC("warning", tol=1e-2)))
ss <- getME(m1, c("theta","fixef"))
# The above model failed to converge, this line takes the previous model fit
# and then the subsequent model builds upon this previous fit
m1.1 <- update(m1, start=ss,control=glmerControl(optCtrl=list(maxfun=1e4),
check.conv.grad=.makeCC("warning", tol=1e-2)))
ss <- getME(m1.1, c("theta","fixef"))
# The above model failed to converge, this line takes the previous model fit
# and then the subsequent model builds upon this previous fit
m1.2 <- update(m1.1, start=ss,control=glmerControl(optCtrl=list(maxfun=1e4),
                                                   check.conv.grad=.makeCC("warning",
                                                                           tol=1e-2)))

ss <- getME(m1.2, c("theta","fixef"))

m1.3 <- update(m1.2, start=ss,control=glmerControl(optCtrl=list(maxfun=1e4),
                                                   check.conv.grad=.makeCC("warning",
                                                                           tol=1e-2)))
ss <- getME(m1.3, c("theta","fixef"))
m1.4 <- update(m1.3, start=ss,control=glmerControl(optCtrl=list(maxfun=1e4),
                                                   check.conv.grad=.makeCC("warning",
                                                                           tol=1e-2)))
ss <- getME(m1.4, c("theta","fixef"))
m1.5 <- update(m1.4, start=ss,control=glmerControl(optCtrl=list(maxfun=1e4),
                                                   check.conv.grad=.makeCC("warning",
                                                                           tol=1e-2)))

ss <- getME(m1.5, c("theta","fixef"))
m1.6 <- update(m1.5, start=ss,control=glmerControl(optimizer="bobyqa",optCtrl=list(maxfun=1e4),
                                                   check.conv.grad=.makeCC("warning",
                                                                           tol=1e-2)))



m2 <- glmer(MgCa ~ Chamber + (testlogsize+Subspecies)^2 + (1|Spot) +
              (1|ID) + (1|Batch), data=mgca,family=Gamma,
            control = glmerControl(check.conv.grad=.makeCC("warning", tol=1e-2)))
ss <- getME(m2, c("theta","fixef"))
m2.1 <- update(m2, start=ss,control=glmerControl(optCtrl=list(maxfun=1e4),
check.conv.grad=.makeCC("warning", tol=1e-2)))

m3 <- glmer(MgCa ~ (Chamber+Subspecies)^2 + testlogsize + (1|Spot) + (1|ID) +
              (1|Batch), data=mgca, family=Gamma,control = glmerControl(
```

```
                check.conv.grad=.makeCC("warning", tol=1e-2)))
ss <- getME(m3, c("theta","fixef"))
m3.1 <- update(m3, start=ss,control=glmerControl(optCtrl=list(maxfun=1e4),
                                                 check.conv.grad=.makeCC("warning",
                                                                         tol=1e-2)))

ss <- getME(m3.1, c("theta","fixef"))
m3.2 <- update(m3.1, start=ss,control=glmerControl(optCtrl=list(maxfun=1e4),
                                                 check.conv.grad=.makeCC("warning",
                                                                         tol=1e-2)))

ss <- getME(m3.2, c("theta","fixef"))
m3.3 <- update(m3.2, start=ss,control=glmerControl(optCtrl=list(maxfun=1e4),
                                                   check.conv.grad=.makeCC("warning",
                                                                           tol=1e-2)))
```

Table C.8: Model comparison for mixed effect models including test size as fixed effect. Random effects are: (1|Spot) + (1|ID) +(1|Batch)

	Fixed effects	npar	df	logLik	Deviance	Chisq	p-value	BIC	AIC	ΔAIC
1	(Chamber+Subspecies)^2 + testlogsize	16	2	-2652.93	5305.86	7.74	0.021	5426.30	5337.86	0.00
2	(Chamber+Subspecies)^2 + (testlogsize+Subspecies)^2	14	2	-2656.80	5313.59	33.80	0.000	5418.98	5341.59	3.74
3	Chamber + (testlogsize+Subspecies)^2	12	NA	-2673.70	5347.39	NA	NA	5437.72	5371.39	33.53

```
## Generalized linear mixed model fit by maximum likelihood (Laplace
##   Approximation) [glmerMod]
##  Family: Gamma  ( inverse )
## Formula: MgCa ~ (Chamber + Subspecies)^2 + testlogsize + (1 | Spot) +
##     (1 | ID) + (1 | Batch)
##    Data: mgca
## Control:
## glmerControl(optCtrl = list(maxfun = 10000), check.conv.grad = .makeCC("warning",
##     tol = 0.01))
##
##      AIC      BIC   logLik deviance df.resid
##   5341.6   5419.0  -2656.8   5313.6     1844
##
## Scaled residuals:
##     Min      1Q  Median      3Q     Max
## -2.2408 -0.6261 -0.1071  0.5077  7.3608
##
## Random effects:
##  Groups   Name        Variance  Std.Dev.
##  ID       (Intercept) 5.439e-04 0.023322
##  Batch    (Intercept) 8.899e-05 0.009434
##  Spot     (Intercept) 4.329e-06 0.002081
##  Residual             5.924e-02 0.243394
## Number of obs: 1858, groups:  ID, 154; Batch, 4; Spot, 3
##
## Fixed effects:
##                                  Estimate Std. Error t value Pr(>|z|)
## (Intercept)                      0.287354   0.020533  13.995  < 2e-16 ***
## ChamberPenultimate              -0.043624   0.004835  -9.022  < 2e-16 ***
```

```
## ChamberAntepenultimate               -0.050456   0.004868 -10.364  < 2e-16 ***
## SubspeciesSL                          0.050324   0.010423   4.828 1.38e-06 ***
## SubspeciesSLE                         0.062096   0.010767   5.767 8.07e-09 ***
## testlogsize                          -0.017434   0.008159  -2.137   0.0326 *
## ChamberPenultimate:SubspeciesSL      -0.037275   0.007383  -5.049 4.45e-07 ***
## ChamberAntepenultimate:SubspeciesSL  -0.035646   0.007421  -4.803 1.56e-06 ***
## ChamberPenultimate:SubspeciesSLE     -0.039679   0.008223  -4.825 1.40e-06 ***
## ChamberAntepenultimate:SubspeciesSLE -0.041376   0.008142  -5.082 3.74e-07 ***
## ---
## Signif. codes:  0 '***' 0.001 '**' 0.01 '*' 0.05 '.' 0.1 ' ' 1
##
## Correlation of Fixed Effects:
##             (Intr) ChmbrP ChmbrA SbspSL SbsSLE tstlgs ChP:SSL ChA:SSL CP:SSLE
## ChmbrPnltmt -0.149
## ChmbrAntpnl -0.140  0.665
## SubspecisSL -0.230  0.309  0.305
## SubspecsSLE -0.291  0.292  0.285  0.459
## testlogsize -0.557 -0.009 -0.019 -0.035  0.076
## ChmbrPn:SSL  0.110 -0.655 -0.435 -0.476 -0.197 -0.015
## ChmbrAn:SSL  0.101 -0.436 -0.656 -0.473 -0.186 -0.007  0.674
## ChmbrP:SSLE  0.092 -0.588 -0.391 -0.184 -0.501  0.000  0.386   0.257
## ChmbrA:SSLE  0.083 -0.398 -0.598 -0.182 -0.502  0.012  0.260   0.392   0.670
```

4.2 Now including chamber size

```
m4 <- glmer(MgCa ~ (Chamber+Subspecies)^2 + (chamberlogsize+Subspecies)^2 + (1|Spot) +
              (1|ID) + (1|Batch),data=mgca, family=Gamma,
            control = glmerControl(check.conv.grad=.makeCC("warning",
                                                           tol=1e-2)))

ss <- getME(m4, c("theta","fixef"))
m4.1<- update(m4, start=ss,control=glmerControl(optCtrl=list(maxfun=1e4),
                                                check.conv.grad=.makeCC("warning",
                                                                        tol=1e-2)))

m5 <- glmer(MgCa ~ Chamber + (chamberlogsize+Subspecies)^2 + (1|Spot) +
              (1|ID) + (1|Batch), data=mgca,family=Gamma,
            control = glmerControl(check.conv.grad=.makeCC("warning", tol=1e-2)))
ss <- getME(m5, c("theta","fixef"))
m5.1<- update(m5, start=ss,control=glmerControl(optCtrl=list(maxfun=1e4),
                                                check.conv.grad=.makeCC("warning",
                                                                        tol=1e-2)))


m6 <- glmer(MgCa ~ (Chamber+Subspecies)^2 + chamberlogsize + (1|Spot) + (1|ID) +
              (1|Batch), data=mgca, family=Gamma,control = glmerControl(
                check.conv.grad=.makeCC("warning", tol=1e-2)))
ss <- getME(m6, c("theta","fixef"))
m6.1<- update(m6, start=ss,control=glmerControl(optCtrl=list(maxfun=1e4),
                                                  check.conv.grad=.makeCC("warning",
                                                                          tol=1e-2)))
```

```
mgca$stricto <- as.factor(mgca$Subspecies == "SS")
m7 <- glmer(MgCa ~ (Chamber*stricto)^2 + (chamberlogsize*stricto) +
              (1|Spot) + (1|ID) + (1|Batch),
            data=mgca, family=Gamma(link="log"))
```

Table C.9: Model comparison for mixed effect models including chamber size as a fixed effect. Random effects are: (1|Spot) + (1|ID) +(1|Batch). The model with the lowest AIC is following grouping, the decrease in AIC compared to the next best fitting model indicates that chamber size has no effect

Fixed effects	npar	df	logLik	Deviance	Chisq	p-value	BIC	AIC	ΔAIC
(Chamber+Subspecies)^2 + (chamberlogsize+Subspecies)^2 (SS vs grouped SL+SLE)	12	0	-2645.41	5290.83	62.64	NA	5381.16	5314.83	0.00
(Chamber+Subspecies)^2 + chamberlogsize	14	2	-2658.36	5316.73	0.00	1.000	5422.11	5344.73	29.90
(Chamber+Subspecies)^2 + (chamberlogsize+Subspecies)^2	16	2	-2657.66	5315.33	1.40	0.497	5435.76	5347.33	32.50
Chamber + (chamberlogsize+Subspecies)^2	12	NA	-2676.73	5353.47	NA	NA	5443.80	5377.47	62.64

```
## Generalized linear mixed model fit by maximum likelihood (Laplace
##   Approximation) [glmerMod]
##  Family: Gamma  ( inverse )
## Formula: MgCa ~ (Chamber + Subspecies)^2 + chamberlogsize + (1 | Spot) +
##     (1 | ID) + (1 | Batch)
##    Data: mgca
## Control:
## glmerControl(optCtrl = list(maxfun = 10000), check.conv.grad = .makeCC("warning",
##     tol = 0.01))
##
##      AIC      BIC   logLik deviance df.resid
##   5344.7   5422.1  -2658.4   5316.7     1844
##
## Scaled residuals:
##     Min      1Q  Median      3Q     Max
## -2.2312 -0.6205 -0.1089  0.5073  7.2060
##
## Random effects:
##  Groups   Name        Variance  Std.Dev.
##  ID       (Intercept) 5.368e-04 0.023169
##  Batch    (Intercept) 8.720e-05 0.009338
##  Spot     (Intercept) 4.349e-06 0.002085
##  Residual             5.934e-02 0.243591
## Number of obs: 1858, groups:  ID, 154; Batch, 4; Spot, 3
##
## Fixed effects:
##                                    Estimate Std. Error t value Pr(>|z|)
## (Intercept)                        0.265599   0.007538  35.237  < 2e-16 ***
## ChamberPenultimate                -0.043643   0.005243  -8.324  < 2e-16 ***
## ChamberAntepenultimate            -0.052321   0.005439  -9.620  < 2e-16 ***
## SubspeciesSL                       0.049500   0.008294   5.968 2.40e-09 ***
## SubspeciesSLE                      0.060264   0.009370   6.432 1.26e-10 ***
## chamberlogsize                    -0.006547   0.005580  -1.173 0.240686
## ChamberPenultimate:SubspeciesSL   -0.037517   0.008008  -4.685 2.80e-06 ***
## ChamberAntepenultimate:SubspeciesSL -0.035193   0.008038  -4.378 1.20e-05 ***
## ChamberPenultimate:SubspeciesSLE  -0.036000   0.009340  -3.854 0.000116 ***
## ChamberAntepenultimate:SubspeciesSLE -0.037691   0.009193  -4.100 4.13e-05 ***
## ---
## Signif. codes:  0 '***' 0.001 '**' 0.01 '*' 0.05 '.' 0.1 ' ' 1
```

```
##
## Correlation of Fixed Effects:
##             (Intr) ChmbrP ChmbrA SbspSL SbsSLE chmbrl ChP:SSL ChA:SSL CP:SSLE
## ChmbrPnltmt -0.451
## ChmbrAntpnl -0.502  0.636
## SubspecisSL -0.489  0.418  0.403
## SubspecsSLE -0.518  0.357  0.424  0.400
## chamberlgsz -0.251 -0.023  0.248  0.001  0.300
## ChmbrPn:SSL  0.296 -0.655 -0.415 -0.646 -0.237  0.018
## ChmbrAn:SSL  0.305 -0.433 -0.644 -0.645 -0.246 -0.035  0.670
## ChmbrP:SSLE  0.339 -0.554 -0.440 -0.237 -0.682 -0.321  0.362   0.255
## ChmbrA:SSLE  0.337 -0.373 -0.631 -0.239 -0.685 -0.305  0.243   0.386   0.701
## optimizer (Nelder_Mead) convergence code: 0 (OK)
## unable to evaluate scaled gradient
## Model failed to converge: degenerate  Hessian with 4 negative eigenvalues
```

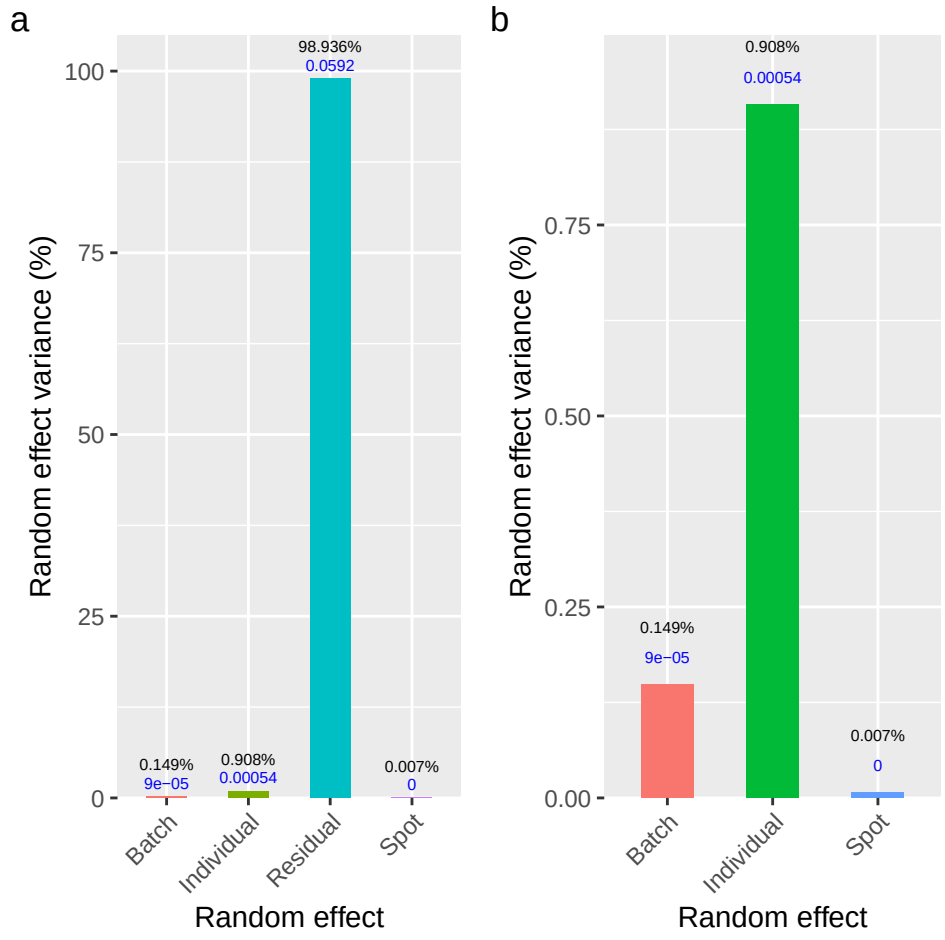

Figure C.5: Percentage variance explained by the random effects of the chosen model (a) Percentage of varaince explained by all the random effects (b) Percentage of variance explained when residual variance is removed. The black text is a print of the percentage of variance wheres blue text is the raw value of variance from the model

5 Stable Isotope Analysis

```
aov(Carbon ~ Subspecies, data=oc)
```

```
## Call:
##    aov(formula = Carbon ~ Subspecies, data = oc)
##
## Terms:
##                 Subspecies Residuals
## Sum of Squares    0.424558 19.482200
## Deg. of Freedom          2        95
##
## Residual standard error: 0.4528529
## Estimated effects may be unbalanced
```

```
aov(Oxygen ~ Subspecies, data = oc)
```

```
## Call:
##    aov(formula = Oxygen ~ Subspecies, data = oc)
##
## Terms:
##                 Subspecies Residuals
## Sum of Squares     0.89919  44.72529
## Deg. of Freedom          2        95
##
## Residual standard error: 0.6861432
## Estimated effects may be unbalanced
```

5.1 Carbon

```
c0 <- lmer(Carbon ~ 1+ (1|ID) + (1|Run), data=oc)
c1 <- lmer(Carbon ~ Subspecies + logsize +(1|ID) + (1|Run), data=oc )
c2 <- lmer(Carbon ~ Subspecies*logsize + (1|ID)+(1|Run), data=oc)
c3 <- lmer(Carbon ~ Subspecies  +(1|ID) + (1|Run), data=oc )
c4 <- lmer(Carbon ~ logsize +(1|ID) + (1|Run), data=oc )
```

5.2 Oxygen

```
o0 <- lmer(Oxygen ~ 1+ (1|ID) + (1|Run), data=oc)
o1 <- lmer(Oxygen ~ Subspecies + logsize +(1|ID) + (1|Run), data=oc )
o2 <- lmer(Oxygen ~Subspecies*logsize + (1|ID)+(1|Run), data = oc)
o3 <- lmer(Oxygen ~ Subspecies  +(1|ID) + (1|Run), data=oc )
o4 <- lmer(Oxygen ~ logsize +(1|ID) + (1|Run), data=oc )
```

Table C.10: Analysis of variance table of carbon

Fixed Effects	Carbon				
	npar	AIC	logLik	Pr(>Chisq)	AICchange
Subspecies*Size	9	113.2095	-47.60474	0.0192438	0.0000000
Size	5	113.3022	-51.65108	0.0000161	0.0926924
Subspecies+Size	7	117.1106	-51.55530	0.0000441	3.9011291
Null Model	4	129.9089	-60.95447	NA	16.6994787
Subspecies	6	131.7963	-59.89813	1.0000000	18.5867887

Table C.11: Analysis of variance table of oxygen

Model	Carbon				
	npar	AIC	logLik	Pr(>Chisq)	AICchange
Subspecies*Size	9	209.6193	-95.80967	0.0216638	0.000000
Null Model	4	210.6937	-101.34685	NA	1.074351
Size	5	210.9480	-100.47402	0.1864228	1.328687
Subspecies+Size	6	213.2380	-100.61899	1.0000000	3.618630
Subspecies	7	213.2836	-99.64179	0.1621129	3.664224

```
mgcagroup <- mgca %>% group_by(Morphological_ID)%>%
  mutate(Chamber_Mean_MgCa = mean(MgCa)) %>%
  mutate(Chamber_Mean_Temp = mean(MgCaTemperature))
oc <- oc %>% unite("Morphological_ID",Subspecies:ID,remove = FALSE,
                   sep="")
stab_trace <- inner_join(mgcagroup,oc,
                         by=c("Morphological_ID","Subspecies"))

stab_trace$Chamber <- factor(stab_trace$Chamber, levels =
                           c("Final","Penultimate","Antepenultimate"))


stab_trace$Subspecies <- factor(stab_trace$Subspecies, levels =
                                  c("SS","SL","SLE"))
```

Table C.12: Linear regression of Chamber Mg/Ca Oxygen in SS

Term	Coefficient	SE	t	p
(Intercept)	4.33	0.19	23.23	<0.001
Oxygen	-0.45	0.12	-3.77	<0.001

Table C.13: Linear regression of Chamber Mg/Ca Oxygen in SL

Term	Coefficient	SE	t	p
(Intercept)	4.34	0.25	17.27	<0.001
Oxygen	-0.73	0.20	-3.64	<0.001

Table C.14: Linear regression of Chamber Mg/Ca Oxygen in SLE

Term	Coefficient	SE	t	p
(Intercept)	3.58	0.14	26.30	<0.001
Oxygen	-0.11	0.10	-1.13	0.262

Table C.15: Linear regression of Chamber Mg/Ca Carbon in SS

Term	Coefficient	SE	t	p
(Intercept)	5.18	0.23	22.83	<0.001
Carbon	-0.27	0.23	-1.15	0.254

Table C.16: Linear regression of Chamber Mg/Ca Carbon in SL

Term	Coefficient	SE	t	p
(Intercept)	5.19	0.27	18.89	<0.001
Carbon	-0.04	0.26	-0.16	0.876

Table C.17: Linear regression of Chamber Mg/Ca Carbon in SLE

Term	Coefficient	SE	t	p
(Intercept)	3.76	0.12	30.52	<0.001
Carbon	-0.07	0.15	-0.47	0.641

Bibliography

Bates, Douglas, Martin Maechler, Ben Bolker, and Steven Walker. 2019. *Lme4: Linear Mixed-Effects Models Using 'Eigen' and S4*. https://CRAN.R-project.org/package=lme4.

Dinno, Alexis. 2018. *Paran: Horn's Test of Principal Components/Factors*. https://CRAN.R-project.org/package=paran.

Fraley, Chris, Adrian E. Raftery, and Luca Scrucca. 2019. *Mclust: Gaussian Mixture Modelling for Model-Based Clustering, Classification, and Density Estimation*. https://CRAN.R-project.org/package=mclust.

Kassambara, Alboukadel. 2020. *Ggpubr: 'Ggplot2' Based Publication Ready Plots*. https://CRAN.R-project.org/package=ggpubr.

R Core Team. 2019. *R: A Language and Environment for Statistical Computing*. Vienna, Austria: R Foundation for Statistical Computing. https://www.R-project.org/.

Wickham, Hadley. 2019. *Tidyverse: Easily Install and Load the 'Tidyverse'*. https://CRAN.R-project.org/package=tidyverse.

Xie, Yihui. 2020. *Knitr: A General-Purpose Package for Dynamic Report Generation in r*. https://CRAN.R-project.org/package=knitr.

Zhu, Hao. 2019. *kableExtra: Construct Complex Table with 'Kable' and Pipe Syntax*. https://CRAN.R-project.org/package=kableExtra.

Bibliography

Agashe, D. (2009). The Stabilizing Effect of Intraspecific Genetic Variation on Population Dynamics in Novel and Ancestral Habitats. *The American Naturalist*, 174 (2), pp.255–267. [Online]. Available at: doi:10.1086/600085.

Akçakaya, H. R. et al. (2020). Assessing ecological function in the context of species recovery. *Conservation Biology*, 34 (3), pp.561–571. [Online]. Available at: doi:10.1111/cobi.13425.

Al-Sabouni, N. et al. (2018). Reproducibility of species recognition in modern planktonic foraminifera and its implications for analyses of community structure. *Journal of Micropalaeontology*, 37 (2), pp.519–534. [Online]. Available at: doi:10.5194/jm-37-519-2018.

Al-Sabouni, N., Kucera, M. and Schmidt, D. N. (2007). Vertical niche separation control of diversity and size disparity in planktonic foraminifera. *Marine Micropaleontology*, 63 (1–2), pp.75–90. [Online]. Available at: doi:10.1016/j.marmicro.2006.11.002.

Anand, P. and Elderfield, H. (2005). Variability of Mg/Ca and Sr/Ca between and within the planktonic foraminifers Globigerina bulloides and Globorotalia truncatulinoides. *Geochemistry, Geophysics, Geosystems*, 6 (11), p.n/a-n/a. [Online]. Available at: doi:10.1029/2004GC000811.

André, A. et al. (2014). SSU rDNA Divergence in Planktonic Foraminifera: Molecular Taxonomy and Biogeographic Implications. Ketmaier, V. (Ed). *PLoS ONE*, 9 (8), p.e104641. [Online]. Available at: doi:10.1371/journal.pone.0104641.

Antczak-Orlewska, O. et al. (2021). Chironomidae Morphological Types and Functional Feeding Groups as a Habitat Complexity Vestige. *Frontiers in Ecology and Evolution*, 8. [Online]. Available at: doi:10.3389/fevo.2020.583831 [Accessed 5 February 2021].

Antonarakou, A. et al. (2015). Biotic and geochemical (δ18O, δ13C, Mg/Ca, Ba/Ca) responses of Globigerinoides ruber morphotypes to upper water column variations during the last deglaciation, Gulf of Mexico. *Geochimica et Cosmochimica Acta*, 170, pp.69–93. [Online]. Available at: doi:10.1016/j.gca.2015.08.003.

Araújo, M. S., Bolnick, D. I. and Layman, C. A. (2011). The ecological causes of individual specialisation. *Ecology Letters*, 14 (9), pp.948–958. [Online]. Available at: doi:10.1111/j.1461-0248.2011.01662.x.

Arimoto, J. et al. (2020). Changes in upper ocean hydrography and productivity across the Middle Eocene Climatic Optimum: Local insights and global implications from the Northwest Atlantic. *Global and Planetary Change*, 193, p.103258. [Online]. Available at: doi:10.1016/j.gloplacha.2020.103258.

Audzijonyte, A. *et al.* (2020) 'Fish body sizes change with temperature but not all species shrink with warming', *Nature Ecology & Evolution*, 4(6), pp. 809–814. doi:10.1038/s41559-020-1171-0.

Aurahs, R. et al. (2011). A revised taxonomic and phylogenetic concept for the planktonic foraminifer species Globigerinoides ruber based on molecular and morphometric evidence. *Marine Micropaleontology*, 79 (1–2), pp.1–14. [Online]. Available at: doi:10.1016/j.marmicro.2010.12.001.

Aze, T. et al. (2011). A phylogeny of Cenozoic macroperforate planktonic foraminifera from fossil data. *Biological Reviews*, 86 (4), pp.900–927. [Online]. Available at: doi:10.1111/j.1469-185X.2011.00178.x.

Bibliography

Aze, T. et al. (2014). Extreme warming of tropical waters during the Paleocene-Eocene thermal maximum. *Geology*, 42 (9), pp.739–742. [Online]. Available at: doi:10.1130/G35637.1.

Bailey, I. W. and Sinnott, E. W. (1915). A Botanical Index of Cretaceous and Tertiary Climates. *Science*, 41 (1066), pp.831–834. *JSTOR*.

Barker, S. et al. (2005). Planktonic foraminiferal Mg/Ca as a proxy for past oceanic temperatures: A methodological overview and data compilation for the Last Glacial Maximum. *Quaternary Science Reviews*, 24 (7-9 SPEC. ISS.), pp.821–834. [Online]. Available at: doi:10.1016/j.quascirev.2004.07.016.

Barnosky, A. D. (2001). Distinguishing the effects of the Red queen and Court Jester on Miocene mammal evolution in the northern Rocky Mountains. *Journal of Vertebrate Paleontology*, 21 (1), pp.172–185. [Online]. Available at: doi:10.1671/0272-4634(2001)021[0172:DTEOTR]2.0.CO;2.

Barnosky, A. D. (2008). Megafauna biomass tradeoff as a driver of Quaternary and future extinctions. *Proceedings of the National Academy of Sciences of the United States of America*, 105 (Suppl 1), pp.11543–11548. [Online]. Available at: doi:10.1073/pnas.0801918105.

Barnosky, A. D. et al. (2011). Has the Earth's sixth mass extinction already arrived? *Nature*, 471 (7336), pp.51–57. [Online]. Available at: doi:10.1038/nature09678.

Bar-On, Y. M., Phillips, R. and Milo, R. (2018). The biomass distribution on Earth. *Proceedings of the National Academy of Sciences*, 115 (25), pp.6506–6511. [Online]. Available at: doi:10.1073/pnas.1711842115.

Bates, D. (2005). Fitting linear mixed models in R. *R News*, 5 (1), pp.27–30.

Bates, D. et al. (2015). Fitting Linear Mixed-Effects Models Using lme4. *Journal of Statistical Software*, 67 (1), pp.1–48. [Online]. Available at: doi:10.18637/jss.v067.i01.

Baum, D. A. (2009). Species as Ranked Taxa. *Systematic Biology*, 58 (1), pp.74–86. [Online]. Available at: doi:10.1093/sysbio/syp011.

Baumfalk, Y. A. et al. (1987). Phenotypic variation of Globorotalia scitula (foraminiferida) as a response to Pleistocene climatic fluctuations. *Marine Geology*, 75 (1), pp.231–240. [Online]. Available at: doi:10.1016/0025-3227(87)90106-X.

Baumiller, T. K. (1993). Survivorship analysis of Paleozoic Crinoidea: effect of filter morphology on evolutionary rates. *Paleobiology*, 19 (3), pp.304–321. [Online]. Available at: doi:10.1017/S0094837300000294.

Bé, A. W. H. (1968). Shell Porosity of Recent Planktonic Foraminifera as a Climatic Index. *Science*, 161 (3844), pp.881–884. [Online]. Available at: doi:10.1126/science.161.3844.881.

Bé, A. W. H. et al. (1977). Laboratory and Field Observations of Living Planktonic Foraminifera. *Micropaleontology*, 23 (2), pp.155–179. [Online]. Available at: doi:10.2307/1485330.

Bé, A. W. H., Caron, D. A. and Anderson, O. R. (1981). Effects of feeding frequency on life processes of the planktonic foraminifer globigerinoides sacculifer in laboratory culture. *Journal of the Marine Biological Association of the United Kingdom*, 61 (1), pp.257–277. [Online]. Available at: doi:10.1017/S002531540004604X.

Bé, A. W. H., Spero, H. J. and Anderson, O. R. (1982). Effects of symbiont elimination and reinfection on the life processes of the planktonic foraminifer Globigerinoides sacculifer. *Marine Biology*, 70 (1), pp.73–86. [Online]. Available at: doi:10.1007/bf00397298.

Beck, J. et al. (2012). What's on the horizon for macroecology? *Ecography*, 35 (8), pp.673–683. [Online]. Available at: doi:10.1111/j.1600-0587.2012.07364.x.

Belyaeva, N. V. and Burmistrova, I. (1984). Critical levels of carbonates accumulation in the Indian Ocean. *Doklady of the USSR Academy of Sciences Earth Science Section 277:652–655*.

Bemis, B. E. et al. (2000). Temperature influence on the carbon isotopic composition of Globigerina bulloides and Orbulina universa(planktonic foraminifera). *Marine Micropaleontology*, 38 (3–4), pp.213–228. [Online]. Available at: doi:10.1016/S0377-8398(00)00006-2.

Bemis, B. E., Spero, H. J. and Bijma, J. (1998). Reevaluation of the oxygen isotopic composition of planktonic foraminifera. *Paleoceanography*, 13 (2), pp.150–160.

Benton, M. J. (2009). The Red Queen and the Court Jester: and Abiotic Factors Through Time. *Science*, 323 (February), pp.728–732. [Online]. Available at: doi:10.1126/science.1157719.

Bentov, S. and Erez, J. (2006). Impact of biomineralization processes on the Mg content of foraminiferal shells: A biological perspective. *Geochemistry, Geophysics, Geosystems*, 7 (1). [Online]. Available at: doi:https://doi.org/10.1029/2005GC001015 [Accessed 17 May 2021].

Berger, W. H. (1969). Kummerform Foraminifera as Clues to Oceanic Environments. *AAPG Bulletin*, 53 (3), pp.706–706. [Online]. Available at: doi:10.1306/5D25C6C1-16C1-11D7-8645000102C1865D.

Berger, W. H. (1970). Planktonic foraminifera: Selective solution and the lysocline. *Marine Geology*, 8, pp.111–138.

Berger, W. H. (1971). Sedimentation of planktonic foraminifera. *Marine Geology*, 11 (5), pp.325–358. [Online]. Available at: doi:10.1016/0025-3227(71)90035-1.

Berger, W. H. (1973). Deep-Sea carbonates: Pleistocene dissolution cycles. *Journal of Foraminiferal Research*, 3 (4), pp.187–195.

Berger, W. H., Killingley, J. S. and Vincent, E. (1978). Stable Isotopes in Deep-Sea Carbonates: Box Core EDRC-92, West Equatorial Pacific. *STABLE ISOTOPES IN DEEP-SEA CARBONATES: BOX CORE ERDC-92, WEST EQUATORIAL PACIFIC.*

Berggren, W. A. (1969). Rates of Evolution in Some Cenozoic Planktonic Foraminifera. *Micropaleontology*, 15 (3), pp.351–365. [Online]. Available at: doi:10.2307/1484931.

Bijl, P. K. et al. (2010). Transient Middle Eocene Atmospheric CO2 and Temperature Variations. *Science*, 330 (6005), pp.819–821. [Online]. Available at: doi:10.1126/science.1193654.

Bijma, J. et al. (1998). Experimental determination of the ontogenetic stable isotope variability in two morphotypes of Globigerinella siphonifera (d'Orbigny). *Marine Micropaleontology*, 35 (3–4), pp.141–160. [Online]. Available at: doi:10.1016/S0377-8398(98)00017-6.

Bijma, J., Erez, J. and Hemleben, C. (1990). Lunar and semi-lunar reproductive cycles in some spinose planktonic foraminifera. *Journal of Foraminiferal Research*, 20 (2), pp.117–127.

Bijma, J., Faber, W. W. and Hemleben, C. (1990). Temperature and salinity limits for growth and survival of some planktonic foraminifers in laboratory cultures. *The Journal of Foraminiferal Research*, 20 (2), pp.95–116. [Online]. Available at: doi:10.2113/gsjfr.20.2.95.

Bijma, J., Spero, H. J. and Lea, D. W. (1999). Reassessing Foraminiferal Stable Isotope Geochemistry: Impact of the Oceanic Carbonate System (Experimental Results). *Use of Proxies in*

Paleoceanography, (1947), pp.489–512. [Online]. Available at: doi:10.1007/978-3-642-58646-0_20.

Birch, H. et al. (2013). Planktonic foraminifera stable isotopes and water column structure: Disentangling ecological signals. *Marine Micropaleontology*, 101, pp.127–145. [Online]. Available at: doi:10.1016/j.marmicro.2013.02.002.

Birks, H. J. B. (2020). Reflections on the Use of Ecological Attributes and Traits in Quaternary Botany. *Frontiers in Ecology and Evolution*, 8. [Online]. Available at: doi:10.3389/fevo.2020.00166 [Accessed 3 February 2021].

Blackmon, P. D. and Todd, R. (1959). Mineralogy of Some Foraminifera as Related to Their Classification and Ecology. *Journal of Paleontology*, 33 (1), pp.1–15.

Boersma, A. and Premoli Silva, I. (1986). Terminal Eocene Events: Planktonic Foraminifera and Isotopic Evidence. Pomerol, Ch. and Premoli-Silva, I. (Eds). *Developments in Palaeontology and Stratigraphy*, 9, pp.213–223. [Online]. Available at: doi:10.1016/S0920-5446(08)70124-9.

Boersma, A. and Silva, I. P. (1991). Distribution of Paleogene planktonic foraminifera--- analogies with the Recent? *Palaeogeography Palaeoclimatology Palaeoecology*, 83, pp.29–48.

Boersma, A., Silva, I. P. and Shackleton, N. J. (1987). Atlantic Eocene planktonic foraminiferal paleohydrographic indicators and stable isotope paleoceanography. *Paleoceanography*, 2 (3), pp.287–331. [Online]. Available at: doi:10.1029/PA002i003p00287.

Bohaty, S. M. et al. (2009). Coupled greenhouse warming and deep-sea acidification in the middle Eocene. *Paleoceanography*, 24 (December 2008), pp.1–16. [Online]. Available at: doi:10.1029/2008PA001676.

Bohaty, S. M. and Zachos, J. C. (2003). Significant Southern Ocean warming event in the late middle Eocene. *Geology*, 31 (11), pp.1017–1020. [Online]. Available at: doi:10.1130/G19800.1.

Bolker, B. M. et al. (2009). Generalized linear mixed models: a practical guide for ecology and evolution. *Trends in Ecology & Evolution*, 24 (3), pp.127–135. [Online]. Available at: doi:10.1016/j.tree.2008.10.008.

Bolnick, D. I. et al. (2003). The ecology of individuals: incidence and implications of individual specialization. *American Naturalist*, 161 (1), pp.1–28. [Online]. Available at: doi:10.1086/343878.

Bolnick, D. I. et al. (2011). Why intraspecific trait variation matters in community ecology. *Trends in Ecology and Evolution*, 26 (4), pp.183–192. [Online]. Available at: doi:10.1016/j.tree.2011.01.009.

Bolton, A. et al. (2011). Environmental versus biological controls on Mg/Ca variability in Globigerinoides ruber (white) from core top and plankton tow samples in the southwest Pacific Ocean. *Paleoceanography*, 26 (2), pp.1–14. [Online]. Available at: doi:10.1029/2010PA001924.

Boltovskoy, E. and Totah, V. I. (1992). PRESERVATION INDEX AND PRESERVATION POTENTIAL OF SOME FORAMINIFERAL SPECIES Three sets of foraminiferal specimens that consist of different areas do not necessarily have the same test. *Journal of Foraminiferal Research*, 22 (3), pp.267–273.

Boscolo Galazzo, F. et al. (2013). Paleoenvironmental changes during the Middle Eocene Climatic Optimum (MECO) and its aftermath: The benthic foraminiferal record from the Alano section (NE Italy). *Palaeogeography, Palaeoclimatology, Palaeoecology*, 378, pp.22–35. [Online]. Available at: doi:10.1016/j.palaeo.2013.03.018.

Boyé, A. *et al.* (2019) 'Trait-based approach to monitoring marine benthic data along 500 km of coastline', *Diversity and Distributions*, 25(12), pp. 1879–1896. doi:10.1111/ddi.12987.

Boyle, P. R. et al. (2017). Cenozoic North Atlantic deep circulation history recorded in contourite drifts, offshore Newfoundland, Canada. *Marine Geology*, 385 (2017), pp.185–203. [Online]. Available at: doi:10.1016/j.margeo.2016.12.014.

Bralower, T. J. et al. (1995). Late Paleocene to Eocene paleoceanography of the equatorial Pacific Ocean: Stable isotopes recorded at Ocean Drilling Program Site 865, Allison Guyot. *Paleoceanography*, 10 (4), pp.841–865. [Online]. Available at: doi:10.1029/95PA01143.

Bregman, T. P., Sekercioglu, C. H. and Tobias, J. A. (2014). Global patterns and predictors of bird species responses to forest fragmentation: Implications for ecosystem function and conservation. *Biological Conservation*, 169, pp.372–383. [Online]. Available at: doi:10.1016/j.biocon.2013.11.024.

Brombacher, A. et al. (2017). The Breakdown of Static and Evolutionary Allometries during Climatic Upheaval. *The American Naturalist*, pp.000–000. [Online]. Available at: doi:10.1086/692570.

Brombacher, A., Wilson, P. A. and Ezard, T. H. G. (2017). Calibration of the repeatability of foraminiferal test size and shape measures with recommendations for future use. *Marine Micropaleontology*, 133, pp.21–27. [Online]. Available at: doi:10.1016/j.marmicro.2017.05.003.

Brousseau, P.-M., Gravel, D. and Handa, I. T. (2018). On the development of a predictive functional trait approach for studying terrestrial arthropods. *Journal of Animal Ecology*, 87 (5), pp.1209–1220. [Online]. Available at: doi:https://doi.org/10.1111/1365-2656.12834.

Brown, C. M. et al. (2013a). Ecological modelling, size distributions and taphonomic size bias in dinosaur faunas: a comment on Codron et al. (2012). *Biology Letters*, 9 (1), p.20120582. [Online]. Available at: doi:10.1098/rsbl.2012.0582.

Brown, C. M. et al. (2013b). Evidence for taphonomic size bias in the Dinosaur Park Formation (Campanian, Alberta), a model Mesozoic terrestrial alluvial-paralic system. *Palaeogeography, Palaeoclimatology, Palaeoecology*, 372, pp.108–122. [Online]. Available at: doi:10.1016/j.palaeo.2012.06.027.

Brummer, G. A., Hemlebent, C. and Spindlert, M. (1986). Planktonic foraminiferal ontogeny and new perspectives for micropalaeontology. *Nature*, 319 (6048), pp.50–52.

Brun, P., Payne, M.R. and Kiørboe, T. (2017) 'A trait database for marine copepods', *Earth system science data*, 9, pp. 99–113.

Burke, J. E. et al. (2018). Factors influencing test porosity in planktonic foraminifera. *Biogeosciences*, 15 (21), pp.6607–6619. [Online]. Available at: doi:10.5194/bg-15-6607-2018.

Burke, J. E. and Hull, P. M. (2017). Effect of gross morphology on modern planktonic foraminiferal test strength under compression. *Journal of Micropalaeontology*, 2, pp.jmpaleo2016-007. [Online]. Available at: doi:10.1144/jmpaleo2016-007.

Burnham, K. and Anderson, D. (2002). *Model Selection and Multi-Model Inference*. [Online]. Available at: doi:10.1002/1521-3773(20010316)40:6<9823::AID-ANIE9823>3.3.CO;2-C.

Cappelli, C. et al. (2019). The Early to Middle Eocene Transition: An Integrated Calcareous Nannofossil and Stable Isotope Record From the Northwest Atlantic Ocean (Integrated Ocean

Bibliography

Drilling Program Site U1410). *Paleoceanography and Paleoclimatology*, 34 (12), pp.1913–1930. [Online]. Available at: doi:10.1029/2019PA003686.

Cardinale, B. J. et al. (2012). Biodiversity loss and its impact on humanity. *Nature*, 489 (7415), pp.326–326. [Online]. Available at: doi:10.1038/nature11373.

Caromel, A. G. M. et al. (2014). Hydrodynamic constraints on the evolution and ecology of planktic foraminifera. *Marine Micropaleontology*, 106, pp.69–78. [Online]. Available at: doi:10.1016/j.marmicro.2014.01.002.

Caromel, A. G. M., Schmidt, D. N. and Rayfield, E. J. (2017). Ontogenetic constraints on foraminiferal test construction. *Evolution & Development*, 19 (3), pp.157–168. [Online]. Available at: doi:https://doi.org/10.1111/ede.12224.

Carter, A. et al. (2017). Differing oxygen isotopic signals of two Globigerinoides ruber (white) morphotypes in the East China Sea: Implications for paleoenvironmental reconstructions. *Marine Micropaleontology*, 131, pp.1–9. [Online]. Available at: doi:10.1016/j.marmicro.2017.01.001.

Ceballos, G. et al. (2015). Accelerated modern human–induced species losses: Entering the sixth mass extinction. *Science Advances*, 1 (5), p.e1400253. [Online]. Available at: doi:10.1126/sciadv.1400253.

Ceballos, G., Ehrlich, P. R. and Raven, P. H. (2020). Vertebrates on the brink as indicators of biological annihilation and the sixth mass extinction. *Proceedings of the National Academy of Sciences*, 117 (24), pp.13596–13602. [Online]. Available at: doi:10.1073/pnas.1922686117.

Chao, A. et al. (2014). Rarefaction and extrapolation with Hill numbers : a framework for sampling and estimation in species diversity studies. *Ecological Monographs*, 84 (1), pp.45–67.

Chao, A., Chiu, C. H. and Jost, L. (2010). Phylogenetic diversity measures based on Hill numbers. *Philosophical Transactions of the Royal Society B: Biological Sciences*, 365 (1558), pp.3599–3609. [Online]. Available at: doi:10.1098/rstb.2010.0272.

Chao, A., Chiu, C.-H. and Jost, L. (2014). Unifying Species Diversity, Phlogenetic Diversity, Functional Diversity, and related similarity and differentiation measures through Hill numbers. *Annual Review of Ecology, Evolution and Systematics*, 45, pp.297–324.

Chao, A. and Jost, L. (2012). Diversity measures. *Encyclopedia of Theoretical Ecology*, pp.203–207.

Chao, A. and Jost, L. (2015). Estimating diversity and entropy profiles via discovery rates of new species. *Methods in Ecology and Evolution*, 6 (8), pp.873–882. [Online]. Available at: doi:10.1111/2041-210X.12349.

Chernihovsky, N. et al. (2020). The daily resolved temperature dependence and structure of planktonic foraminifera blooms. *Scientific Reports*, 10 (1), p.17456. [Online]. Available at: doi:10.1038/s41598-020-74342-z.

Chiarucci, A., Bacaro, G. and Scheiner, S. M. (2011). Old and new challenges in using species diversity for assessing biodiversity. *Philosophical Transactions of the Royal Society B: Biological Sciences*, 366 (1576), pp.2426–2437. [Online]. Available at: doi:10.1098/rstb.2011.0065.

Chiu, C. H. and Chao, A. (2014). Distance-based functional diversity measures and their decomposition: A framework based on hill numbers. *PLoS ONE*, 9 (7). [Online]. Available at: doi:10.1371/journal.pone.0100014.

Cléroux, C. et al. (2008). Mg/Ca and Sr/Ca ratios in planktonic foraminifera: Proxies for upper water column temperature reconstruction. *Paleoceanography*, 23 (3), p.n/a-n/a. [Online]. Available at: doi:10.1029/2007PA001505..

Colwell, R. K. (2009). Biodiversity: Concepts, Patterns, and Measurement. In: *The Princeton Guide to Ecology*. Princeton, NJ, UDA: Princeton University Press. pp.257–263.

Colwell, R. K., Coddington, J. A. and Hawksworth, D. L. (1994). Estimating terrestrial biodiversity through extrapolation. *Philosophical Transactions of the Royal Society of London. Series B: Biological Sciences*, 345 (1311), pp.101–118. [Online]. Available at: doi:10.1098/rstb.1994.0091.

Constandache, M., Yerly, F. and Spezzaferri, S. (2013). Internal pore measurements on macroperforate planktonic Foraminifera as an alternative morphometric approach. *Swiss Journal of Geosciences*, 106 (2), pp.179–186. [Online]. Available at: doi:10.1007/s00015-013-0134-8.

Coxall, H. K. et al. (2000). Hantkeninid depth adaptation: An evolving life strategy in a changing ocean. *Geology*, 28 (1), pp.87–90. [Online]. Available at: doi:10.1130/0091-7613(2000)28<87:HDAAEL>2.0.CO.

Coxall, H. K. et al. (2005). Rapid stepwise onset of Antarctic glaciation and deeper calcite compensation in the Pacific Ocean. *Nature*, 433 (7021), pp.53–57. [Online]. Available at: doi:10.1038/nature03135.

Coxall, H. K. et al. (2007). Iterative Evolution of Digitate Planktonic Foraminifera. *Paleobiology*, 33 (4), pp.495–516. [Online]. Available at: doi:10.2307/4500169.

Cramer, B. S. et al. (2009). Ocean overturning since the Late Cretaceous : Inferences from a new benthic foraminiferal isotope compilation. *Paleoceanography*, 24 (July), pp.1–14. [Online]. Available at: doi:10.1029/2008PA001683.

Cramwinckel, M. J. et al. (2018). Synchronous tropical and polar temperature evolution in the Eocene. *Nature*, 559 (7714), pp.382–386. [Online]. Available at: doi:10.1038/s41586-018-0272-2.

Cramwinckel, M. J. et al. (2019). Harmful algae and export production collapse in the equatorial Atlantic during the zenith of Middle Eocene Climatic Optimum warmth. *Geology*, 47 (3), pp.247–250. [Online]. Available at: doi:10.1130/G45614.1.

Creech, J. B. et al. (2010). Eocene sea temperatures for the mid-latitude southwest Pacific from Mg/Ca ratios in planktonic and benthic foraminifera. *Earth and Planetary Science Letters*, 299 (3–4), pp.483–495. [Online]. Available at: doi:10.1016/j.epsl.2010.09.039.

Crutsinger, G. M. (2006). Plant Genotypic Diversity Predicts Community Structure and Governs an Ecosystem Process. *Science*, 313 (5789), pp.966–968. [Online]. Available at: doi:10.1126/science.1128326.

Currano, E. D. et al. (2017). *Fossil insect folivory tracks paleotemperature for six million years Published by : Wiley on behalf of the Ecological Society of America Stable URL : http://www.jstor.org/stable/20787449 REFERENCES Linked references are available on JSTOR for this article*. 80 (4), pp.547–567.

Damassa, T. D. et al. (2006). Enhanced multidecadal climate variability in the seventeenth century from coral isotope records in the western Indian Ocean. *Paleoceanography*, 21 (2). [Online]. Available at: doi:10.1029/2005PA001217.

Bibliography

Dangles, O. and Crespo Pérez, V. (2020). Editorial overview: Devastating locust swarms and pandemics: the same pressing need for sustainability science. *Current Opinion in Insect Science*, 40, pp.v–ix. [Online]. Available at: doi:10.1016/j.cois.2020.08.004.

Darling, K. F. et al. (1997). Planktic foraminiferal molecular evolution and their polyphyletic origins from benthic taxa. *Marine Micropaleontology*, 30 (4), pp.251–266. [Online]. Available at: doi:10.1016/S0377-8398(96)00057-6.

Darling, K. F. et al. (2009). Surviving mass extinction by bridging the benthic/planktic divide. *Proceedings of the National Academy of Sciences*, 106 (31), pp.12629–12633. [Online]. Available at: doi:10.1073/pnas.0902827106.

Darling, K. F. and Wade, C. M. (2008). The genetic diversity of planktic foraminifera and the global distribution of ribosomal RNA genotypes. *Marine Micropaleontology*, 67 (3–4), pp.216–238. [Online]. Available at: doi:10.1016/j.marmicro.2008.01.009.

Davis, C. V. et al. (2020). Extensive morphological variability in asexually produced planktic foraminifera. *Science Advances*, 6 (28), p.eabb8930. [Online]. Available at: doi:10.1126/sciadv.abb8930.

Dekens, P. S. et al. (2002). Core top calibration of Mg/Ca in tropical foraminifera: Refining paleotemperature estimation*. *Geochemistry Geophysics Geosystems*, 3 (4), pp.1–29. [Online]. Available at: doi:10.1029/2001gc000200.

Di Martino, E. and Liow, L. H. (2021). Trait–fitness associations do not predict within-species phenotypic evolution over 2 million years. *Proceedings of the Royal Society B: Biological Sciences*, 288 (1943), p.20202047. [Online]. Available at: doi:10.1098/rspb.2020.2047.

Diamond, J. (1984). 'Normal' extinctions of isolated populations. In: Nitecki, M. H. (Ed). *Extinctions*. pp.191–246.

Dinno, A. (2018). *paran: Horn's Test Of Principal Components/Factors*.

Dirzo, R. et al. (2014). Defaunation in the Anthropocene. *Science*, 345 (6195), pp.401–406. [Online]. Available at: doi:10.1126/science.1251817.

Doncaster, C. P. et al. (2016). Early warning of critical transitions in biodiversity from compositional disorder. *Ecology*, 97 (11), pp.3079–3090. [Online]. Available at: doi:10.1002/ecy.1558.

Donohue, I. et al. (2016). Navigating the complexity of ecological stability. *Ecology letters*, 19 (9), pp.1172–1185. [Online]. Available at: doi:10.1111/ele.12648.

Dueñas-Bohórquez, A. et al. (2011). Interindividual variability and ontogenetic effects on Mg and Sr incorporation in the planktonic foraminifer Globigerinoides sacculifer. *Geochimica et Cosmochimica Acta*, 75 (2), pp.520–532. [Online]. Available at: doi:10.1016/j.gca.2010.10.006.

Dunson, W. A. and Travis, J. (1991). The Role of Abiotic Factors in Community Organization. *American Naturalist*, 138 (5), pp.1067–1091. [Online]. Available at: doi:10.2307/2678832.

Dutton, A., Lohmann, K. C. and Leckie, R. M. (2005). Insights from the Paleogene tropical Pacific: Foraminiferal stable isotope and elemental results from Site 1209, Shatsky Rise. *Paleoceanography*, 20 (3). [Online]. Available at: doi:10.1029/2004PA001098 [Accessed 28 October 2020].

Edgar, K. M. et al. (2007). No extreme bipolar glaciation during the main Eocene calcite compensation shift. *Nature*, 448 (August), pp.908–911. [Online]. Available at: doi:10.1038/nature06053.

Edgar, K. M. et al. (2013). Symbiont 'bleaching' in planktic foraminifera during the Middle Eocene Climatic Optimum. *Geology*, 41 (1), pp.15–18. [Online]. Available at: doi:10.1130/G33388.1.

Edgar, K. M. et al. (2020). New composite bio- and isotope stratigraphies spanning the Middle Eocene Climatic Optimum at tropical ODP Site 865 in the Pacific Ocean. *Journal of Micropalaeontology*, 39 (2), pp.117–138. [Online]. Available at: doi:10.5194/jm-39-117-2020.

Edgar, K. M., Hull, P. M. and Ezard, T. H. G. G. (2017). Evolutionary history biases inferences of ecology and environment from δ13C but not δ18O values. *Nature Communications*, 8 (1), pp.1106–1106. [Online]. Available at: doi:10.1038/s41467-017-01154-7.

Eggins, S. M., De Deckker, P. and Marshall, J. (2003). Mg/Ca variation in planktonic foraminifera tests: implications for reconstructing palaeo-seawater temperature and habitat migration. *Earth and Planetary Science Letters*, 212 (3–4), pp.291–306. [Online]. Available at: doi:10.1016/S0012-821X(03)00283-8.

Eggins, S. M., Sadekov, A. and De Deckker, P. (2004). Modulation and daily banding of Mg/Ca in Orbulina universa tests by symbiont photosynthesis and respiration: a complication for seawater thermometry? *Earth and Planetary Science Letters*, 225 (3), pp.411–419. [Online]. Available at: doi:10.1016/j.epsl.2004.06.019.

Elderfield, H., Vautravers, M. and Cooper, M. (2002). The relationship between shell size and Mg/Ca, Sr/Ca, D 18 O, and D 13 C of species of planktonic foraminifera. *Geochemistry, Geophysics, Geosystems*, 3 (8), pp.1–13. [Online]. Available at: doi:10.1029/2001GC000194.

Ellison, A. M. (2010). Partitioning diversity. *Ecology*, pp.1962–1963. [Online]. Available at: doi:10.1890/09-1692.1.

Emiliani, C. (1954). Depth habitats of some species of pelagic Foraminifera as indicated by oxygen isotope ratios. *American Journal of Science*, 252 (3), pp.149–158. [Online]. Available at: doi:10.2475/ajs.252.3.149.

Enquist, B. J. et al. (2016). *Cyberinfrastructure for an integrated botanical information network to investigate the ecological impacts of global climate change on plant biodiversity*. PeerJ Inc. [Online]. Available at: doi:10.7287/peerj.preprints.2615v2 [Accessed 10 February 2021].

Epstein, S. et al. (1951). Carbonate-Water isotopic Tempreature Scale. *Bulletin of the geological society of Americaociety of America*, 62 (April), pp.417–426.

Epstein, S. et al. (1953). Revised Carbonate-Water isotopic temperature scale. *GSA Bulletin*, 64 (11), pp.1315–1326. [Online]. Available at: doi:10.1130/0016-7606(1953)64[1315:RCITS]2.0.CO;2.

Epstein, S. and Lowenstam, H. A. (1954). Temperature-Shell-Growth Relations of Recent and Interglacial Pleistocene Shoal-Water Biota from Bermuda. *The Journal of Geology*, 61 (5), pp.424–438. [Online]. Available at: doi:10.1086/626110.

Erez, J. (1978). Vital effect on stable-isotope composition seen in foraminifera and coral skeletons. *Nature*, 273 (5659), pp.199–202. [Online]. Available at: doi:10.1038/273199a0.

Erez, J. and Luz, B. (1983). Experimental paleotemperature equation for planktonic foraminifera. *Geochimica et Cosmochimica Acta*, 47 (6), pp.1025–1031. [Online]. Available at: doi:10.1016/0016-7037(83)90232-6.

Bibliography

Eronen, J. T. et al. (2010). Ecometrics: The traits that bind the past and present together. *Integrative Zoology*, 5 (2), pp.88–101. [Online]. Available at: doi:10.1111/j.1749-4877.2010.00192.x.

Estes, L. et al. (2018). The spatial and temporal domains of modern ecology. *Nature Ecology and Evolution*, 2 (5), pp.819–826. [Online]. Available at: doi:10.1038/s41559-018-0524-4.

Evans, D. et al. (2016). Revisiting carbonate chemistry controls on planktic foraminifera Mg / Ca: Implications for sea surface temperature and hydrology shifts over the Paleocene-Eocene Thermal Maximum and Eocene-Oligocene transition. *Climate of the Past*, 12 (4), pp.819–835. [Online]. Available at: doi:10.5194/cp-12-819-2016.

Evans, D. and Mller, W. (2012). Deep time foraminifera Mg/Ca paleothermometry: Nonlinear correction for secular change in seawater Mg/Ca. *Paleoceanography*, 27 (4), pp.1–11. [Online]. Available at: doi:10.1029/2012PA002315.

Eyring, V. et al. (2021). Human Influence on the Climate System. In: *Climate Change 2021: The Physical Science Basis.* Sixth Assessment Report of the Intergovernmental Panel on Climate Change. Cambridge Univeristy Press.

Ezard, T. H. G. et al. (2011). Interplay Between Changing Climate and Species' Ecology Drives Macroevolutionary Dynamics. *Science*, 332 (6027), pp.349–351. [Online]. Available at: doi:10.1126/science.1203060.

Ezard, T. H. G., Edgar, K. M. and Hull, P. M. (2015). Environmental and biological controls on size-specific ^{13}C and ^{18}O in recent planktonic foraminifera. *Paleoceanography*, 30 (3), pp.151–173. [Online]. Available at: doi:10.1002/2014PA002735.

Ezard, T. H. G. and Purvis, A. (2016). Environmental changes define ecological limits to species richness and reveal the mode of macroevolutionary competition. *Ecology Letters*, 19 (8), pp.899–906. [Online]. Available at: doi:10.1111/ele.12626.

Ezard, T. H. G., Quental, T. B. and Benton, M. J. (2016). The challenges to inferring the regulators of biodiversity in deep time. *Philosophical transactions of the Royal Society of London. Series B, Biological sciences*, 371 (1691), pp.20150216-. [Online]. Available at: doi:10.1098/rstb.2015.0216.

Fairbanks, R. G. et al. (1982). Vertical distribution and isotopic fractionation of living planktonic foraminifera from the Panama Basin. *Nature*, 298 (5877), pp.841–844. [Online]. Available at: doi:10.1038/298841a0.

Fairbanks, R. G., Wiebe, P. H. and Bé, A. W. H. (1980). Vertical Distribution and Isotopic Composition of Living Planktonic Foraminifera in the Western North Atlantic. *Science*, 207 (4426), pp.61–63. [Online]. Available at: doi:10.1126/science.207.4426.61.

Farnsworth, K. D., Albantakis, L. and Caruso, T. (2017). Unifying concepts of biological function from molecules to ecosystems. *Oikos*, 126 (10), pp.1367–1376. [Online]. Available at: doi:https://doi.org/10.1111/oik.04171.

Fehrenbacher, J. S. et al. (2017). Link between light-triggered Mg-banding and chamber formation in the planktic foraminifera Neogloboquadrina dutertrei. *Nature Communications*, 8 (May), pp.1–10. [Online]. Available at: doi:10.1038/ncomms15441.

Fehrenbacher, J. S. et al. (2018). Ba/Ca ratios in the non-spinose planktic foraminifer Neogloboquadrina dutertrei: Evidence for an organic aggregate microhabitat. *Geochimica et Cosmochimica Acta*, 236, pp.361–372. [Online]. Available at: doi:10.1016/j.gca.2018.03.008.

Fenton, I. S. et al. (2016a). Environmental predictors of diversity in recent planktonic foraminifera as recorded in marine sediments. *PLoS ONE*, 11 (11), pp.1–22. [Online]. Available at: doi:10.1371/journal.pone.0165522.

Fenton, I. S. et al. (2016b). The impact of Cenozoic cooling on assemblage diversity in planktonic foraminifera. *Philosophical transactions of the Royal Society of London. Series B, Biological sciences*, 371 (1691), p.20150224. [Online]. Available at: doi:10.1098/rstb.2015.0224.

Fenton, I. S. et al. (2021). Triton, a new species-level database of Cenozoic planktonic foraminiferal occurrences. *Scientific Data*, 8 (1), p.160. [Online]. Available at: doi:10.1038/s41597-021-00942-7.

Fordham, D. A. et al. (2020). Using paleo-archives to safeguard biodiversity under climate change. *Science*, 369 (6507). [Online]. Available at: doi:10.1126/science.abc5654 [Accessed 2 September 2020].

Fortelius, M. et al. (2016). An ecometric analysis of the fossil mammal record of the Turkana Basin. *Philosophical Transactions of the Royal Society B: Biological Sciences*, 371 (1698), p.20150232. [Online]. Available at: doi:10.1098/rstb.2015.0232.

Fraass, A. J., Kelly, D. C. and Peters, S. E. (2015). Macroevolutionary History of the Planktic Foraminifera. *Annual Review of Earth and Planetary Sciences*, 43 (1), pp.139–166. [Online]. Available at: doi:10.1146/annurev-earth-060614-105059.

Fraley, C. and Raftery, A. E. (1996). Model-based methods of classification: Using the mclust software in chemometrics. *Journal of Statistical Software*, 18 (6), pp.1–13.

Fried, G. et al. (2019). Functional traits modulate plant community responses to alien plant invasion. *Perspectives in Plant Ecology, Evolution and Systematics*, 37, pp.53–63. [Online]. Available at: doi:10.1016/j.ppees.2019.02.003.

Friedrich, O. et al. (2012). Influence of test size, water depth, and ecology on Mg/Ca, Sr/Ca, δ 18O and δ 13C in nine modern species of planktic foraminifers. *Earth and Planetary Science Letters*, 319–320, pp.133–145. [Online]. Available at: doi:10.1016/j.epsl.2011.12.002.

Galazzo, F. B. et al. (2014). The middle Eocene climatic optimum (MECO): A multiproxy record of paleoceanographic changes in the southeast Atlantic (ODP Site 1263, Walvis Ridge). *Paleoceanography*, pp.1143–1161. [Online]. Available at: doi:10.1002/2014PA002670.Received.

Galazzo, F. B. et al. (2015). The planktic foraminifer Planorotalites in the Tethyan middle Eocene. *Journal of Micropalaeontology*, pp.2014–2030. [Online]. Available at: doi:10.1144/jmpaleo2014-030.

Gaston, K. J. (2008). Biodiversity and extinction: the importance of being common. *Progress in Physical Geography*, 32 (1), pp.73–79. [Online]. Available at: doi:10.1177/0309133308089499.

Gaston, K. J. and Fuller, R. A. (2007). Biodiversity and extinction. *Progress in Physical Geography*, 31 (2), pp.213–225. [Online]. Available at: doi:10.1177/0309133307076488.

gbif.org. (2020). *GBIF: The Global Biodiversity Information Facility (2021) What is GBIF?.* [Online]. Available at: https://www.gbif.org/what-is-gbif.

Gebhardt, H. et al. (2013). Middle to Late Eocene paleoenvironmental changes in a marine transgressive sequence from the northern Tethyan margin (Adelholzen, Germany). *Austrian journal of earth sciences : an international journal of the Austrian Geological Society*, 106 (2), pp.45–72.

Bibliography

Gill, B. J. and Martinson, P. (1991). *New Zealand's Extinct Birds*. Random Century. [Online]. Available at: https://books.google.co.uk/books?id=3qTwAAAAMAAJ.

Gillies, C. S. et al. (2006). Application of random effects to the study of resource selection by animals. *Journal of Animal Ecology*, 75 (4), pp.887–898. [Online]. Available at: doi:10.1111/j.1365-2656.2006.01106.x.

Glaubke, R. H. et al. (2021). Discerning Changes in High-Frequency Climate Variability Using Geochemical Populations of Individual Foraminifera. *Paleoceanography and Paleoclimatology*, 36 (2), p.e2020PA004065. [Online]. Available at: doi:https://doi.org/10.1029/2020PA004065.

Godhe, A. and Rynearson, T. (2017) 'The role of intraspecific variation in the ecological and evolutionary success of diatoms in changing environments', *Philosophical Transactions of the Royal Society B: Biological Sciences*, 372(1728), p. 20160399. doi:10.1098/rstb.2016.0399.

Gradstein, F. M. et al. (2012). *The geologic time scale 2012*. elsevier.

Gray, W. R. et al. (2018). The effects of temperature, salinity, and the carbonate system on Mg/Ca in Globigerinoides ruber (white): A global sediment trap calibration. *Earth and Planetary Science Letters*, 482, pp.607–620. [Online]. Available at: doi:10.1016/j.epsl.2017.11.026.

Greenwood, D. R. et al. (2004). Paleotemperature estimation using leaf-margin analysis: Is Australia different? *Palaios*, 19 (2), pp.129–142. [Online]. Available at: doi:10.1669/0883-1351(2004)019<0129:PEULAI>2.0.CO;2.

Grenié, M. et al. (2018). Functional rarity of coral reef fishes at the global scale: Hotspots and challenges for conservation. *Biological Conservation*, 226, pp.288–299. [Online]. Available at: doi:10.1016/j.biocon.2018.08.011.

Groeneveld, J., Ho, S. L. and Mohtadi, M. (2019). *Deciphering the Variability in Mg / Ca and Stable Oxygen Isotopes of Individual Foraminifera Paleoceanography and Paleoclimatology*. pp.755–773. [Online]. Available at: doi:10.1029/2018PA003533.

Guo, Z., Zhang, L. and Li, Y. (2010). Increased Dependence of Humans on Ecosystem Services and Biodiversity. *PLOS ONE*, 5 (10), p.e13113. [Online]. Available at: doi:10.1371/journal.pone.0013113.

Hallmann, C. A. et al. (2017). More than 75 percent decline over 27 years in total flying insect biomass in protected areas. *PLOS ONE*, 12 (10), p.e0185809. [Online]. Available at: doi:10.1371/journal.pone.0185809.

Hallock, P., Silva, I. P. and Boersma, A. (1991). Similarities between planktonic and larger foraminiferal evolutionary trends through Paleogene paleoceanographic changes. *Palaeogeography Palaeoclimatology Palaeoecology*, 83, pp.49–64.

Hannisdal, B. et al. (2017). Common species link global ecosystems to climate change: dynamical evidence in the planktonic fossil record. *Proceedings of the Royal Society B: Biological Sciences*, 284 (1858), p.20170722. [Online]. Available at: doi:10.1098/rspb.2017.0722.

Hart, M. B. et al. (2003). The search for the origin of the planktic Foraminifera. *Journal of the Geological Society*, 160 (3), pp.341–343. [Online]. Available at: doi:10.1144/0016-764903-003.

Hart, S. P., Schreiber, S. J. and Levine, J. M. (2016a). How variation between individuals affects species coexistence. *Ecology Letters*, 19 (8), pp.825–838. [Online]. Available at: doi:10.1111/ele.12618.

Hart, S. P., Schreiber, S. J. and Levine, J. M. (2016b). How variation between individuals affects species coexistence. *Ecology Letters*, 19 (8), pp.825–838. [Online]. Available at: doi:10.1111/ele.12618.

Hautmann, M. (2020). What is macroevolution? *Palaeontology*, 63 (1), pp.1–11. [Online]. Available at: doi:10.1111/pala.12465.

Hemleben, C. et al. (1991). Surface Texture and the First Occurrence of Spines in Planktonic Foraminifera from the Early Tertiary. *Geol. Jb. A*, 128, pp.117–146.

Hemleben, C., Spindler, M. and Anderson, O. R. (1989). *Modern planktonic foraminifera*. New York: Springer verlag.

Hendricks, J. R. et al. (2014). The Generification of the Fossil RecordGENERIFICATION OF THE FOSSIL RECORD. *Paleobiology*, 40 (4), pp.511–528. [Online]. Available at: doi:10.1666/13076.

Henehan, M. J. et al. (2017). Size-dependent response of foraminiferal calcification to seawater carbonate chemistry. *Biogeosciences*, 14 (13), pp.3287–3308. [Online]. Available at: doi:https://doi.org/10.5194/bg-14-3287-2017.

Henehan, M. J. et al. (2020). Revisiting the Middle Eocene Climatic Optimum “Carbon Cycle Conundrum” With New Estimates of Atmospheric pCO2 From Boron Isotopes. *Paleoceanography and Paleoclimatology*, 35 (6), p.e2019PA003713. [Online]. Available at: doi:https://doi.org/10.1029/2019PA003713.

Henn, J. J. et al. (2018). Intraspecific Trait Variation and Phenotypic Plasticity Mediate Alpine Plant Species Response to Climate Change. *Frontiers in Plant Science*, 9, p.1548. [Online]. Available at: doi:10.3389/fpls.2018.01548.

Heritier-Robbins, P. et al. (2021). Beach sand oil spills select for generalist microbial populations. *The ISME Journal*, pp.1–5. [Online]. Available at: doi:10.1038/s41396-021-01017-6.

Hernitz Kucenjak, M. (2014). The test size and abundance variations in planktonic foraminifera Chiloguembelina cubensis and C. Ototara as response to climatic events in the Oligocene. *Rendiconti online della Società Geologica Italiana*, 31, pp.103–104. [Online]. Available at: doi:10.3301/ROL.2014.68.

Hill, M. O. (1973). Diversity and Evenness: A Unifying Notation and Its Consequences. *Ecology*, 54 (2), pp.427–432. [Online]. Available at: doi:10.2307/1934352.

Hohenegger, J. (2014). Species as the basic units in evolution and biodiversity: Recognition of species in the Recent and geological past as exemplified by larger foraminifera. *Gondwana Research*, 25 (2), pp.707–728. [Online]. Available at: doi:10.1016/j.gr.2013.09.009.

Holland, K. et al. (2020). Constraining multiple controls on planktic foraminifera Mg/Ca. *Geochimica et Cosmochimica Acta*. [Online]. Available at: doi:10.1016/j.gca.2020.01.015.

Hönisch, B. et al. (2003). The influence of symbiont photosynthesis on the boron isotopic composition of foraminifera shells. *Marine Micropaleontology*, 49 (1–2), pp.87–96. [Online]. Available at: doi:10.1016/S0377-8398(03)00030-6.

Hönisch, B. *et al.* (2013) ‘The influence of salinity on Mg/Ca in planktic foraminifers - Evidence from cultures, core-top sediments and complementary δ18O’, *Geochimica et Cosmochimica Acta*, 121, pp. 196–213. doi:10.1016/j.gca.2013.07.028.

Bibliography

Hsiang, A. Y., Elder, L. E. and Hull, P. M. (2016). Towards a morphological metric ofassemblage dynamics in the fossil record a test case using planktonic foraminifera.pdf. *Philosophical transactions of the Royal Society of London. Series B, Biological sciences*, 371, pp.1–24.

Huber, B. T., Bijma, J. and Darling, K. (1997). Cryptic speciation in the living planktonic foraminifer Globigerinella siphonifera (d'Orbigny). *Paleobiology*, 23 (1), pp.33–62. [Online]. Available at: doi:10.2307/2401156.

Hunt, G. and Roy, K. (2006) 'Climate change, body size evolution, and Cope's Rule in deep-sea ostracodes', *Proceedings of the National Academy of Sciences*, 103(5), pp. 1347–1352. doi:10.1073/pnas.0510550103.

Hutchinson, D. K. et al. (2021). The Eocene–Oligocene transition: a review of marine and terrestrial proxy data, models and model–data comparisons. *Climate of the Past*, 17 (1), pp.269–315. [Online]. Available at: doi:https://doi.org/10.5194/cp-17-269-2021.

Imura, D., Toquenaga, Y. and Fujii, K. (2003). Genetic variation can promote system persistence in an experimental host-parasitoid system. *Population Ecology*, 45 (3), pp.205–212. [Online]. Available at: doi:10.1007/s10144-003-0154-8.

Ishino, S. and Suto, I. (2020). Late Pliocene sea-ice expansion and its influence on diatom species turnover in the Southern Ocean. *Marine Micropaleontology*, 160, p.101895. [Online]. Available at: doi:10.1016/j.marmicro.2020.101895.

Ivanova, E. V. (2009). Paleoceanography of the Northern Indian Ocean: Linkages to Monsoon and Global Thermohaline Paleocirculation. In: *The Global Thermohaline Paleocirculation*. Dordrecht: Springer Netherlands. pp.107–145. [Online]. Available at: doi:10.1007/978-90-481-2415-2_5.

Jablonski, D. and Finarelli, J. A. (2009). Congruence of morphologically-defined genera with molecular phylogenies. *Proceedings of the National Academy of Sciences*, 106 (20), pp.8262–8266. [Online]. Available at: doi:10.1073/pnas.0902973106.

Jackson, S. T. and Blois, J. L. (2015). Community ecology in a changing environment: Perspectives from the Quaternary. *Proceedings of the National Academy of Sciences*, 112 (16), pp.4915–4921. [Online]. Available at: doi:10.1073/pnas.1403664111.

Jackson, S. T. and Overpeck, J. T. (2000). Responses of plant populations and communities to environmental changes of the late Quaternary. *Paleobiology*, 26 (S4), pp.194–220. [Online]. Available at: doi:10.1017/S0094837300026932.

Jax, K. (2005). Function and "functioning" in ecology: what does it mean? *Oikos*, 111 (3), pp.641–648. [Online]. Available at: doi:10.1111/j.1600-0706.2005.13851.x.

Jehle, S. et al. (2019). Paleoceanographic changes across the Latest Danian Event in the South Atlantic Ocean and planktic foraminiferal response. *Palaeogeography, Palaeoclimatology, Palaeoecology*, p.#pagerange#-#pagerange#. [Online]. Available at: doi:10.1016/J.PALAEO.2019.03.024.

Jochum, K. P. et al. (2007). GeoReM: A New Geochemical Database for Reference Materials and Isotopic Standards. *Geostandards and Geoanalytical Research*, 29 (3). [Online]. Available at: https://onlinelibrary.wiley.com/doi/10.1111/j.1751-908X.2005.tb00904.x [Accessed 21 April 2020].

Jochum, K. P. et al. (2011). Determination of Reference Values for NIST SRM 610–617 Glasses Following ISO Guidelines. *Geostandards and Geoanalytical Research*, 35 (4), pp.397–429. [Online]. Available at: doi:https://doi.org/10.1111/j.1751-908X.2011.00120.x.

Jonkers, L. and Kučera, M. (2017). Quantifying the effect of seasonal and vertical habitat tracking on planktonic foraminifera proxies. *Climate of the Past*, 13 (6), pp.573–586. [Online]. Available at: doi:10.5194/cp-13-573-2017.

Jost, L. (2007). PARTITIONING DIVERSITY INTO INDEPENDENT ALPHA AND BETA COMPONENTS. *Ecology*, 88 (10), pp.2427–2439. [Online]. Available at: doi:10.1002/ecy.1730.

Jost, L. (2010a). Independence of alpha and beta diversities. *Ecology*, 91 (7), pp.1969–1974. [Online]. Available at: doi:10.1890/09-0368.1.

Jost, L. (2010b). The Relation between Evenness and Diversity. *Diversity*, 2, pp.207–232. [Online]. Available at: doi:10.3390/d2020207.

Jung, V. et al. (2010). Intraspecific variability and trait-based community assembly. *Journal of Ecology*, 98 (5), pp.1134–1140. [Online]. Available at: doi:10.1111/j.1365-2745.2010.01687.x.

Kang, S. et al. (2016). Hill number as a bacterial diversity measure framework with high-throughput sequence data. *Scientific Reports*, 6 (1), p.38263. [Online]. Available at: doi:10.1038/srep38263.

Kattge, J. et al. (2020). TRY plant trait database – enhanced coverage and open access. *Global Change Biology*, 26 (1), pp.119–188. [Online]. Available at: doi:https://doi.org/10.1111/gcb.14904.

Kaufman, L. (1992). Catastrophic Change in Species-Rich Freshwater Ecosystems. *BioScience*, 42 (11), pp.846–858. [Online]. Available at: doi:10.2307/1312084.

Kawahata, H. (2005). Stable isotopic composition in the subtropical Gtobigerinoi des ruber (white) in the North Pacific identified. *Paleontological Research*, 9 (1), pp.27–35.

Kearns, L. E. et al. (2021). Searching for Function: Reconstructing Adaptive Niche Changes Using Geochemical and Morphological Data in Planktonic Foraminifera. *Frontiers in Ecology and Evolution*, 9. [Online]. Available at: doi:10.3389/fevo.2021.679722 [Accessed 6 July 2021].

Keller, G. (1983). Paleoclimatic analyses of middle Eocene through Oligocene planktic foraminiferal faunas. *Palaeogeography, Palaeoclimatology, Palaeoecology*, 43 (1), pp.73–94. [Online]. Available at: doi:10.1016/0031-0182(83)90049-4.

Keller, G., MacLeod, N. and Barrera, E. (1992). Eocene-Oligocene Faunal Turnover in Planktic Foraminifera, and Antarctic Glaciation. In: *Eocene-Oligocene Climatic and Biotic Evolution*. Princeton University Press. pp.218–244. [Online]. Available at: https://www.degruyter.com/document/doi/10.1515/9781400862924.218/html [Accessed 13 July 2021].

Kelly, D. C., Bralower, T. J. and Zachos, J. C. (1997). Evolutionary consequences of the latest Paleocene thermal maximum for tropical planktonic foraminifera. *Palaeogeography, Palaeoclimatology, Palaeoecology*, 141 (1–2), pp.139–161. [Online]. Available at: doi:10.1016/S0031-0182(98)00017-0.

Kisakürek, B. et al. (2008). Controls on shell Mg/Ca and Sr/Ca in cultured planktonic foraminiferan, Globigerinoides ruber (white). *Earth and Planetary Science Letters*, 273 (3–4), pp.260–269. [Online]. Available at: doi:10.1016/j.epsl.2008.06.026.

Kleyer, M. et al. (2008). The LEDA Traitbase: a database of life-history traits of the Northwest European flora. *Journal of Ecology*, 96 (6), pp.1266–1274. [Online]. Available at: doi:https://doi.org/10.1111/j.1365-2745.2008.01430.x.

Bibliography

Kling, M. M. et al. (2020). Multiple axes of ecological vulnerability to climate change. *Global Change Biology*, 26 (5), pp.2798–2813. [Online]. Available at: doi:10.1111/gcb.15008.

Kontakiotis, G. et al. (2017). Morphological recognition of Globigerinoides ruber morphotypes and their susceptibility to diagenetic alteration in the eastern Mediterranean Sea. *Journal of Marine Systems*, 174, pp.12–24. [Online]. Available at: doi:10.1016/j.jmarsys.2017.05.005.

Kretschmer, K. et al. (2018). Modeling seasonal and vertical habitats of planktonic foraminifera on a global scale. *Biogeosciences*, 15 (14), pp.4405–4429. [Online]. Available at: doi:10.5194/bg-15-4405-2018.

Kroon and the Shipboard Scientific Party. (2010). *Tropical temperature history during Paleogene Global Warming (GLOW) events NIOZ Site Survey Cruise Report*.

Kucera, M. et al. (2005). Reconstruction of sea-surface temperatures from assemblages of planktonic foraminifera: multi-technique approach based on geographically constrained calibration data sets and its application to glacial Atlantic and Pacific Oceans. *Quaternary Science Reviews*, 24 (7), pp.951–998. [Online]. Available at: doi:10.1016/j.quascirev.2004.07.014.

Kucera, M. (2007). Chapter Six: Planktonic Foraminifera as Tracers of Past Oceanic Envrionments. In: *Proxies in Late Cenozoic Paleoceanography*. 1. Elsevier. pp.213–262.

Kucera, M. et al. (2017). Caught in the act: anatomy of an ongoing benthic–planktonic transition in a marine protist. *Journal of Plankton Research*, 39 (3), pp.436–449. [Online]. Available at: doi:10.1093/plankt/fbx018.

Kuroyanagi, A. et al. (2008). The occurrence of two genotypes of the planktonic foraminifer Globigerinoides ruber (white) and paleo-environmental implications. *Marine Micropaleontology*, 68 (3–4), pp.236–243. [Online]. Available at: doi:10.1016/j.marmicro.2008.04.004.

Kuroyanagi, A. and Kawahata, H. (2004). Vertical distribution of living planktonic foraminifera in the seas around Japan. *Marine Micropaleontology*, 53 (1–2), pp.173–196. [Online]. Available at: doi:10.1016/j.marmicro.2004.06.001.

Labandeira, C. C., Johnson, K. R. and Wilf, P. (2002). Impact of the terminal Cretaceous event on plant-insect associations. *Proceedings of the National Academy of Sciences*, 99 (4), pp.2061–2066. [Online]. Available at: doi:10.1073/pnas.042492999.

Lacourse, T. (2009). Environmental change controls postglacial forest dynamics through interspecific differences in life-history traits. *Ecology*, 90 (8), pp.2149–2160. [Online]. Available at: doi:https://doi.org/10.1890/08-1136.1.

Lagomarsino, L. P. et al. (2016). The abiotic and biotic drivers of rapid diversification in Andean bellflowers (Campanulaceae). *New Phytologist*, 210 (4), pp.1430–1442. [Online]. Available at: doi:10.1111/nph.13920.

Lamanna, C. et al. (2014). Functional trait space and the latitudinal diversity gradient. *Proceedings of the National Academy of Sciences*, 111 (38), pp.13745–13750. [Online]. Available at: doi:10.1073/pnas.1317722111.

Lankau, R. A. and Strauss, S. Y. (2007). Mutual Feedbacks Maintain Both Genetic and Species Diversity in a Plant Community. *Science*, 317 (5844), pp.1561–1563. [Online]. Available at: doi:10.1126/science.1147455.

Larsen, T. H., Williams, N. M. and Kremen, C. (2005). Extinction order and altered community structure rapidly disrupt ecosystem functioning. *Ecology Letters*, 8 (5), pp.538–547. [Online]. Available at: doi:10.1111/j.1461-0248.2005.00749.x.

Lavorel, S. and Garnier, E. (2002). Predicting changes in community composition and ecosystem functioning from plant traits: revisiting the Holy Grail. *Functional Ecology*, 16 (5), pp.545–556. [Online]. Available at: doi:https://doi.org/10.1046/j.1365-2435.2002.00664.x.

Lazarus, D. (1983). Paleontological Society Speciation in Pelagic Protista and Its Study in the Planktonic Microfossil Record : A Review Speciation in pelagic Protista and its study in the planktonic microfossil record : a review. *Paleobiology*, 9 (4), pp.327–340.

Le, J. and Shackleton, N. J. (1992). Carbonate dissolution fluctiations int he western equitorial pacific durign the late qauternary. *Paleoceanography*, 7 (1), pp.21–42.

Lea, D. W. et al. (2002). Reconstructing a 350 ky history of sea level using planktonic Mg/Ca and oxygen isotope records from a Cocos Ridge core. *Quaternary Science Reviews*, 21 (1–3), pp.283–293. [Online]. Available at: doi:10.1016/S0277-3791(01)00081-6.

Lea, D. W., Mashiotta, T. A. and Spero, H. J. (1999). Controls on magnesium and strontium uptake in planktonic foraminifera determined by live culturing. *Geochimica et Cosmochimica Acta*, 63 (16), pp.2369–2379. [Online]. Available at: doi:10.1016/S0016-7037(99)00197-0.

Lennon, J. J. et al. (2004). Contribution of rarity and commonness to patterns of species richness. *Ecology Letters*, 7 (2), pp.81–87. [Online]. Available at: doi:10.1046/j.1461-0248.2004.00548.x.

Leon-rodriguez, L. and Dickens, G. R. (2010). Constraints on ocean acidi fi cation associated with rapid and massive carbon injections : The early Paleogene record at ocean drilling program site 1215 , equatorial Paci fi c Ocean. *Palaeogeography, Palaeoclimatology, Palaeoecology*, 298 (3–4), pp.409–420. [Online]. Available at: doi:10.1016/j.palaeo.2010.10.029.

Li Qianyu and Radford, S. S. (1991). Evolution and biogeography of Paleogene microperforate planktonic foraminifera. *Palaeogeography, Palaeoclimatology, Palaeoecology*, 83 (1), pp.87–115. [Online]. Available at: doi:10.1016/0031-0182(91)90077-5.

Lin, H. L., Wang, W. C. and Hung, G. W. (2004). Seasonal variation of planktonic foraminiferal isotopic composition from sediment traps in the South China Sea. *Marine Micropaleontology*, 53 (3–4), pp.447–460. [Online]. Available at: doi:10.1016/j.marmicro.2004.08.004.

Litchman, E. and Klausmeier, C.A. (2008) 'Trait-Based Community Ecology of Phytoplankton', *Annual Review of Ecology, Evolution, and Systematics*, 39(1), pp. 615–639. doi:10.1146/annurev.ecolsys.39.110707.173549.

Liu, C. and Olsson, R. K. (1992). Evolutionary radiation of microperforate planktonic Foraminifera following the K/T mass extinction event. *The Journal of Foraminiferal Research*, 22 (4), pp.328–346. [Online]. Available at: doi:10.2113/gsjfr.22.4.328.

Liu, L. et al. (2012). Dental functional traits of mammals resolve productivity in terrestrial ecosystems past and present. *Proceedings of the Royal Society B: Biological Sciences*, 279 (1739), pp.2793–2799. [Online]. Available at: doi:10.1098/rspb.2012.0211.

Lončarić, N. et al. (2006). Oxygen isotope ecology of recent planktic foraminifera at the central Walvis Ridge (SE Atlantic). *Paleoceanography*, 21 (3). [Online]. Available at: doi:https://doi.org/10.1029/2005PA001207 [Accessed 4 May 2021].

Löwemark, L. et al. (2005). A test of different factors influencing the isotopic signal of planktonic foraminifera in surface sediments from the northern South China Sea. *Marine Micropaleontology*, 55 (1–2), pp.49–62. [Online]. Available at: doi:10.1016/j.marmicro.2005.02.004.

Lowery, C. M. and Fraass, A. J. (2019). Morphospace expansion paces taxonomic diversification after end Cretaceous mass extinction. *Nature Ecology & Evolution*. [Online]. Available at: doi:10.1038/s41559-019-0835-0.

Luciani, V. et al. (2010). Ecological and evolutionary response of Tethyan planktonic foraminifera to the middle Eocene climatic optimum (MECO) from the Alano section (NE Italy). *Palaeogeography, Palaeoclimatology, Palaeoecology*, 292 (1–2), pp.82–95. [Online]. Available at: doi:10.1016/j.palaeo.2010.03.029.

Luciani, V. et al. (2020). Which was the habitat of early Eocene planktic foraminifer Chiloguembelina? Stable isotope paleobiology from the Atlantic Ocean and implication for paleoceanographic reconstructions. *Global and Planetary Change*, 191, p.103216. [Online]. Available at: doi:10.1016/j.gloplacha.2020.103216.

Luxem, K. E., Ellwood, M. J. and Strzepek, R. F. (2017). Intraspecific variability in Phaeocystis antarctica's response to iron and light stress. *PLOS ONE*, 12 (7), p.e0179751. [Online]. Available at: doi:10.1371/journal.pone.0179751.

Lyle, M. W. et al. (2005). Biogenic sedimentation in the Eocene equatorial Pacific: the stuttering greenhouse and Eocene carbonate compensation depth. *ODP Scientific Results*, 199. [Online]. Available at: doi:10.2973/odp.proc.sr.199.219.2005 [Accessed 2 July 2021].

Lynch-stieglitz, J. et al. (2015). Glacial-interglacial changes in central tropical Pacific surface seawater property gradients. *Paleoceanography*, 30 (5), pp.423–438. [Online]. Available at: doi:10.1002/2014PA002746.

Lyons, K. G. et al. (2005). Rare species and ecosystem functioning. *Conservation Biology*, 19 (4), pp.1019–1024. [Online]. Available at: doi:10.1111/j.1523-1739.2005.00106.x.

Mace, G. M. et al. (2014). Approaches to defining a planetary boundary for biodiversity. *Global Environmental Change*, 28 (1), pp.289–297. [Online]. Available at: doi:10.1016/j.gloenvcha.2014.07.009.

Mace, G. M., Norris, K. and Fitter, A. H. (2012). Biodiversity and ecosystem services: a multilayered relationship. *Trends in Ecology & Evolution*, 27 (1), pp.19–26. [Online]. Available at: doi:10.1016/j.tree.2011.08.006.

Macleod, N., Keller, G. and Kitchell, J. A. (1990). Progenesis in Late Eocene populations of Subbotina linaperta (Foraminifera) from the western Atlantic. *Marine Micropaleontology*, 16 (3), pp.219–240. [Online]. Available at: doi:10.1016/0377-8398(90)90005-7.

Macumber, A. L. et al. (2020). Freshwater Testate Amoebae (Arcellinida) Response to Eutrophication as Revealed by Test Size and Shape Indices. *Frontiers in Ecology and Evolution*, 8. [Online]. Available at: doi:10.3389/fevo.2020.568904 [Accessed 5 February 2021].

Malmgren, B. A. (1987). Differential dissolution of upper Cretaceous planktonic foraminfera from a temperate region of the South Atlantic ocean. *Marine Micropaleontology*, 11, pp.251–271.

Marr, J. P. et al. (2011). Ecological and temperature controls on Mg/Ca ratios of Globigerina bulloides from the southwest Pacific Ocean. *Paleoceanography*, 26 (2), pp.1–15. [Online]. Available at: doi:10.1029/2010PA002059.

Mayr, E. (1942). *Systemetics and the Origin of Species*. New York: Columbia University Press.

Mayr, E. and Ashlock, P. D. (1991). *Principles of systematic biology*. New York: McGraw-Hill.

McClain, C. R., Nunnally, C. and Benfield, M. C. (2019). Persistent and substantial impacts of the Deepwater Horizon oil spill on deep-sea megafauna. *Royal Society Open Science*, 6 (8), p.191164. [Online]. Available at: doi:10.1098/rsos.191164.

McClanahan, T. (1988). Seasonality in East Africa's coastal waters. *Marine Ecology Progress Series*, 44, pp.191–199. [Online]. Available at: doi:10.3354/meps044191.

McConnell, M. C. and Thunell, R. C. (2005). Calibration of the planktonic foraminiferal Mg/Ca paleothermometer: Sediment trap results from the Guaymas Basin, Gulf of California. *Paleoceanography*, 20 (2), p.n/a-n/a. [Online]. Available at: doi:10.1029/2004PA001077.

McGill, B. J. et al. (2006). Rebuilding community ecology from functional traits. *Trends in Ecology & Evolution*, 21 (4), pp.178–185. [Online]. Available at: doi:10.1016/j.tree.2006.02.002.

McGuire, J. L. and Lauer, D. A. (2020). Linking patterns of intraspecific morphology to changing climates. *Journal of Biogeography*, 47 (11), pp.2417–2425. [Online]. Available at: doi:https://doi.org/10.1111/jbi.13954.

McLean, M. *et al.* (2019) 'Trait structure and redundancy determine sensitivity to disturbance in marine fish communities', *Global Change Biology*, 25(10), pp. 3424–3437. doi:10.1111/gcb.14662.

Meilland, J. et al. (2019). *Highly replicated sampling reveals no diurnal vertical migration but stable species-speci fi c vertical habitats in planktonic foraminifera*. 41, pp.127–141. [Online]. Available at: doi:10.1093/plankt/fbz002.

Metcalfe, B., Feldmeijer, W. and Ganssen, G. M. (2019). Oxygen Isotope Variability of Planktonic Foraminifera Provide Clues to Past Upper Ocean Seasonal Variability. *Paleoceanography and Paleoclimatology*, 34 (3), pp.374–393. [Online]. Available at: doi:10.1029/2018PA003475.

Miller, J. I. et al. (2020). Microbial Communities across Global Marine Basins Show Important Compositional Similarities by Depth. *mBio*, 11 (4), pp.e01448-20. [Online]. Available at: doi:10.1128/mBio.01448-20.

Moebius, I. et al. (2015). Episodes of intensified biological productivity in the subtropical Atlantic Ocean during the termination of the Middle Eocene Climatic Optimum (MECO). *Paleoceanography*, 30 (8), pp.1041–1058. [Online]. Available at: doi:10.1002/2014PA002673.

Mohtadi, M. et al. (2009). Low-latitude control on seasonal and interannual changes in planktonic foraminiferal flux and shell geochemistry off south Java: A sediment trap study. *Paleoceanography*, 24 (1). [Online]. Available at: doi:https://doi.org/10.1029/2008PA001636 [Accessed 4 May 2021].

Montoya, J. M., Donohue, I. and Pimm, S. L. (2017). Planetary Boundaries for Biodiversity: Implausible Science, Pernicious Policies. *Trends in Ecology and Evolution*, 33 (2), pp.71–73. [Online]. Available at: doi:10.1016/j.tree.2017.10.004.

Morard, R. et al. (2015). PFR ^{2} : a curated database of planktonic foraminifera 18S ribosomal DNA as a resource for studies of plankton ecology, biogeography and evolution. *Molecular Ecology Resources*, 15 (6), pp.1472–1485. [Online]. Available at: doi:10.1111/1755-0998.12410.

Bibliography

Morard, R. et al. (2019). Genetic and morphological divergence in the warm-water planktonic foraminifera genus Globigerinoides. *PLoS ONE*, 14 (12). [Online]. Available at: doi:10.1371/journal.pone.0225246.

Nadeau, C. P. and Urban, M. C. (2019). Eco-evolution on the edge during climate change. *Ecography*, p.ecog.04404. [Online]. Available at: doi:10.1111/ecog.04404.

Naik, S. S. (2016). A comparison of Mg/Ca ratios in Globigerinoides ruber (white): sensu stricto versus a mixture of genotypes. *Journal of the Geological Society of India*, 87 (3), pp.323–326. [Online]. Available at: doi:10.1007/s12594-016-0399-4.

Nevoux, M. et al. (2010). Bet-hedging response to environmental variability, an intraspecific comparison. *Ecology*, 91 (8), pp.2416–2427. [Online]. Available at: doi:10.1890/09-0143.1.

Nguyen, T. M. P. et al. (2011). Dissolution susceptibility of Paleocene – Eocene planktic foraminifera : Implications for palaeoceanographic reconstructions. *Marine Micropaleontology*, 81 (1–2), pp.1–21. [Online]. Available at: doi:10.1016/j.marmicro.2011.07.001.

Nguyen, T. M. P., Petrizzo, M. R. and Speijer, R. P. (2009). Experimental dissolution of a fossil foraminiferal assemblage (Paleocene-Eocene Thermal Maximum, Dababiya, Egypt): Implications for paleoenvironmental reconstructions. *Marine Micropaleontology*, 73 (3–4), pp.241–258. [Online]. Available at: doi:10.1016/j.marmicro.2009.10.005.

Nguyen, T. M. P. and Speijer, R. P. (2014). A new procedure to assess dissolution based on experiments on Pliocene–Quaternary foraminifera (ODP Leg 160, Eratosthenes Seamount, Eastern Mediterranean). *Marine Micropaleontology*, 106, pp.22–39. [Online]. Available at: doi:10.1016/j.marmicro.2013.11.004.

Ni, Y. et al. (2007). A core top assessment of proxies for the ocean carbonate system in surface-dwelling foraminifers. *Paleoceanography*, 22 (3), p.n/a-n/a. [Online]. Available at: doi:10.1029/2006PA001337.

Nogués-Bravo, D. et al. (2018). Cracking the Code of Biodiversity Responses to Past Climate Change. *Trends in Ecology & Evolution*, 33 (10), pp.765–776. [Online]. Available at: doi:10.1016/j.tree.2018.07.005.

Norris, R. D. (1992). Extinction selectivity and ecology in planktonic foraminifera. *Palaeogeography, Palaeoclimatology, Palaeoecology*, 95 (1–2), pp.1–17. [Online]. Available at: doi:10.1016/0031-0182(92)90161-W.

Norris, R. D. (1996). Symbiosis as an Evolutionary Innovation in the Radiation of Paleocene Planktic Foraminifera. *Paleobiology*, 22 (4), pp.461–480.

Norris, R. D. (2000). Paleontological Society Pelagic Species Diversity , Biogeography , and Evolution Pelagic species diversity , biogeography , and evolution. *Paleobiology*, 26 (4), pp.236–258.

Norris, R. D. et al. (2014). *Proceedings of the Integrated Ocean Drilling Program; Paleogene Newfoundland sediment drifts and MDHDS test; Expedition 342 of the riserless drilling platform, St. George, Bermuda, to St. John's, Newfoundland (Canada); Sites U1402-U1411, 2 June-1 August 2*.

Norris, R. D., Corfield, R. M. and Cartlidge, J. E. (1993). Evolution of depth ecology in the planktic foraminifera lineage Globorotalia (Fohsella).pdf. *Geology*, 21 (11), pp.975–978. [Online]. Available at: doi:10.1130/0091-7613(1993)021<0975:eodeit>2.3.co;2.

Numberger, L. et al. (2009). Habitats, abundance patterns and isotopic signals of morphotypes of the planktonic foraminifer Globigerinoides ruber (d'Orbigny) in the eastern Mediterranean Sea since the Marine Isotopic Stage 12. *Marine Micropaleontology*, 73 (1–2), pp.90–104. [Online]. Available at: doi:10.1016/j.marmicro.2009.07.004.

Ogle, D. H., Wheeler, P. and Dinno, A. (2021). *FSA: Fisheries Stock Analysis*. [Online]. Available at: https://github.com/droglenc/FSA.

Oksanen, O. et al. (2019). A Humboldtian approach to life and climate of the geological past: Estimating palaeotemperature from dental traits of mammalian communities. *Journal of Biogeography*, 46 (8), pp.1760–1776. [Online]. Available at: doi:https://doi.org/10.1111/jbi.13586.

Olsson, R. K. (1973). What Is a Kummerform Planktonic Foraminifer? *Journal of Paleontology*, 47 (2), pp.327–329.

Oppo, D. W. and Fairbanks, R. G. (1989). Carbon isotope composition of tropical surface water during the past 22,000 years. *Paleoceanography*, 4 (4), pp.333–351. [Online]. Available at: doi:https://doi.org/10.1029/PA004i004p00333.

paleobiodb.org. (2021). *PBDB*. [Online]. Available at: paleobiodb.org.

Pälike, H. et al. (2012). A Cenozoic record of the equatorial Pacific carbonate compensation depth. *Nature*, 488 (7413), pp.609–614. [Online]. Available at: doi:10.1038/nature11360.

Parker, F. L. (1962). Planktonic Foraminiferal Species in Pacific Sediments. *Micropaleontology*. [Online]. Available at: doi:10.2307/1484745.

Parr, C. S. et al. (2012). Evolutionary informatics: unifying knowledge about the diversity of life. *Trends in Ecology and Evolution*, 27 (2), pp.94–103.

Pärtel, M., Szava-Kovats, R. and Zobel, M. (2011). Dark diversity: shedding light on absent species. *Trends in Ecology & Evolution*, 26 (3), pp.124–128. [Online]. Available at: doi:10.1016/j.tree.2010.12.004.

Patzkowsky, M. E. and Holland, S. M. (2007). Diversity partitioning of a Late Ordovician marine biotic invasion: controls on diversity in regional ecosystems. *Paleobiology*, 33 (2), pp.295–309. [Online]. Available at: doi:10.1666/06078.1.

Payne, J. L. et al. (2012). A shift in the long-term mode of foraminferan size evolution caused by the end-Permian mass extinction. *Evolution*, 67 (3), pp.816–827. [Online]. Available at: doi:10.5061/dryad.5pr86.

Pearson, P. N. (1998). Stable Isotopes and the Study of Evolution in Planktonic Foraminifera. *The Paleontological Society Papers*, 4, pp.138–178. [Online]. Available at: doi:10.1017/S1089332600000425.

Pearson, P. N. et al. (2001). Warm tropical sea surface temperatures in the Late Cretaceous and Eocene epochs. *Nature*, 413, pp.481–488.

Pearson, P. N. et al. (2006). *Atlas of Eocene Planktonic Foraminifera*.

Pearson, P. N. et al. (2008). Extinction and environmental change across the Eocene-Oligocene boundary in Tanzania. *Geology*, 36 (2), pp.179–182. [Online]. Available at: doi:10.1130/G24308A.1.

Pearson, P. N. (2012). Oxygen Isotopes in Foraminifera: Overview and Historical Review. *The Paleontological Society Papers*, 18, pp.1–38. [Online]. Available at: doi:10.1017/s1089332600002539.

Pearson, P. N. and Wade, B. S. (2015). Systematic Taxonomy of Exceptionally Well-Preserved Planktonic Foraminifera From the Eocene / Oligocene Boundary of Tanzania. *Cushman Foundation Special Publication*, (45), pp.1–85.

Peeters, F. J. C., Brummer, G. J. A. and Ganssen, G. (2002). The effect of upwelling on the distribution and stable isotope composition of Globigerina bulloides and Globigerinoides ruber (planktic foraminifera) in modern surface waters of the NW Arabian Sea. *Global and Planetary Change*, 34 (3–4), pp.269–291. [Online]. Available at: doi:10.1016/S0921-8181(02)00120-0.

Peppe, D. J. et al. (2011). Sensitivity of leaf size and shape to climate: global patterns and paleoclimatic applications. *New Phytologist*, 190 (3), pp.724–739. [Online]. Available at: doi:10.1111/j.1469-8137.2010.03615.x.

Pereira, H. M. et al. (2010). Scenarios for Global Biodiversity in the 21st Century. *Science*, 330 (6010), pp.1496–1501. [Online]. Available at: doi:10.1126/science.1196624.

Peres-Neto, P. R., Jackson, D. A. and Somers, K. M. (2005). How many principal components? stopping rules for determining the number of non-trivial axes revisited. *Computational Statistics & Data Analysis*, 49 (4), pp.974–997. [Online]. Available at: doi:10.1016/j.csda.2004.06.015.

Petrizzo, M. R. et al. (2008). DISSOLUTION SUSCEPTIBILITY OF SOME PALEOGENE PLANKTONIC FORAMINIFERA FROM ODP SITE 1209 (SHATSKY RISE, PACIFIC OCEAN). *Journal of Foraminiferal Research*, 38 (4), pp.357–371. [Online]. Available at: doi:10.2113/gsjfr.38.4.357.

Petro, S. M., Pivel, M. A. and Coimbra, J. C. (2018). Foraminiferal solubilty rankings: A contribution to the search for consensus. *Journal of Foraminiferal Research*, 48 (4), pp.301–313.

Pfuhl, H. A. and Shackleton, N. J. (2004). Two proximal , high-resolution records of foraminiferal fragmentation and their implications for changes in dissolution. *Deep Sea Research Part I: Oceanographic Research Papers*, 51, pp.809–832. [Online]. Available at: doi:10.1016/j.dsr.2004.02.003.

Phillimore, A. B. and Owens, I. P. F. (2006). Are subspecies useful in evolutionary and conservation biology? *Proceedings of the Royal Society B: Biological Sciences*, 273 (1590), pp.1049–1053. [Online]. Available at: doi:10.1098/rspb.2005.3425.

Pimiento, C. et al. (2017). The Pliocene marine megafauna extinction and its impact on functional diversity. *Nature Ecology and Evolution*, 1 (8), pp.1100–1106. [Online]. Available at: doi:10.1038/s41559-017-0223-6.

Pimm, S. L. et al. (2014). The biodiversity of species and their rates of extinction, distribution, and protection. *Science*, 344 (6187), pp.1246752–1246752. [Online]. Available at: doi:10.1126/science.1246752.

Pracht, H., Metcalfe, B. and Peeters, F. J. C. (2019). Oxygen isotope composition of the final chamber of planktic foraminifera provides evidence of vertical migration and depth-integrated growth. *Biogeosciences*, 16 (2), pp.643–661. [Online]. Available at: doi:10.5194/bg-16-643-2019.

Preston, F. W. (1948). The Commonness, And Rarity, of Species. *Ecology*, 29 (3), pp.254–283. [Online]. Available at: doi:10.2307/1930989.

Purvis, A. and Hector, A. (2000). Getting the measure of biodiversity. *Nature*, 405 (6783).

R Core Team. (2020). *R: A Language and Environment for Statistical Computing*. Vienna, Austria: R Foundation for Statistical Computing. [Online]. Available at: https://www.R-project.org/.

Raia, P. et al. (2016). Progress to extinction: increased specialisation causes the demise of animal clades. *Scientific Reports*, 6 (1), p.30965. [Online]. Available at: doi:10.1038/srep30965.

Rego, B. L. et al. (2012). Within- and among-genus components of size evolution during mass extinction, recovery, and background intervals: a case study of Late Permian through Late Triassic foraminifera. *Paleobiology*, 38 (04), pp.627–643. [Online]. Available at: doi:10.1666/11040.1.

Reich, P. B. et al. (2012). Impacts of Biodiversity Loss Escalate Through Time as Redundancy Fades. *Science*, 336 (6081), pp.589–592. [Online]. Available at: doi:10.1126/science.1217909.

Renaud, S. et al. (2005). Morphological evolution, ecological diversification and climate change in rodents. *Proceedings of the Royal Society B: Biological Sciences*, 272 (1563), pp.609–617. [Online]. Available at: doi:10.1098/rspb.2004.2992.

Renaud, S. and Schmidt, D. N. (2003). Habitat tracking as a response of the planktic foraminifer Globorotalia truncatulinoides to environmental fluctuations during the last 140 kyr. *Marine Micropaleontology*, 49 (1), pp.97–122. [Online]. Available at: doi:10.1016/S0377-8398(03)00031-8.

Reydon, T. A. C. (2019). Are Species Good Units for Biodiversity Studies and Conservation Efforts? In: Casetta, E., Marques da Silva, J. and Vecchi, D. (Eds). *From Assessing to Conserving Biodiversity: Conceptual and Practical Challenges*. History, Philosophy and Theory of the Life Sciences. Cham: Springer International Publishing. pp.167–193. [Online]. Available at: doi:10.1007/978-3-030-10991-2_8 [Accessed 20 July 2021].

Rillo, M. C. et al. (2017). The unknown planktonic foraminiferal pioneer Henry A. Buckley and his collection at The Natural History Museum, London. *Journal of Micropalaeontology*, 36 (2), pp.191–194. [Online]. Available at: doi:10.1144/jmpaleo2016-020.

Rillo, M. C. et al. (2020). Intraspecific size variation in planktonic foraminifera cannot be consistently predicted by the environment. *Ecology and Evolution*, 10 (20), pp.11579–11590. [Online]. Available at: doi:10.1002/ece3.6792.

Rivero-Cuesta, L. et al. (2019). Paleoenvironmental Changes at ODP Site 702 (South Atlantic): Anatomy of the Middle Eocene Climatic Optimum. *Paleoceanography and Paleoclimatology*, 34 (12), pp.2047–2066. [Online]. Available at: doi:https://doi.org/10.1029/2019PA003806.

Robbins, L. L. and Healy-Williams, N. (1991). Toward a classification of planktonic foraminifera based on biochemical, geochemical, and morphological criteria. *Journal of Foraminiferal Research*, 21 (2).

Rockstrom, J. et al. (2009). A safe operating space for humanity. *Science*, 461 (September).

Rolland, J. and Salamin, N. (2016). Niche width impacts vertebrate diversification. *Global Ecology and Biogeography*, 25 (10), pp.1252–1263. [Online]. Available at: doi:10.1111/geb.12482.

Román-Palacios, C. and Wiens, J. J. (2020). Recent responses to climate change reveal the drivers of species extinction and survival. *Proceedings of the National Academy of Sciences*, 117 (8), pp.4211–4217. [Online]. Available at: doi:10.1073/pnas.1913007117.

Rosenthal, Y., Boyle, E. A. and Slowey, N. (1997). Temperature control on the incorporation of magnesium, strontium, flourine, and cadmium into benthic foraminiferal shells from the Little

Bibliography

Bahama Bank: Prospects for thermocline paleoceanography. *Geochimica et Cosmochimica Acta*, 61 (17), pp.3633–3643.

Russell, A. D. et al. (2004). Effects of seawater carbonate ion concentration and temperature on shell U, Mg, and Sr in cultured planktonic foraminifera. *Geochimica et Cosmochimica Acta*, 68 (21), pp.4347–4361. [Online]. Available at: doi:10.1016/j.gca.2004.03.013.

Rutherford, S., D'Hondt, S. and Prell, W. (1999). Environmental controls on the geographic distribution of zooplankton diversity. *Nature*, 400 (6746), pp.749–753. [Online]. Available at: doi:10.1038/23449.

Sadekov, A. et al. (2008). Uncertainties in seawater thermometry deriving from intratest and intertest Mg/Ca variability in Globigerinoides ruber. *Paleoceanography*, 23 (1), pp.1–12. [Online]. Available at: doi:10.1029/2007PA001452.

Sadekov, A. et al. (2009). Surface and subsurface seawater temperature reconstruction using Mg/Ca microanalysis of planktonic foraminifera Globigerinoides ruber, Globigerinoides sacculifer, and Pulleniatina obliquiloculata. *Paleoceanography*, 24 (3), pp.1–17. [Online]. Available at: doi:10.1029/2008PA001664.

Sadekov, A., Eggins, S. M. and Deckker, P. D. (2005). Characterization of Mg/Ca distributions in planktonic foraminifera species by electron microprobe mapping. *Geochemistry, Geophysics, Geosystems*, 6 (12). [Online]. Available at: doi:https://doi.org/10.1029/2005GC000973 [Accessed 4 May 2021].

Sanderson, E. W. et al. (2002). The Human Footprint and the Last of the Wild. *BioScience*, 52 (10), pp.891–891. [Online]. Available at: doi:10.1641/0006-3568(2002)052[0891:THFATL]2.0.CO;2.

Schiebel, R. and Hemleben, C. (2008). Protozoa, Planktonic Foraminifera. *Encyclopedia of Ocean Sciences: Second Edition*, pp.606–612. [Online]. Available at: doi:10.1016/B978-012374473-9.00192-2.

Schiebel, R. and Hemleben, C. (2017). Classification and Taxonomy of Extant Planktic Foraminifers. In: Schiebel, R. and Hemleben, C. (Eds). *Planktic Foraminifers in the Modern Ocean*. Berlin, Heidelberg: Springer. pp.11–110. [Online]. Available at: doi:10.1007/978-3-662-50297-6_2 [Accessed 13 September 2021].

Schmidt, D. N. (2004). Abiotic Forcing of Plankton Evolution in the Cenozoic. *Science*, 303 (5655), pp.207–210. [Online]. Available at: doi:10.1126/science.1090592.

Schmidt, D. N. et al. (2004). Size distribution of Holocene planktic foraminifer assemblages: biogeography, ecology and adaptation. *Marine Micropaleontology*, 50 (3), pp.319–338. [Online]. Available at: doi:10.1016/S0377-8398(03)00098-7.

Schmidt, D. N. et al. (2006). Biogeography and evolution of body size in marine plankton. *Earth-Science Reviews*, 78 (3), pp.239–266. [Online]. Available at: doi:10.1016/j.earscirev.2006.05.004.

Schmidt, D. N., Thierstein, H. R. and Bollmann, J. (2004). The evolutionary history of size variation of planktic foraminiferal assemblages in the Cenozoic. *Palaeogeography, Palaeoclimatology, Palaeoecology*, 212 (1–2), pp.159–180. [Online]. Available at: doi:10.1016/j.palaeo.2004.06.002.

Schmitt, A. et al. (2019). Single foraminifera Mg/Ca analyses of past glacial-interglacial temperatures derived from G. ruber sensu stricto and sensu lato morphotypes. *Chemical Geology*, 511, pp.510–520. [Online]. Available at: doi:10.1016/j.chemgeo.2018.11.007.

Schulte, P. et al. (2010). The Chicxulub Asteroid Impact and Mass Extinction at the Cretaceous-Paleogene Boundary. *Science*, 327 (5970), pp.1214–1218. [Online]. Available at: doi:10.1126/science.1177265.

Schwarz, G. (1978). Estimating the Dimension of a Model. *The Annals of Statistics*, 6 (2), pp.461–464. [Online]. Available at: doi:10.1214/aos/1176344136.

Scrucca, L. et al. (2016). mclust 5: clustering, classification and density estimation using Gaussian finite mixture models. *The R Journal*, 8 (1), pp.289–317.

Seddon, P. J., Armstrong, D. P. and Maloney, R. F. (2007). Developing the Science of Reintroduction Biology. *Conservation Biology*, 21 (2), pp.303–312. [Online]. Available at: doi:10.1111/j.1523-1739.2006.00627.x.

Seears, H. A., Darling, K. F. and Wade, C. M. (2012). Ecological partitioning and diversity in tropical planktonic foraminifera. *BMC Evolutionary Biology*, 12 (1), p.54. [Online]. Available at: doi:10.1186/1471-2148-12-54.

Sexton, P. F., Wilson, P. A. and Pearson, P. N. (2006a). Microstructural and geochemical perspectives on planktic foraminiferal preservation: "Glassy" versus "Frosty". *Geochemistry, Geophysics, Geosystems*, 7 (12). [Online]. Available at: doi:https://doi.org/10.1029/2006GC001291 [Accessed 15 January 2021].

Sexton, P. F., Wilson, P. A. and Pearson, P. N. (2006b). Palaeoecology of late middle Eocene planktic foraminifera and evolutionary implications. *Marine Micropaleontology*, 60 (1), pp.1–16. [Online]. Available at: doi:10.1016/j.marmicro.2006.02.006.

Si, W. and Aubry, M. P. (2018). Vital Effects and Ecologic Adaptation of Photosymbiont-Bearing Planktonic Foraminifera During the Paleocene-Eocene Thermal Maximum, Implications for Paleoclimate. *Paleoceanography and Paleoclimatology*, 33 (1), pp.112–125. [Online]. Available at: doi:10.1002/2017PA003219.

Silvertown, J. et al. (2006). The Park Grass Experiment 1856–2006: its contribution to ecology. *Journal of Ecology*, 94 (4), pp.801–814. [Online]. Available at: doi:10.1111/j.1365-2745.2006.01145.x.

Silvestro, D. et al. (2015). The role of clade competition in the diversification of North American canids. *Proceedings of the National Academy of Sciences*, 112 (28), pp.8684–8689. [Online]. Available at: doi:10.1073/pnas.1502803112.

Smith, A. B. and Jeffery, C. H. (1998). Selectivity of extinction among sea urchins at the end of the Cretaceous period. *Nature*, 392 (6671), pp.69–71. [Online]. Available at: doi:10.1038/32155.

Solórzano, A. et al. (2019). Data from: Biotic and abiotic factors driving the diversification dynamics of Crocodylia. *Dryad Digital Repository*, p.https://doi.org/10.5061/dryad.sb5844c-https://doi.org/10.5061/dryad.sb5844c. [Online]. Available at: doi:10.5061/dryad.sb5844c.

Spero, H. J. (1987). *SYMBIOSIS IN T H E PLANKTONIC FORAMINIFER , ORBULZLVA UNIVERSA , AND T H E ISOLATION O F I T S SYMBIOTIC DINOFLAGELLATE , GYMVODZNZUA4 BEZZ SP . NOV .' and close association of these algae with host cyto- At least two types of algae are known to establish*. (1 982), pp.37–46.

Spero, H. J. et al. (1997). Effect of seawater carbonate concentration on foraminiferal carbon and oxygen isotopes. *Nature*, 390 (6659), pp.497–500. [Online]. Available at: doi:10.1038/37333.

Bibliography

Spero, H. J. (1998). Life History and Stable Isotope Geochemistry of Planktonic Foraminifera. *The Paleontological Society Papers*, 4, pp.7–36. [Online]. Available at: doi:10.1017/s1089332600000383.

Spero, H. J. et al. (2015). Timing and mechanism for intratest Mg/Ca variability in a living planktic foraminifer. *Earth and Planetary Science Letters*, 409, pp.32–42. [Online]. Available at: doi:10.1016/j.epsl.2014.10.030.

Spero, H. J. and Deniro, M. J. (1987). The influence of Symbiont Photosynthesis on the Oxygen and Carbon isotope values of Planktonic Foraminiferal Shell Calcite. *Symbiosis*, 4, pp.213–228.

Spero, H. J. and Lea, D. W. (1993). Intraspecific stable isotope variability in the planktic foraminifera Globigerinoides sacculifer: Results from laboratory experiments. *Marine Micropaleontology*, 22 (3), pp.221–234. [Online]. Available at: doi:10.1016/0377-8398(93)90045-Y.

Spero, H. J. and Lea, D. W. (1996). Experimental determination of stable isotope variability in Globigerina bulloides: Implications for paleoceanographic reconstructions. *Marine Micropaleontology*, 28 (3–4), pp.231–246. [Online]. Available at: doi:10.1016/0377-8398(96)00003-5.

Spero, H. J., Lerche, I. and Williams, D. F. (1991). *Opening the carbon isotope 'vital effect' black box 2, quantative model for interesting foraminiferal carbon isotope data*. 6 (6), pp.639–655.

Spero, H. J. and Williams, D. F. (1989b). Opening the carbon isotope 'vital effect' black box 1. Seasonal tempratures in the euphotic zone. *Paleoceanography*, 4 (6), pp.593–601.

Spofforth, D. J. A. et al. (2010). Organic carbon burial following the middle Eocene climatic optimum in the central western Tethys. *Paleoceanography*, 25 (3). [Online]. Available at: doi:https://doi.org/10.1029/2009PA001738 [Accessed 15 December 2020].

Stap, L. et al. (2010). Coherent pattern and timing of the carbon isotope excursion and warming during Eocene Thermal Maximum 2 as recorded in planktic and benthic foraminifera. *Geochemistry, Geophysics, Geosystems*, 11 (11). [Online]. Available at: doi:10.1029/2010GC003097 [Accessed 10 June 2020].

Stavert, J. R. et al. (2016). Hairiness: the missing link between pollinators and pollination. *PeerJ*, 4, p.e2779. [Online]. Available at: doi:10.7717/peerj.2779.

Steffen, W. et al. (2018). Trajectories of the Earth System in the Anthropocene. *Proceedings of the National Academy of Sciences*, 115 (33), pp.8252–8259. [Online]. Available at: doi:10.1073/pnas.1810141115.

Steineck, P. L. (1971). Middle Eocene Refrigeration — New Evidence from California Planktonic Foraminiferal Assemblages. *Lethaia*, 4 (2), pp.125–129. [Online]. Available at: doi:10.1111/j.1502-3931.1971.tb01284.x.

Steinke, S. et al. (2005). Mg/Ca ratios of two Globigerinoides ruber (white) morphotypes: Implications for reconstructing past tropical/subtropical surface water conditions. *Geochemistry, Geophysics, Geosystems*, 6 (11), pp.1–12. [Online]. Available at: doi:10.1029/2005GC000926.

Steinke, S. et al. (2010). East Asian summer monsoon weakening after 7.5 Ma: Evidence from combined planktonic foraminifera Mg/Ca and δ18O (ODP Site 1146; northern South China Sea). *Palaeogeography, Palaeoclimatology, Palaeoecology*, 289, pp.33–43. [Online]. Available at: doi:10.1016/j.palaeo.2010.02.007.

Steinthorsdottir, M. et al. (2016). Fossil plant stomata indicate decreasing atmospheric CO 2 prior to the Eocene – Oligocene boundary. *Climate of the past*, 12, pp.439–454. [Online]. Available at: doi:10.5194/cp-12-439-2016.

Stenseth, N. C. and Smith, J. M. (1984). Coevolution in Ecosystems: Red Queen Evolution or Stasis? *Evolution*, 38 (4), pp.870–880. [Online]. Available at: doi:10.1111/j.1558-5646.1984.tb00358.x.

Stewart, J. A. et al. (2012). Geochemical assessment of the palaeoecology, ontogeny, morphotypic variability and palaeoceanographic utility of 'Dentoglobigerina' venezuelana. *Marine Micropaleontology*, 84–85, pp.74–86. [Online]. Available at: doi:10.1016/j.marmicro.2011.11.003.

Stuart-Smith, R.D. *et al.* (2013) 'Integrating abundance and functional traits reveals new global hotspots of fish diversity', *Nature*, 501(7468), pp. 539–542. doi:10.1038/nature12529.

Takagi, H. et al. (2019). Characterizing photosymbiosis in modern planktonic foraminifera. *Biogeosciences*, 16 (17), pp.3377–3396. [Online]. Available at: doi:10.5194/bg-2019-145.

Taylor, B. J. et al. (2018). Distribution and ecology of planktic foraminifera in the North Pacific: Implications for paleo-reconstructions. *Quaternary Science Reviews*, 191, pp.256–274. [Online]. Available at: doi:10.1016/j.quascirev.2018.05.006.

Thirumalai, K. et al. (2013). Statistical constraints on El Niño Southern Oscillation reconstructions using individual foraminifera: A sensitivity analysis. *Paleoceanography*, 28 (3), pp.401–412. [Online]. Available at: doi:https://doi.org/10.1002/palo.20037.

Thirumalai, K. et al. (2014). Globigerinoides ruber morphotypes in the Gulf of Mexico: a test of null hypothesis. *Scientific reports*, 4, pp.1–7. [Online]. Available at: doi:10.1038/srep06018.

Thunell, R. C. (1976). Calcium Carbonate Dissolution History in Late Quaternary Deep-Sea Sediments , Western Gulf of Mexico. *Quaternary Researcg*, 297, pp.281–297.

Tierney, J. E. et al. (2020). Past climates inform our future. *Science*, 370 (6517). [Online]. Available at: doi:10.1126/science.aay3701 [Accessed 12 February 2021].

Tolderlund, D. S. and Bé, A. W. H. (1971). *Seasonal distribution of planktonic foraminifera in the western North Atlantic*.

Trip, E.D. *et al.* (2014) 'Temperature-related variation in growth rate, size, maturation and life span in a marine herbivorous fish over a latitudinal gradient', *Journal of Animal Ecology*, 83(4), pp. 866–875. doi:10.1111/1365-2656.12183.

Trueman, C. N., Chung, M.-T. and Shores, D. (2016). Ecogeochemistry potential in deep time biodiversity illustrated using a modern deep-water case study.pdf. *Philosophical transactions of the Royal Society of London. Series B, Biological sciences*, 371.

Urban, M. C. et al. (2016). Improving the forecast for biodiversity under climate change. *Science*, 353 (6304), pp.aad8466–aad8466. [Online]. Available at: doi:10.1126/science.aad8466.

Urey, H. C. (1947). The thermodynamic properties of isotopic substances. *Journal of the Chemical Society (Resumed)*, (0), pp.562–581. [Online]. Available at: doi:10.1039/JR9470000562.

Bibliography

Urey, H. C. et al. (1951). Measurement of Paleotemperatures and Temperatures and the Southeastern United States. *Bulletin of the geological society of America*, 62 (April), pp.399–416. [Online]. Available at: doi:10.1130/0016-7606(1951)62[399:MOPATO]2.0.CO;2.

Van Peer, T. E., Liebrand, D. ,. Xuan, C. ,. Lippert, P. C. ,. Agnini, C. ,. Blum, N. ,. Blum, P. ,. Bohaty, S. M. ,. Bown, P. ,. Greenop, R. and Kordesch, W. E. (2017). *Data report: revised composite depth scale and splice for IODP Site U1406*.

Van Valen, L. (1973). *A new evolutionary law.*

Van Valkenburgh, B. (2004). Cope's Rule, Hypercarnivory, and Extinction in North American Canids. *Science*, 306 (5693), pp.101–104. [Online]. Available at: doi:10.1126/science.1102417.

de Vargas, C. et al. (1999). Molecular evidence of cryptic speciation in planktonic foraminifers and their relation to oceanic provinces. *Proceedings of the National Academy of Sciences of the United States of America*, 96 (6), pp.2864–2868. [Online]. Available at: doi:10.1073/pnas.96.6.2864.

Villa, G. et al. (2008). Middle Eocene-late Oligocene climate variability: Calcareous nannofossil response at Kerguelen Plateau, Site 748. *Marine Micropaleontology*, 69 (2), pp.173–192. [Online]. Available at: doi:10.1016/j.marmicro.2008.07.006.

Villa, G. et al. (2013). Middle Eocene to Late Oligocene Antarctic gla-ciation/deglaciation and Southern Ocean productivity, Paleoceanography, 29, doi: 10.1002/2013PA002518. *Academia.Edu*, pp.223–237. [Online]. Available at: doi:10.1002/2013PA002518.Received.

Vincent, E. and Berger, W. H. (1981). Planktonic foraminifera and their use in paleoceanography. *The sea*, 7, pp.1025–1119.

Violle, C. et al. (2007). Let the concept of trait be functional! *Oikos*, 116 (5), pp.882–892. [Online]. Available at: doi:10.1111/J.0030-1299.2007.15559.X.

Violle, C. et al. (2012). The return of the variance: Intraspecific variability in community ecology. *Trends in Ecology and Evolution*, 27 (4), pp.244–252. [Online]. Available at: doi:10.1016/j.tree.2011.11.014.

Voje, K. L. et al. (2015). The role of biotic forces in driving macroevolution: beyond the Red Queen. *Proceedings of the Royal Society B: Biological Sciences*, 282 (1808), pp.20150186–20150186. [Online]. Available at: doi:10.1098/rspb.2015.0186.

Wade, B. (2004). Planktonic foraminiferal biostratigraphy and mechanisms in the extinction of Morozovella in the late middle Eocene. *Marine Micropaleontology*, 51 (1–2), pp.23–38. [Online]. Available at: doi:10.1016/j.marmicro.2003.09.001.

Wade, B. et al. (2008). Symbiont bleaching in fossil planktonic foraminifera. *Evolutionary Ecology*, 22 (2), pp.253–265. [Online]. Available at: doi:10.1007/s10682-007-9176-6.

Wade, B. et al. (2011). Review and revision of Cenozoic tropical planktonic foraminiferal biostratigraphy and calibration to the geomagnetic polarity and astronomical time scale. *Earth Science Reviews*, 104 (1–3), pp.111–142. [Online]. Available at: doi:10.1016/j.earscirev.2010.09.003.

Wade, B. et al. (2018). *Atlas of Oligocene Planktonic Foraminifera*. Cushman Foundation Special Publication.

Wade, B. and Olsson, R. K. (2009). Investigation of pre-extinction dwar fi ng in Cenozoic planktonic foraminifera. *Palaeogeography, Palaeoclimatology, Palaeoecology*, 284 (1–2), pp.39–46. [Online]. Available at: doi:10.1016/j.palaeo.2009.08.026.

Wade, B. and Pearson, P. N. (2008). Planktonic foraminiferal turnover , diversity fluctuations and geochemical signals across the Eocene / Oligocene boundary in Tanzania. *Marine Micropaleontology*, 68, pp.244–255. [Online]. Available at: doi:10.1016/j.marmicro.2008.04.002.

Wang, L. (2000). Isotopic signals in two morphotypes of Globigerinoides ruber (white) from the South China Sea: Implications for monsoon climate change during the last glacial cycle. *Palaeogeography, Palaeoclimatology, Palaeoecology*, 161 (3–4), pp.381–394. [Online]. Available at: doi:10.1016/S0031-0182(00)00094-8.

Wei, K. -Y and Kennett, J. P. (1986). Taxonomic evolution of Neogene planktonic foraminifera and paleoceanographic relations. *Paleoceanography*, 1 (1), pp.67–84. [Online]. Available at: doi:10.1029/PA001i001p00067.

Weiner, A. K. M. et al. (2015). Genetic and morphometric evidence for parallel evolution of the Globigerinella calida morphotype. *Marine Micropaleontology*, 114, pp.19–35. [Online]. Available at: doi:10.1016/j.marmicro.2014.10.003.

Weiner, S. (2005). An Overview of Biomineralization Processes and the Problem of the Vital Effect. *Reviews in Mineralogy and Geochemistry*, 54 (1), pp.1–29. [Online]. Available at: doi:10.2113/0540001.

Weinkauf, M. et al. (2014). Disruptive selection and bet-hedging in planktonic Foraminifera: shell morphology as predictor of extinctions. *Frontiers in Ecology and Evolution*, 2. [Online]. Available at: doi:10.3389/fevo.2014.00064 [Accessed 11 May 2021].

Weinkauf, M. et al. (2019). An extinction event in planktonic Foraminifera preceded by stabilizing selection. Rosa, R. (Ed). *PLOS ONE*, 14 (10), p.e0223490. [Online]. Available at: doi:10.1371/journal.pone.0223490.

Weinkauf, M. et al. (2020). Stable Oxygen Isotope Composition Is Biased by Shell Calcification Intensity in Planktonic Foraminifera. *Paleoceanography and Paleoclimatology*, 35 (11), p.e2020PA003941. [Online]. Available at: doi:https://doi.org/10.1029/2020PA003941.

Weisser, W. W. et al. (2017). Biodiversity effects on ecosystem functioning in a 15-year grassland experiment: Patterns, mechanisms, and open questions. *Basic and Applied Ecology*, 23, pp.1–73. [Online]. Available at: doi:10.1016/j.baae.2017.06.002.

Westerhold, T. et al. (2018). Global Extent of Early Eocene Hyperthermal Events: A New Pacific Benthic Foraminiferal Isotope Record From Shatsky Rise (ODP Site 1209). *Paleoceanography and Paleoclimatology*, 33 (6), pp.626–642. [Online]. Available at: doi:https://doi.org/10.1029/2017PA003306.

Westerhold, T. et al. (2020). An astronomically dated record of Earth's climate and its predictability over the last 66 million years. *Science*, 369 (6509), pp.1383–1387. [Online]. Available at: doi:10.1126/science.aba6853.

Williams, J. W. et al. (2018). The Neotoma Paleoecology Database, a multiproxy, international, community-curated data resource. *Quaternary Research*, 89 (1), pp.156–177. [Online]. Available at: doi:10.1017/qua.2017.105.

Bibliography

Wintle, B. A. et al. (2003). The Use of Bayesian Model Averaging to Better Represent Uncertainty in Ecological Models. *Conservation Biology*, 17 (6), pp.1579–1590. [Online]. Available at: doi:10.1111/j.1523-1739.2003.00614.x.

Wit, J. C. et al. (2010). Approaches to unravel seasonality in sea surface temperatures using paired single-specimen foraminiferal δ18O and Mg/Ca analyses. *Paleoceanography*, 25 (4), pp.1–15. [Online]. Available at: doi:10.1029/2009PA001857.

Witkowski, J. et al. (2012). Enhanced siliceous plankton productivity in response to middle Eocene warming at Southern Ocean ODP Sites 748 and 749. *Palaeogeography, Palaeoclimatology, Palaeoecology*, 326–328, pp.78–94. [Online]. Available at: doi:10.1016/j.palaeo.2012.02.006.

Witkowski, J. et al. (2014). Rapid fluctuations in mid-latitude siliceous plankton production during the Middle Eocene Climatic Optimum (ODP Site 1051, western North Atlantic). *Marine Micropaleontology*, 106, pp.110–129. [Online]. Available at: doi:10.1016/j.marmicro.2014.01.001.

Wood, S. N. (2011). Fast stable restricted maximum likelihood and marginal likelihood estimation of semiparametric generalized linear models. *Journal of the Royal Statistical Society: Series B (Statistical Methodology)*, 73 (1), pp.3–36. [Online]. Available at: doi:10.1111/j.1467-9868.2010.00749.x.

Wood, S. N. (2017). *Generalized Additive Models: An Introduction with R, Second Edition*. 2nd edition. Chapman and Hall/CRC. [Online]. Available at: https://www.routledge.com/Generalized-Additive-Models-An-Introduction-with-R-Second-Edition/Wood/p/book/9781498728331 [Accessed 10 June 2021].

Yamamoto, Y. et al. (2018). Data report: updated magnetostratigraphy for IODP Sites U1403, U1408, U1409, and U1410. *Proceedings of the Integrated Ocean Drilling Program,. 342: College Station, TX (Integrated Ocean Drilling Program).* [Online]. Available at: doi:10.2204/iodp.proc.342.2014 [Accessed 11 March 2021].

Yasuhara, M. et al. (2008). *Abrupt climate change and collapse of deep-sea ecosystems*.

Yasuhara, M. et al. (2016). *Biodiversity – ecosystem functioning relationships in long-term time series and palaeoecological records : deep sea as a test bed*.

Yasuhara, M. et al. (2020). Past and future decline of tropical pelagic biodiversity. *Proceedings of the National Academy of Sciences*, 117 (23), pp.12891–12896. [Online]. Available at: doi:10.1073/pnas.1916923117.

Zachos, J. C. et al. (2001). Trends, Global Rhythms, Aberrations in Global Climate 65Ma to Present. *Science*, 292 (5517), pp.686–693. [Online]. Available at: doi:10.1126/science.1059412.

Zachos, J. C., Dickens, G. R. and Zeebe, R. E. (2008). An early Cenozoic perspective on greenhouse warming and carbon-cycle dynamics. *Nature*, 451 (7176), pp.279–283. [Online]. Available at: doi:10.1038/nature06588.

Zachos, J. C., Quinn, T. M. and Salamy, K. A. (1996). High-resolution (104 years) deep-sea foraminiferal stable isotope records of the Eocene-Oligocene climate transition. *Paleoceanography*, 11 (3), pp.251–266. [Online]. Available at: doi:10.1029/96PA00571.

Zar, J. H. (2010). *Biostatistical Analysis*. Prentice Hall. [Online]. Available at: https://books.google.co.uk/books?id=LCRFAQAAIAAJ.

Zeebe, R. E. and Wolf-Gladrow, D. (2001). *CO2 in Seawater: Equilibrium, Kinetics, Isotopes*. Elsevier.

Žliobaitė, I. et al. (2016). Herbivore teeth predict climatic limits in Kenyan ecosystems. *Proceedings of the National Academy of Sciences*, 113 (45), pp.12751–12756. [Online]. Available at: doi:10.1073/pnas.1609409113.